Generating Molecularly-Controlled Biomaterials Using Host-Guest Guided Peptide Amphiphile Self-Assembly

Carlos A. Redondo Gómez

January 2020

Submitted in partial fulfillment of the requirements of the
Degree of Doctor of Philosophy

School of Engineering and Materials Science
Queen Mary, University of London

Declaration

I, Carlos Alberto Redondo Gómez, confirm that the research included within this thesis is my own work or that where it has been carried out in collaboration with, or supported by others, that this is duly acknowledged below and my contribution indicated. Previously published material is also acknowledged below.

I attest that I have exercised reasonable care to ensure that the work is original, and does not to the best of my knowledge break any UK law, infringe any third party's copyright or other Intellectual Property Right, or contain any confidential material.

I accept that the College has the right to use plagiarism detection software to check the electronic version of the thesis.

I confirm that this thesis has not been previously submitted for the award of a degree by this or any other university.

The copyright of this thesis rests with the author and no quotation from it or information derived from it may be published without the prior written consent of the author.

Signature:

Carlos A. Redondo Gómez

Date: 21-01-2020

Supervisory team

Primary supervisor: Prof. Alvaro Mata
Secondary supervisor: Dr. Helena S. Azevedo

Details of collaborations

Mr. Yamin Abdouni (School of Engineering and Materials Science, Queen Mary University of London) & Dr. Remzi C. Becer (Department of Chemistry, University of Warwick.

- Organised the synthesis and availability of monoazido-β-cyclodextrin and per-thio-β-cyclodextrin for chapters 4 & 5.

Miss Soraya Padilla-Lopátegui (School of Engineering and Materials Science, Queen Mary University of London).

- Acquired confocal images in chapters 5 & 6.

Publications

Please see Appendix A (page 192) for a list of related publications and collaborations.

Abstract

Supramolecular chemistry offers a unique opportunity to assemble biomaterials with molecular precision. Though biomaterials based on self-assembling peptides often exhibit limited control over their hierarchical assembly, mechanical properties or biological relevance. This dissertation addresses these challenges by bringing together the scopes of peptide self-assembly and host-guest interactions.

The thesis opens with a literature revision chapter on supramolecular biomaterials and multicomponent self-assembly as a strategy to design complex biomedically relevant hydrogels. The following three experimental chapters constitute examples of biomedically relevant peptide amphiphile (PA)-based hydrogels based on the co-assembly of peptides bearing host-guest recognition motifs.

Firstly, a report on a new family of supramolecular hydrogels based on the non-covalent crosslinking between PAs bearing either β-Cyclodextrin (β**CD**) or Adamantane (**Ada**) host-guest cues is presented. The resulting hydrogels exhibit enhanced mechanical properties, including stiffness and resistance to degradation, while retaining good in vitro biocompatibility.

The next chapter explores on the non-covalent tethering of biologically relevant epitopes to self-assembled PA nanofibers through β**CD**/**Ada** complexations as a modular approach for developing more complex and dynamic PA hydrogels. Incorporating host-guest peptide pairs endowed control from nano to macroscale in the materials, as well as its mechanical control, biological tunability and the possibility to imprint them higher levels of dynamic spatiotemporal properties.

Lastly, the use of another host-guest interaction family based on the ternary complexation of aromatic amino acid-bearing PAs and cucurbit[8]uril (**CB[8]**) is presented. An unreported non-ionic gelation mechanism is presented as well as the structural and mechanical comparison of the PA-**CB[8]** gels versus conventional ionically-gelled PAs.

Altogether, this work presents new approaches to develop more controlled and functional peptide-based nanomaterials with broad implications in the self-assembling and bioengineering communities.

Acknowledgements

First I want to thank my mother Lourdes, Tía Elieth and the rest of my family for all their love, continued support, tireless encouragement and words of wisdom.

I would like to thank everyone in the Mata & Azevedo Groups for their valuable support during difficult times and tremendous input during our lab meetings. In some occasions I ended up spending more time in the lab than at home, inevitably some of these wonderful human beings became like family, and for that I could not be any more grateful.

I am indebted to Clara, Anna, Alessia, Gastón, Estelle, Elham and Ana Karen for their help in the lab, endless proofreading sessions and valuable discussions. I would like to thank Miss Soraya Padilla & Mr. Yamin Abdouni for their kind help in the lab and Mr. Miguel Quetzeri for his technical assistance on preparing this dissertation.

None of this would had been possible without the thoughtful support from my supervisors: Prof. Alvaro Mata and Dr. Helena S. Azevedo, from whom I was able to learn way more than just about biomedical materials and bioengineering, but also priceless life lessons on the value of hard work, attention to detail and how we should never forget about the human side of science and engineering research.

I want to express my endless appreciation for my friends Mauricio, Elías & Anthony, whose encouraging messages helped me through the hardest moments.

Finally, I would like to thank all the institutions that have contributed funding to the herein reported projects: The European Research Council (ERC) Starting Grant (STROFUNSCAFF), and specially the Government of the Republic of Costa Rica.

My deepest gratitute goes to the Program for Innovation and Human Capital (PINN) from the Ministry of Science, Technology, and Telecommunications (MICITT) of the Republic of Costa Rica (Contract MICITT-PINN-PED-014-2015-2), whose generous support covered my tuition fees and stipend during these lovely four years in London.

Contents

List of Abbreviations

1D	One-dimensional
^{1}H-NMR	Proton nuclear magnetic resonance
2D	Two-dimensional
3D	Three-dimensional
A	Alanine
AD	Adamantyl
Ada	Adamantane
βCD	β-Cyclodextrin
βCD-AuNPs	β-Cyclodextrin capped gold nanoparticles
BSA	Bovine serum albumin
BTA	Benzenetricarboxamide
$CaCl_2$	Calcium chloride
CB[5]	Cucurbit[5]uril
CB[6]	Cucurbit[6]uril
CB[7]	Cucurbit[7]uril
CB[8]	Cucurbit[8]uril
CB[n]	Cucurbit[n]uril
CCD	Charge-coupled device
CDs	Cyclodextrins
CD	Circular Dichroism
CLSM	Confocal laser scanning microscope
cpp	Critical packing parameter
CuAAC	Copper(I)-catalysed alkyne–azide cycloaddition
D	Aspartic acid
D_2O	Deuterium oxide
D_3COD	Deuterated methanol
DAPI	4’,6-Diamidino-2-phenylindole
DCM	Dichloromethane
DIC	N,N’-diisopropylcarbodiimide
DMEM	Dulbecco’s modified Eagle medium
DMF	N,N-Dimethylformamide
E	Glutamic acid
ELP	Elastin-like polypeptide
ESI-MS	Electrospray ionisation mass spectrometry
EthD-1	Ethidium homodimer-1
F	Phenylalanine
FBS	Fetal bovine serum
FC	Ferrocene
FITC	Fluorescein isothiocyanate
Fmoc	N-fluorenyl-methoxycarbonyl

G	Glycine
G’	Shear storage modulus
G”	Shear loss modulus
G*	Complex dynamic shear modulus
H	Histidine
HA	Hyaluronic acid
HBSS	Hank’s balanced salt solution
HEPES	4-(2-Hydroxyethyl)-1-piperazine -ethanesulfonic acid
HFIP	1,1,1,3,3,3-Hexafluoro-2-propanol
HOBT	1-Hydroxybenzotriazole
I	Isoleucine
ITC	Isothermal titration calorimetry
K	Lysine
K_D	Dissociation constant
K_{dim}	Dimerisation constant
K_{eq}	Equilibrium constant
L	Leucine
MALDI-TOF-MS	Matrix-assisted laser desorption/ionisation mass spectroscopy
MBHA	4-Methylbenzhydrylamine
MWCO	Molecular weight cut-off
NaOD	Sodium deuteroxide
NOESY	Nuclear Overhauser effect spectroscopy
ODNP	Overhauser Dynamic Nuclear Polarisation Relaxometry
P/S	Penicillin/Streptomycin
PA	Peptide amphiphile
PAM	Polyacrylamide
PDMS	Polydimethylsiloxane
PEG	Polyethylene glycol
PFA	Paraformaldehyde
PVA	Polyvinyl alcohol
R	Arginine
RP-HPLC	Reverse Phase High-Performance Liquid Chromatography

S	Serine
SAXS	Small angle X-rays scattering
SEM	Scanning electron microscopy
SSPS	Solid-state peptide synthesis
TEM	Transmission electron microscopy
TFA	Trifluoroacetic acid
TGA	Thermogravimetric analysis
TIS	Triisopropylsilane
Upy	2-Ureido-4-[1H]pyrimidone
UV	Ultraviolet
UV-Vis	Ultraviolet-Visible
V	Valine
W	Tryptophan

List of Figures

List of Tables

Part I

Introductory Section

Chapter 1

Opening Remarks

This chapter presents the motivation behind the herein described projects, provides the thesis statement as well as an outline on how this dissertation is organised.

1.1 Motivation

There is growing realisation about the role that the extracellular surroundings play in regulating cell responses.[1] Morphological, rheological and compositional hints can indeed have profound effects on cell behaviour and functions.[2,3]

Even though standard cell culture materials (glass and polystyrene in tissue culture plastic for example) have provided cell and molecular biology studies with valuable information on cell function and response, these materials exhibit unphysiologically high stiffness and notable lack of structural complexity, thus promoting flattened cell shape, deviant polarisation, unrealistic response to drugs, among other abnormal behaviours.[4] Some studies even indicate that cells retain memory of past mechanical environments.[5]

Cell culture systems able to recapitulate native cellular environments are required as alternatives to conventional cultures as more biological studies and bioengineering applications demand more complex in vivo milieus. In this regard, hydrogels have emerged as very promising alternatives to develop cell culture alternatives, as hydrogels mimic the high water content and mechanical properties that match soft tissues of the native extracellular matrix (ECM).[6]

Hydrogels are considered water-swollen polymer networks formed through the crosslinking (either covalent or non-covalent) of hydrophilic polymer chains,[7] their entangled polymer network provides a simple biomimetic 3D environment, useful for either tissue production by seeded cells or for positioning of these cells for in vivo delivery. Even though hydrogels based on naturally ocurring biomolecules like collagen and assortments of ECM proteins (such as Matrigel[8]) are routinely used by biologists, these often exhibit enormous variability in composition and outcome results, calling their biological relevance into question.[9]

Luckily, there are many other hydrogel alternatives, and advances in the design and synthesis of on-demand sequence-controlled biomacromolecules together with non-natural synthesis routes have allowed for an impressive tool kit for the design of synthetic hydrogels with user-defined properties (Figure 1.1).[10]

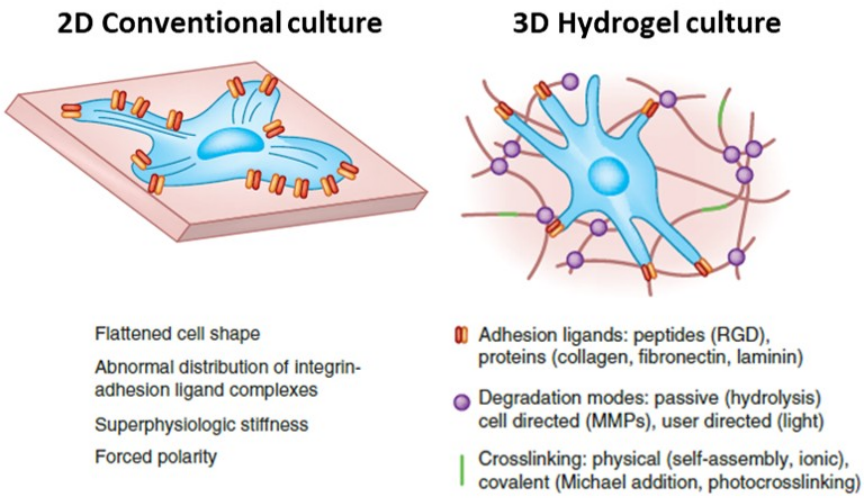

Figure 1.1: *Advantages of hydrogel cell culture technologies. Conventional 2D culture on superphysiologically stiff substrates versus 3D hydrogels that can be engineered to present a more realistic microenvironment to cells [Adapted from Caliari et al.[4]].*

Given their ubiquity in nature, their biodegradability and ease of synthesis, peptide-based hydrogels have arise as promising candidates. The most common method to fabricate peptide-based hydrogels relies on molecular self-assembly of peptide units into well defined supramolecular nanostructures.[11,12,13]

Polypeptide-based hydrogels are particularly useful in cell culture applications, given the control they offer over their assemblies, leading to tunable properties that can be modulated to emulate those exhibited by covalent polymers, not to mention the possibility to assembly into hierarchical length-variable structures. Peptide Amphiphiles (PAs) represent a particular self-assembling peptide family based on lipidated short peptides that actually exhibits all of the just mentioned characteristics.

PAs excel at recapitulating aspects of native ECMs, can assemble in modular ratiometric fashions, and their molecular structure can be altered via rather simple covalent modifications, thus allowing for a myriad of studies on how to tune the fine array of intermolecular forces that give raise to their functionality as in vitro cell culture scaffolds and in vivo regenerative materials.

There is a plentiful collection of intermolecular forces guiding PA molecular self-assembly,[14] ranging from dispersive hydrophobic interactions, to intrafiber hydrogen bonding, metal - ion electrostatic forces and hydrogen bonding phenomena involving water molecules captured from the solvent bulk.[15,16]

In spite of this, the full potential of PA nanofibers has not been fully exploited as interactions based on high affinity, molecular recognition and selectivity remain yet to be either fully understood[17] or unexploited.

Even though PA hydrogels are conventionally formed via electrostatic screening, more sophisticated and dynamic hydrogelation mechanisms might help to improve their design and application. **The motivation for the research presented in this thesis stems from the desire to enhance structural, mechanical and stability aspects of self-assembling PA-based hydrogels**.

Self-assembled PA nanofibers have traditionally been seen as mere static epitope presenters to cells cultured atop or encapsulated in the hydrogels. Therefore, approaches that turn these nanofibers into more dynamic entities are very much required, this will allow PA hydrogels to improve matching the complexity and dynamics of native tissues and will boost advancements that will add up to the reduced number of reports on PA hierarchical structuring[18,19] and spatiotemporal dynamics,[20] consequently, tackling challenges associated to increasing biological complexity in biomedically relevant systems.[4]

1.2 Thesis Statement

Based on the motivation, a concise research statement was formulated which will serve as the overarching aim of this thesis;

This doctoral thesis concentrates on the systematic study of integrating host-guest interactions into peptide amphiphile-based materials. This attempts to increase our current toolbox of interactions useful in the molecular design of self-assembled supramolecular biomaterials. Combining dynamic host-guest molecular recognition motifs with the valuable structural features of peptide amphiphiles will allow to augment their capacities to emulate dynamic spatiotemporal and hierarchical complexity aspects of native extracellular matrixes.

This work presents interdisciplinary research projects between materials and organic synthesis, supramolecular chemistry, peptide biophysics and cell biology. The aim and objectives of this thesis are presented in Sections 3.1 & 3.2 right after the literature review that helped to refine them.

1.3 Thesis Outline

This thesis has been structured in seven chapters and one appendix. Chapter 1 opens Section I presenting the motivation for the studies, presents the thesis statement, and closes presenting the current outline on how the dissertation is structured. Chapter 2 presents a literature review on the principles of supramolecular self-assembly, self-assembling hydrogels and self-assembling peptides, focusing especially on the peptide amphiphiles (PAs) family. Chapter 3, provides the thesis aim and objectives.

Chapter 4 opens Section II and is the first out of three experimental chapters. It presents the outcome result of derivatising cationic PA molecules with host-guest cues enabling the formation of Adamantane/β-cyclodextrin (**Ada/βCD**) anchoring points between self-assembled nanofibers, addressing the main focus of the thesis; originating mechanically tunable hydrogels, with increased stability and suitable for cell culture. The characterisation of the molecules is provided, followed by spectroscopic, morphological, mechanical and biological investigations on the resulting non-covalently cross-linked PA hydrogels.

Chapter 5 takes advantage of the **Ada/βCD** host-guest phenomena detailed in Chapter 4 in order to promote non-covalent display of cell adhesion epitopes at the surface of negatively charged self-assembled PA nanofibers. In the first section of the chapter the molecular design of the system is discussed, followed by the corresponding supramolecular aggregation studies. Also details on the resulting hydrogels' characterisation and cell culture studies that show the functionality of the approach to promote cell attachment are provided.

Section III focuses on a different family of host-guest interactions: the one based on cucurbit[n]urils, **CB[8]** to be precise. Chapter 6 is the last experimental chapter and describes the development of dynamically cross-linked PA hydrogels based on an unreported strategy to generate PA hydrogels based on the formation of a host-guest homoternary complex with **CB[8]** and aromatic amino acid-bearing PA nanofibers. This novel host-guest PA gelation approach is presented as an alternative to ion-screening-based PA hydrogels, to which a structural and rheological comparison is presented along the chapter, closing with preliminary cell viability assays.

Chapter 7 is included in Section IV as it provides a summary of the research work, perspectives and future directions, as well as a discussion on the significance of the work in relation to published studies. Lastly, Appendix A supports the dissertation by presenting all published material during the development of the experimental studies (publications, collaborations and book chapter) and provides a list of all conference presentations concerning this thesis. Figure 1.2 aims to illustrate the interconnections between the above described thesis chapters and contents.

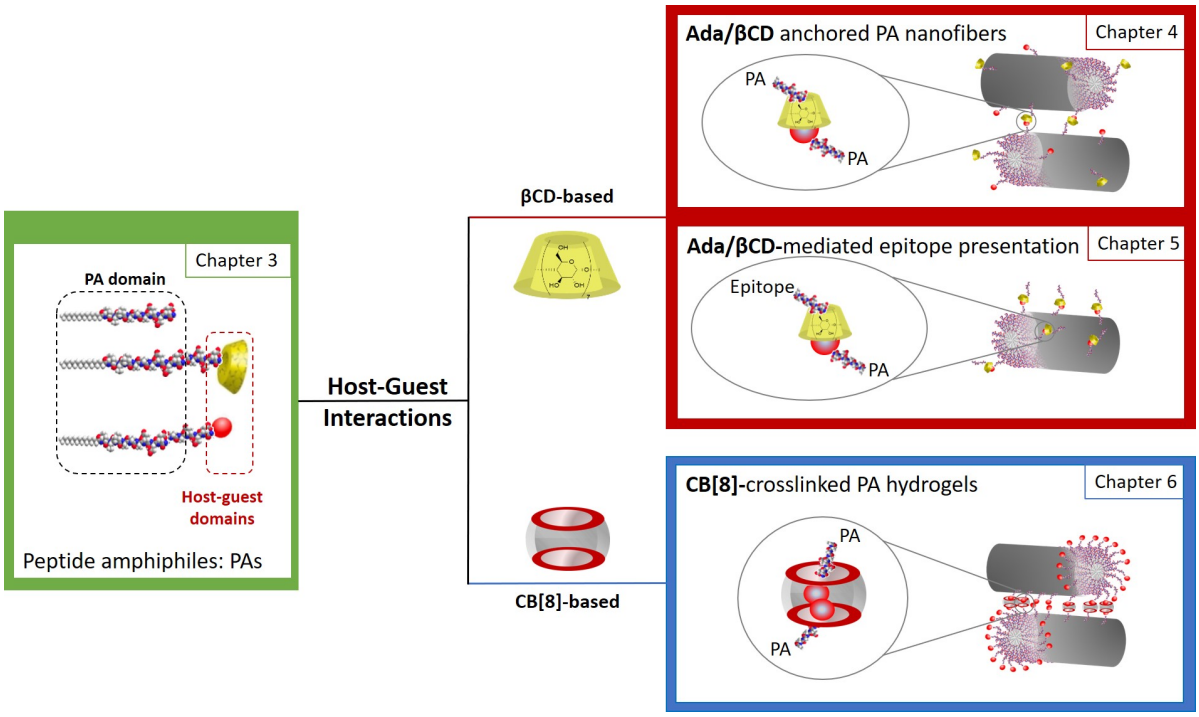

Figure 1.2: *Schematics illustrating the thesis chapter structure.*

Chapter 2

Literature Review

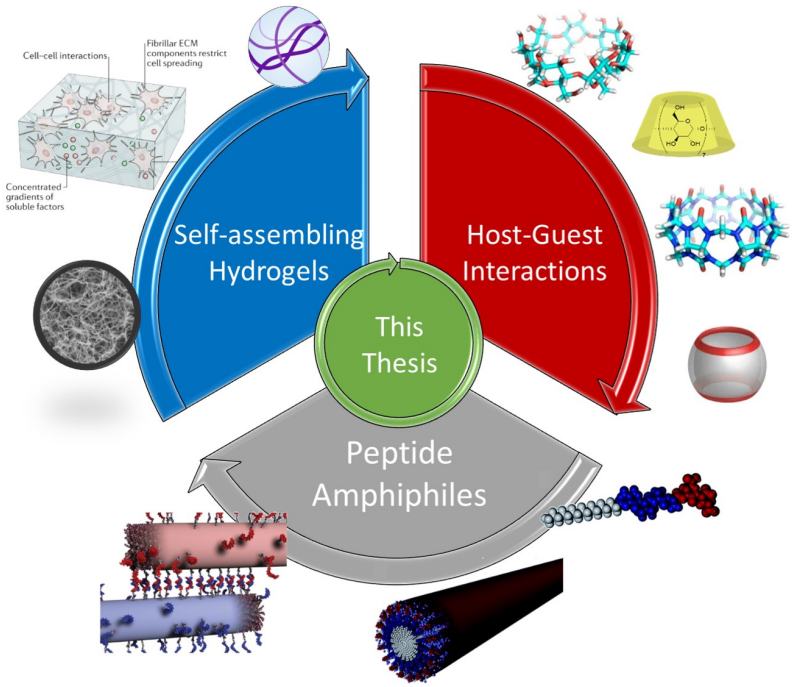

Figure 2.1: *Schematics showing integration of the three main topics of this thesis.*

This chapter presents a literature review on the principles of molecular self-assembly, self-assembling peptides, host-guest interactions and how this dissertation pursues to integrate these concepts into new families of self-assembling hydrogels.

Selected sections of this chapter have been published in:

- Okesola, B. O.; **Redondo-Gómez, C.**; Mata, A. Multicomponent Self-Assembly: Supramolecular Design of Complex Hydrogels for Biomedical Applications. In *Self-assembling Biomaterials: Molecular Design, Characterization and Application in Biology and Medicine*; Azevedo, H. S., da Silva, R. M. P., Eds.; Elsevier Ltd.: **2018**; pp 371-397.[21]

2.1 Molecular Self-assembly

The past three decades have witnessed a true revolution when it comes to think of the way matter (including living organisms) gets organised and reaches high structural and functional complexity levels. Much of this has been enabled by the pioneering works of Charles Pedersen, Donald J. Cram and Jean-Marie Lehn on the “development and use of molecules with structure-specific interactions of high selectivity”, that were jointly recognised with the Nobel Prize in Chemistry in 1987 for laying out the foundations for supramolecular chemistry as we know it today. Lehn, in particular, broadened the perspective in the following years with his vision of "chemistry beyond the molecule" towards the self- assembly of various structures.[22]

Supramolecular chemistry has developed as “the chemistry of the entities generated by intermolecular non-covalent interactions”[23] and has rapidly evolved into the chemistry of molecular information, i.e. one involving the storage of information in the particular array of atoms in a molecule. Molecular structure ultimately determines its interaction with other entities through defined sequential algorithms based on patterns we now call non-covalent interactions (hydrophobic, aromatic, dipole-dipole, ion-dipole, and ion-ion interactions, van der Waals forces, hydrogen bonds, metal-ligand coordination sites, host-guest complexations, among others).[24]

Self-assembling systems undergo autonomous organisation via interaction of multiple smaller components into larger well-defined structures.[25] This definition does not restrict the size of the objects undergoing self-organisation, thus having control over structural features ultimately determines interactions and control over higher organisation levels. In the case of molecular self-assembly it is actually molecules (or parts of them) than undergo spontaneous formation of ordered aggregates with no human intervention.[26]

Evolution of molecular self-assemblies relies on two processes: molecular recognition and self-organisation. Molecular recognition is based on molecular pre-organisation and design, and carries out information storage and processing. Meanwhile self-organisation involves the initiation, growth and termination of the assemblies through sequential binding of multiple components in the correct disposition.[23]

2.1.1 Molecular Fabrication

A deeper understanding of the processes dictating molecular self-assembly, i.e. molecular recognition and self-organisation, has originated molecular structures with controlled chemical complementarity and structural compatibility, and has opened the possibility to imprint materials with control over their molecular composition and arrangement, thus allowing exciting possibilities for molecular and nanofabrication based on the noncovalent interactions that bind building blocks together during self-assembly.[27]

Using natural processes as a guide, substantial advances have been achieved at the interface of nanomaterials and biology allowing development of new biomaterials that can undergo self-assembly into well-ordered structures at the nanometer scale.[27] Molecular recognition and self-organisation principles from self-assembly do govern structure and function in biologically relevant scenarios, from DNA replication, to vesicle formation, transport of solutes, protein synthesis, just to name a few.[28] There is also a number of naturally occurring self-assembling biomolecules like amyloid fibrils, actin filaments, and microtubules[29] where to borrow inspiration from in order to tailor stimuli responsiveness, adaptation, recognition, transport, and catalysis phenomena in materials and biomaterials.[30]

Using these principles based on the rational design of non-covalent molecular recognition motifs has led to obtaining a myriad of molecularly fabricated materials and has also offered exciting opportunities to develop new generations of smarter biomaterials.[31]

2.2 Supramolecular Biomaterials

Exploration of the principles of molecular self-assembly has led to the deliberate manipulation of intermolecular interactions, allowing for new generations of autonomous, dynamic, adaptive and “smarter” biomaterials, whose constituents are linked through reversible associations and may undergo assembly and de-assembly processes in specific conditions.[25]

Supramolecular biomaterials are often composed of constitutionally dynamic supramolecular polymers. This term often evokes immediate analogy to their classical covalent counterparts. Covalent polymers are mechanically and chemically robust, while most supramolecular polymers are much weaker in many cases. This apparent lack of robustness has oriented supramolecular polymeric materials towards applications where tough mechanical and chemical stability are not necessarily required.[29]

The lability and reversibility of these associations allow for growing, shortening or reconstitution of their nano and meso-structures in response to stimuli. This spontaneous but controlled generation of well-defined, functional supramolecular nanostructures through self-organisation allows a very powerful alternative to biomaterials nanofabrication,[23] while the self-assembled nature of supramolecular biomaterials confers unmatched processing, processing, recyclability, self-healing, stimuli responsiveness, and evolvable properties by association/growth/dissociation sequential events that covalent polymers can rarely achieve.[26]

The specific benefits of supramolecular biomaterials emerge from the nature of the dynamic non-covalent interactions that hold them together, which confer control over properties in a reversible, highly tunable, dynamic and modular fashion, allowing in many cases a good biomimetic recapitulation of native biological structural cues (Figure 2.2.a).[31]

Based on their supramolecular formation mechanisms, supramolecular biomaterials have been traditionally split into two categories (Figure 2.2.B):

I. **Supramolecular chain extension and/or crosslinking biomaterials**: Where small olygomer units are chain extended or large polymer units are cross-linked via supramolecular recognition motifs. These will be discussed in Section 2.2.1.

II. **Supramolecular stacking biomaterials**: Prepared from high-aspect-ratio 1D assemblies of molecular stacking motifs. These will be discussed in Section 2.2.2.

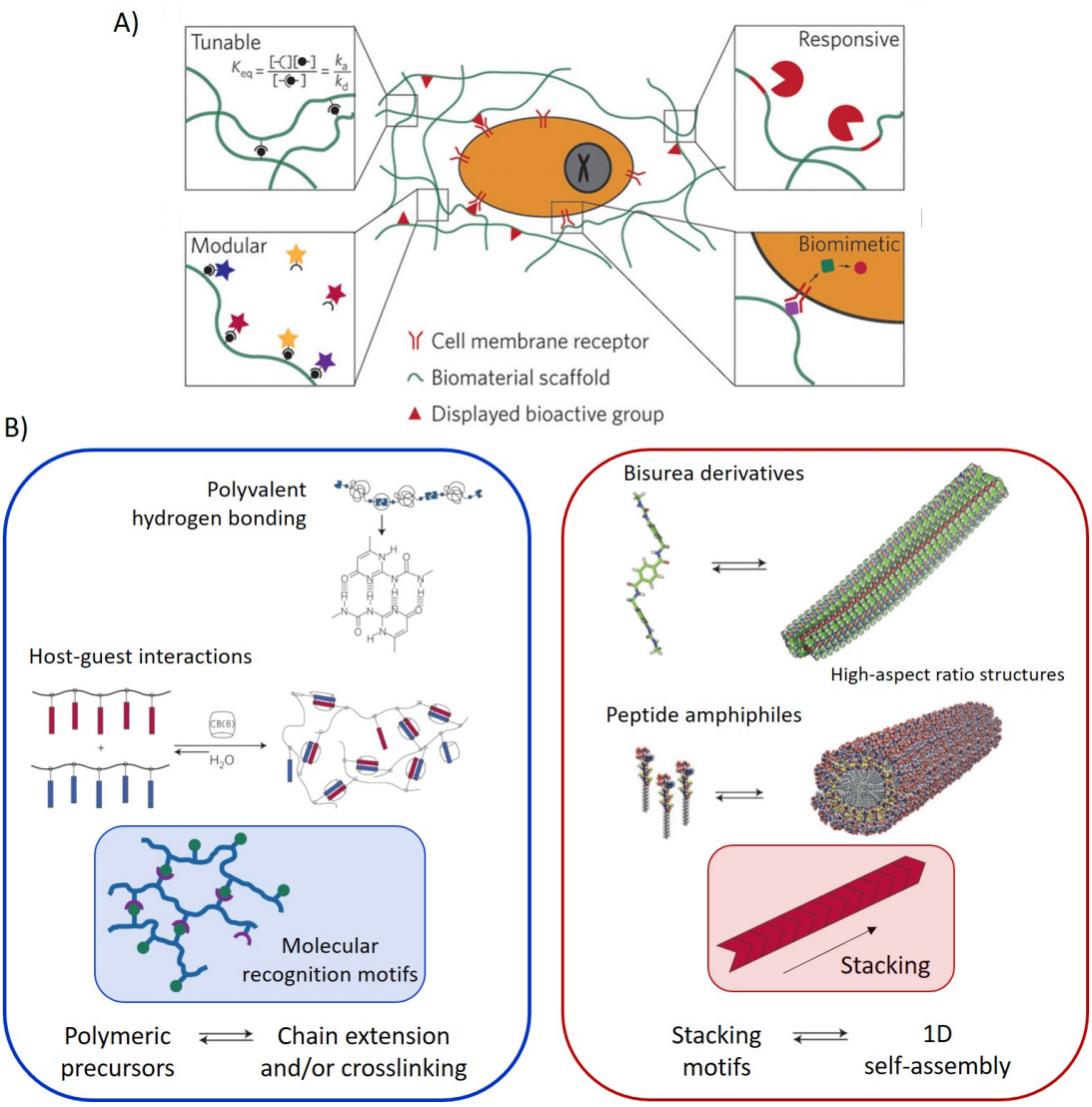

Figure 2.2: *Design of supramolecular biomaterials. A) Specific benefits of supramolecular biomaterials. B) Classification of supramolecular biomaterials created i) through engineered molecular recognition motifs for the crosslinking of polymeric precursors and ii) through the assembly of molecular stacking motifs [Adapted from Webber et al.[31]].*

2.2.1 Supramolecular Chain Extension or Crosslinking

These biomaterials are based on covalent macromers (oligomer or polymer units) that have been appended with motifs able to undergo molecular self-complementary (X:X) or complementary (X:Y) recognition processes. When these motifs are conjugated to the ends of polymer chains, their association leads to supramolecular chain extension. On the other hand, when these motifs are pendant from a polymer chain their association leads to supramolecular crosslinking and network formation.[31] These systems include polymeric chains crosslinked through directional and reversible noncovalent interactions whose environmental responsiveness, viscoelasticity, and cargo release can be engineered as a function of the polymeric architecture and thermodynamic and kinetic parameters of association.[32]

The degree of association of these materials is dictated by their concentration and thermodynamic equilibrium constant, meanwhile their dynamic nature is dictated by their binding kinetics.[31] The motifs used in this type of biomaterials fall into three main families:

- Polyvalent hydrogen-bonding units: Including the ureido-pyrimidinone (2-ureido-4-[1H]pyrimidone, UPy) motif, a quadruple hydrogen-bonding motif able to exhibit X:X self-complementarity (K_{dim} = 6×10^7 M^{-1}) and X:Y complementary with other motifs like 2,7-diamido-1,8-napthyridine (K_{eq} = 5×10^6 M^{-1}). Polyvalent hydrogen bonding-forming motifs include also DNA-inspired units like guanisines,[33] as well as stacking units of bisureas,[34] and benzenetricarboxamides (BTAs) systems.[35]

- Metal–ligand binding pairs: Such as metal–terpyridine, histidine, imidazole or cathecol interactions, whereby two moieties of the same ligand motif are complexed through a single metal ion (X:Y:X), where Y includes Zn^{2+}, Fe^{2+} or Fe^{3+}, among other cations. Even though this platform has been the least-explored, it offers great potential given the use of predictable and strong interactions with biologically relevant metal ion species.[36]

- Host-Guest binding motifs: Macrocyclic host–guest interactions represent one of the most recognizable motifs in supramolecular chemistry. The non-covalent interaction between host molecules like cyclodextrins or cucurbit[n]urils and small hydrophobic guest molecules has also been used as a recognition motif in order to crosslink polymeric precursors and to prepare supramolecular biomaterials.[31] This particular platform will be further extensively discussed in Section 2.5.

2.2.2 Supramolecular Stacking

It was Jean-Marie Lehn himself who introduced the concept of supramolecular polymerisation in 1990 by using molecular recognition events based on complementary triple hydrogen bonding between ditopic diacylaminopyridines and ditopic uracil derivatives to generate the first supramolecular main- chain polymer.[37] The assembly of small molecules (0D objects) typically relies on either facial or lateral aggregation of molecular components and leads to the formation of high aspect-ratio 1D fibrillar structures that account for the supramolecular polymer structure.[38] Preparation of these supramolecular stacks can be controlled either kinetically or thermodynamically, often finding kinetically trapped aggregates — i.e. aggregates that exist in a local free-energy minimum that happens to be highly dependent on the aggregation pathway.[39,40]

Since the report of the first self-assembling peptide by Zhang and collaborators in 1993 (AEAEAKAKAEAEAKAK, known as EAK16)[41] the platform of self-assembling peptides has been greatly expanded and has produced several seminal works in the field of supramolecular biomaterials.[42]

The peptide motifs used in this type of stacking biomaterials fall into the following four main families (Figure 2.3):[43,44,28]

- β-Sheet forming peptides: peptide-based stacks self-assemble by forming β-sheet-like hydrogen bonding networks parallel to the filamentous one-dimensional assemblies axis.[31] Several peptide families belong in this category, including self-complementary oligopeptides like RAD16 and EAK16,[41] glutamine rich peptides like P11,[45,46] surfactant-like peptides,[47] multidomain peptides[48] and β-hairpin peptides.[49]

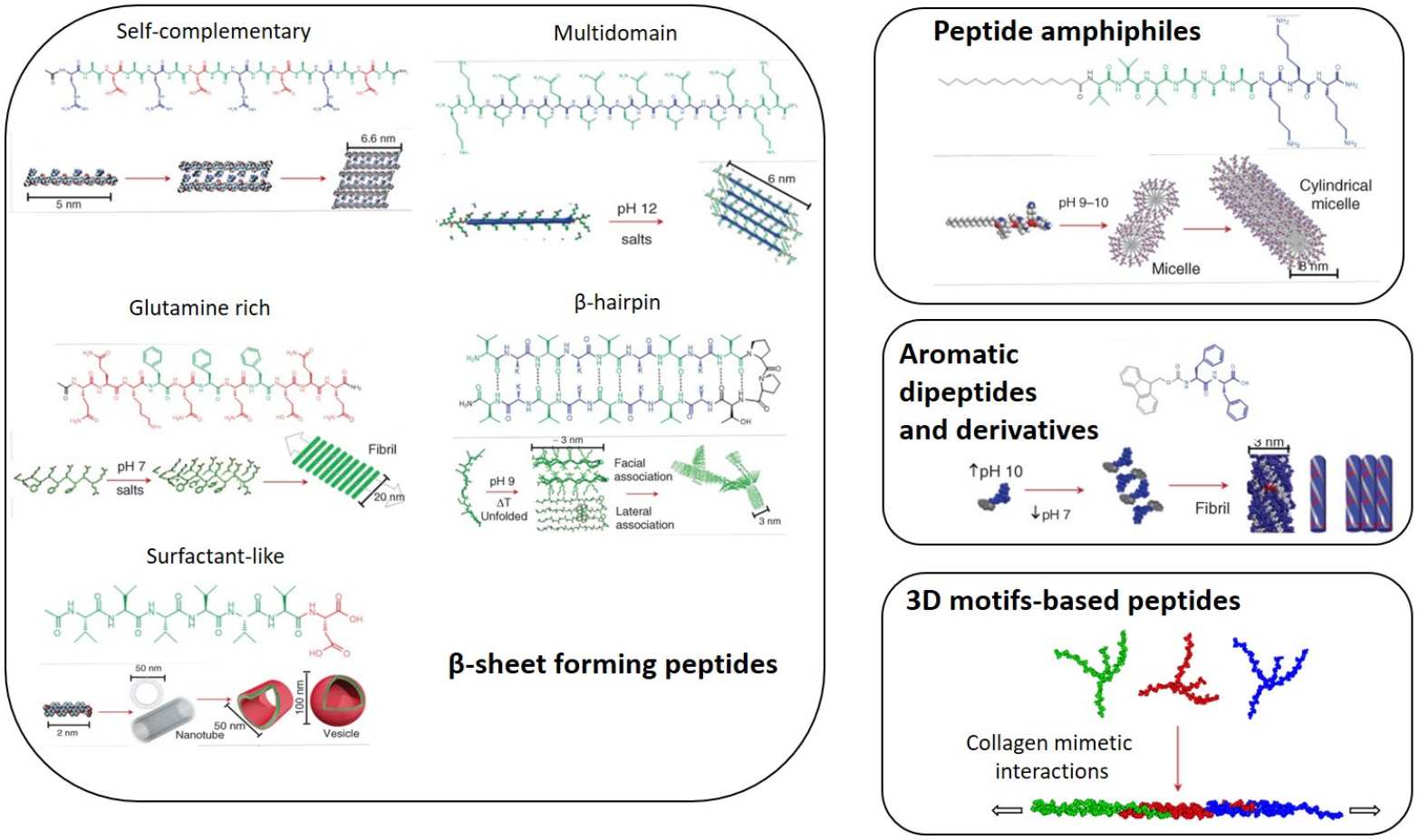

Figure 2.3: *Families of self-assembling peptides [Adapted from Mendes et al.[28]].*

- Three-dimensional motifs-based peptides: based on triple-helical collagen-mimetic interactions[50] and coiled-coil or leucine-zipper interactions.[51]

- Aromatic dipeptides and derivatives: including diphenylalanine (FF-OH)[13,52] and peptides hybridised with aromatic non-peptidic structural moieties, such as aromatic units like: N-fluorenyl-methoxycarbonyl (Fmoc), naphtyl, azobenzyl, and pyrenyl groups.[53] The presence of aromatic moieties incorporates additional driving forces for the peptide stacking through aromatic interactions.[54,12]

- Peptide amphiphiles (PAs): oligopeptides hydridised with long alkyl chains that incorporate additional hydrophobic driving forces for stacking formation.[55,56] PAs will be discussed in detail in Section 2.4.

Other semi-synthetic self-assembling derivatives undergo supramolecular stacking, including biogenic molecules like bile salts derivatives[57] and other lipidic amphiphiles whose self-assembling design principles remain yet elusive.[58] In any case, the assembly of small-molecule-stacking motifs is primarily dictated by their molecular structure, and their resulting supramolecular structures can be partially described by the balance between attractive and repulsive intermolecular forces, as it also obeys principles dictated by molecular packing theory.[31]

The "critical packing parameter" or "cpp" provides a rationale for the relation between a particular molecular shape and its resulting aggregate morphology.[59] In the case of surfactant molecules a particular value of the cpp can be translated into specific shape and size for a resulting equilibrium aggregate.[60] In this case cpp can be defined as:

$$cpp = \frac{v}{l_c a_s} \tag{2.1}$$

where v and l_c are the volume and extended length of the hydrophobic alkyl chain and a_s is the optimum interfacial area occupied by an amphiphilic molecule at the aggregate–water interface.[61] Increasingly repulsive intermolecular forces induce an increase in a_s and l_c, henceforth a decrease in cpp is observed.

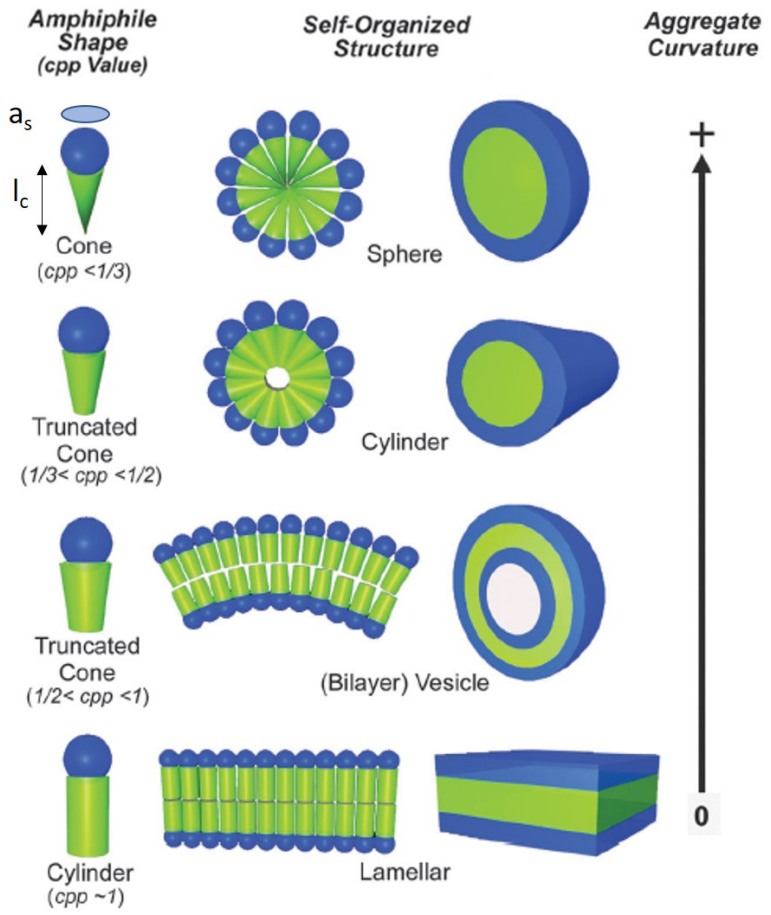

Figure 2.4: *Relation between critical packing parameter of amphiphilic mole-cules and their preferred supramolecular aggregates [Modified from Ramathan et al.[61]].*

Molecular packing factors indicate that wedge-shaped molecules are likely to form cylindrical supramolecular stacks (1/3 < cpp < 1/2).[59] These considerations will prove even more useful when discussing the molecular design of peptide amphiphiles and their supramolecular stacking in Section 2.4.1. In any case, one-dimensional self-assembled nanostructures can further entangle to form hydrogels, yet the interactions that give rise to hydrogel formation are not usually originated by preorganised molecular recognition motifs, but pH changes, the addition of enzymes, or multivalent cations that form salt bridges can originate fibre bundling.[31] Furthermore, bundle length, stiffness and crosslinking between fibres produces a solid-like 3D network that entraps water and determine the mechanical properties of the resulting hydrogels.[21]

2.3 Hydrogels

Hydrogels are a fascinating class of 3D networks formed by hydrophilic polymer chains embedded in a water-rich environment.[62] Hydrogels based on natural components like collagen, fibrin, alginate, hyaluronic acid or synthetic polymers like polyacrylamide (PAM), polyethylene glycol (PEG) or polyvinyl alcohol (PVA) are routinely used for 3D cell culture.[4] In the case of protein-based hydrogels like collagen and fibrin high composition variability is observed as in other ECM-derived proteins. By contrast, synthetic polymer hydrogels fail to mimic the fibrous architecture of the native ECM.[63,64]

Supramolecular hydrogels based on stacking motifs (Section 2.2.2) are a sub-class of man-made fibrillar hydrogels that overcome these obstacles, by benefiting from the precision and control that drives their self-assembly and by exhibiting controllable and reproducible filamentous architectures as those from native ECMs.[63] Supramolecular hydrogels have emerged as promising alternatives to develop cell culture scaffolds for tissue engineering applications,[6] given their capacity to mimic aspects of the ECM by providing cells with structural support and biochemical cues to direct their growth and phenotype.[63]

2.3.1 Hydrogels and the Extracellular Matrix

In fact, ECMs in vivo are made of hydrogel-like networks of fibrous proteins like elastin, laminin, fibronectin, and collagens, all embedded in a matrix of complex proteoglycans (like agregans and syndecans) and glucosaminoglycans (for instance, chondroitin sulfate and hyaluronan) in which cells reside in all tissues and organs.[65] Native ECMs are highly dynamic structural networks and continuously undergo remodeling and reconfiguration of their biochemical cues, present high water content, and are permeable to gases, waste and nutrients.[63,66]

Changes in composition in ECM fibres dictate the properties of the surrounding cell and tissue environment.[65] For instance, unbalances in elastin fibres (responsible for the elasticity of tissues) and collagen fibres (considerably less extensible than elastin) can compromise tissue function as in age-related skin wrinkling or stiffening of arteries, tumour stroma formation among others.[67]

Other aspects of native ECMs is the structure, dimensions and arrangement of fibers, for instance, the organization of collagen fibrils is largely responsible for transparency and refraction of cornea, lens and vitreous body,[68] while excessive deposition of collagen occurs during fibrosis and tumour stroma formation.[63] Fibre alignment occurs in many tissues, like the cornea, the myocardium, skin, and produces an anisotropic environment for cell migration, proliferation and differentiation.

2.3.2 Self-assembling Hydrogels

Self-assembling hydrogels remain one of the most appealing material candidates for biomedical applications owing to their high water content, high porosity for oxygen and nutrient permeability, biocompatibility, biodegradability, tunable stiffness, and responsiveness and reversibility to environmental stimuli.[69,70,71,72]

Conventional polymeric hydrogels are composed of either synthetic or biological macromolecules, crosslinking of these macromer units can be of either covalent or non-covalent nature.[73] Covalently crosslinked polymeric hydrogels are generally permanent, brittle, irreversible and with low cytocompatibility and are of little interest in biomedical applications. On the other hand, non-covalently crosslinked polymeric hydrogels are usually weaker, exhibit shear-thinning and self-healing behaviours, and are susceptible to external stimulation Figure 2.5.

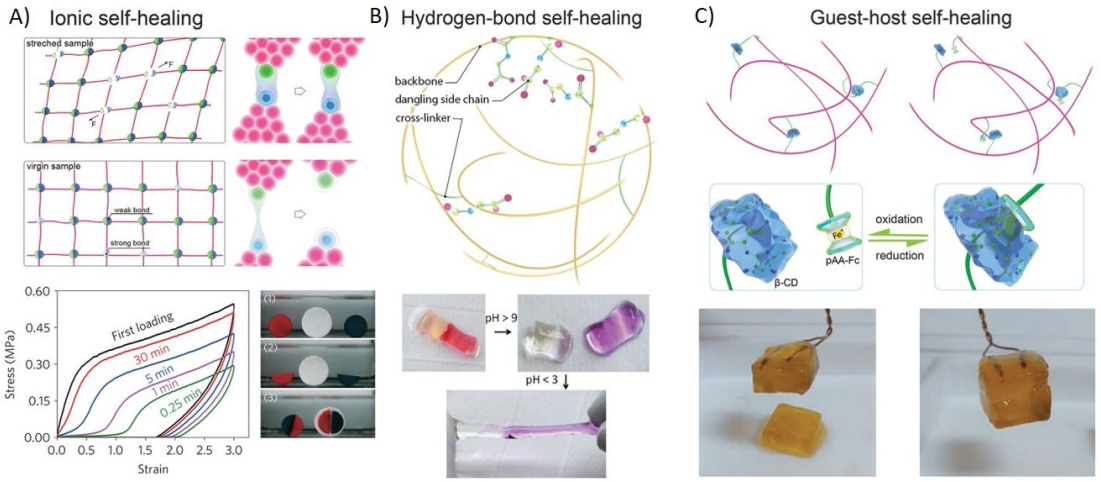

Figure 2.5: *Self-healing hydrogels based on ionic interactions, hydrogen bonds, and host-guest coupling.*
A) Ionic interactions in polyampholyte-based hydrogels (polymers bearing randomly dispersed cationic and anionic repeat groups). (Bottom left) Recovery of gels for different waiting times. (Bottom right) Self-healing between either two freshly cut surfaces (red and blue) or a fresh and an aged surface (white) of samples.[74]
B) Hydrogen bond-based self-healing in polyacryloyl-6-aminocaproic acid gels. (Bottom) The healed hydrogels at low pH separate after exposure to a high-pH solution (with pH > 9), and the separated hydrogels could reheal upon exposure to acidic solution (pH < 3).[75]
C) Host-guest coupling. (Bottom) The cut hydrogel spread with NaClO aqueous solution did not heal after 24 hours, but readhesion was observed 24 hours after spreading reduced glutathione aqueous solution onto the oxidized cut surface[76] *[Modified from Zhang and Khademhosseini.*[62]*].*

Supramolecular stacking of hydrogelators results in nanofibers or other mesoscale assemblies that are transient, often thermally reversible or easily respond to certain stimuli, their major limitation is their mechanical strength. Figure 2.6 compares other features of self-assembled hydrogels versus conventional polymeric hydrogels.[77]

Many formation mechanisms behind the self-assembly of hydrogelators share non-covalent, 3D, responsive, adaptative and dynamic characteristics of certain biological processes (for instance, the assembly/dis-assembly dynamics of cytoskeleton actin filaments and tubulin microtubules), thus making them easy to integrate into the dynamics that reconfigure the ECM or even mimic the cellular recognition events involved in native tissues.[63]

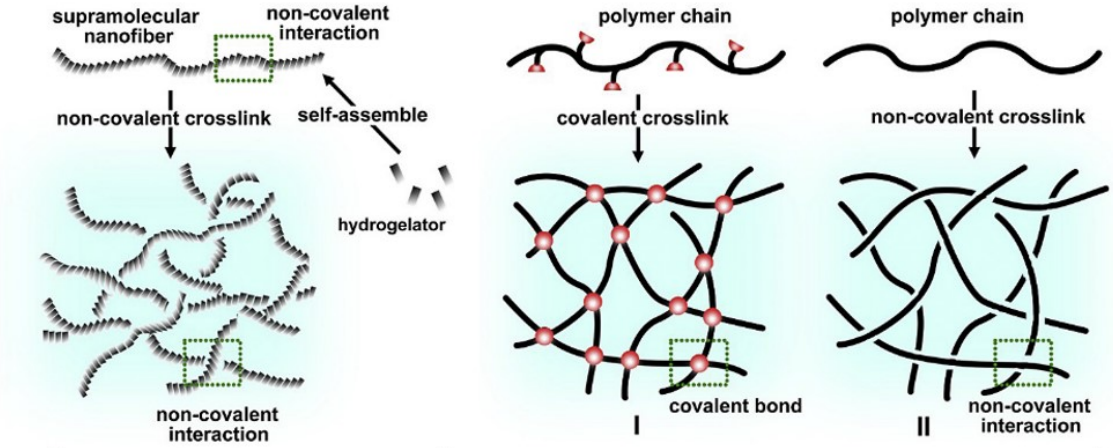

	Self-assembled hydrogels	Polymeric hydrogels	
		Covalent crosslink	Non-covalent crosslink
Mechanical strength	weak	extremely strong	relatively strong
Tunability	excellent	poor	good
Responsiveness to biological stimuli	excellent	poor	medium to excellent
Biocompatibility	excellent	not good	medium to excellent
Mimicry of extracellular matrices	good to excellent	poor	excellent
Reversibility	reversible	brittle and irreversible	less reversible
Degradation/clearance	excellent	poor	medium to excellent
Incorporation of multiple biological functionalities	excellent	poor	excellent

Figure 2.6: *Comparison between polymeric hydrogels and supramolecular hydrogels [Adapted from Zhou et al.[77]].*

Despite the widespread applications of supramolecular hydrogels (like drug delivery,[78] 3D cell culture,[79,80] tissue engineering[81]), the vast majority of reported hydrogels are homotypic, consisting of only one type of molecule. New approaches involving the use of multiple molecular components can significantly enhance the diversity of the resulting self-assembled hydrogels, thus avoiding limits on the emergence of complexity that homogeneity imposes Figure 2.7.[21]

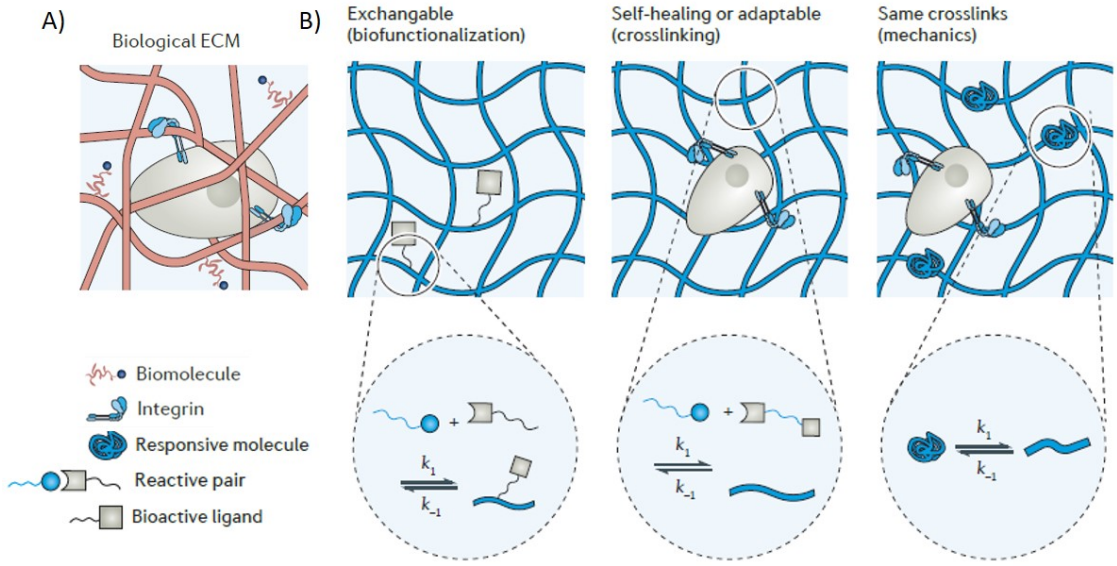

Figure 2.7: *Native ECM and mimicking synthetic strategies involving hydrogel reversible chemistries. A) Native ECM is a heterogeneous fibrillar network that can be emulated via B) Reversible chemistries for hydrogels, including dynamic presentation of cell signalling molecules (left panel), self-healing or adaptable crosslinks (middle panel) and strategies to alter the crosslinking density without changing the network connectivity (right panel) [Modified from Rosales et al.[82]].*

Recently, Eelkema and Pich have reviewed the properties of both supramolecular and macromolecular gelators,[83] reaching to the conclusion that -individually- both kinds of hydrogelators begins to show some principles and properties required to reach the level of biological hydrogels, and both hydrogel families have areas where they outperform the other, proposing that a merge of both supramolecular and macromolecular gels appears to be the optimal strategy to design "life-like adaptative hydrogels".

A hydrogel design strategy based on the coassembly of two or more components is a step forward toward unlocking the full potential of hydrogels in biomedical applications.[84] This approach, referred to as multicomponent coassembly, results in multicomponent or heterotypic hydrogels. In this kind of hydrogels complex morphologies can be more readily accessed as a result of "social" or "self-sorting" interactions between the building blocks, giving raise to different thermodynamically favoured morphologies.[21]

Using mixtures of components with different propensity to self-assemble is therefore a paramount design strategy for the bottom-up nanofabrication of complex multicomponent hydrogels.[21]

Following these principles, self-assembling hydrogels derived from natural building blocks have been prepared. Amino acids, peptides, nucleobases, mono and polysaccharides, as well as their derivatives have been incorporated into supramolecular hydrogels,[77] and their macroscopic morphologies have been engineered using additive manufacturing technologies as well.[85]

2.3.3 Characterisation of Hydrogels

Mechanical Properties of Hydrogels

Hydrogel stiffness (in fibrillar systems like those originated by supramolecular stacking) can be determined through tensile strength and toughness measurements,[63] but it is most commonly characterized by shear modulus (G) or their compressional Young's modulus (E), two values that are related to each other as a function of the material's Poisson's ratio (ν):[4]

$$E = 2G(1 + \nu) \tag{2.2}$$

Most hydrogels exhibit a Poisson's ratio of around 0.45 – 0.5, resulting in $E \approx 3G$.

Shear moduli determinations are usually carried out in a rheometer, particularly in a parallel plate or cone and plate test configuration in oscillatory mode.[86] The hydrogel is placed on the plate as shown in Figure 2.8.A and torque and angular displacement are monitored.[87]

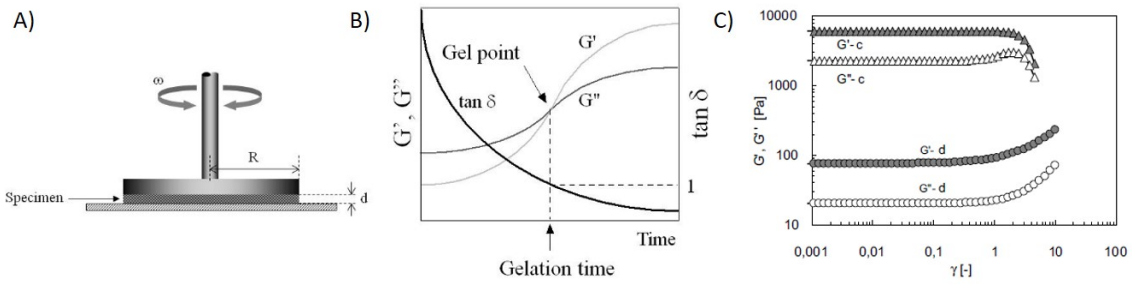

Figure 2.8: *Rheological characterisation of hydrogels. A) Schematic diagram of a controlled-stress rheometer in a parallel plate configuration. B) Schematic representation of dynamic viscoelastic properties of gelation system as a function of reaction time. C) Typical strain dependences of viscoelastic moduli: (c) agar gel, and (d) crosslinked poly(4-vinylpyridine) network [Modified from Murata[86] and Lapasin[88]].*

The complex dynamic shear modulus (G∗) can be expressed as a function of the shear storage modulus (G'), the shear loss modulus (G") and loss tangent (tan δ), defined as follows:[86,88]

$$|G*| = G' + i \cdot G'' \tag{2.3}$$

$$G' = |G*| \cdot cos(\delta) \tag{2.4}$$

$$G'' = |G*| \cdot sin(\delta) \tag{2.5}$$

$$tan(\delta) = \frac{G''}{G'} \tag{2.6}$$

where i = $\sqrt{-1}$, and δ is the phase angle between stress and strain. G' represents the elastic component of material behavior, whereas G" represents the viscous component of material behavior.[86] Contrary to viscous liquids, hydrogels are characterized by G' > G" over several decades of oscillatory shear frequency (Figure 2.8.B).[86] Hydrogels often exhibit viscoelastic properties, in which both storage and loss moduli do not significantly vary over a range of increasing shear strain or frequency (Figure 2.8.C), a range commonly denominated the "viscoelastic region".[87]

In covalently cross-linked polymeric gels (see Figure 2.6) covalent bonds constrain polymer chain mobility in the hydrogels, turning them into elastic spring-like structures that translate into largely elastic material properties,[82]

meaning that the gel strains linearly when a stress is applied only to linearly return to its original shape.[32] This implies that even if a cell exerts enough tension to the hydrogel, there is little chances for it to impart large structural rearrangements. In these gels the storage (elastic) modulus G' is much larger than the loss (viscous) modulus G", while their shear modulus (G$*$) is independent of the frequency or strain applied over a large range (Figure 2.9.A).

Non-covalently crosslinked and supramolecular hydrogels present mechanical properties more similar to the native ECM. Their dynamic physical linkages allow for hydrogel structure remodeling, allowing the gel to dissipate energy by rearranging its structure when a stress is applied. In these gels G" has a larger contribution to G$*$, and both G' and G" show stronger frequency dependency (Figure 2.9.B).

In the case of self-assembling hydrogels G' values can be described in terms of the size and concentration of the fibril building blocks "a" and C_A, as the hydrogel mesh size (ζ, defined as the average distance between constituent fibres) is dictated by:[63]

$$\zeta \approx \frac{1}{\sqrt{aC_A}} \tag{2.7}$$

and G' can be estimated as a function of hydrogel mesh size and the bending modulus of its constitutent filaments (κ):

$$G' \approx \frac{\kappa^2}{K_B T}\zeta^{-5} \tag{2.8}$$

that can be expressed as:

$$G' \approx \frac{\kappa^2}{K_B T}(aC_A)^{5/2} \tag{2.9}$$

K_B and T are the Boltzmann constant and temperature, respectively.[89]

Interestingly, G' of self-assembled hydrogels shows a stronger dependence on network density than polymeric hydrogels, where G' can be described as:[90]

$$G' \approx K_B T \zeta^{-3} \tag{2.10}$$

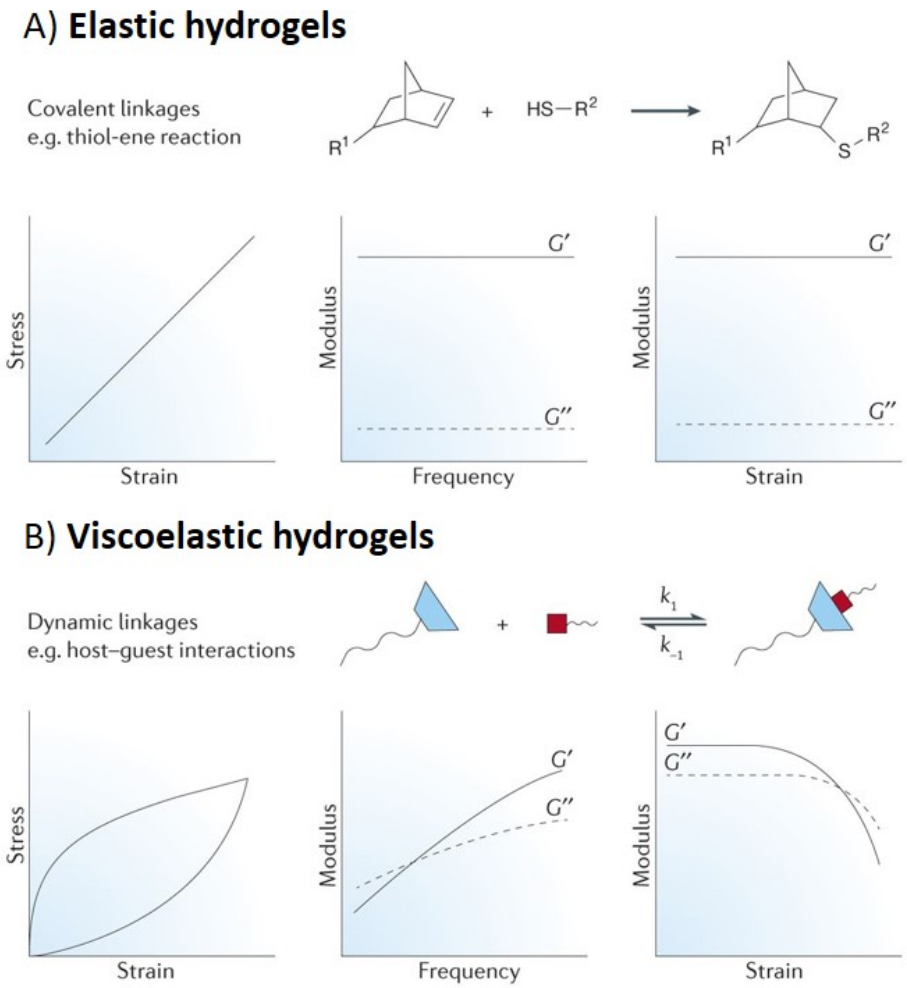

Figure 2.9: *Rheological differences in elastic and viscoelastic hydrogels. A) Elastic gels display a linear stress–strain curve for small deformations (left panel) and shear modulus is is frequency and strain independent (center and right panels). B) The dynamic linkages in viscoelastic gels impart a more liquid-like behaviour to the gel, showing hysteresis in their stress–strain curve (left panel), while the modulus displays frequency dependence (middle panel), and many of these gels show shear-thinning behaviour (the decrease in modulus upon the application of high strain; right panel) [Modified from Rosales et al.[82]].*

This scalling of G' with the concentration of building blocks shows relatively good agreement in self-assembled gels based on *β*-hairpin peptides[91] and peptide amphiphiles.[92] Tuning of hydrogels' stiffness by increasing filament stiffnes (*κ*) has been demonstrated in PA-based hydrogels, in which fiber rigidity can be tailored by supramolecular interactions;[93] increasing the strength of hydrogen bonding in the *β*-sheets increased stiffness values of the resulting hydrogels,[94] meanwhile introducing branched groups into the PA building blocks weakened intrafiber hydrogen bonds resulting in a decrease in G'.[93]

Supramolecular hydrogels often exhibit shear-thinning behaviour, i.e. a decrease in viscosity as a result of increasing shear strain.[86] When exposed to a shear stress, the hydrogels flow with very low viscosity, while the physical bonds between the building blocks restore their original rigidity upon the removal of the stress.[77] Shear-thinning is a rather desirable property for drug delivery and tissue engineering applications as it enables the injection of hydrogels as well as their extrusion during printing processes.[85]

Mass Transport Properties of Hydrogels

The molecular architecture of both polymeric and self-assembled hydrogels can give raise to tissue-like viscoelastic behaviour as well as diffusive transport and interstitial flow, allowing mass properties like the delivery of growth factors, drugs and nutrients as well as gas exchange, the removal of waste products and even cell migration throughout the gel network.[66]

Polymeric hydrogels typically exhibit mesh sizes in a range of $\sim 4 - 30$ nm, whereas self-assembled hydrogels present mesh size values in the order of microns,[63,87] thus self-assembled hydrogels are better materials in terms of mass transport phenomena than their polymeric counterparts.[66]

Hydraulic (also known as Darcy) permeability and probe diffusion coefficient determinations are employed to assess mass transport phenomena within the hydrogel matrix.[63] Permeability is a measure of the ability of water to flow through the hydrogel network under a constant pressure difference ΔP. Permeability coefficients (K) can be derived from Darcy's law as a function of the volumetric water flow rate (Q) through a specific length and cross-sectional area (L and A) and μ is the intrinsic viscosity of water at a specific temperature:

$$K = \frac{Q\mu L}{A\Delta P} \tag{2.11}$$

Polymeric hydrogels exhibit permeability coefficients up to 5 orders of magnitude smaller than self-assembled hydrogels.[63]

Diffusion coefficients of probe molecules within hydrogels provide an indication of the impact of the hydrogel network on the diffusion of solutes. Physical obstruction of the polymer chains control the solute movement in hydrogel network, producing an increased diffusional path length, in this fashion, diffusion coefficients usually increase with increasing pore sizes.[95]

Thorough characterisation of mass transport phenomena in self-assembled hydrogels still remains a challenge mostly due to the experimental challenges related to the hydrogels themselves, as well as the proper choice of probe and experimental method for its tracking.[63]

2.4 Peptide Amphiphiles

First reported in 2001 by the Stupp laboratory,[96] PAs represent a highly promising family of self-assembling stacking peptides able to form high-aspect ratio cylindrical nanofibers, these fibers originate hydrogels when charge density on the supramolecular assemblies surface is low.[97]

Almost two decades of research on PAs have produced hundreds of high quality papers, the goal of this section is rather to provide a general overview of their state of the art rather than a systematic presentation of findings of all these papers, for which the reader is kindly referred to excellent review papers.[98,55,97]

2.4.1 PA Molecular Design

PAs represent a straightforward implementation of the structure-shape concept.[31] PAs consist of a short peptide sequence often conjugated to a hydrophobic tail via their N-terminus (Region 1 in Figure 2.10.A), those three to five amino acids in the proximity of this tail often form β-sheets along the fiber axis (Region 2), while the residues farthest from the tail are charged to promote water solubility (Region 3) and in some cases contain a bioactive sequence (Region 4 in Figure 2.10.A-C).[97]

This careful combination of structural features confers PA monomers with an appropriate balance of repulsive and attractive interactions, affording wedge shapes and cpp values suitable for cylindrical micelle formation (see Section 2.2.2 & Figure 2.10.D).[59]

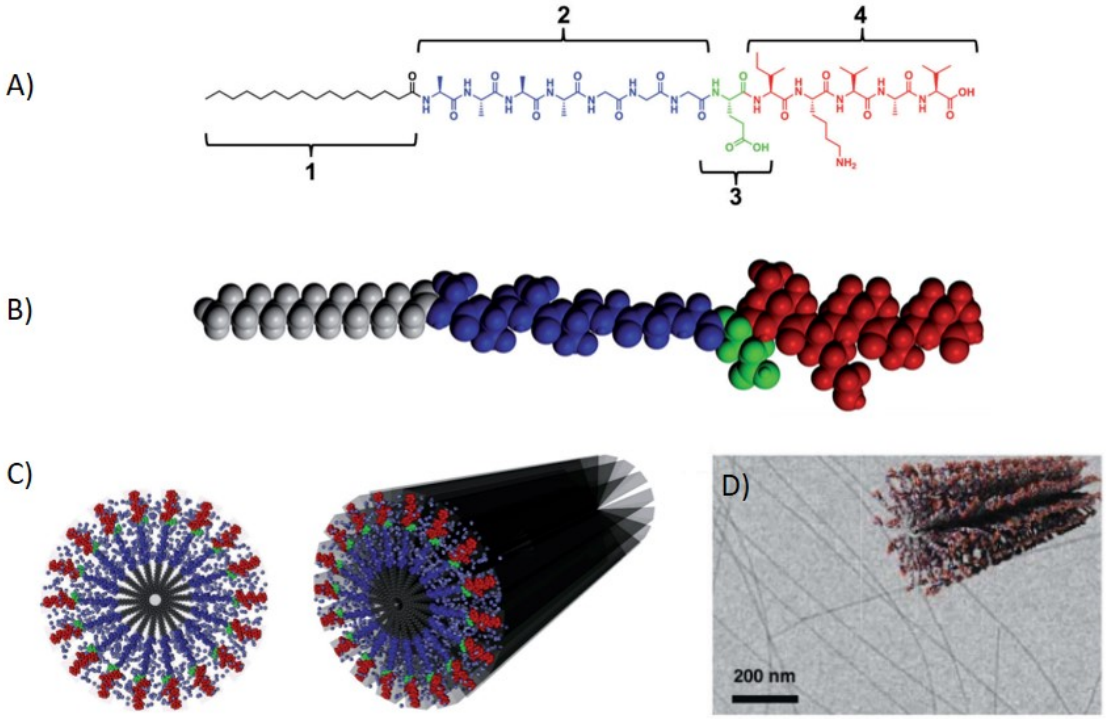

Figure 2.10: *A) Structure of a representative PA molecule with four rationally designed regions (see text for details). B) Schematics of the PA molecule from A) and C) its self-assembly into cylindrical nanofibers. D) Cryogenic Transmission Electron Micrograph (Cryo-TEM) image and a schematic illustration of sulfated PA forming nanofibers [Adapted from Webber et al.[55] and Sato et al.[97]].*

PA supramolecular polimerisation is kept going thanks to the careful balance of intermolecular forces held between PA monomers, hydrogen bonds play a particular role due to their directionality and versatility.[99,100] The strength of the noncovalent interaction between PA monomers in a supramolecular polymer implies that cooperative effects are required to observe large degrees of polimerisation, this implies that additional noncovalent forces must be implied in PA nanofiber formation.[99]

Supramolecular polimerisation degree depends on the concentration and affinity constant between monomers, supramolecular polimerisations tend to exhibit a large range of affinity constants, for instance the host-guest-mediated polimerisations reported by Huang et al. show affinity constants from 10^9 to 10^5 M^{-1}, while hydrogen bond-driven Upy systems show Ka values from 10^4

to 10^5.[99] PA affinity constant values for PA systems have not been yet systematically quantified, yet their value is expected to fall somewhere between this wide range as it depends on a number of factors like: ionic strength, PA concentration,[101] sample preparation protocol[102] among others.

Extensive work has been done on presenting diverse moieties at the surface of self-assembled PA nanofibers, including imaging contrast agents,[103] biotin-avidin motifs,[104] cyclic peptides,[105] sulfated sugars (Figure 2.10.D),[106] DNA strands[17] and bioactive peptide sequences found in ECM cell adhesion molecules, such as arginine-glycine-aspartic acid-serine (RGDS)[107] found in fibronectin, and isoleucine-lysine-valine-alanine-valine (IKVAV)[108] found in laminin.

2.4.2 PA Co-assembly

Co-assembly of two or more PAs offers a simple approach to modulate PA fiber structure[109,110] and biological function.[55] Despite the widespread applications of PAs in biomedicine, a reduced number of examples of co-assembled PA hydrogels have been reported. Electrostatically driven co-assembly has been demostrated as a strategy to produce co-asembled PA nanofibers made of two oppositely charged PAs simultaneously presenting the epitopes on their surface.[111]

The bioactivity, biocompatibility and tunability of PAs has motivated the systematic study on how cellular response is influenced by the spatial presentation of biological epitopes on nanofibers surface.[97,112] Co-assembling of a bioactive PA with a short and nonbioactive PA has been leveraged to enhance spacing of bioactive epitopes for optimal recognition of proteins or receptors as this diluent non-bioactive molecule facilitates the display of the epitope on the fiber surface.[113]

This strategy has been employed for spacing RGDS motifs along nanofibers and thereby maximizes cell adhesion to PA nanostructures.[114] Also, in a study by Sur et al. RGDS motifs have been systematically separated from PA nanofibers surface by one, three, or five glycine residues, finding the strongest effect on cell morphology in PAs with the longest spacer with a resulting strong adhesion between cells and substrate.[115]

2.4.3 PA Hierarchical Self-assembly

PA nanofibers have been shown to allign into monodomain viscoelastic strings over centimeters long as a result of a thermal annealing and their mechanical dragging into salty media (Figure 2.11.A) .[18] These noodle-shaped viscoelastic strings are highly bioactive and can actually dictate growth direction of neurites from neurons when formed with epitope-displaying PAs.[116] Studies of this nature have demonstrated the possibility to organise PA-based materials in a hierarchical fashion (Figure 2.11.B & C).

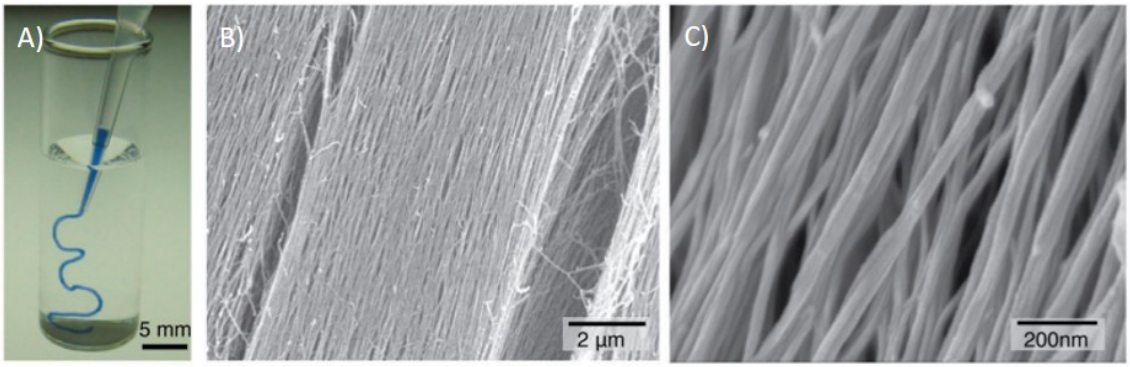

Figure 2.11: *PA viscoelastic string formation. A) A PA solution dyed with trypan blue extruded into a buffered saline solution after annealing. B,C) Scanning electron micrographs (SEM) images of aligned PA fibers within macroscopic strings made by dragging annealed PA solutions into salty media [Adapted from Zhang et al.[18]].*

Beyond their assembly into nanofibers and related nanostructures the strategy of coassembling PAs with supramolecular building blocks of significantly higher molecular weight has been harnessed to develop complex multicomponent hydrogels and particularly high-order PA architectures of biomedical interest,[98] not only for their morphological organization but also for their chemical gradients, hierarchical organisation, and dynamic properties such as self-healing.[21]

Two remarkable examples are herein presented, both systems are based on the interaction of positively charged PAs and either a negatively charged polysaccharide (hyaluronic acid (HA)) or polypeptide (elastin-like polypeptide (ELP)).

Stupp and coworkers reported the formation of a highly ordered membranous architecture arising at the liquid-liquid interface between a solution of a cationic PA (**K_3-PA**, see page 72) and another of high molecular weight hyaluronic acid (HA).[117] Upon contact, PA and HA molecules immediately assemble into a membrane driven by a dynamic synergy between osmotic pressure of ions and static self-assembly.[98] This membrane exhibits three well-defined regions including: (1) an amorphous region formed on the side of the membrane with HA, (2) a dense fibrous network, and (3) a region made from perpendicular fibers growing toward the PA side (Figure 2.12.E).

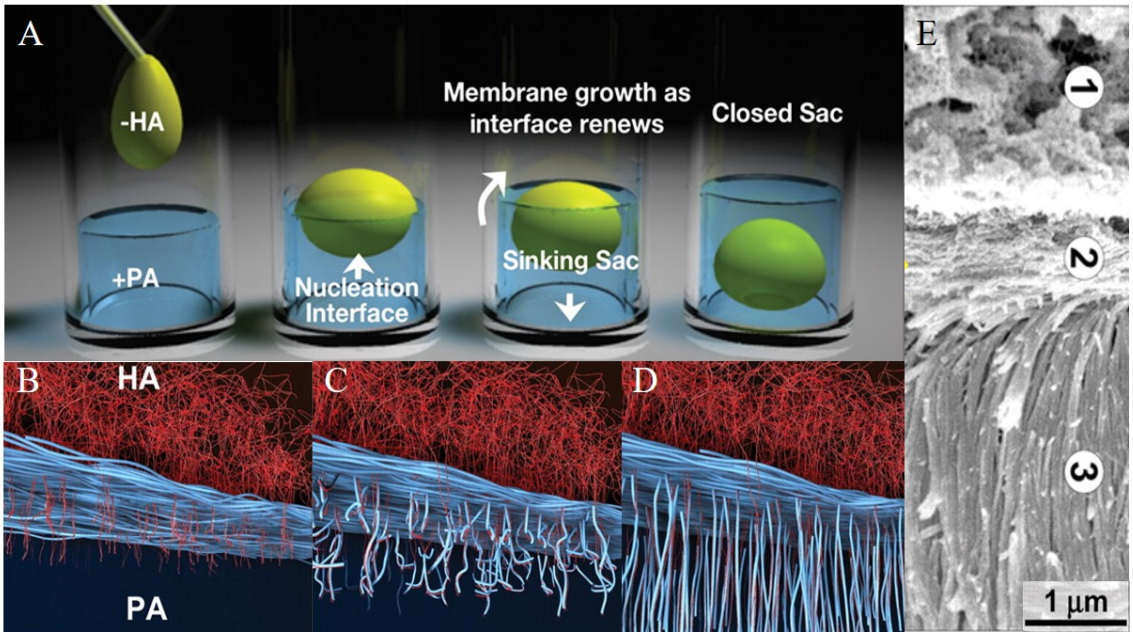

Figure 2.12: *HA-PA co-assembly. A) Schematics of the formation of the co-assembled HA-PA sacs. Formation mechanism of the structure includes the B) penetration of HA stubs (in red) through the diffusion barrier formed at the interface between the two solutions, C) the self-assembly of PA nanofibers (in blue) initiated by the stubs, and the D) growth of the nanofibers perpendicular to the interface over time E). Microstructure of a cross section of the co-assembled membrane showing a distinctive three-layered architecture [Adapted from Capito et al.[117]].*

When the HA solution is embedded within a larger PA solution, the membrane forms around the HA drop, generating a closed sac (Figure 2.12.A). The system forms by rapidly creating a diffusion barrier at the HA-PA interface,[118] which allows the establishment of an osmotic gradient that acts as driving force for the extrusion of HA fibers through the interfacial PA layer (Figure 2.12.B-D). The membrane is permeable to other biomolecules and can support growth and differentiation of mesenchymal stem cells (MSCs) into chondrocytes.[21]

Another example of a hierarchical architecture based on a positively charged PA and a negatively charged macromolecule is based on elastin-like polypeptides (ELPs).[119] This polypeptide comprised four domains based on the pentameric sequence VPGXG (with X being isoleucine (I), valine (V), or glutamic acid (E)) derived from natural elastin while also included a fifth domain with the cell adhesion RGDS motif derived from fibronectin.

When a small volume of PA solution is immersed in a large volume of an ELP solution, a dynamic interfacial assembly spontaneously develops, and a closed membrane is formed, entrapping the PA solution inside it and leaving the ELP solution outside (Figure 2.13).

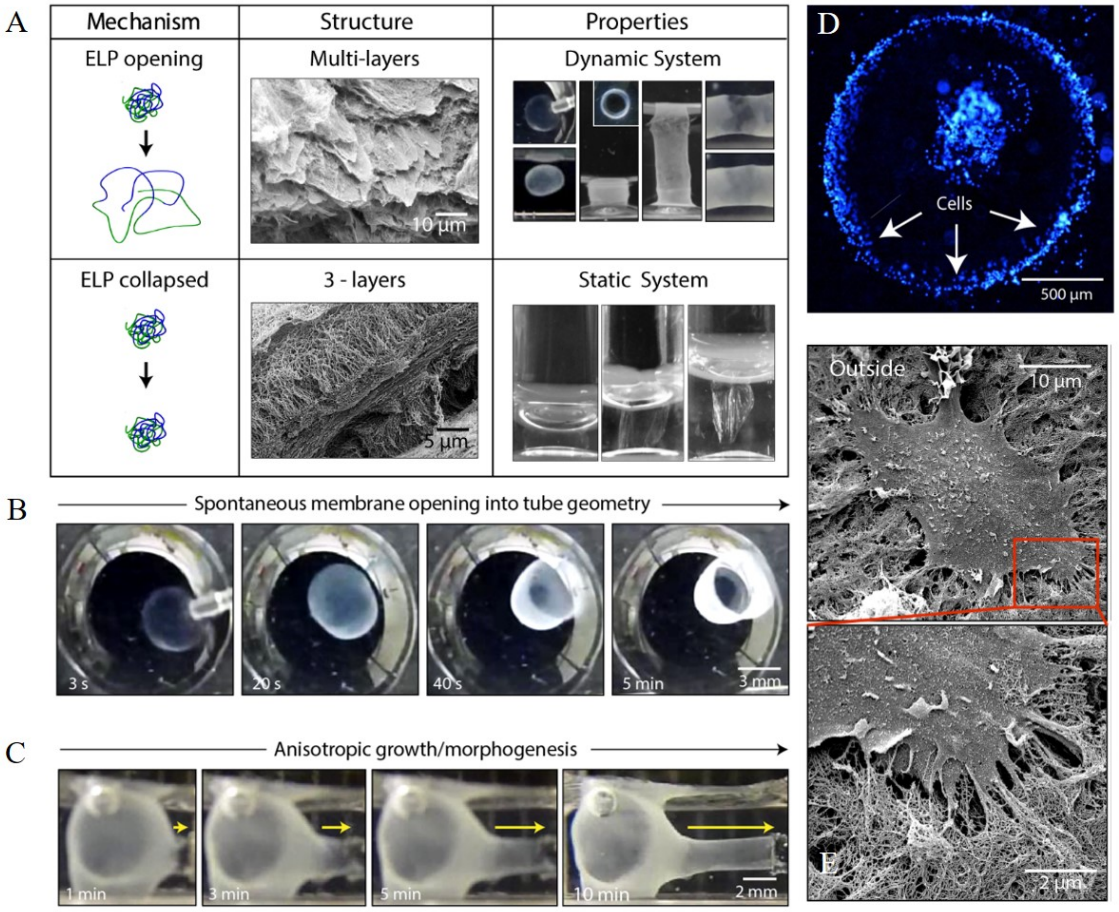

Figure 2.13: *ELP-PA co-assembly. A) Effect of using two different PAs in the coassembly with an ELP. The charged nature of PAs proved to strongly affect its ability to provoke conformational changes in the ELP molecule, thus finally leading to either static (when a two lysine residues bearing PA is used) or dynamic systems (when a three lysine residues bearing PA is used). B) Dynamic self-assembly ELP-PA-based system to grow tubular vascular-like scaffolds and time evolution of an ELP/PA co-assembly from a closed membrane into a tube-like geometry is shown. C) On-demand growth of side tubes by touching and displacing the membrane. D) Human umbilical vein endothelial cells (hUVECs) attached inside and outside the tubes. E) Mouse adipose-derived stem cells (mADSCs) spread on the inner side of the co-assembled tubular structure [Modified from Inostroza-Brito et al.[119]].*

Shortly after the formation of the structure and upon contact with a surface, the membrane opens, adheres, and seals to the surface, creating a tubular structure (Figure 2.13.B & C). Small-angle X-ray scattering (SAXS) and scanning electron microscopy (SEM) have demonstrated that the coassembly process in this case is determined primarily by conformational changes of the ELP triggered by coassembly with PA molecules.

This work demonstrates that by slightly modifying the PA sequence, it is possible to access different coassembling processes, which in turn generate different hierarchical structures -and consequently- biomaterial properties (Figure 2.13.B). The most remarkable assets of this ELP-PA system are its capability to access nonequilibrium for substantial periods of time as well as to enable growth and morphogenesis into vascular-like tubular structures that can serve as scaffolds for tissue engineering without the use of molds or templates (Figure 2.13.D & E).

2.4.4 PAs Biomedical Relevance

Materials originated by PA self-assembly have been proved functional for tissue engineering, regenerative medicine and cancer therapy,[98] mostly owed to their ability to interact with cells through a high density of surface signals as to mimic biomechanical aspects of the ECM.[120]

PA-based systems have been developed to stimulate specific biological processes such as in vitro cell migration[121,122] and differentiation of progenitor cells into neurons (while suppressing the development of astrocytes),[108] and in vivo regeneration of axons,[123] blood vessels,[124] bone,[125] enamel,[126] and cartilage.[127]

Recent works report on the in vitro tumoricidal activity of the cationic α-helical $(KLAKLAK)_2$ peptide (known to induce cancer cell death by membrane disruption) attached to PA nanofibers, as well as in vivo reduction of tumor cell proliferation and tumor growth in a mouse xenograft model of breast cancer.[128] Lastly, PA-based hydrogels are able to reversibly reprogram the phenotype of neural cells.[17]

2.5 Host-Guest Interactions & Biomaterials

Macrocyclic host–guest interactions are one of the most recognizable motifs in supramolecular chemistry,[32] the characteristic feature of these interactions is a macrocycle host container with a cavity that harbours small molecules, pharmaceuticals and biomolecules in it.[129]

All together, the specificity of host–guest interactions plus the ability to tune their strength (Figure 2.14.C) and directionality of this kind of interaction by selection of the guest, enable excellent control when designing supramolecular materials using host–guest binding to facilitate cross-linking.[31]

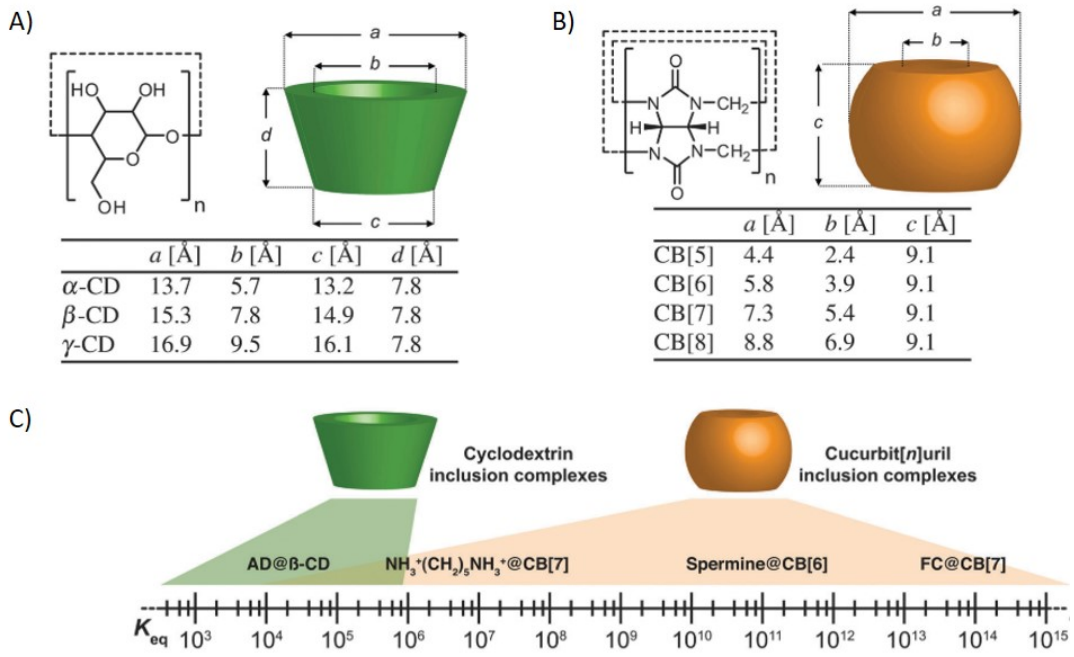

	a [Å]	b [Å]	c [Å]	d [Å]
α-CD	13.7	5.7	13.2	7.8
β-CD	15.3	7.8	14.9	7.8
γ-CD	16.9	9.5	16.1	7.8

	a [Å]	b [Å]	c [Å]
CB[5]	4.4	2.4	9.1
CB[6]	5.8	3.9	9.1
CB[7]	7.3	5.4	9.1
CB[8]	8.8	6.9	9.1

Figure 2.14: *Schematic representations of A) cyclodextrins and B) cucurbit[n]urils. C) Ranges of binding affinities between cyclodextrins and CB[n]s and suitable guests (AD: Adamantane, FC: Ferrocene) [Modified from Mann et al.[32] and Yu et al.[129]].*

As mentioned in Section 2.2.1, host-guest interactions constitute appealing molecular recognition motifs given the high affinity and range of interaction strengths achievable through different host-guest pairs. Decades of synthetic efforts have produced a myriad of man-made macrocyclic hosts: crown ethers, cyclophanes, catenanes, porphyrins, cryptophanes, carcerands, and cavitands such as calix[n]arenes, and cucurbit[n]urils (CB[n], as well as the naturally ocurring cyclodextrins (CD).[129,130]

Cyclodextrins and cucurbit[n]urils are the most studied host-guest systems in biomaterials design and plenty of applications. For instance, cyclodextrins are extensively used in food industry, drug delivery, theranostics (specific targeted therapies based on specific targeted diagnostic tests), protein and surface modification, 3D printing and smart hydrogel design (Figure 2.14.A&B).[129,31] While cucurbit[n]urils are employed in household products,[131] pharmaceutical formulations,[132] and clean up of waste streams.[133]

Cyclodextrins and cucurbit[n]urils are biocompatible macrocycles and are already utilized in real-world applications, therefore, they are produced in industrial scale. Moreover, the incorporation of various functional groups is better established for CD systems than other aqueous host systems, which renders them optimal candidates for covalent functionalisation of macromolecules.[130]

Synthetic polymers (such as PAM)[134] or naturally ocurring biopolymers (such as HA)[135] routinely used as part of biomaterials and polymeric hydrogels (Section 2.3.2) can be grafted with either a macrocylic host or its complementary guest partner to prepare non-covalently cross-linked hydrogels (Figure 2.6).[136] When host and guest-functionalised polymers are present in the same bulk hydrogel the dynamic and reversible host-guest binding endows the material with self-healing and shear-thinning properties.[32]

To date, hydrogel systems based on the co-assembly between multiple types of macromolecules have been less explored than those between smaller size components. While the majority of these materials include synthetic polymers,[137] there is an important number of protein[138,139] or polysaccharide-based ones.[140] Incorporation of cyclodextrins is next discussed in Section 2.5.1 and the use of cucurbit[n]urils in supramolecular hydrogels will be presented in Section 2.5.2.

2.5.1 Cyclodextrin-based Biomaterials

Cyclodextrins (CDs) are naturally occurring macrocyclic oligosaccharides, typically composed of 6, 7 or 8 D-glucose repeating units (forming α-, β- or γ-CD, respectively) coupled through α-1,4-glucosidic linkages that endow a macrocycle (Figure 2.14.A).[130]

CD's 3D structure can be approximated to a truncated cone positioning the primary hydroxyl groups on the smaller rim, as the inner cavity presents a hydrophobic environment it is suitable to host small hydrophobic molecules. This complexation is mainly driven by hydrophobic and van der Waals interactions, although the release of CD ring strain and formation of hydrogen bonds with CD hydroxyl groups also play a role in some cases.[73]

Frequent guest molecules for CD systems include adamantane, ferrocene, azobenzene, cholesterol and bile acid derivatives, as well as hydrophobic drugs.[130,129] The most frequently utilized guest group for βCD is adamantane (Ada), which fits very efficiently into its cavity (log K = 5.04).[141] Perhaps the most important property of CD-guest complexes is their responsive nature to a variety of stimuli (Figure 2.15).[130]

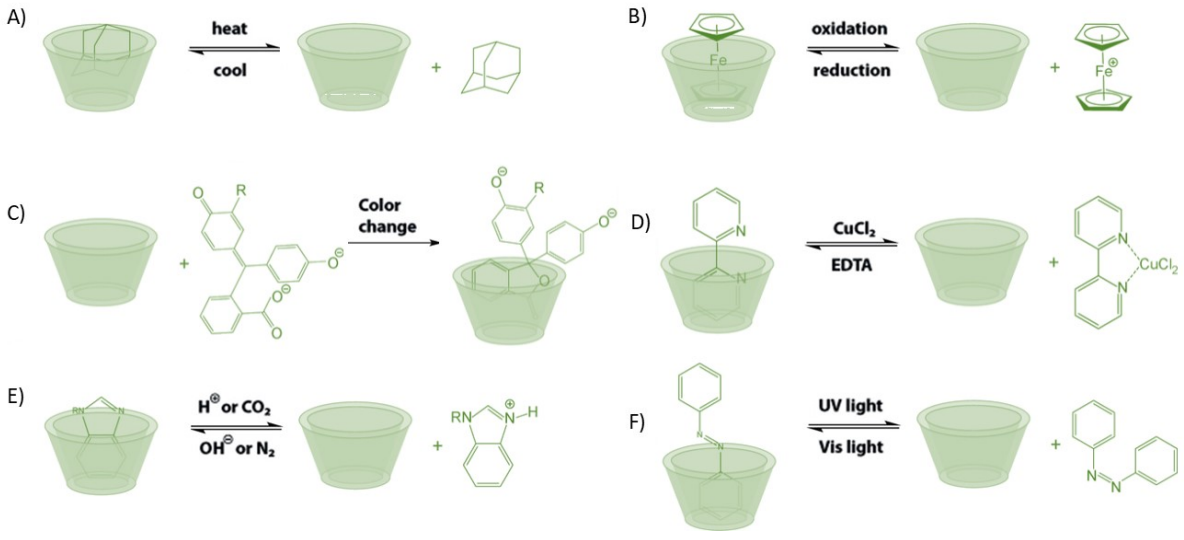

Figure 2.15: *Stimuli-resposiveness character of CD-host complexes. A) Thermoresponsive adamantane complex, B) Redox-responsive ferrocene complex, C) Colour-changing phenolphthalein complex, D) Metal-ion-responsive bipyridine complex, E) pH-Responsive benzimidazole complex, and F) Light-responsive azobenzene complex [Modified from Schmidt et al.[130]].*

Inclusion complex formation by CDs has been utilised as a reversible binding motif for the development of non-covalently cross-linked polymeric networks, these polymeric systems have been investigated in pharmaceutical and biomedical applications as drug delivery systems and biocompatible scaffolds for tissue engineering and medical diagnostics.[73,77] PAM,[142] PEG multi-arm star polymers,[143] poly(sodium acrylate) co-polymers,[144] poly(lysine),[145] and poly(acrylic acid)[76] (see Figure 2.5.C) are just a few examples where hydrogels have been developed by the covalent attachment of a CD host to a polymer chain and mixing with a similarly functionalised guest-containing polymer.[130]

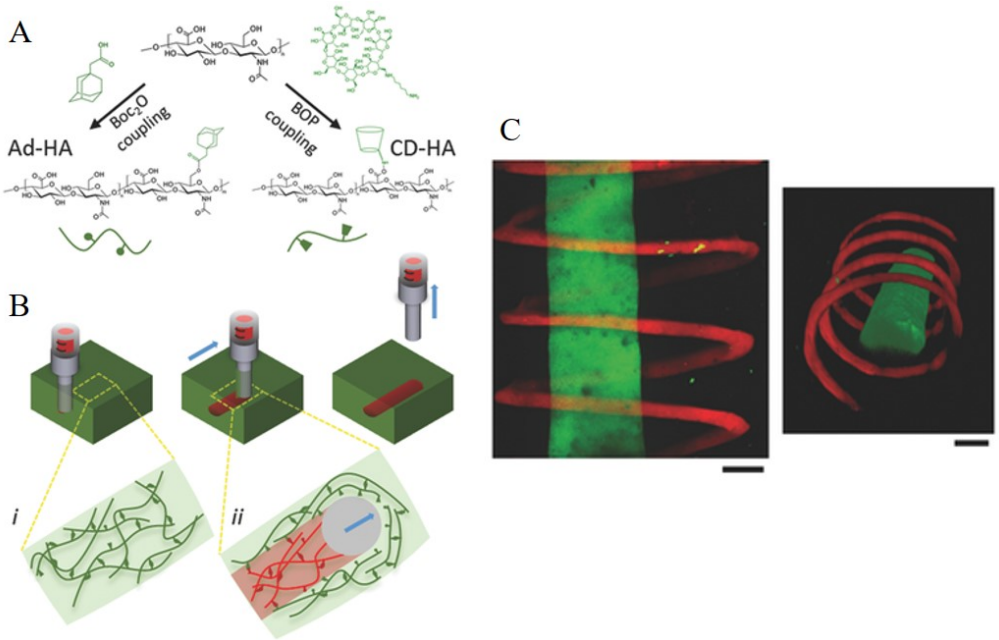

Figure 2.16: *3D-printing with a β-CD/Ada-HA ink A) Conjugation of adamantane (Ad, guest) and β-cyclodextrin (CD, host) to hyaluronic acid (HA). B) Illustration of the extrusion of a supramolecular ink (red) into a supramolecular support gel (green). (C) Printing of a spiral red-labeled gel spiral around a green-labeled filament embedded in an unlabeled support gel [Modified from Highley et al.[135]].*

Burdick and coworkers reported the use of one-step functionalised HA hydrogels with either Ada or *β*-CD moieties to create a material that exhibited self-healing and shear-thinning behaviours, which has enabled its use as an "ink" for 3D printing (Figure 2.16.A). The system requires that the hydrogel is directly linked into another self-healing "support" gel; this is possible due to the quick formation of the inclusion complex between the printed and the support gels mediated by host-guest interactions (Figure 2.16.B). The printed material displays remarkable control of structural complexity and can support the concomitant culture of multiple cell types (Figure 2.16.C).[135]

2.5.2 Cucurbit[n]uril-based Biomaterials

Cucurbit[n]urils (CB[n], n = 5–8, 10) are synthetic macrocyclic oligomers based on repeating monomer units of glycoluril.[146] Unlike CDs, CB[n]s present two identical portals surrounded by ureido-carbonyl groups that lead access to their hydrophobic cavity (Figure 2.14.B).[147,32]

A complex interplay of intermolecular interactions turn CB[n]s into ideal recognition motifs for molecular binding, on one side there is an important interplay between the release of 'high-energy' water molecules upon inclusion of non-polar organic guests and concomitant van der Waals interactions inside the cavity, similar to CDs, CB[n] rims are also involved in hydrogen bonding formation upon guest inclusion.[73,129]

Increasing amount of glycoluryl repeating units in CB[n]s originates increasing sizes of both the inner cavity and the distance between portals, resulting in different molecular recognition properties within the CB[n]s family.[146] The smallest, CB[5], can encapsulate gases and metal cations, CB[6] can bind to them too, in adition to protonated aminoalkanes (for instance, 1,6-diaminohexane (or spermine in Figure 2.14.C) yields a 1:1 complex with K_{eq} up to $10^{12} M^{-1}$).[148] CB[7] forms strong 1 : 1 complexes with positively charged amphiphilic guests including Ada, FC, and p-xylylene amino derivatives, as well as viologen.[147]

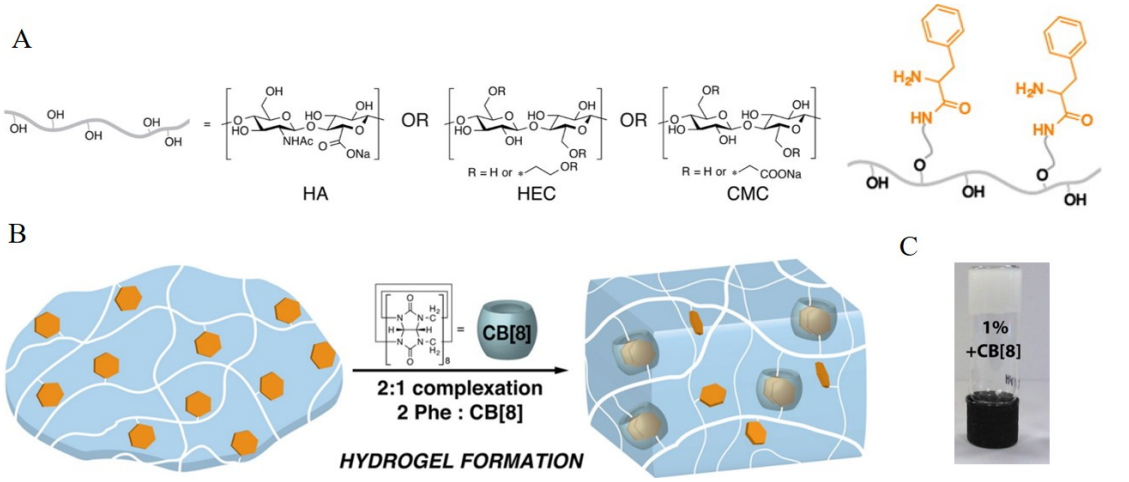

Figure 2.17: *A) Phenylalanine-bearing polysaccharides (HA, hydroxyethyl cellulose, and carboxymethyl cellulose) for binding of **CB[8]**. B) Schematic showing the coassembly of the modified polysaccharides and **CB[8]** triggering hydrogel formation. (C) Turbid hydrogel formed by modified HA and **CB[8]** [Modified from Rowland et. al[140]].*

In contrast to CB[5–7], the cavity of **CB[8]** is large enough to originate ternary complexes by harbouring two organic guests simultaneously.[146,129] Several recognition motifs have been described as part of ternary complexes with CB[8], including naphthalene derivatives,[73,129] viologen,[147] as well as amino acids like tryptophan and phenylalanine.[149]

This CB[8] ability to bind two guests simultaneously has been utilised for the reversible assembly of supramolecular diblock copolymers,[150] protein dimerisation,[151,152] and the assembly of supramolecular glycopolymers[153] and polymeric hydrogels.[136,73,32]

Appel and co-workers reported in 2010 the first example of a supramolecular polymeric hydrogel based on **CB[8]**–viologen/naphtoxy inclusion complexes.[154] Ever since the Scherman laboratory has devoted significant efforts to study the thermodynamics and kinetics of physically cross-linked hydrogels prepared by mixing polymers containing pendant guest motifs with freely diffusible **CB[8]** units to form ternary complexes (Figure 2.2.B).[32]

For instance, the system based on pendant phenylalanine residues attached to HA and cellulose derivatives presented in Figure 2.17.A,[140] where the host-guest complexation and further electrostatic interactions stabilize the supramolecular complex that holds the macromolecular chains together and thus enable the establishment of the hydrogel (Figure 2.17.B&C).[140]

2.6 Perspective and Opportunities

This review chapter has featured the diversity and potential of supramolecular building blocks and the possibilities that their careful tuning and design offer to develop molecularly precise biomaterials.

There is an increasing interest to develop supramolecular strategies capable of generating more complex and functional materials. The herein reviewed examples demonstrate that a range of combinations of covalent and non-covalent polymeric architectures can be used to fabricate with self-assembly-based materials. In this chapter it has been described how approaches based on self-assembling multiple types of components are establishing new routes to achieve this goal. These systems are enabling new molecular interactions, more diverse structures, higher levels of functionalities, and ultimately new and innovative properties.

Each one of the co-assembling approaches herein discussed offers different advantages and are also subjected to different challenges. The broader opportunities for design and function that emerge by combining multiple types of supramolecular building blocks are also subjected to a higher need for control and predictability. In particular, self-assembled hydrogels and their promising biomedical and tissue engineering applications offer possibilities to improve their design in order to boost their dynamic morphological and spatiotemporal ECM mimicking capacities.

For instance, no system is reported in the literature that merges the two supramolecular formation mechanisms described in Figure 2.2, i.e. supramolecular crosslinking via molecular recognition motifs and supramolecular stacking biomaterials like peptide amphiphiles. Nonetheless, embracing higher levels of complexity that co-assembling different kinds of self-assembling systems comprise, will enable new discoveries and push the boundaries of complex biomaterials design.

These identified opportunities were used to refine the thesis statement (Section 1.2) into the final thesis aim and objectives as presented in the following chapter (Chapter 3).

Chapter 3

Aims and Objectives

This brief chapter provides the aims and objectives for the experimental section, stating how this dissertation pursues integration of host-guest interactions into new families of self-assembling hydrogels.

3.1 Aim

The aim of this thesis is to generate novel self-assembling peptide platforms that combine the dynamic and molecular recognition features of host-guest interactions and the benefits of peptide amphiphile capacities towards hydrogel scaffolds with improved functionality and stability.

3.2 Objectives

Objective 1

Synthesise and characterise cationic complementary PA molecules bearing **adamantane** and *β*-**cyclodextrin** motifs. Focus on the establishment of host-guest interactions among this pair. Determine the possibility to formulate co-assembled hydrogels with tunable stability and mechanical properties based on the non-covalent binding of the host-guest pair. Determine the suitability of these hydrogels as scaffolds for tissue engineering and regenerative medicine applications.

Objective 2

Synthesise and characterise anionic PA molecules bearing **adamantane** motifs as binding sites to *β*-**cyclodextrin**-derivatives. Determine the most suitable guest-bearing molecule to incorporate in a co-assembled hydrogel. Formulate co-assem-bled hydrogels incorporating the non-covalent tethering of the adamantane units and a *β*-**cyclodextrin-RGDS** derivative. Determine the suitability of these hydrogel scaffolds to display bioactivity in order to control cell adhesion for tissue engineering and regenerative medicine applications.

Objective 3

Synthesise and characterise **phenylalanine** and **tryptophan**-bearing PA molecules suitable for homoternary binding with cucurbit[8]uril **CB[8]**. Develop a proof-of-concept study on PA hydrogel formation via dynamic non-covalent dimerisation. Compare this novel PA hydrogelation mechanism to the conventionally ion-based method. Study the suitability of these co-assembled hydrogels as scaffolds for tissue engineering and regenerative medicine applications.

Part II

Peptide Amphiphiles & Adamantane/β-Cyclodextrin Interactions

Chapter 4

Self-Assembling Hydrogels Based on a Complementary Cationic Host-Guest Peptide Amphiphile Pair

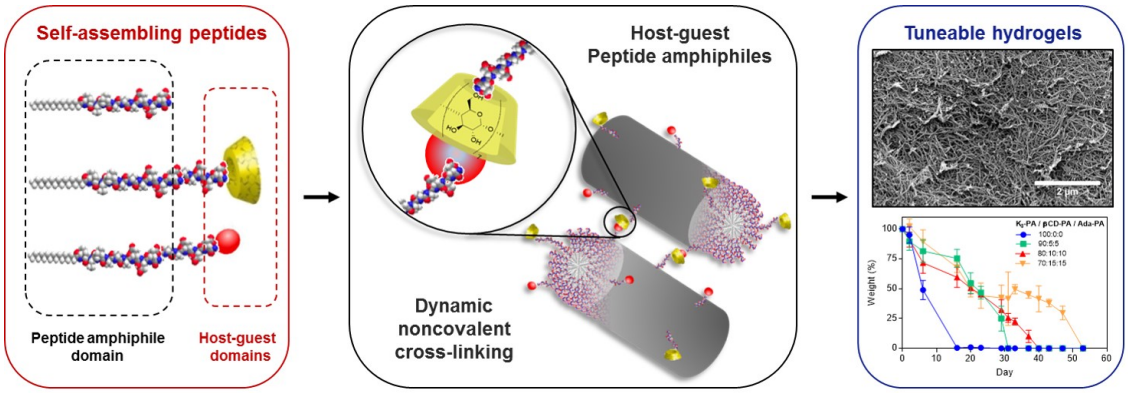

Figure 4.1: *Schematics showing the host-guest PA hydrogels concept.*

This chapter presents the development of supramolecular hydrogels based on *β*-Cyclodextrin•Adamantane interactions between cationic PA molecules. The rationale behind the molecules' design is firstly presented, then their supramolecular study and incorporation into hydrogels of biomedical relevance, lastly the functionality of the resulting gels is demonstrated.

This study has been published in:

Redondo-Gómez, C.; Abdouni, Y.; Becer, C. R.; Mata, A. Self-Assembling Hydrogels Based on a Complementary Host–Guest Peptide Amphiphile Pair. *Biomacromolecules*, **2019** 20 (6):2276-2285.[155]

4.1 Overview

Supramolecular polymer-based biomaterials play a significant role in current biomedical research. In particular, PAs represent a promising material platform for biomedical applications given their modular assembly, tunability, and capacity to render materials with structural and molecular precision. However, the possibility to provide dynamic cues within PA-based materials would increase our capacity to modulate their mechanical and physical properties and consequently enhance their functionality and broader use.

In this chapter, the synthesis of a cationic PA pair bearing complementary Ada and β-CD host-guest cues and their capacity to be further incorporated into self-assembled nanostructures are presented.

The possibility of these recognition motifs to selectively bind is presented, enabling noncovalent cross-linking between PA nanofibers, and endowing the resulting supramolecular hydrogels with enhanced mechanical properties, including stiffness and resistance to degradation, while retaining in vitro biocompatibility. The incorporation of the host-guest PA pairs in the resulting hydrogels allowed not only for macroscopic mechanical control from the molecular scale but also for the possibility to engineer further spatiotemporal dynamic properties, opening opportunities for broader potential applications of PA-based materials.

4.2 Introduction

Over the past decade, supramolecular chemistry has increasingly facilitated the design of a wide variety of functional biomaterials with enhanced precision and versatility.[30,27] In particular, self-assembling approaches offer modularity, tunability, and the possibility to engineer macroscopic properties through molecular modifications.[32]

These characteristics arise from the reversible nature of the noncovalent interactions that hold self-assembling biomaterials together, and allows for their ability to assemble in a modular and controllable fashion.[31] Based on these principles, a wide variety of self-assembling systems have been reported based on for example polymers,[135] peptides,[156] proteins,[139] DNA,[157] peptide derivatives,[158] and conjugates of them.[17]

PAs are a particularly promising family of self-assembling peptides, which are programmed to assemble in aqueous environments. These molecules comprise a lipid hydrophobic component, a β-sheet forming peptide segment, and charged amino acid residues that provide water-solubility and the possibility to carry bioactive sequences (see Figure 2.10).[96] The dispersive interactions among the hydrophobic tails and the establishment of a hydrogen bonding network between the oligopeptide segments drive the self-assembly processes of PAs in a cooperative fashion, yielding ordered and micrometre-long 1D structures.[98]

As the resulting supramolecular network assembles, a nanofibrous hydrogel forms, which can be designed to mimic both structural and functional features of the natural ECM.[159] These biomimetic systems have been developed to stimulate specific biological processes such as cell migration[121,122] and differentiation[108] in vitro as well as in vivo regeneration of axons,[123] blood vessels,[124] bone,[125] and cartilage.[127]

Hydrogels (see Section 2.3) are attractive materials for biomedical applications given their molecular-scale control over mechanical and bioresponsive properties.[7,6] While stiffness has been shown to be a key hydrogel parameter to control and drive cell response,[2,160,161] its tunability remains challenging.

Traditional approaches to tune hydrogel stiffness have mostly relied on modifying either gel concentration or crosslinking density, which can concomitantly modify porosity, network connectivity, and consequently affect bioactivity and degradation.[62]

Therefore, other approaches that can selectively control stiffness without affecting other hydrogel parameters would enhance the precision and versatility with which these biomaterials are designed. In particular, supramolecular hydrogels represent an attractive platform to enable such capability due to both the dynamic binding of their molecular components and the weak non-covalent nature of their interactions.[162]

The last three decades have witnessed the use of macrocyclic host-guest interactions to endow materials with dynamic, reversible, and responsive properties (see Section 2.5).[163] CDs constitute one of the best studied supramolecular hosts as they exhibit good biocompatibility, degradability, and a wide repertoire of functional groups that render their conjugation with biomacromolecules.[130] The strength and specificity of the CD–guest interaction enables excellent control over material functionality when designing both covalent[76] and supramolecular[164] polymer-based materials.

β-Cyclodextrin (β**CD**) comprises seven α-D-glucopyranoside units linked by ($\alpha\rightarrow$1,4)-glycosidic bonds, rendering a truncated cone structure with a hydrophilic exterior surface and a hydrophobic interior cavity. This structure is suitable for association with hydrophobic guest motifs of appropriate size and polarity such as Ada derivatives.[130,165,166,167]

A number of **CD/Ada** peptide-based systems have proven functional as soft materials,[168] delivery devices,[169,170] and chemo-[171] and bio-sensors.[172] However, to our knowledge, both the benefits and functionalities of this host-guest pair have not yet been translated into PA self-assembled hydrogels.

As a strategy to ameliorate the control of mechanical properties of PA hydrogels, we herein report a new family of supramolecular hydrogels prepared through the noncovalent crosslinking between PAs bearing either β**CD** or **Ada** host-guest motifs. We describe the synthesis of both cationic isostructural PA conjugates, the underlying mechanism of both peptide self-assembly and host-guest complexation, as well as the resulting properties of assembled hydrogels. Furthermore, the potential biofunctionality of the system is demonstrated using cell-culture experiments.

4.3 Host-guest PAs self-assembly

4.3.1 Design and rationale of host-guest PA molecules

The main goal of this work was to generate a molecularly-designed functional hydrogel that exhibits the benefits of both peptide self-assembly and host-guest interactions. The covalent incorporation of host-guest motifs took place by synthesizing two PA-conjugates bearing either a β**CD** residue (**K_3G_3-βCD-PA**, host-PA) or an **Ada** residue (**K_3G_3-Ada-PA**, guest-PA). Both **K_3G_3-βCD-PA** and **K_3G_3-Ada-PA** conjugates are isostructural to the well-characterised cationic **K_3-PA**, which we employed as a control (Table 4.1).

Table 4.1: Structural information of cationic host-guest co-assembled peptide amphiphiles.

Peptide	Sequence	Schematics
K_3G_3-βCD-PA	$C_{15}H_{31}CONH$-$V_3A_3K_3G_3$-(β-Cyclodextrin)-$CONH_2$	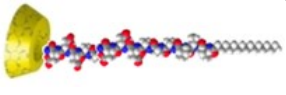
K_3G_3-Ada-PA	$C_{15}H_{31}CONH$-$V_3A_3K_3G_3$-(Adamantane)-$CONH_2$	
K_3-PA	$C_{15}H_{31}CONH$-$V_3A_3K_3$-$CONH_2$	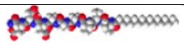

Note:
$*$ As can be inferred by the schematics above, **K_3G_3-βCD-PA** and **K_3G_3-Ada-PA** exhibit slightly larger sizes than **K_3-PA**. In this fashion, fibers formed by the latter are expected to be around 8 nm in diameter,[173] meanwhile the former ones are expected to be around 10 - 11 nm.

These new host-guest derivatives comprise a hydrophobic palmitoil tail (C_{16}-), an oligopeptide motif with a strong tendency to form β-sheets (-V_3A_3-), an ionizable region that is also responsible for further hydrogelation (-K_3-), a triglyine spacer (-G_3-) to enhance further fiber display of the host-guest cues, and a 1,2,3-triazole linker that positioned the corresponding **βCD** and **Ada** residues nearby the C-terminus of the respective PA (Figure 4.2).

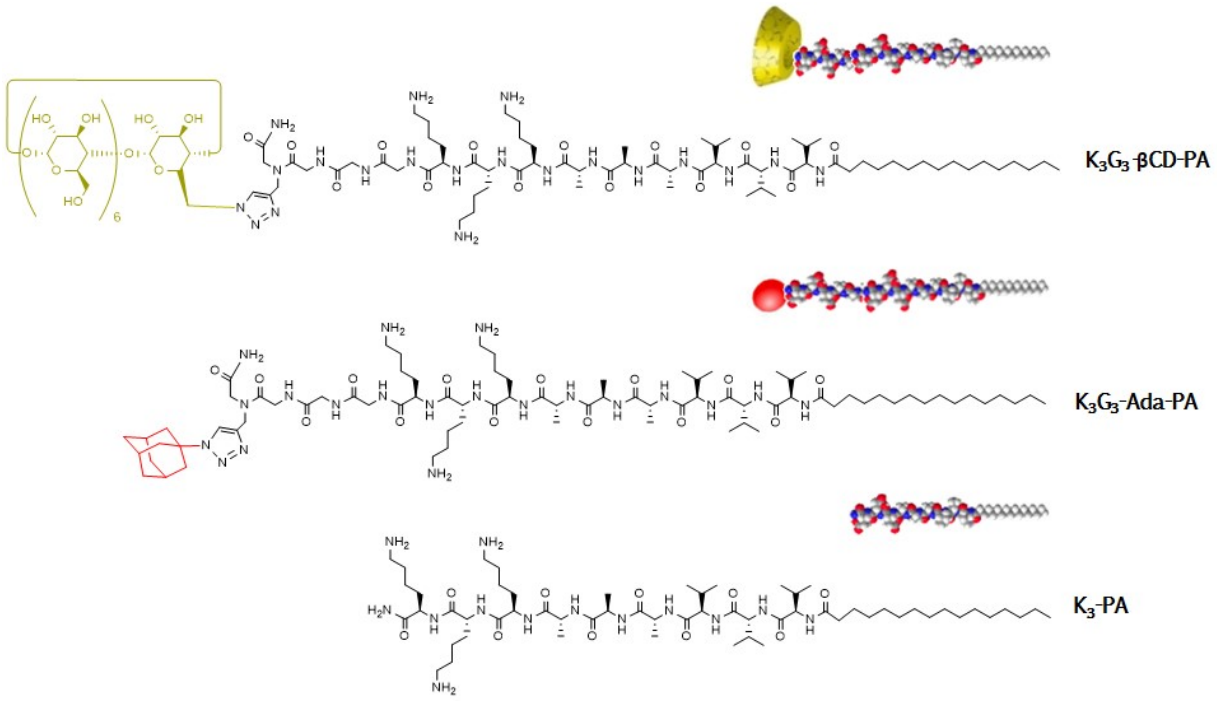

Figure 4.2: *Molecular structures of the peptide amphiphile (PA) molecules reported in this chapter. The complementary host-guest PA pair is represented by* ***K_3G_3-βCD-PA*** *and* ***K_3G_3-Ada-PA****. The former bears a β-cyclodextrin moiety and acts as the host-PA, while the latter bears an adamantane residue and acts as the guest-PA. Both peptides are isostructural to* ***K_3-PA****.*

4.3.2 Host-Guest PAs purity and characterisation

Both **K_3G_3-βCD-PA** and **K_3G_3-Ada-PA** derivatives were synthesised using solid state peptide synthesis (SSPS) followed by further copper(I)-catalysed alkyne–azide cycloaddition (CuAAC) coupling, also known as the Huisgen reaction.[174] Extensive details on their synthesis routes and purification steps can be found in Section 4.12.1 of this thesis.

Host-PA **K_3G_3-βCD-PA** was obtained with 93% sequence purity, and both ESI-MS and MALDI-TOF-MS provided mass confirmation of the conjugate: 860.53 $[M+3H]^{3+}$, 1289.6 $[M+2H]^{2+}$, and 2598.3 $[M+Na]^{+}$ (Figure 4.3). Guest-PA **K_3G_3-Ada-PA** purity was found to be close to 94% and presented three main ionisation adducts on ESI-MS: 797.7 $[M+2H]^{2+}$, 1594.3 $[M+H]^{+}$ and 1615.3 $[M+Na]^{+}$ (Figure 4.4).

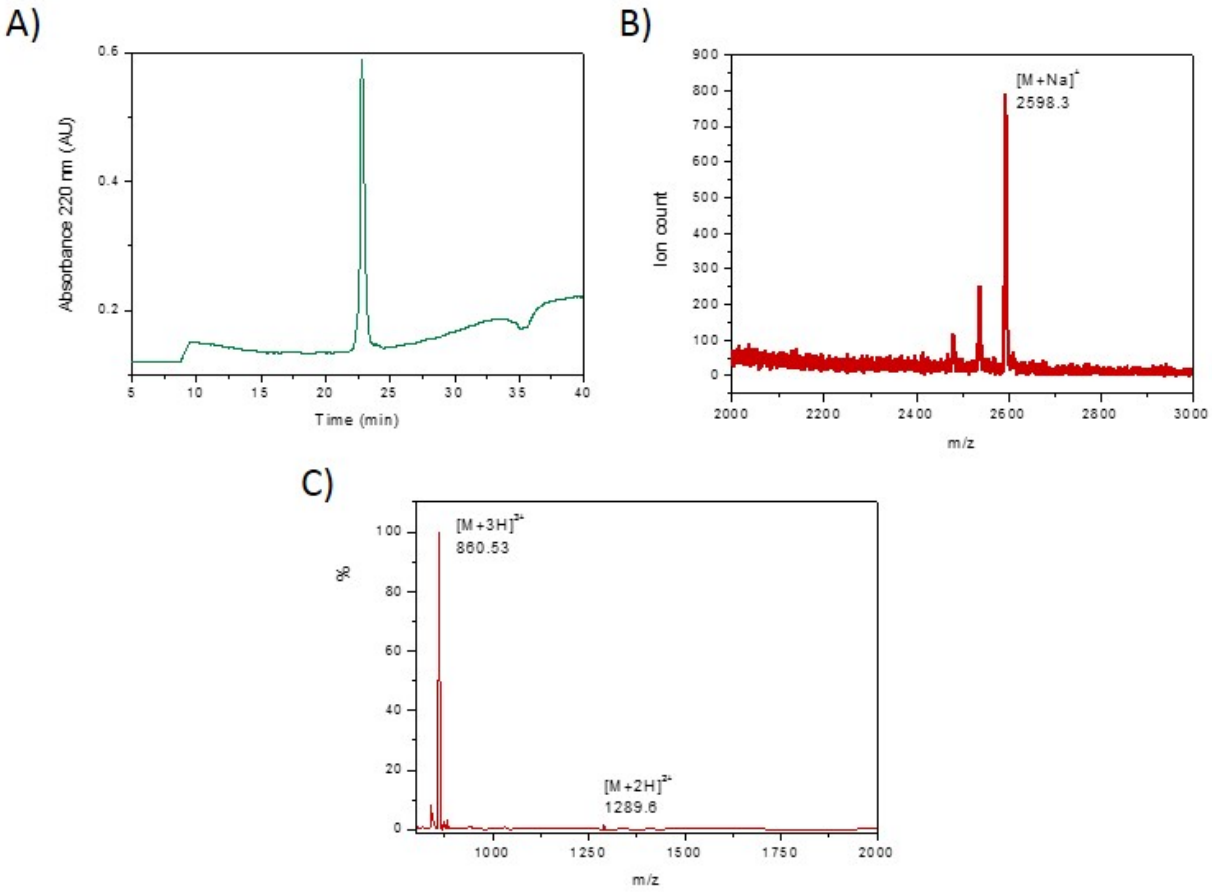

Figure 4.3: *Purity and molecular weight confirmation for **K_3G_3-βCD-PA**. A) RP-HPLC, B) ESI-MS and C) MALDI-TOF-MS traces.*

Filler-PA **K_3-PA** was obtained with 96% purity and its ESI-MS spectrum showed three main ionisation adducts: 576.2 $[M+2H]^{2+}$, 1150.1 $[M+H]^{+}$ and 1173.1 $[M+Na]^{+}$ (Figure 4.4).All of these results are briefed in Table 4.2.

It is worth mentioning that in all PAs presented in this chapter there can be found the presence of either a trifluoroacetate (TFA) or a chloride counterion, therefore, all purity values represent sequence purities. Though all concentrations must require a slight correction due to this effect, the traditional approach used to report concentrations was followed.

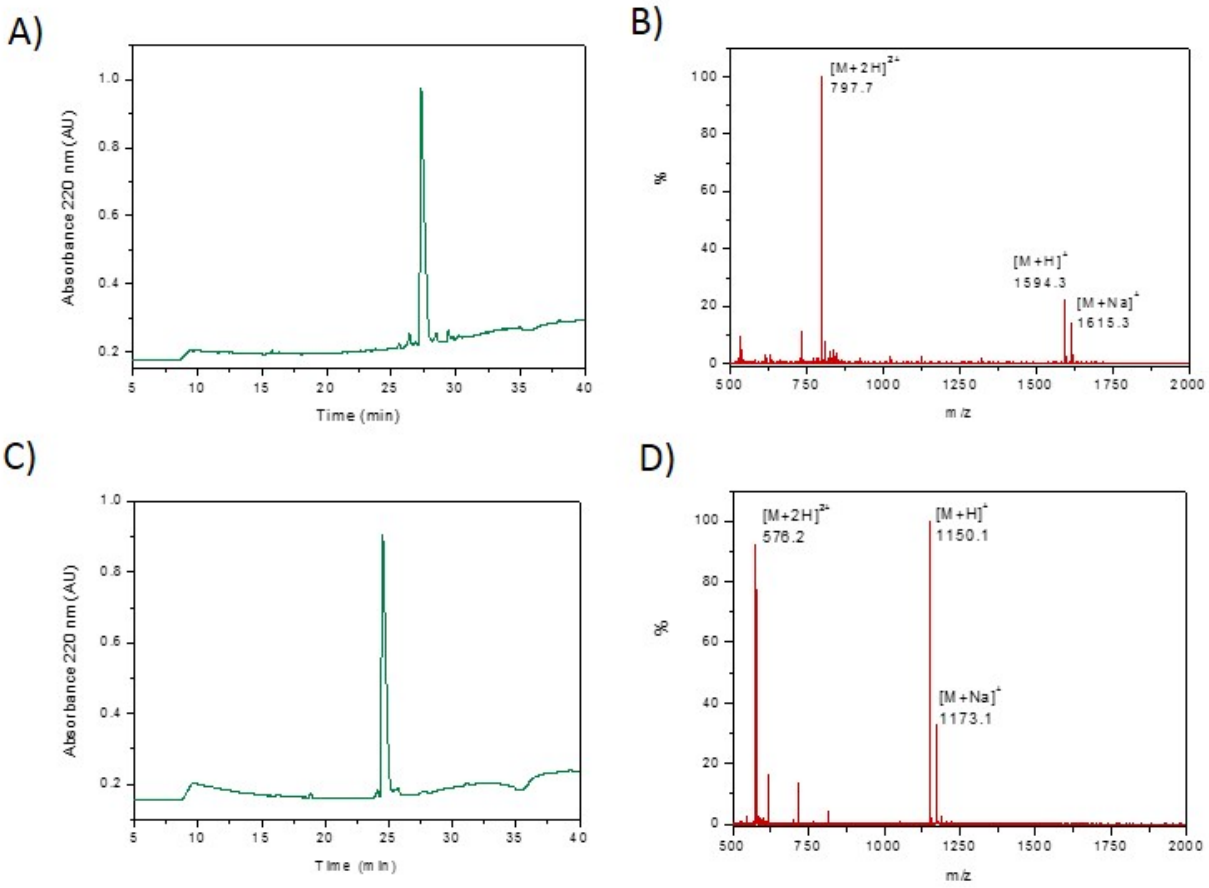

Figure 4.4: *Purity and molecular weight confirmation for* ***K*$_3$*G*$_3$*-Ada-PA*** *and* ***K*$_3$*-PA***. *Panels A,C) RP-HPLC and B,D) ESI-MS correspond to* ***K*$_3$*G*$_3$*-Ada-PA*** *and* ***K*$_3$*-PA*** *respectively.*

4.3.3 Fiber forming individual PA molecules

Transmission electron micrographs (TEM) revealed that both host-guest PAs self-assemble individually into nanofibers when dissolved in water in a micro-molar concentration range (Figures 4.5.A & 4.6.A). While both **K$_3$G$_3$-βCD-PA** and **K$_3$G$_3$-Ada-PA** exhibited comparable fiber diameters (9.8 ± 1.4 nm and 9.6 ± 1.3 nm, respectively) their length varied significantly (184 ± 130 nm and 666 ± 386 nm, respectively) and both exhibited shorted lengths compared to conventional micrometer-long PA fibers (Figures 4.5.B,D & 4.6.B,D).

This length shortening suggests that the allocation of bulky/hydrophilic β**CD** or small/hydrophobic **Ada** residues on the surface of the PA nanostructures may originate packing disruptions, resulting in shorter self-assembled fibers.

Table 4.2: Chemical characterisation of the herein reported cationic peptide amphiphiles.

Peptide	Molecular mass (g/mol)	Found mass (m/z)	ζ (mV, ∇)	Purity (%, ♯)
K_3G_3-βCD-PA	2575.34	2598.3 $[M+Na]^+$ ∗	20.4 ± 3.6	93
K_3G_3-Ada-PA	1594.12	1611.53 $[M+Na]^+$ Ø	28.2 ± 4.5	94
K_3-PA	1150.61	1150.1 $[M+H]^+$ Ø	24.2 ± 3.6	96

Notes:
∗ Determined through MALDI-TOF,
Ø Determined through ESI-MS,
∇ Determined from a 0.01 wt% solution in water at pH 7,
♯ Assessed through RP-HPLC.

Despite this potential intrusion in fiber formation, zeta potential (ζ) measurements revealed that both self-assembled **K_3G_3-βCD-PA** and **K_3G_3-Ada-PA** fibers exhibit a net positive charge along a wide range of pH values, suggesting that the presence of the host-guest motifs does not intrude on the surface display of the positively charged lysine residues once the fibers have assembled (Figures 4.7.D & 4.8.D).

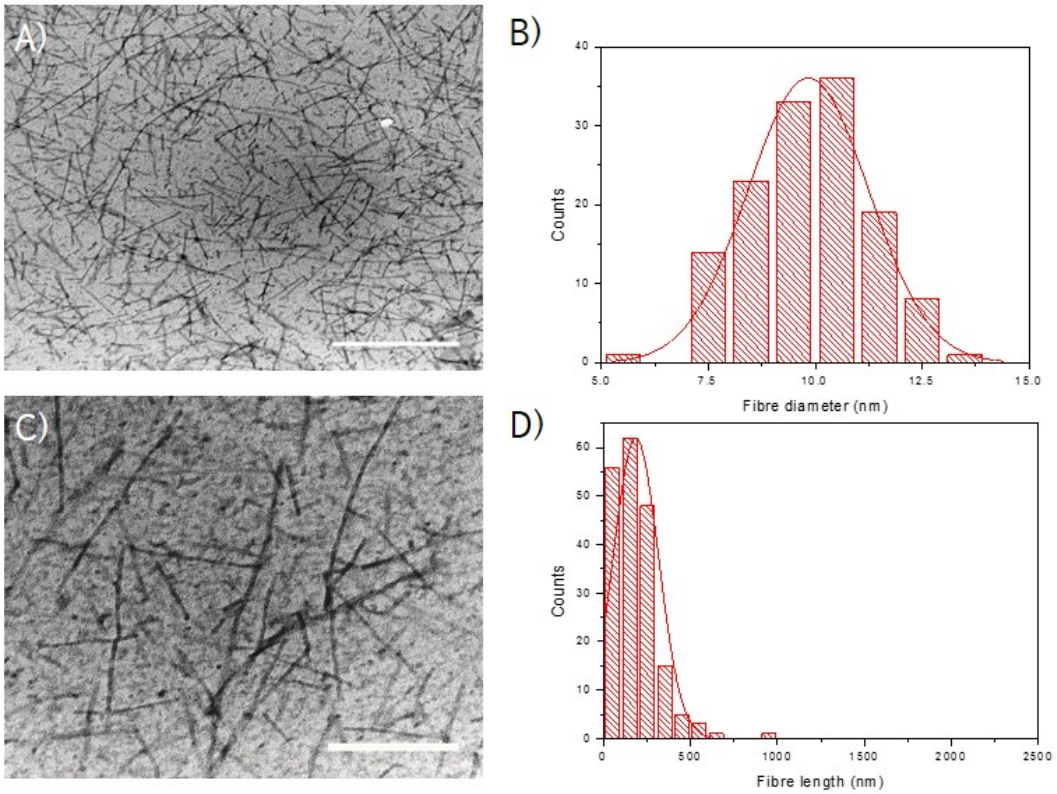

Figure 4.5: *Characterisation of **K_3G_3-βCD-PA** nanofibers. A,C) TEM micrographs of **K_3G_3-βCD-PA** fibers in water (scale bars = 500 mm and 250 nm in panels A and C respectively, [**K_3G_3-βCD-PA**] = 38 μM) B,D) Fibre diameter and length distributions.*

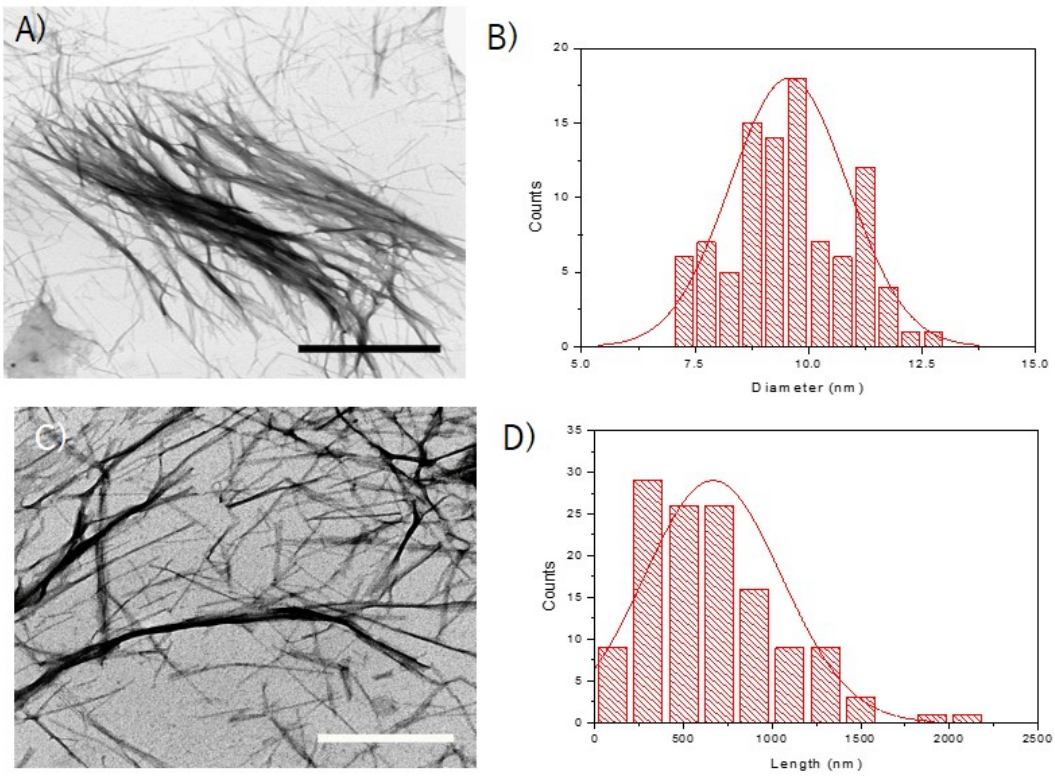

Figure 4.6: *Characterisation of* ***K*$_3$*G*$_3$*-Ada-PA*** *nanofibers. A,C) TEM micrographs of* ***K*$_3$*G*$_3$*-Ada-PA*** *fibers in water (scale bars = 1 μm and 250 nm in panels A and C respectively, [****K*$_3$*G*$_3$*-Ada-PA****] = 63 μM) B,D) Fibre diameter and length distributions.*

4.3.4 K_3G_3-βCD-PA secondary structure in water and HEPES

It is agreed that the assembly of PAs into fibers in aqueous environments is driven by both the hydrophobic association of the alkyl tail and the cohesive formation of a regular hydrogen bonding network (i.e. β-sheets). Interestingly, circular dichroism (CD) measurements revealed that **K_3G_3-βCD-PA** fibers do not attain the expected β-sheets in water at 25 ºC (Figures 4.7.A & 4.9.A) but rather a β-turn-like secondary structure.[175]

Formation of β-turn-like secondary structures might involve the interaction of at least two **K_3G_3-βCD-PA** molecules and could be attributed to the complexation of a C_{16} tail from a PA molecule into the cyclodextrin cavity of a second one. Some evidence of this alkyl tail complex formation was gathered through NOESY experiments, though a full spectroscopic study of this kind remains elusive due to the limitations of this technique in this type of macromolecular systems (see page 93).

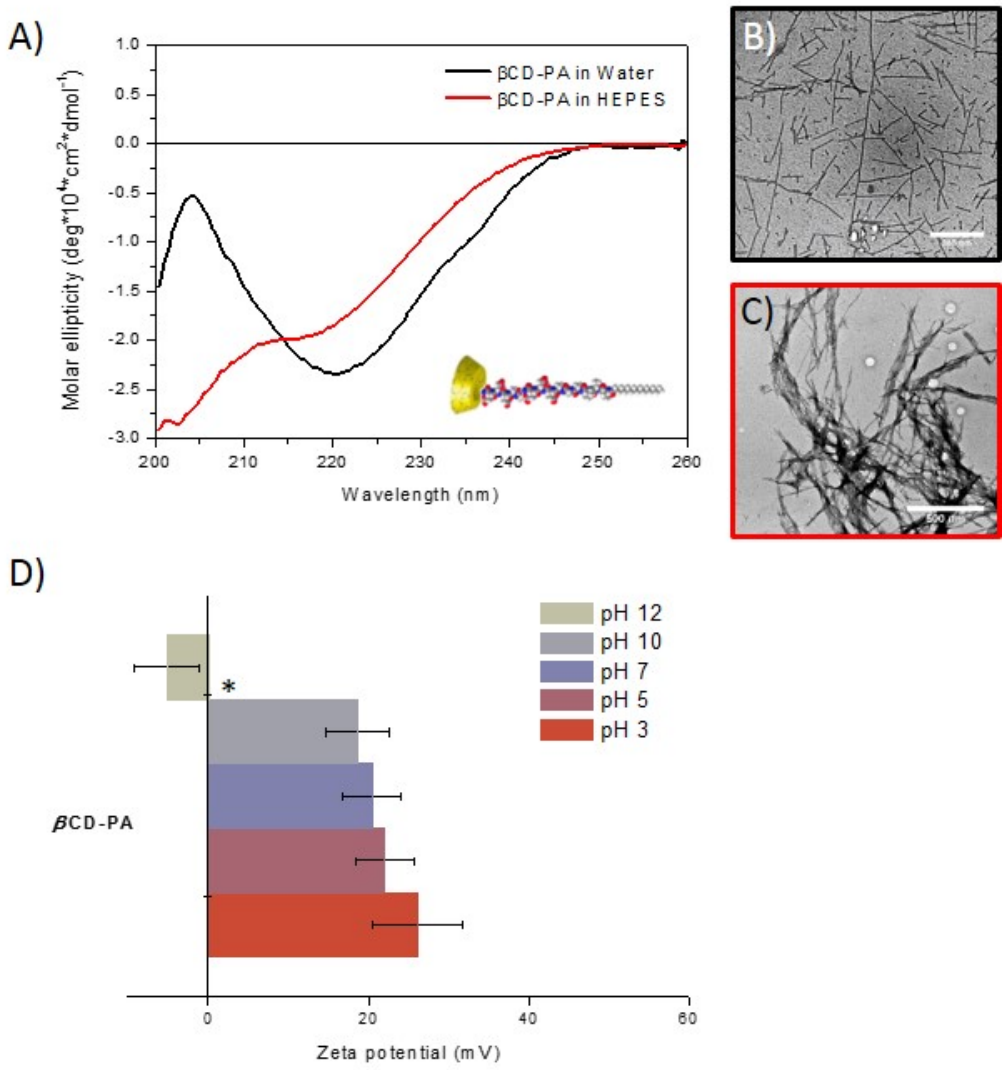

Figure 4.7: *Self-assembly of* ***K*$_3$*G*$_3$*-βCD-PA*** *into nanofibers in aqueous media. A) Circular dichroism (CD) spectra and B) transmission electron microscopy (TEM) images of* ***K*$_3$*G*$_3$*-βCD-PA*** *[38 μM] in water (black) and C) HEPES buffer (red). D) Zeta potential (ζ) measurements of solutions of* ***K*$_3$*G*$_3$*-βCD-PA*** *in water (n = 3, mean ± s.d., * marks the PA isoelectric point).*

Compared to a classical PA such as **K$_3$-PA**,[19] the geometrical packing parameters in **K$_3$G$_3$-*β*CD-PA** have been modified by the presence of the voluminous ***β*CD** motifs at the C-terminus (see Section 2.2.2 and Figure 2.4).

It can be speculated that allocating these moieties at the surface of the self-assembled nanofibers could restrict the peptide backbone and promote the observed *β*-turn conformation (Figure 4.7.A) as reported in dipalmitoylated PA systems.[176]

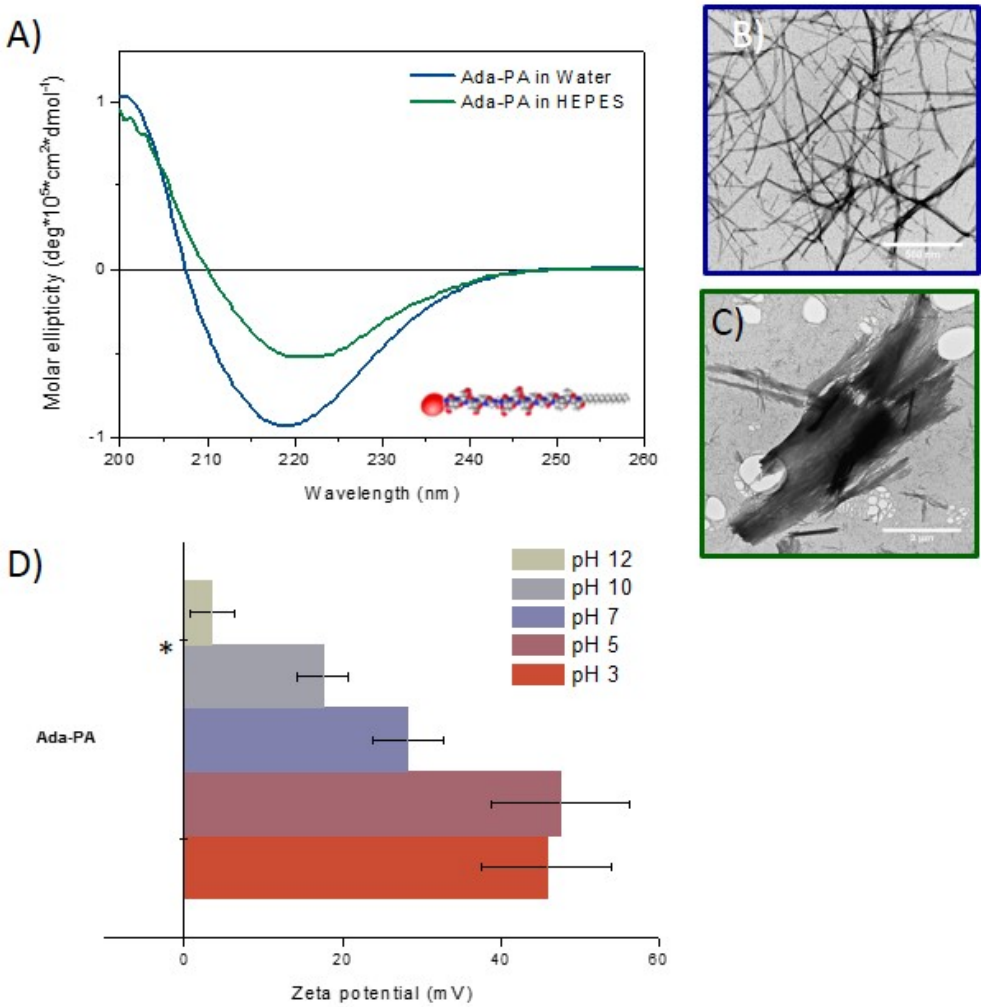

Figure 4.8: *Self-assembly of* ***K*$_3$*G*$_3$*-Ada-PA*** *into nanofibers in aqueous media. A) Circular dichroism (CD) spectra and B) transmission electron microscopy (TEM) images of* ***K*$_3$*G*$_3$*-Ada-PA*** *[63 μM] in water (blue) and C) HEPES buffer (green). D) Zeta potential (ζ) measurements of solutions of* ***K*$_3$*G*$_3$*-Ada-PA*** *in water (n = 3, mean ± s.d., * marks the PA isoelectric point).*

Interestingly, these *β*-turns could be switched to a random coil conformation when assembled at room temperature and under physiological conditions (i.e. in HEPES pH 7.4, [NaCl] = 0.9 wt%), maintaining a fibrous morphology and exhibiting a slight tendency to form bundles (Figures 4.7.C & 4.9.A).

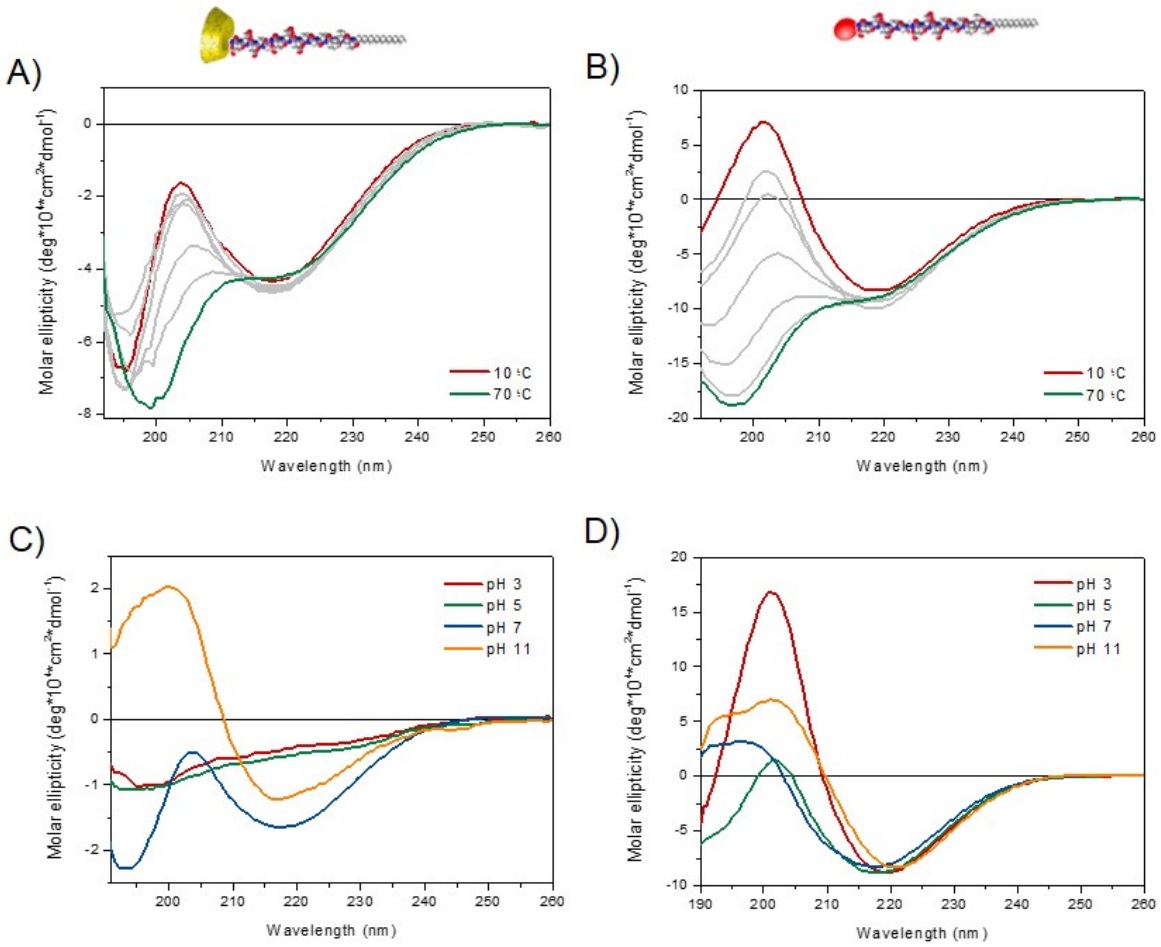

Figure 4.9: *Conformational changes of* ***K*$_3$*G*$_3$*-βCD-PA*** *and* ***K*$_3$*G*$_3$*-Ada-PA*** *as a function of temperature and pH. A) Temperature dependent CD spectra of* ***K*$_3$*G*$_3$*-βCD-PA*** *and B)* ***K*$_3$*G*$_3$*-Ada-PA*** *in water. C) pH dependent CD spectra of* ***K*$_3$*G*$_3$*-βCD-PA*** *and D)* ***K*$_3$*G*$_3$*-Ada-PA*** *in water.*

4.3.5 K$_3$G$_3$-Ada-PA secondary structure in water and HEPES

In contrast, CD investigations revealed that **K$_3$G$_3$-Ada-PA** nanofibers exhibited well-defined β-sheet conformations in both water and HEPES buffer (Figure 4.8.A).

One interesting aspect related to changes in the pKa values of lysines in **K$_3$G$_3$-Ada-PA** was found during pH-dependent zeta potential experiments. When one compares the variation of zeta potentials of both **K$_3$G$_3$-βCD-PA** (Figure 4.7.D) and **K$_3$G$_3$-Ada-PA** (Figure 4.8.D) it is possible to observe differences in zeta potential changes over different pH values, the **K$_3$G$_3$-βCD-PA** system showed a smooth decrease in zeta values and beyond pH 12 zeta potential dropped to practically zero as expected for lysine containing peptides, whose pKa value is close to 10.76.[177]

In the case of **K_3G_3-Ada-PA** zeta potential values did not drop all at once at values close to the expected pKa value of 10.76, but they exhibited two main jumps, one before pH and another after pH 12 (Figure 4.8.D) suggesting that lysine residues in **K_3G_3-Ada-PA** might exhibit two different pKa values. It is well known that some structural factors can modify the pKa of side chain aminoacid residues, such as small conformational reorganisation or changes in the environment surrounding the ionisable groups,[178] though these changes have usually reported in larger protein systems.[179] Perhaps some computational studies might throw some light on this phenomenon in the particular case of the slightly hydrophobic **K_3G_3-Ada-PA** derivative.

TEM micrographs revealed that while single **K_3G_3-Ada-PA** fibers exist in water and HEPES buffer at low concentration regimes (Figure 4.11), at higher concentrations these fibers tend to bundle into small fibrils, that eventually appear to coalesce into larger raft-like objects of heterogeneous morphology and size (Figures 4.8.C & 4.11), similar to the nanosheets reported by Nam et al.[180]

It is speculated that these structures form through van der Waals interactions amid adjacent **Ada** residues. In an attempt to dismantle these rafts it was found that 1,1,1,3,3,3-hexafluoro-2-propanol (HFIP) dissolves them to completion. CD spectra of **K_3G_3-Ada-PA** shows that in 100% HFIP media the peptide exists as free monomers, while increasing the concentration of water promotes assembly of **K_3G_3-Ada-PA** into the rafts (Figure 4.10), similar results have obtained with other PA systems,[181] however, further investigations on the nature of this peptide rafts formations are required.

Both **K_3G_3-Ada-PA** and **K_3G_3-βCD-PA** exhibited temperature-driven conformational changes in accordance to previous studies,[182] Figure 4.9 shows that our system might retain a substantial content of their native secondary structure at physiologically relevant conditions. These results demonstrate that incorporation of small hydrophobic moieties in **K_3G_3-Ada-PA** fibers does not significantly affect the peptide backbone conformation in aqueous environments, but can lead to fiber bundling at higher concentration regimes.

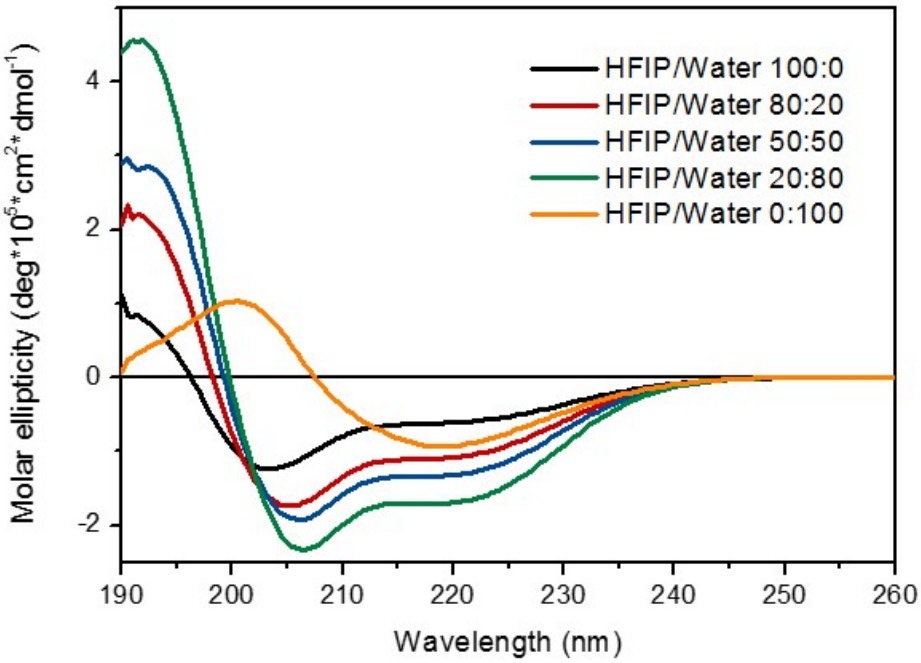

Figure 4.10: *Circular dichroism (CD) spectra of* ***K*$_3$*G*$_3$*-Ada-PA*** *dissolved in different fractions of HFIP/water [****K*$_3$*G*$_3$*-Ada-PA****] = 63 µM.*

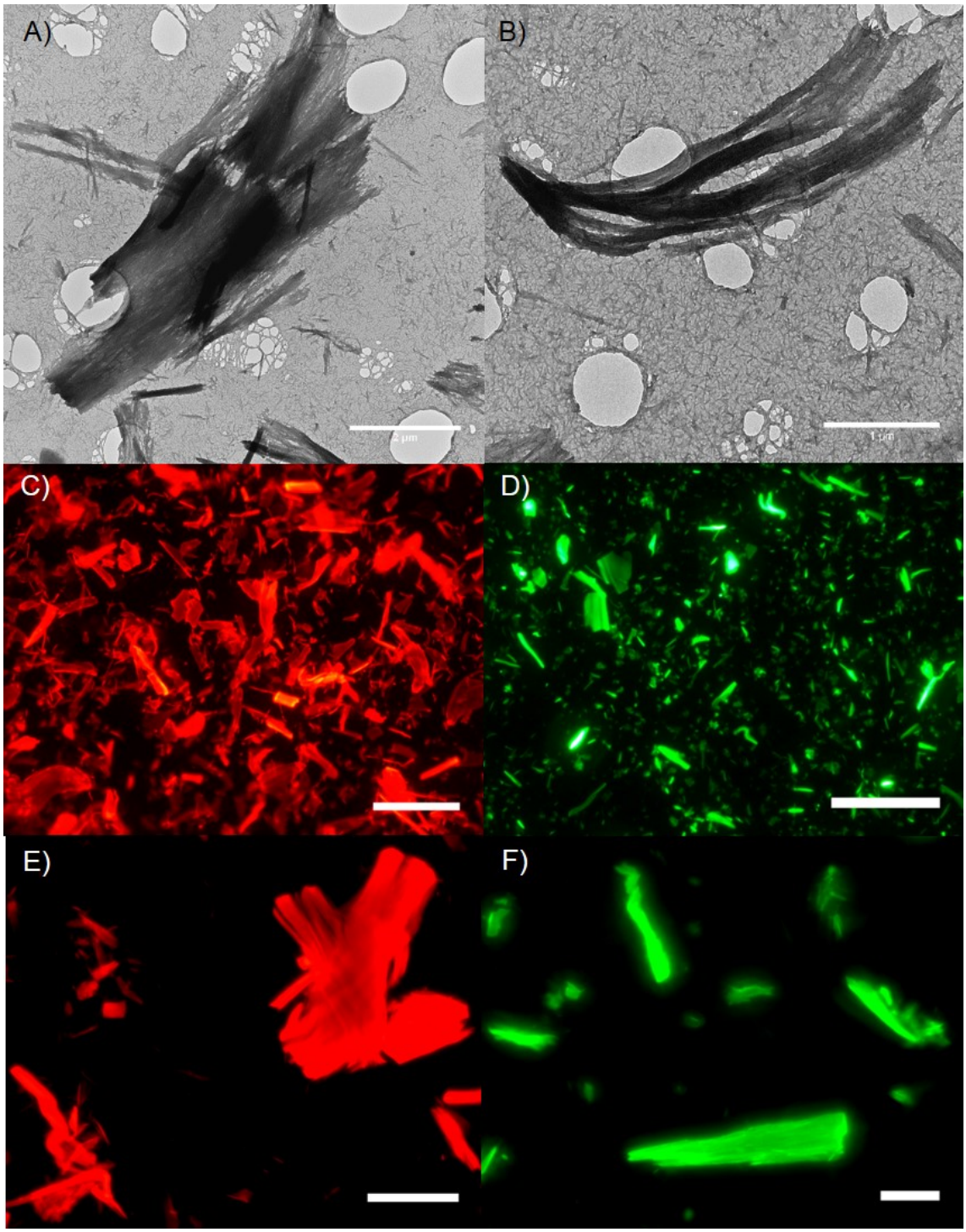

Figure 4.11: *Micrographs showing the diversity of sizes and shapes of the peptide rafts formed by* ***K_3G_3-Ada-PA*** *in HEPES buffer. A,B) TEM images of the rafts. C,E) Epifluorescence micrographs of stained rafts using Nile Red or D,F) 6-deoxy-6-[(5/6)-fluoresceinylthioureido]-β-cyclodextrin (FITC-β-CD) as fluorescent probes (scale bars = 200 μm and [****K_3G_3-Ada-PA****] = 400 μM for panels A-D & scale bars = 50 μm and [****K_3G_3-Ada-PA****] = 150 μM for panels E,F).*

4.4 Tracking adamantyl residues on K_3-PA/K_3G_3-Ada-PA co-assembled nanofibers

The possibility to track **Ada** residues in co-assembled nanofibers was explored, for this purpose *β*-Cyclodextrin capped gold nanoparticles (*β*CD-AuNPs) were synthesised as detailed by Shi and co-workers (**Figure 4.12**).[183] UV-Vis spectroscopy investigations revealed a λspr = 514 nm, Thermogravimetric analysis (TGA) indicated a functionalisation degree of about 210 ***β*CD** units attached per Au nanoparticle, while analysis of TEM micrographs indicated a *β*CD-AuNPs size distribution of about (5.6 ± 0.9) nm (Figure 4.13) in good agreement with previous reports.[183]

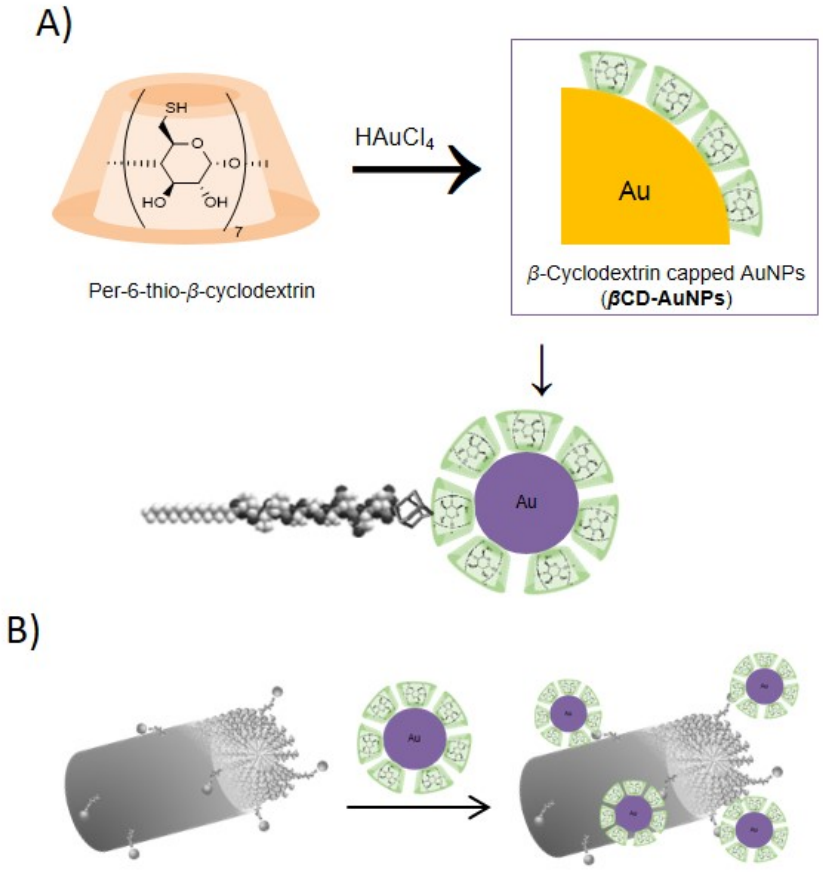

Figure 4.12: *β-Cyclodextrin capped gold nanoparticles (βCD-AuNPs). A) Preparation of βCD-AuNPs and further complexation with* ***K*$_3$*G*$_3$*-Ada-PA**. *B) Decoration of self-assembled* ***K*$_3$*G*$_3$*-Ada-PA** *nanofibers with βCD-AuNPs.*

PA samples were incubated with an excess of βCD-AuNPs were incubated at room temperature, and further imaged on TEM via negative staining, the resulting images are presented in Figure 4.14. Figure 4.14.A shows pristine **K_3G_3-Ada-PA**, while panels B-C evidence how βCD-AuNPs were able to bind to adamantyl motifs in the self-assembled nanofibers. Less binding was found when **K_3G_3-Ada-PA** nanofibers were blocked with non-capped **βCD** first and then incubated with capped βCD-AuNPs (Figure 4.14.D). Unexpectedly, **K_3-Ada-PA** controls (Figure 4.14 E) also exhibited affinity for βCD-AuNPs, indicating that the binding must be also determined by electrostic factors on top of the host-guest interactions. Further discussion on the utility of this βCD-AuNP-based tracking system is presented in Chapter 5, when its functionality for tracking **Ada** units in anionic PA systems is addressed.

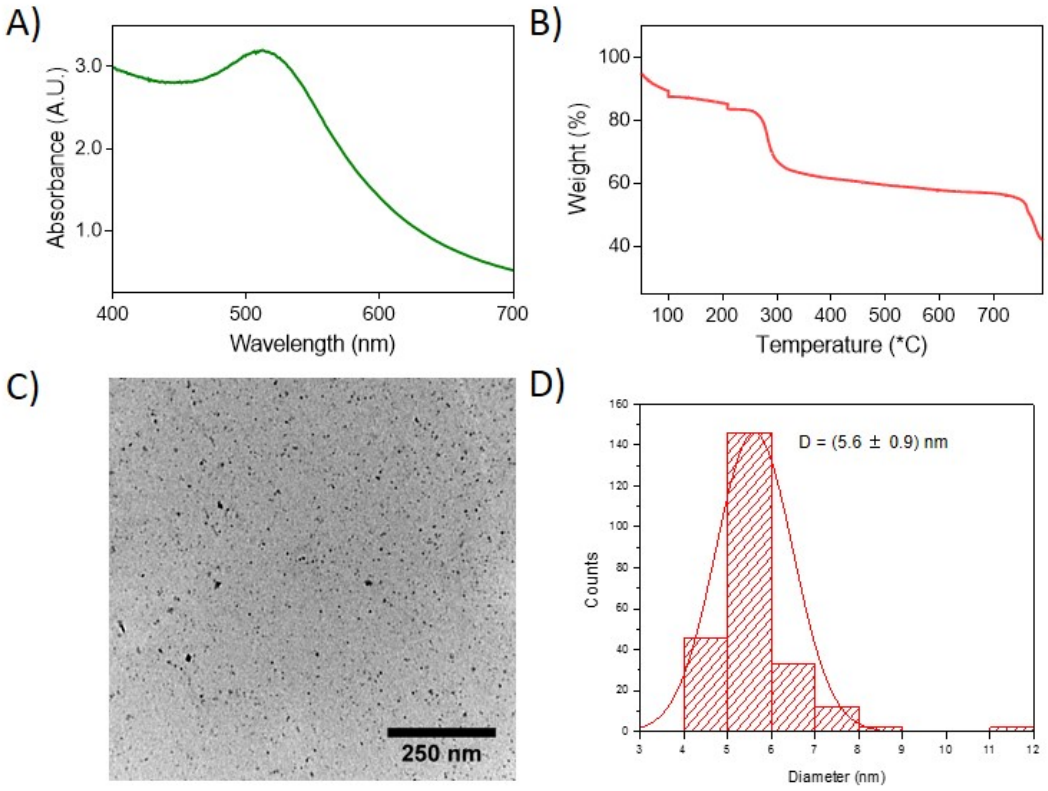

Figure 4.13: *Characterisation of βCD-AuNPs. A) UV-Vis spectra [βCD-AuNPs = 0.01%]. B) TGA thermogram showing thermal degradation of βCD-AuNPs. C) TEM micrograph of βCD-AuNPs in water. D) βCD-AuNPs diameter distribution from panel C).*

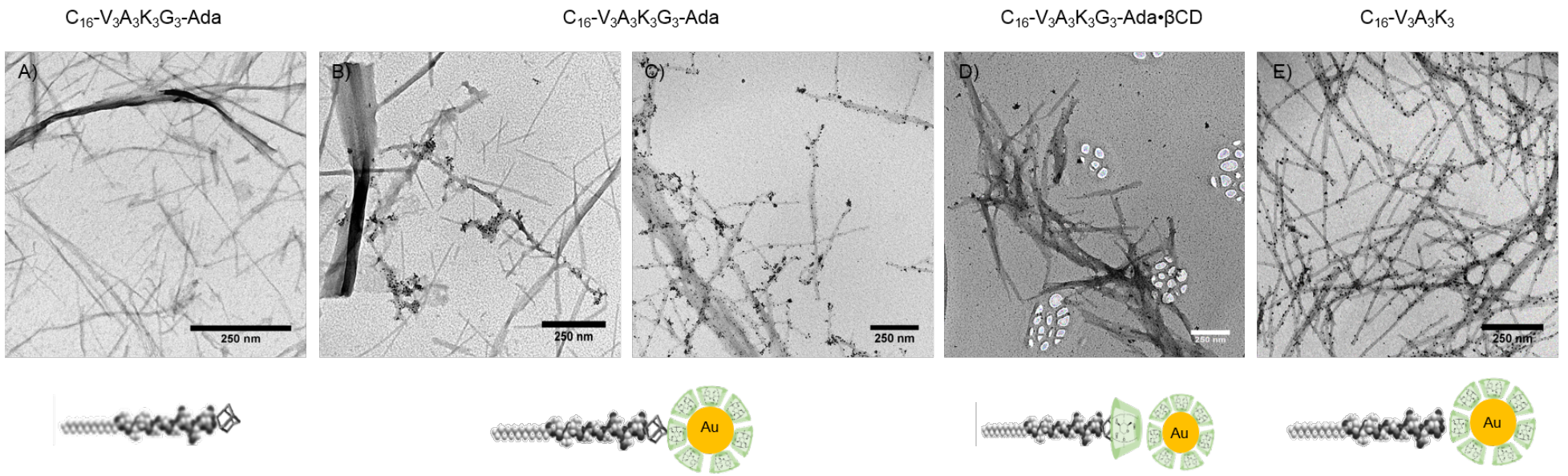

Figure 4.14: *TEM micrographs showing A)* ***K*$_3$*G*$_3$*-Ada-PA*** *nanofibers and evidencing the interaction between B,C) βCD-AuNPs and* ***K*$_3$*G*$_3$*-Ada-PA****, D)* ***K*$_3$*G*$_3$*-Ada-PA•βCD*** *and E)* ***K*$_3$*-PA*** *(scale bars = 250 nm).*

4.5 Supramolecular decoration of K_3G_3-βCD-PA and K_3G_3-Ada-PA self-assembled nanofibers

As host-guest motifs are presented on the surface of both **K_3G_3-βCD-PA** and **K_3G_3-Ada-PA** nanofibers, these cues elicit the formation of inclusion complexes with free complementary partners in solution. When **K_3G_3-βCD-PA** nanofibers were incubated with rimantadine (a water soluble **Ada** derivative) in HEPES buffer, the formation of a well-known 1:1 inclusion complex took place between self-assembled **βCD** units and free **Ada** moieties in solution.

TEM micrographs revealed that this noncovalent interaction has no significant impact on fiber morphology (Figure 4.15.B), but CD studies indicated that the **K_3G_3-βCD-PA** undergoes a conformational change from a random coil to a β-sheet conformation upon binding **Ada** units (**Figure 4.15.A**).

To further investigate whether these inclusion complexes can be formed at the surface of self-assembled **K_3G_3-Ada-PA**, isothermal titration calorimetry (ITC) experiments were performed. Titration of assembled **K_3G_3-Ada-PA** nanofibers with free **βCD** revealed a 1:1 binding mode (Figure 4.16, Table 5.3), same evidence was collected through nuclear Overhauser effect spectroscopy (NOESY) (Figures 4.17-4.19).

Table 4.3: Thermodynamic parameters associated to the host-guest interactions in **βCD•K$_3$G$_3$-Ada-PA** and **K$_3$G$_3$-βCD-PA•K$_3$G$_3$-Ada-PA**.

System	N	K_D (μM)	K_a (x 10^4 M^{-1})	ΔH (kJ•mol^{-1})	ΔG (kJ•mol^{-1})	-T•ΔS (kJ•mol^{-1})
K$_3$G$_3$-Ada-PA•βCD	0.95 ± 0.07	25.6 ± 6.4	3.91 ± 0.98	-14.56 ± 2.3	-26.23	-11.67
K$_3$G$_3$-Ada-PA•K$_3$G$_3$-βCD-PA	1.02 ± 0.05	13.2 ± 4.4	7.6 ± 2.5	-9.41 ± 0.84	-27.87	-18.45

TEM micrographs showed that this noncovalent complexation had little effect on fiber morphology (Figure 4.15.D). Furthermore, CD studies revealed that the **K_3G_3-Ada-PA** undergoes a conformational change when binding to free *β***CD** moieties, switching conformation from *β*-sheet to random coil (Figure 4.15.C).

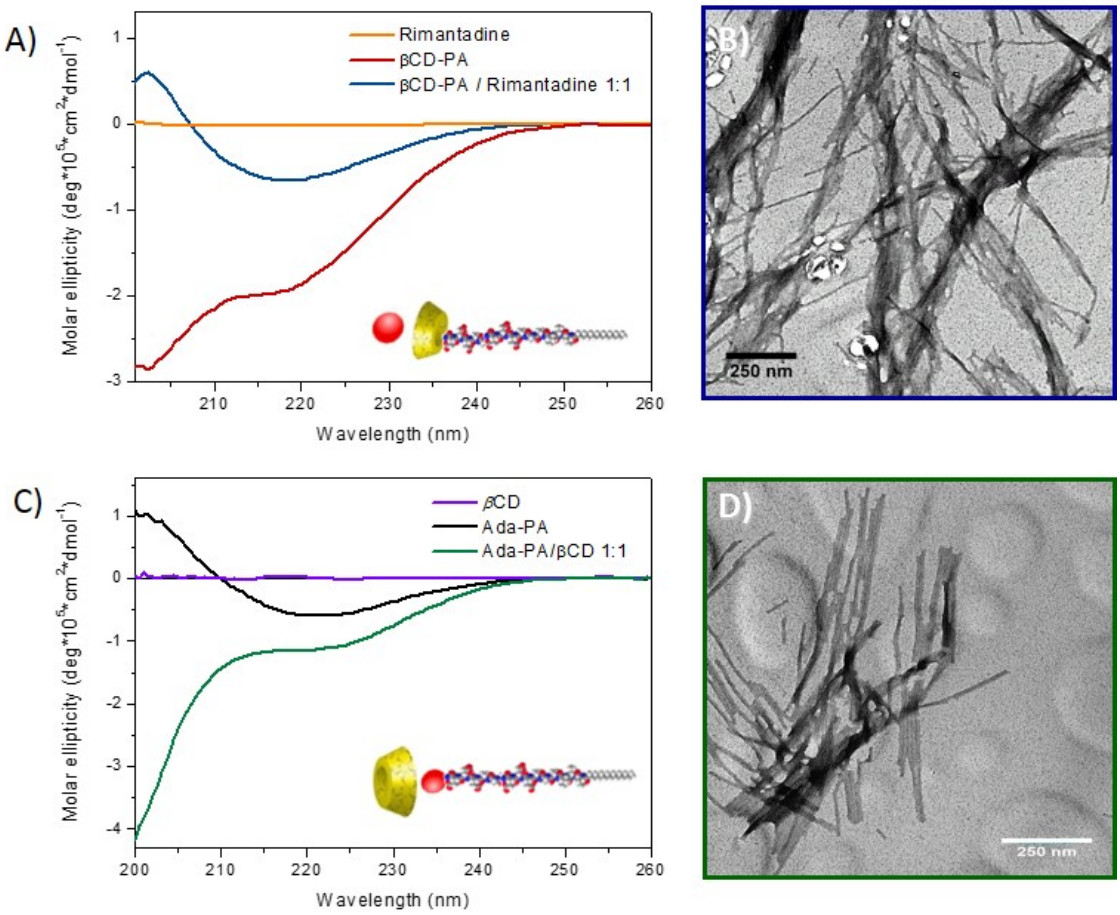

Figure 4.15: *Noncovalent decoration of **K_3G_3-βCD-PA** and **K_3G_3-Ada-PA** fibers with complementary host/guest motifs in HEPES buffer. A) Circular dichroism (CD) spectra of an equimolar mixture of **K_3G_3-βCD-PA** and rimantadine and B) transmission electron microscopy (TEM) micrograph of the resulting nanofibers [38 μM, blue]. C) CD spectra of an equimolar mixture of **K_3G_3-Ada-PA** and **β-cyclodextrin**, and D) TEM micrograph of the resulting nanofibers [63 μM, green].*

These results suggest that host-guest complexations could be used as a tool to tune peptide conformations with little morphological alterations on their resulting self-assembled nanostructures. Moreover, this host-guest PA platform widens the possibility to decorate self-assembled peptide nanostructures with suitable complementary partners bearing bioactive motifs,[184,185] thus providing new modular assembly strategy of biomaterials with increasing complexity and functionality beyond traditional covalent approaches.

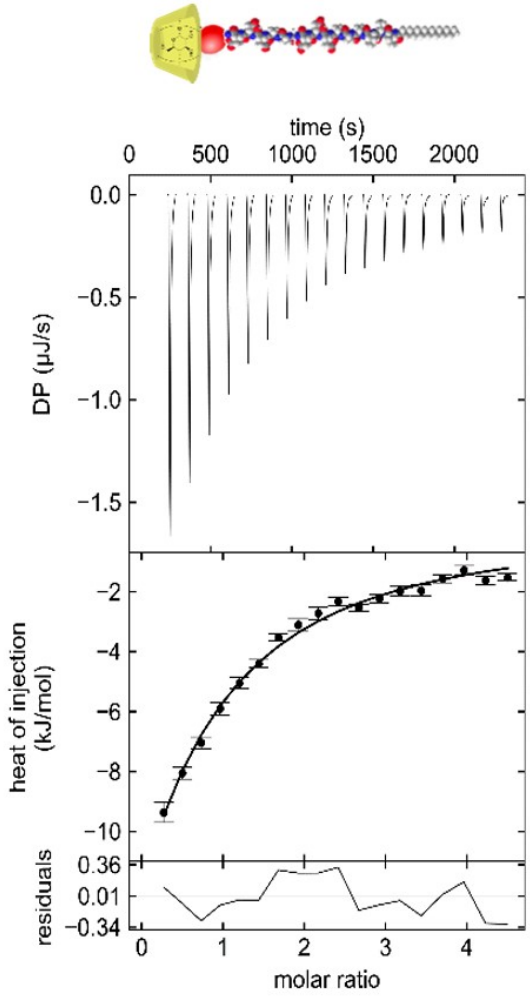

Figure 4.16: *ITC titration of* ***K_3G_3-Ada-PA*** *with* ***βCD*** *evidencing the formation of a 1:1 Host-Guest inclusion complex, [****K_3G_3-Ada-PA****] = 45 µM, [****βCD****] = 1050 µM, 19x20µL injections, T = 25ºC, HEPES buffer 10 µM.*

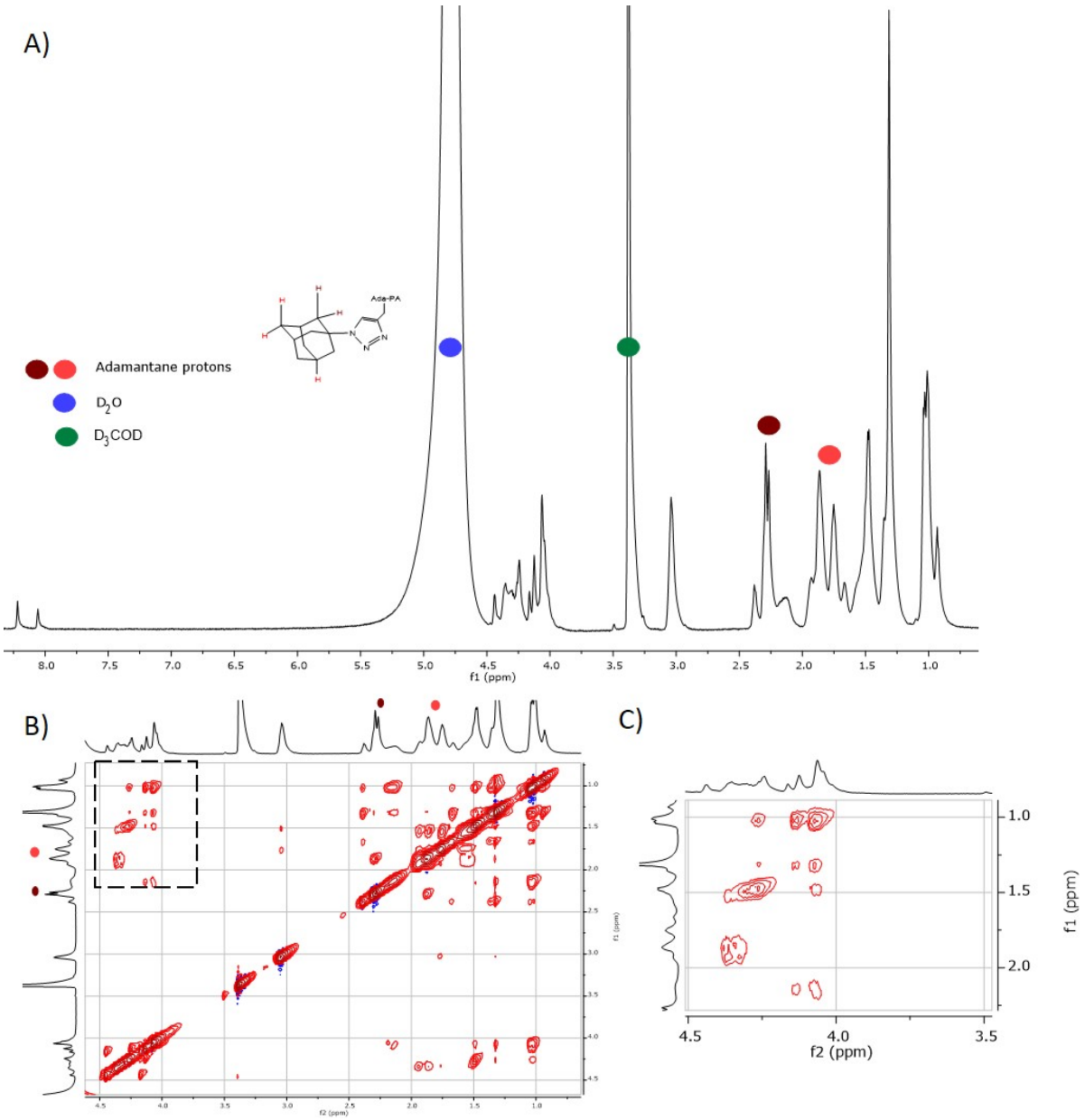

Figure 4.17: *NMR spectra corresponding to* ***K*$_3$*G*$_3$*-Ada-PA*** *and its complex with free β-cyclodextrin (β****CD****). A)* ^{1}*H-NMR and B) NOESY spectra corresponding to* ***K*$_3$*G*$_3$*-Ada-PA*** *(600 MHz, 7.5 mM, D*$_2$*O/D*$_3$*COD 2:1, 298 K). C) Zoom of the indicated region from panel B).*

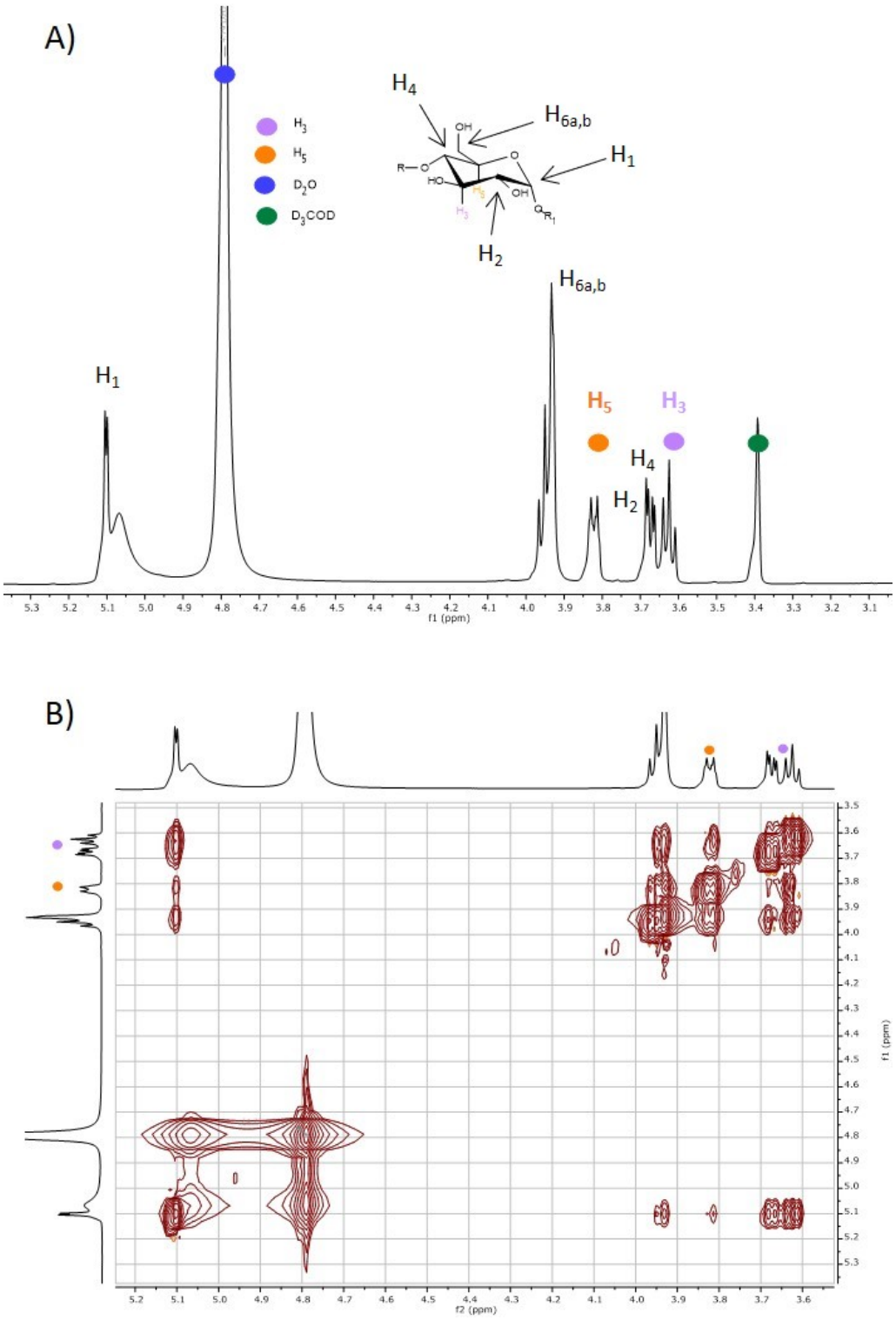

Figure 4.18: *A) ^{1}H-NMR spectrum corresponding to β-cyclodextrin (β**CD**) (600 MHz, 7.5 mM, D_2O/D_3COD 2:1, 298 K). B) NOESY spectrum of the same sample.*

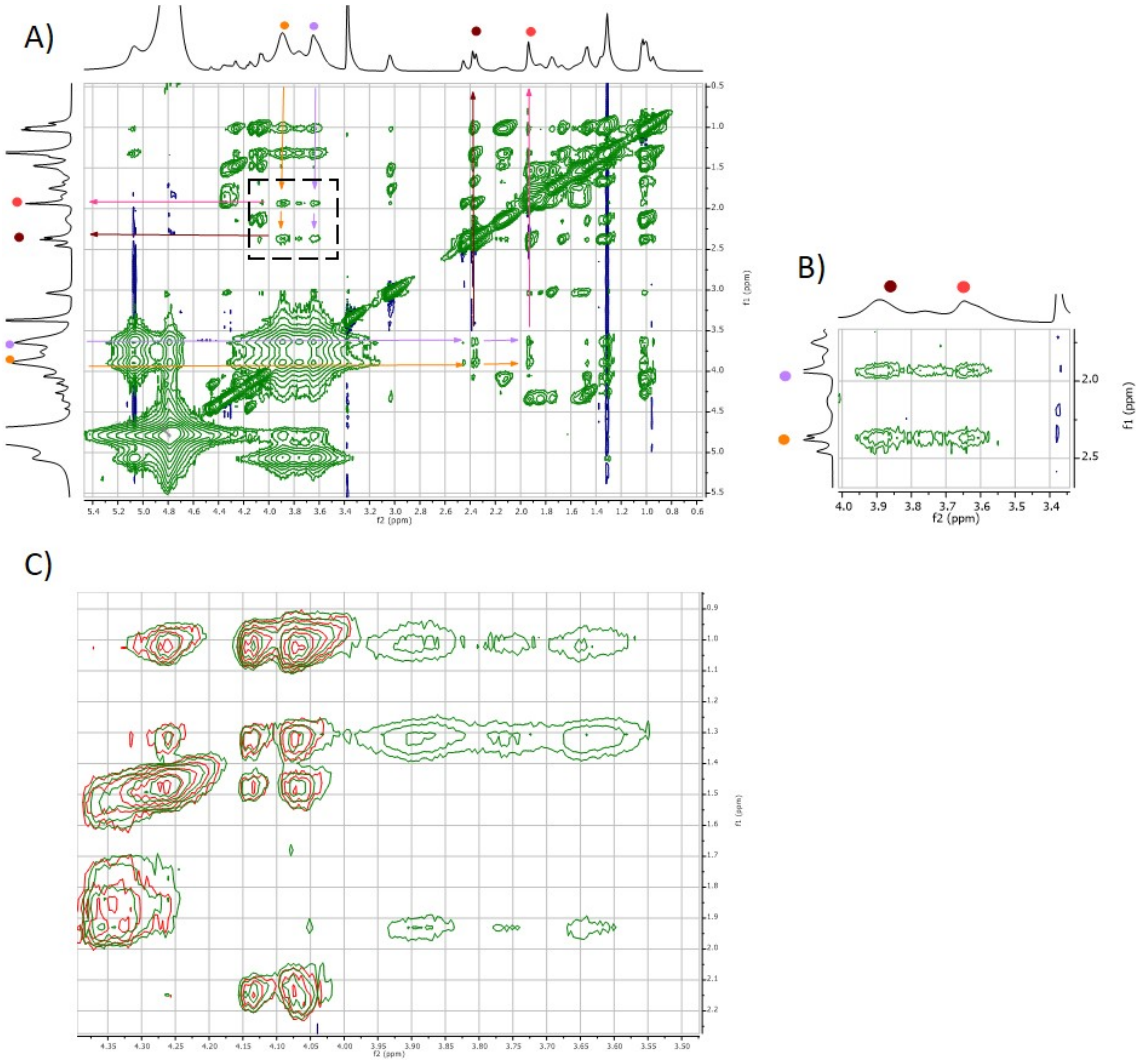

Figure 4.19: *A) NOESY spectra corresponding to* ***K_3G_3-Ada-PA*** *mixed with* ***(βCD)*** *(600 MHz, 7.5 mM each, D_2O/D_3COD 2:1, 298 K). B). G) Zoom of the indicated region from panel A). C) Superposition of panels 4.17.C (in red) and 4.19.B (in green) showing that the cross-peaks in green arise from the interaction between adamantane protons of* ***K_3G_3-Ada-PA*** *and H_3 (violet) and H_5 (orange) protons from* ***βCD****.*

4.6 K_3G_3-βCD-PA/K_3G_3-Ada-PA interaction

After confirming that both **K_3G_3-βCD-PA** and **K_3G_3-Ada-PA** can form inclusion complexes with their complementary standalone partners in solution, we proceeded to assess the noncovalent binding between these two host-guest PAs.

ITC titrations revealed that both **K_3G_3-βCD-PA** and **K_3G_3-Ada-PA** bind to each other following a 1:1 stoichiometry (N), exhibiting a dissociation constant (K_D) of 13.2 ± 4.4 μM as well as enthalpic, enthropic and free energy values similar to those of **K_3G_3-Ada-PA** titrated with free **βCD** (Figure 4.22, Table 4.3).[169,186]

NOESY experiments (Figure 4.21) revealed cross-peaks between the signals at 3.0 - 4.5 ppm assigned to the inner protons of **βCD** and the signals at 1.5 - 2.2 ppm assigned to **Ada**. Perhaps a word on the quality of these NOESY results is required. NOESY cross-peaks appear when two protons are in close proximity in space (less than 5 Å)[187] and their intensity largely depends on the tumbling rate of the originating molecule,[188] the slow tumbling of larger macromolecules or fixed aggregates in solution (like PA nanofibers) leads to faster relaxation of transverse magnetization thus complicating the recording of high-resolution NOE spectra.

A typical solution to this issue is to increase the overall molecular tumbling rate by recording NMR spectra at elevated temperatures.[188,187] Sadly, this possibility disrupts the host-guest interaction between **K_3G_3-βCD-PA** and **K_3G_3-Ada-PA** thus leading to obtaining no signal at all. In future NOESY experiments on PA systems it is suggested to use rotating frame experiments instead in order to increase the signal to noise ratio in the outcome spectra. In any case, both NOESY and ITC determinations point in the same directions: the allocation of **Ada** residues into the cavity of their complementary **βCD** motifs, resulting in the formation of the noncovalent **K_3G_3-βCD-PA•K_3G_3-Ada-PA** complex (Figures 4.20 & 4.21).[186]

CD spectroscopy confirmed that the noncovalent **K_3G_3-βCD-PA•K_3G_3-Ada-PA** complex exhibits different secondary structures in water and HEPES buffer, forming β-sheets and β-turn-like structures, respectively (Figure 4.22.B). This difference in conformation is expected, as isostructural systems to ours exhibit conformational transitions when ionic strength is increased.[101]

Nonetheless, TEM micrographs of equimolar mixtures of **K_3G_3-βCD-PA** and **K_3G_3-Ada-PA** demonstrated that their binding did not unsettle fiber formation (Figure 4.22.C-D), thus indicating that they can be incorporated into a PA hydrogel without compromising its fibrous structure.

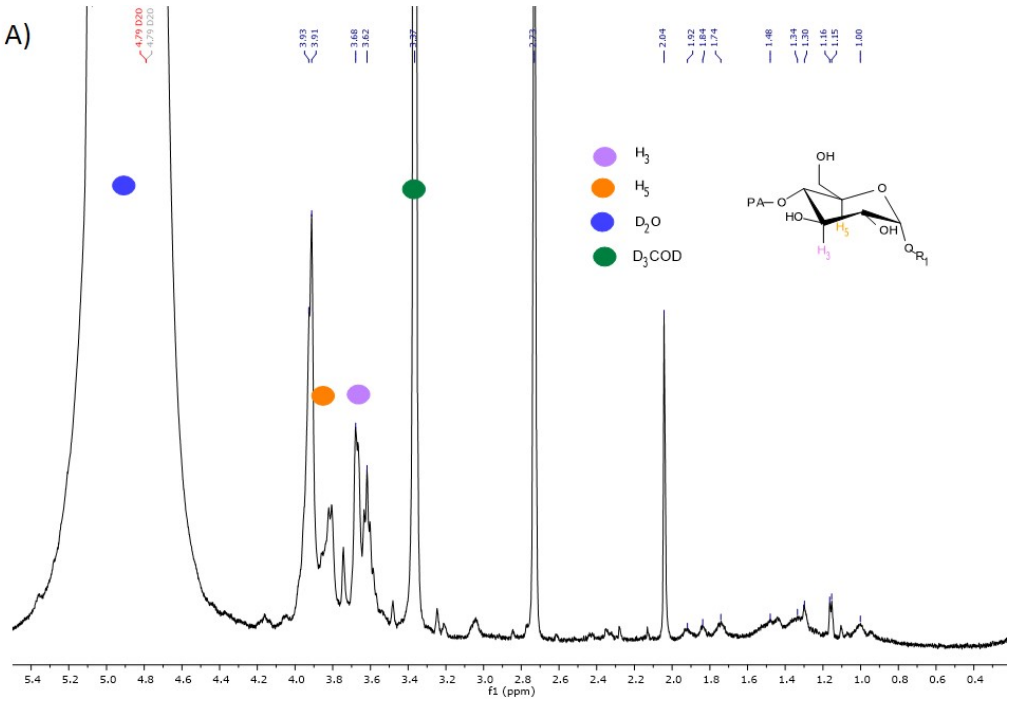

Figure 4.20: *A) ^{1}H-NMR spectra corresponding to **K_3G_3-βCD-PA** (600 MHz, 7.5 mM, D_2O/D_3COD 2:1, 298 K).*

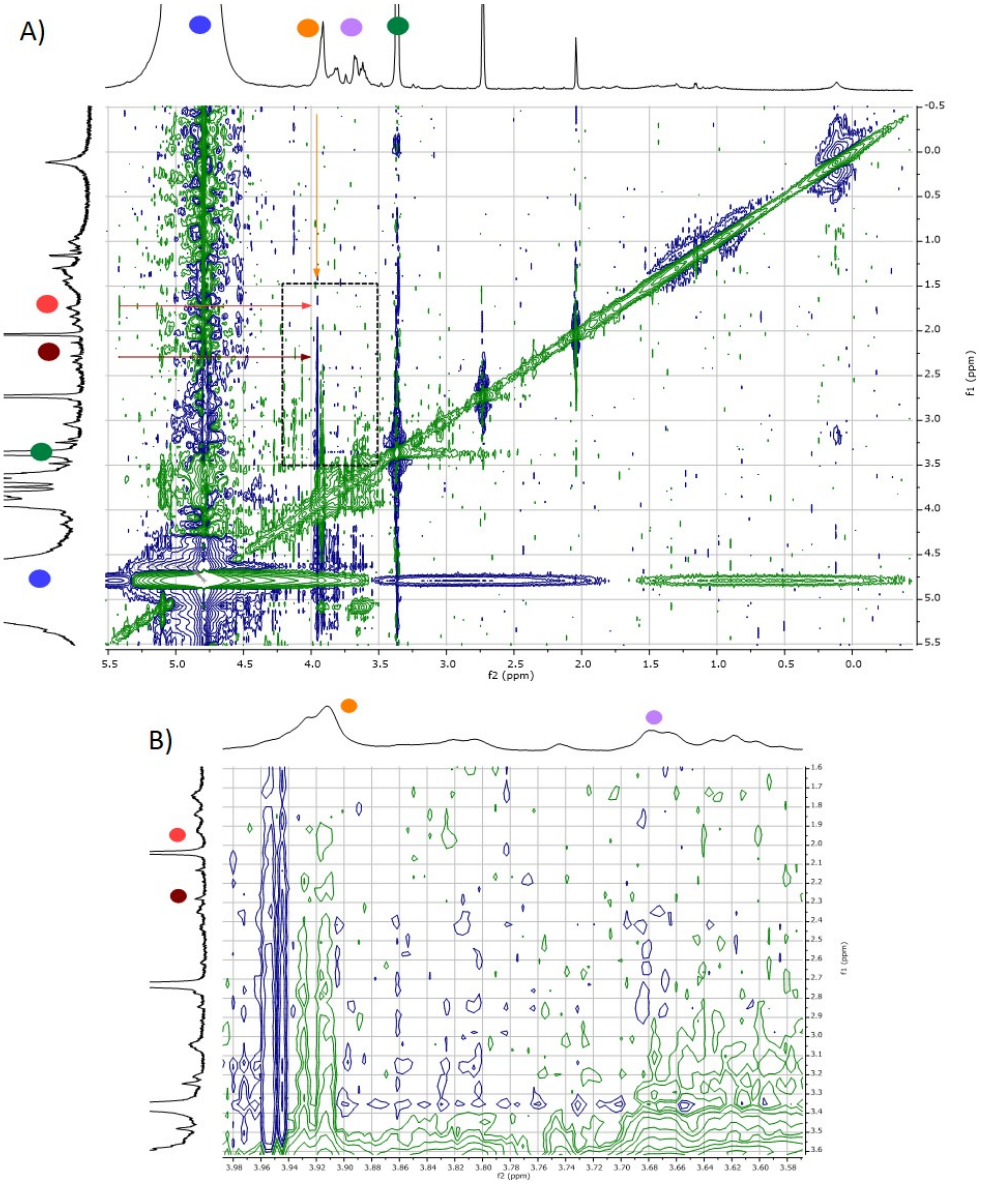

Figure 4.21: *A) NOESY spectra corresponding to* ***K*$_3$*G*$_3$*-Ada-PA*** *mixed with* ***K*$_3$*G*$_3$*-β**CD-PA*** *(600 MHz, 7.5 mM each, D_2O/D_3COD 3:1, 298 K). B) Zoom of the indicated region from panel A).*

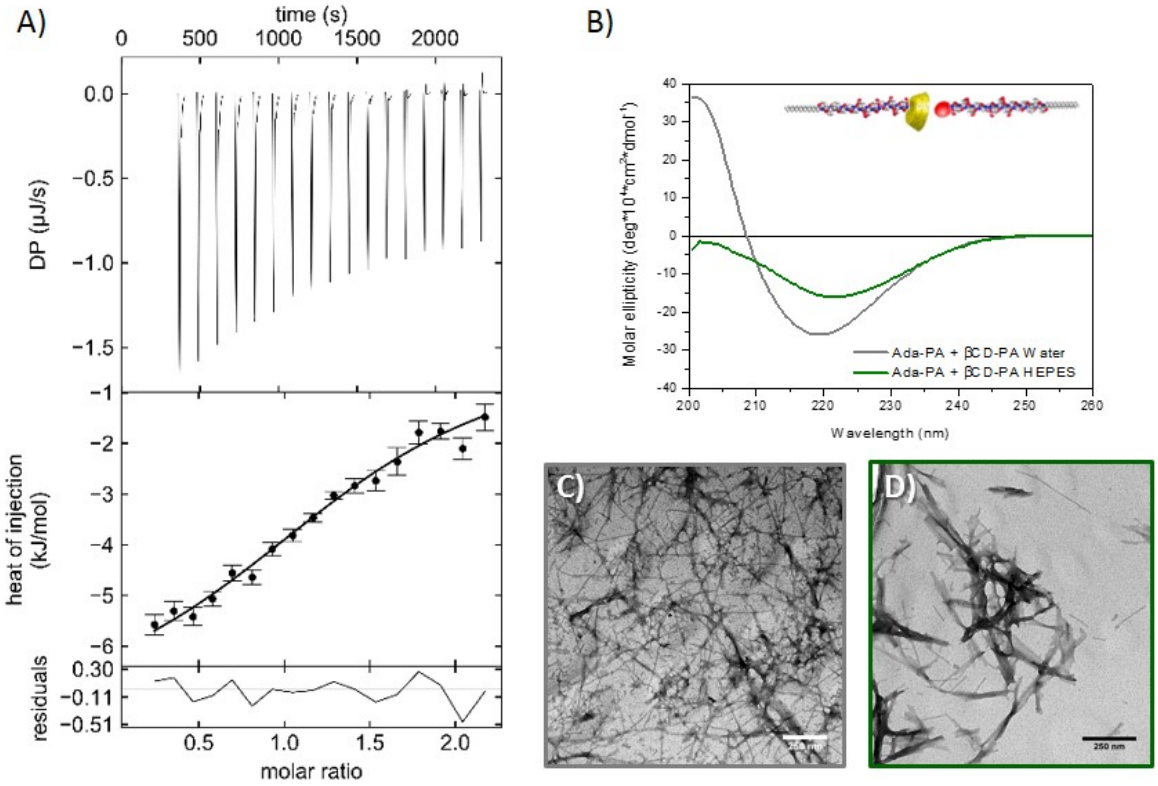

Figure 4.22: *Molecular binding between* ***K*$_3$*G*$_3$*-βCD-PA*** *and* ***K*$_3$*G*$_3$*-Ada-PA***. *A) Isothermal titration Calorimetry (ITC) titration of* ***K*$_3$*G*$_3$*-Ada-PA*** *with* ***K*$_3$*G*$_3$*-βCD-PA*** *evidencing the formation of a 1:1 host-guest inclusion complex ([****K*$_3$*G*$_3$*-Ada-PA***] = 75 µM, [****K*$_3$*G*$_3$*-βCD-PA***] = 600 µM, T = 25ºC, 19x10 µL injections). B) Circular dichroism (CD) spectra and transmission electron microscopy (TEM) micrographs of equimolar mixtures of* ***K*$_3$*G*$_3$*-Ada-PA*** *and* ***K*$_3$*G*$_3$*-βCD-PA*** *in C) water and D) HEPES buffer.*

4.7 K_3G_3-βCD-PA and K_3G_3-Ada-PA assemblies in hydrogels

A main objective of this study was to generate **K_3G_3-βCD-PA•K_3G_3-Ada-PA** complexes that would allow noncovalent tethering between PA-fibers, resulting in hydrogel networks with improved structural integrity. In order to provide further tunability of these tethering interactions, we self-assembled both **K_3G_3-βCD-PA** and **K_3G_3-Ada-PA** in presence of an excess of the cationic filler-PA **K_3-PA**, which permits control over the spacing and concentration of both **K_3G_3-βCD-PA** and **K_3G_3-Ada-PA**.

It is reported that heating **K_3-PA** solutions to 80 ºC and then gently cooling them down can lead to lengthening of subsequently self-assembled nanofibers.[98] Furthermore, scaffolds made from such longer PA fibers consist of long bundled fibers, that can lead to improved cell spreading and proliferation.[101,189] Consequently, mixtures of **K_3G_3-βCD-PA**, **K_3G_3-Ada-PA**, and an excess of **K_3-PA** were carefully prepared and thermally treated to obtain longer and more cytocompatible PA fibers (Figure 4.23.A).

SEM micrographs of hydrogels composed of **K_3-PA** and identical increasing content of **K_3G_3-βCD-PA** and **K_3G_3-Ada-PA**, revealed that the presence of the host-guest PAs caused neither phase separation in the resulting hydrogels nor disturbed the morphology or dimensions of the fibrillar nanostructures (Figure 4.23.B). This PA gel-forming network preservation in presence of **βCD/Ada** joints demonstrated the possibility to use them as interfiber cross-linking cues within a PA-hydrogel (Figure 4.23.C).

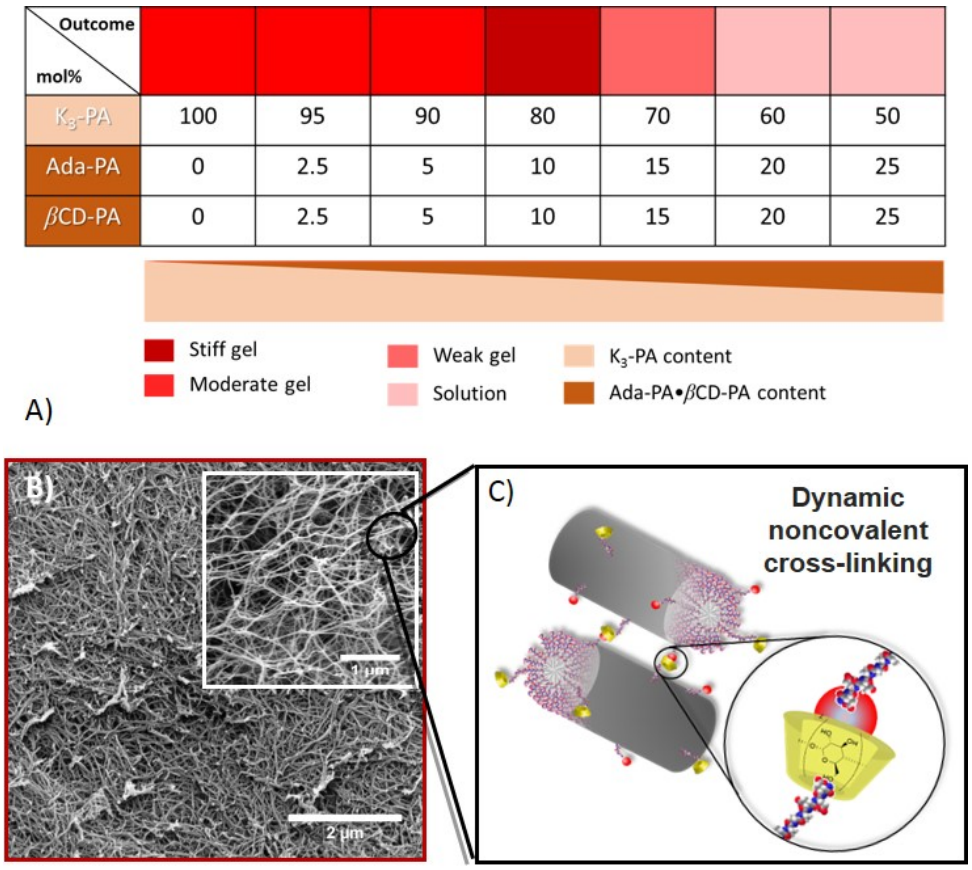

Figure 4.23: *Ternary co-assembly between* ***K*$_3$*-PA*** *and* ***K*$_3$*G*$_3$*-βCD-PA•K*$_3$*G*$_3$*-Ada-PA***. *A) Heat map showing the relative strength of different* ***K*$_3$*-PA/K*$_3$*G*$_3$*-βCD-PA/K*$_3$*G*$_3$*-Ada-PA*** *hydrogels. B) Scanning electron micrographs (SEMs) of a* ***K*$_3$*-PA/K*$_3$*G*$_3$*-βCD-PA/K*$_3$*G*$_3$*-Ada-PA*** *80:10:10 mol% hydrogel demonstrating the persistence of a fibrous network after the noncovalent binding of* ***βCD*** *and* ***Ada*** *motifs. C) Schematics illustrating the underlying host-guest interaction mechanism between PA nanofibers.*

4.8 K$_3$-PA/K$_3$G$_3$-βCD-PA•K$_3$G$_3$-Ada-PA hydrogel stiffness

Given these results, it was reasoned that **K$_3$-PA** gels containing increasing content of **K$_3$G$_3$-βCD-PA** and **K$_3$G$_3$-Ada-PA** would increase in stiffness as more interfiber binding takes place. To confirm this possibility, the stiffness and response to deformation of the hydrogels were assessed through dynamic rheology (see Section 2.3.3). Amplitude and frequency sweep experiments were used to quantify the storage modulus (G') and loss modulus (G") of **K$_3$-PA/K$_3$G$_3$-βCD-PA/K$_3$G$_3$-Ada-PA** 1 wt% hydrogels containing increasing fractions of host-guest PAs (90:5:5, 80:10:10, and 70:15:15 mol%) (Figure 4.24 & 4.26).

Control **K_3-PA** hydrogels exhibited G' values of 2.8 ± 0.5 kPa while **K_3-PA/K_3G_3-βCD-PA/K_3G_3-Ada-PA** hydrogels displayed higher G' and G" values (Table 4.4, Figure 4.26).

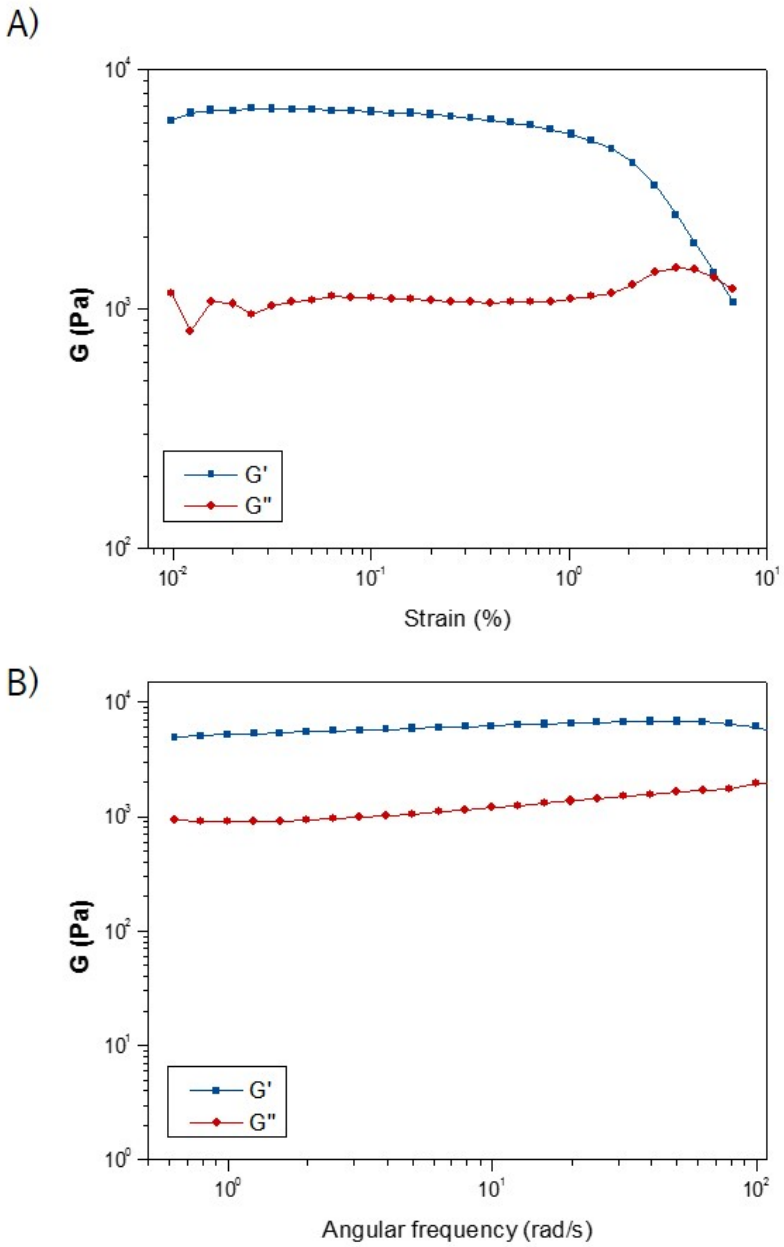

Figure 4.24: *A) Oscillatory strain and B) oscillatory frequency sweeps of a representative ternary **K_3-PA/K_3G_3-βCD-PA/K_3G_3-Ada-PA** 70:15:15 mol% gel (1 wt%).*

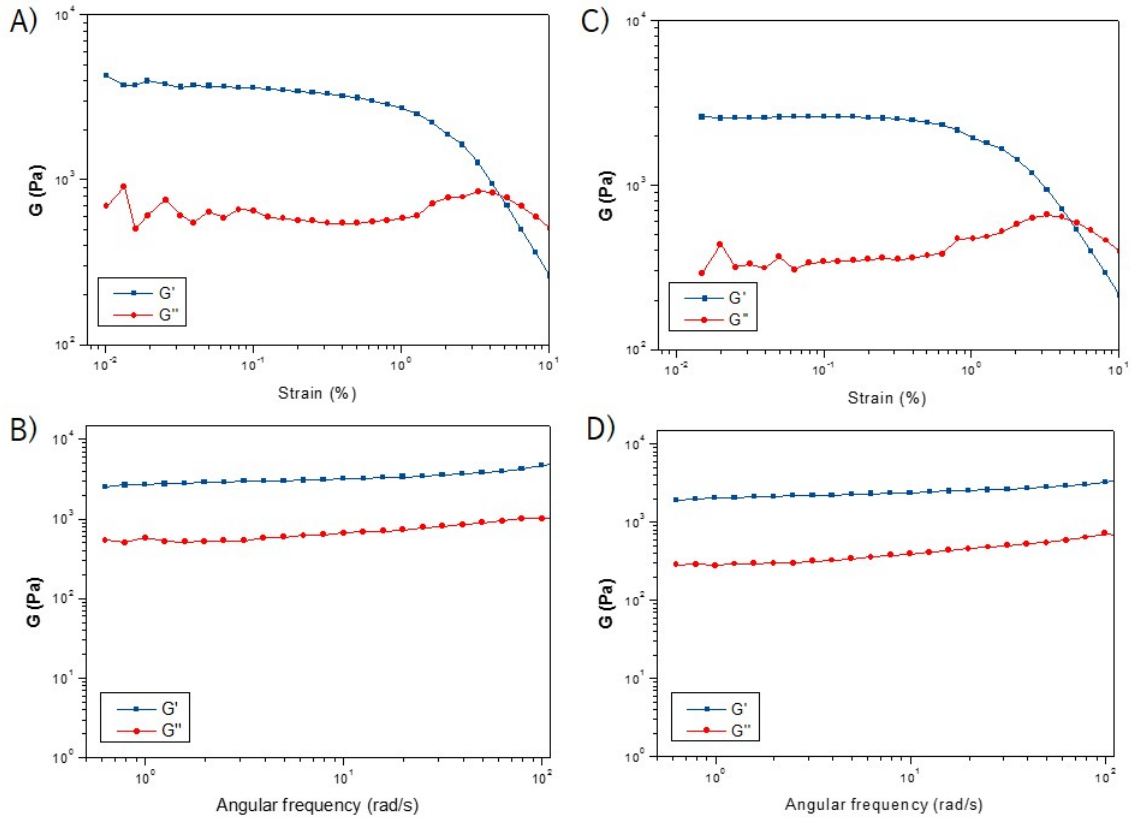

Figure 4.25: *A) Oscillatory strain and B) oscillatory frequency sweeps of a binary* ***K*$_3$-PA/K$_3$G$_3$-βCD-PA** *70:30 hydrogel (1 wt%). C) Oscillatory strain and D) oscillatory frequency sweeps of a binary* ***K*$_3$-PA/K$_3$G$_3$-Ada-PA** *70:30 hydrogel (1 wt%).*

Table 4.4: Storage (G') and loss (G") moduli of hydrogels with increasing concentration of **K$_3$G$_3$-βCD-PA•K$_3$G$_3$-Ada-PA** host-guest pair [∀]

K$_3$-PA/K$_3$G$_3$-βCD-PA•K$_3$G$_3$-Ada-PA ratio (mol%)	**G'** (Pa)	**G"** (Pa)
100:0:0	2806 ± 466	401 ± 80
90:5:5	4470 ± 1206	905 ± 270
80:10:10	5152 ± 880	1161 ± 247
70:15:15	3100 ± 575	756 ± 120

Note: [∀] ± S.D. n > 3.

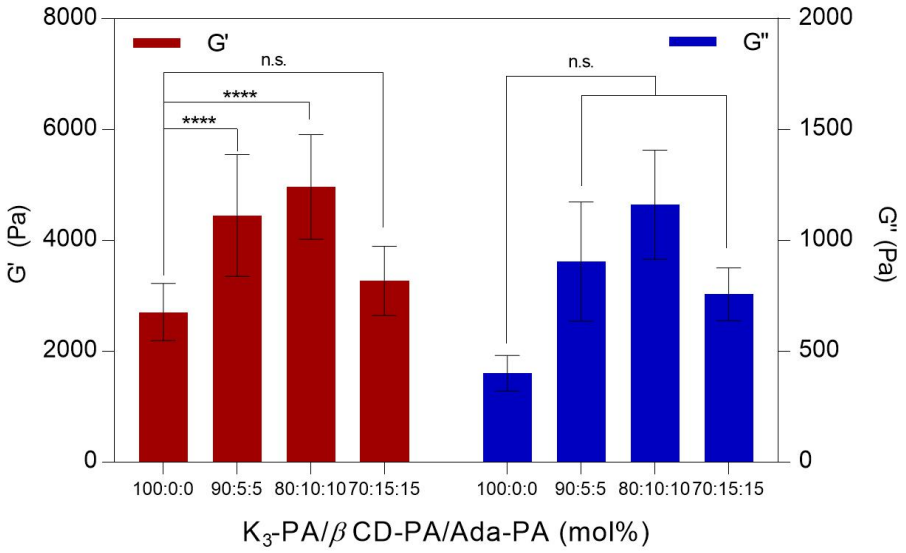

Figure 4.26: *Storage (G') and loss (G") moduli values of different* ***K_3-PA/K_3G_3-Ada-PA/K_3G_3-βCD-PA*** *hydrogels (1 wt%) determined by oscillatory rheology (see text, **** $p < 0.0001$, n.s. no significant difference, $n > 3$).*

Values for both G' and G" increased with the concentration of the **K_3G_3-βCD-PA•K_3G_3-Ada-PA** pair in the hydrogels, gel stiffness increased significantly (compared to control **K_3-PA** hydrogels) until reaching a maximum of 5.1 ± 0.8 kPa when the fractions of **K_3G_3-βCD-PA** and **K_3G_3-Ada-PA** were 10 mol% each (80:10:10 gels, $p < 0.0001$, $n > 3$, Table 4.4). Increasing **K_3G_3-βCD-PA•K_3G_3-Ada-PA** pair concentration above 20 mol% was detrimental for hydrogel stiffness.

Hydrogels containing **K_3-PA/K_3G_3-βCD-PA/K_3G_3-Ada-PA** 70:15:15 mol% exhibited a similar stiffness as **K_3-PA** control gels, while mixtures incorporating higher ratios of the host-guest pair than 70:15:15 mol% rendered only solutions in presence of the PBS gellator, most likely due to a decrease in nanofiber length (Figures 4.23.A and 4.26).

Nonetheless, neither **K_3-PA/K_3G_3-βCD-PA** nor **K_3-PA/K_3G_3-Ada-PA** binary hydrogels exhibited an increase in stiffness compared to control **K_3-PA** ones assembled at the same 1 wt% concentration (Figure 4.25). This suggests that the host-guest binding between nanofibers bearing **K_3G_3-βCD-PA** and those bearing **K_3G_3-Ada-PA** is likely responsible for the observed increase in stiffness in the ternary gels.

Other approaches aiming to modulate PA hydrogel stiffness rely on modification of their intrafiber hydrogen bonding network strength,[94] pH,[92] concentration,[92] covalent capture via hydrophobic domains,[122] covalent interfiber crosslinking[190] or mixing with other PAs,[191] proteins,[20,192] phospholipids,[193] and metal counterions.[194]

On the other hand, our non-covalent crosslinking approach allows for enhancing stiffness without altering other gel parameters such as peptide concentration and porosity. Besides these benefits, the integration of dynamic host-guest chemistry into supramolecular PA hydrogels allows for the possibility to engineer further temporal and morphological properties, which are relevant within cell environments and other therapeutically applications.[6]

4.9 Self-healing and resistance to degradation of ternary host-guest-PAs hydrogels

In addition to enhancing gel stiffness, we hypothesized that the precise and reversible nature of the host-guest interactions would elicit additional effects on the structural integrity of the **K_3-PA**/**K_3G_3-βCD-PA**/**K_3G_3-Ada-PA** hydrogels.

First, given the supramolecular and noncovalent nature of these materials,[92] we tested the self-healing and shear-thinning properties of the hydrogels by step strain measurements. When undergoing changes from large (100%) to small (0.10%) strain values, the hydrogels exhibited a reversible gel-sol transition and rapidly recovered up to 90% of their G' and G" after sheared for up to 4 cycles (Figure 4.27.B).

K_3-PA/**K_3G_3-βCD-PA**/**K_3G_3-Ada-PA** hydrogels proved to withstand more damage than control **K_3-PA** hydrogels under the same exhibited strain, but were also able to recover in a similar way to the control gels (Figure 4.27.B).

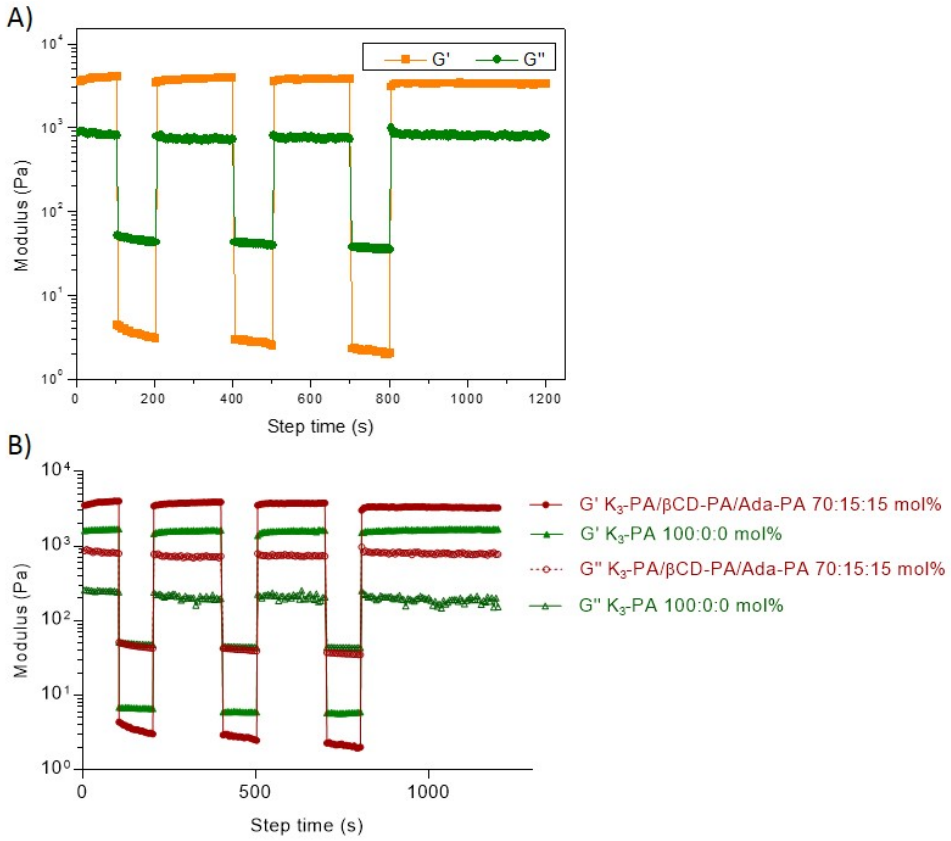

Figure 4.27: *Self-healing ability of host-guest PA hydrogels. A) G' (blue) and G" (red) of a* ***K*$_3$*-PA/K*$_3$*G*$_3$*-Ada-PA•K*$_3$*G*$_3$*-βCD-PA*** *80:10:10 mol% hydrogel in continuous step strain measurements (1 wt%, T = 25 ºC). Large strains (100 %) inverted the G' and G" values to render the sol state. On the other hand, G' was recovered under small strains (0.1 %) within less than 30 s. B) Continuous step strain measurements (creep and recovery) of control* ***K*$_3$*-PA*** *hydrogel (1 wt%, green traces) and* ***K*$_3$*-PA/K*$_3$*G*$_3$*-βCD-PA/K*$_3$*G*$_3$*-Ada-PA*** *70:15:15 mol% hydrogel (1 wt%, red traces).*

In addition, the effect of the host-guest motifs on the stability of the PA hydrogels upon degradation was tested. Gels when incubated in HEPES at 25 ºC and weight remaining ratios were monitored after exhaustive removal of buffer and determination of the residual hydrogel mass (see Section 4.12.16 for experimental details).[195]

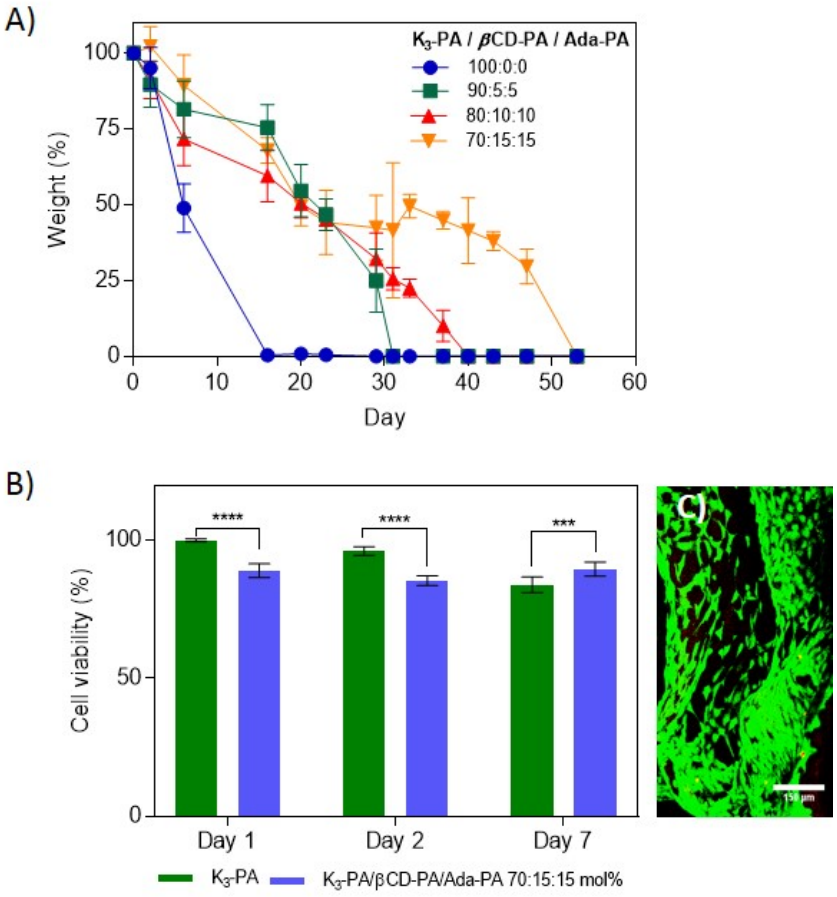

Figure 4.28: *Host-guest PA hydrogels behaviour under physiologically relevant conditions. A) Degradation profile of* ***K*$_3$*-PA/K*$_3$*G*$_3$*-Ada-PA/K*$_3$*G*$_3$*-βCD-PA*** *hydrogels in time. Weight remaining ratios of 90:5:5, 80:10:10 and 70:15:15 mol% hydrogels as well as* ***K*$_3$*-PA*** *control hydrogels are shown. B) Cell viability determinations of NIH-3T3 fibroblasts cultured atop* ***K*$_3$*-PA/K*$_3$*G*$_3$*-Ada-PA/K*$_3$*G*$_3$*-βCD-PA*** *70:15:15 mol% hydrogels (blue),* ***K*$_3$*-PA*** *gels were used as controls (green, 1 wt% in both cases) (**** $p < 0.0001$, *** $p < 0.001$, $n > 3$) C) LIVE-DEAD image from the host-guest based hydrogels at day 7 (green: calcein AM, alive cells; red: ethidium homodimer-1 (EthD-1), dead cells).*

The results indicate that 70:15:15 mol% **K$_3$-PA/K$_3$G$_3$-βCD-PA/K$_3$G$_3$-Ada-PA** hydrogels are able to withstand this buffer exchange process for up to 7 weeks before full degradation compared to **K$_3$-PA**, which completely degraded after 2 weeks time (Figure 4.28.A). It can be speculated that the host-guest interfiber tethering sites provide an additional anchoring force that confines individual PA molecules to the fibrillar hydrogel network, decreasing Fickian diffusion of free PA-monomers, thus slowing the rate of gel erosion.[196]

These results not only demonstrate that the **βCD/Ada** system enhances the stability of PA hydrogels by helping to preserve their structural integrity, but also allows for the tuning of their time-dependent properties, which could be of use when present in tissue regeneration and development sites.[6]

4.10 Biocompatibility of K_3-PA/K_3G_3-βCD-PA•K_3G_3-Ada-PA hydrogels

To assess the potential of our modified PA hydrogels to be used in biological applications, NIH-3T3 fibroblasts were cultured atop either **K_3-PA/K_3G_3-βCD-PA/K_3G_3-Ada-PA** or **K_3-PA** control hydrogels for up 7 days. Cells attached and exhibited a spread morphology on both hydrogel systems after two days of culture (Figures 4.28.B & 4.30), and cells seeded atop **K_3-PA** control gels showed higher viability at this point.

However, on day 7, cells growing atop ternary **K_3-PA/K_3G_3-βCD-PA/K_3G_3-Ada-PA** hydrogels exhibited higher viability (89.6 ± 2.6 %) compared to cells growing on **K_3-PA** controls (83.9 ± 2.8 %) (Figure 4.28.B). We speculate that the host-guest motifs play a role in partially screening the positive charges from the cationic nanofibers, in fact, NIH-3T3 fibroblasts viability assays in solution showed higher cell survival in **K_3G_3-βCD-PA** than **K_3-PA** (Figure 4.29).

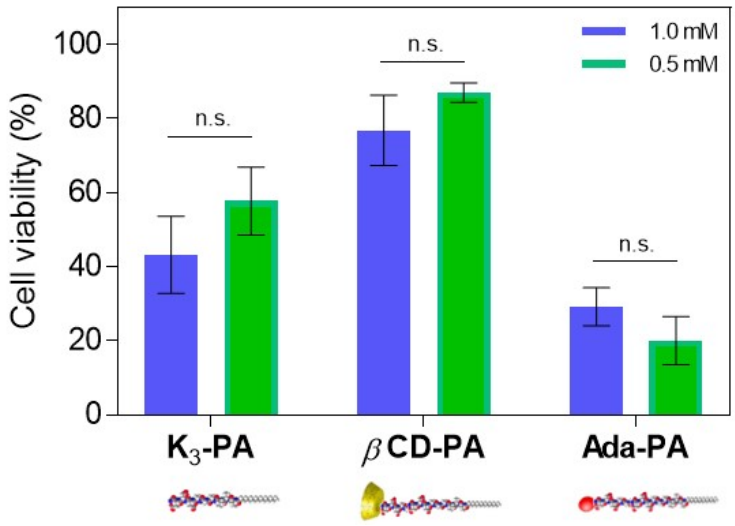

Figure 4.29: *NIH-3T3 fibroblasts monolayer LIVE-DEAD assay after culture in 1.0 mM and 0.5 mM **K_3-PA**, **K_3G_3-Ada-PA** and **K_3G_3-βCD-PA** solutions.*

Also, the noncovalent interfiber binding leads to obtaining stiffer hydrogels, which could promote the expression of mechanosensitive proteins.[161] It is possible that this observed increased cell viability observed in our **K_3-PA/K_3G_3-βCD-PA/K_3G_3-Ada-PA** hydrogels after 7 days of culture results from a stiffer gel as a result of our host guest interaction, studies have reported an effect on increasing cell viability as a result of matrix stiffness.[197] It is noteworthy

that our approach enables an increase in stiffness without affecting nanofiber density (as total amount of self-assembling PAs remain constant), therefore, network crosslinking and cell microenvironments shall remain similar to those of conventional **K_3-PA** gels, in terms of cell nutrient access, gas exchange and other physiological parameters.

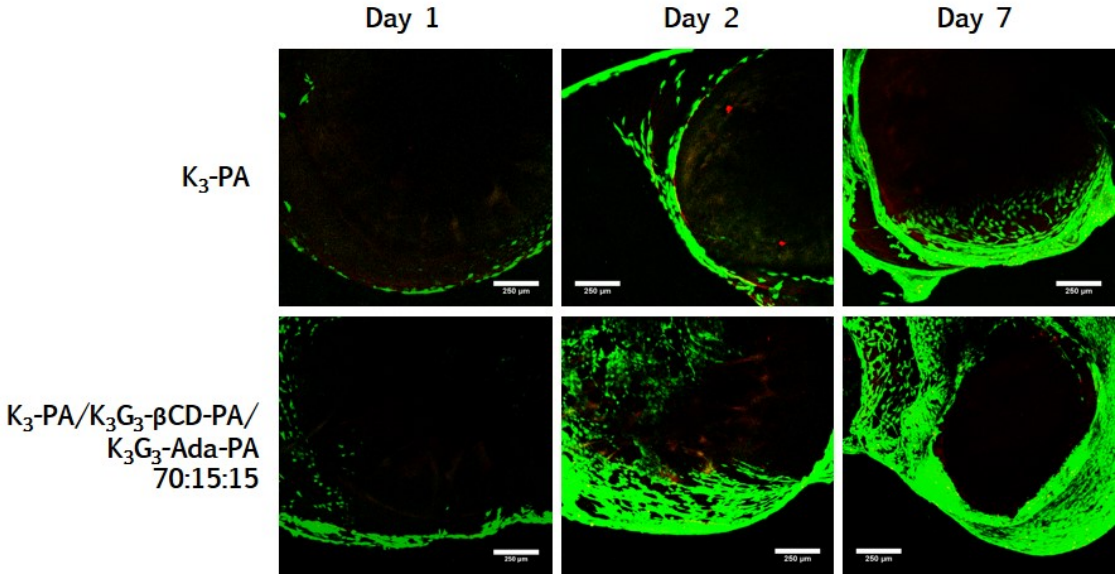

Figure 4.30: *NIH-3T3 fibroblasts LIVE-DEAD assay (green: calcein AM, alive cells; red: ethidium homodimer-1 (EthD-1), dead cells) after culture onto* ***K_3-PA/K_3G_3-Ada-PA•K_3G_3-βCD-PA*** *70:15:15 mol% and* ***K_3-PA*** *1 wt% hydrogels.*

This capacity could have a significant effect on cell function, for instance cell differentiation.[3] Taking advantage of the capacity to modulate supramolecular hydrogel properties as a result of our host-guest approach, further optimisation of the hydrogel stiffness would be possible, but it might depend on specific cell type behaviours and therapeutic use.

It is noteworthy that when cells were embedded within the hydrogel materials, a significant decrease in viability was observed in both **K_3-PA/K_3G_3-βCD-PA/K_3G_3-Ada-PA** and **K_3-PA** control hydrogels. This effect is likely a result of the positively charged PAs used, as it is well-known that cationic peptides cytotoxicity can be tuned.[189,112]

4.11 Closing remarks

In this study, we report on the synthesis, supramolecular aggregation, and structural improvement of a new family of PA hydrogels based on the dynamic noncovalent binding of β**-CD** and **Ada** motifs. Through this approach, we aim to develop a robust and versatile noncovalent cross-linking strategy for peptide-based biomaterials. The work validated the possibility to incorporate host-guest binding motifs on self-assembling PA molecules to generate hydrogel biomaterials with enhanced stiffness and structural integrity without altering parameters such as total peptide concentration.

To validate the applicability of the biomaterial, we showed that the system can be assembled with different PA molecules and serve as substrates for in vitro cell-culture. The study described in this chapter demonstrates that host-guest interactions represent an attractive and viable tool to not only improve mechanical and structural features in PA-based hydrogels, but also to further incorporate dynamic guests and structural complexity levels of PA hydrogels. The system may find applications in the development of novel therapies for disease and regenerative medicine.

In the next chapter, the design and selection process of a host-guest PA-peptide pair able to exhibit bioactivity via non-covalent co-assembly are presented.

4.12 Materials and methods

4.12.1 Peptide synthesis and characterisation

Conventional PA synthesis

PAs were synthesised using 4-methylbenzhydrylamine (MBHA) Rink Amide resin (0.52 mmol/g, Novabiochem Corporation, UK).

MBHA resin functionalisation

In the case of **K_3G_3-βCD-PA** and **K_3G_3-Ada-PA** the resin was bromoacetylated and functionalised with propargylamine following the peptoid synthesis solid phase submonomer method.[198]

Resin bromoacetylation was carried out as follows (Figure 4.31): In a dry and Argon flushed reactor 10 equivalents of bromoacetic acid **1** and **5** equivalents of N,N'-diisopropylcarbodiimide (DIC) were dissolved in 5 mL of dry DCM, the mixture was stirred for 30 min and then transferred to another vessel containing previously DCM swollen and Fmoc deprotected resin.

The mixture was shaken for 2 h, filtered off, washed with DCM and DMF x4. The resin-bound bromide **5** was then displaced with propargylamine (10 equivalents in 5 mL of DMF), shaken for 8 h at room temperature, filtered and washed three times with DMF, methanol, chloroform and diethyl ether respectively. In this fashion, propargylated MHBA resin **6** was afforded (Figure 4.31).

Synthesis of Host-PAs

For the synthesis of **K_3G_3-βCD-PA**, propargylated resin **6** was loaded in an automated peptide synthesiser (CS Bio, USA), solid phase peptide synthesis (SPPS) couplings were performed using four equivalents of Fmoc-protected amino acids (Novabiochem Corporation, UK), four equivalents of 1-hydroxybenzotriazole (HOBT, Carbosynth Limited, UK) and six equivalents of N,N'-diisopropylcarbodiimide (DIC, Sigma–Aldrich, UK), Fmoc deprotections were performed with 20% piperidine (Sigma-Aldrich, UK) in DMF (Figure 4.31).

Following Fmoc removal from the N-terminus the palmitoyl tail was manu-

ally conjugated using four equivalents of palmitic acid (Calbiochem, UK), four equivalents of HOBT, six equivalents of DIC in DMF/DCM 2:3 until negative for Kaiser Test, tail-coupled peptide **8** was afforded in this fashion.

6-Monodeoxy-6-monoazido-beta-cyclodextrin (N_3-βCD) was prepared as reported[199,200] and clicked to the PA backbone using a copper(I)-catalised azide-alkyne cycloaddition (CuAAC) procedure as reported in literature.[201]

Cleaving of the crude **K_3G_3-βCD-PA** product from the resin was carried out using a mixture of TFA (Sigma-Aldrich, UK)/triisopropylsilane (TIS, Alfa Aesar, UK)/water (95:2.5:2.5) for 3 h at room temperature, solvent was removed in vacuo allowing the precipitation of the peptide **9**: **K_3G_3-βCD-PA** using diethyl ether at -20ºC.

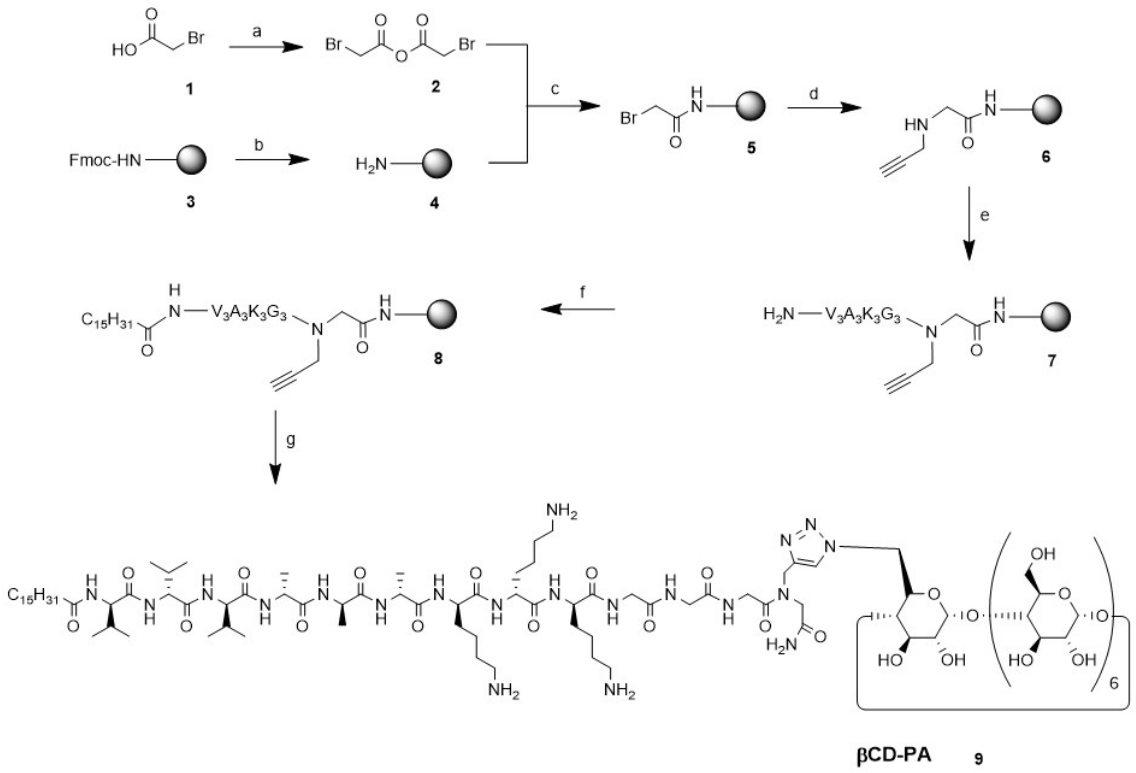

Figure 4.31: *Synthetic route followed for the preparation of **K_3G_3-βCD-PA**. a) Bromoacetic acid 10 eq., DIC 5 eq., DCM, r.t., 30 min. b) MHBA resin, piperidine 20% in DMF, r.t., 15 min. c) DCM, r.t., 2 h. d) Propargylamine 20 eq., DMF, r.t., 8 h. e) SPPS. f) Palmitic acid/HOBT/DIC 4:4:6 in DMF/DCM 2:3, r.t., 3 h. g) 1. CuBr/ascorbic acid/N_3-βCD in DMF/acetonitrile, DIPEA, 2,6-lutidine, r.t., 8 h; 2. TFA/TIPS/Water, r.t., 3 h.*

Synthesis of Guest-PAs

The synthesis of **K_3G_3-Ada-PA** (Figure 4.32) firstly involved the clicking of the propargylated resin **6** with 1-azidoadamantane to afford the triazole **10**, fur-

ther Fmoc SPPS, alkyl tail coupling and cleaving operations were performed as described above to afford the adamantane peptide **12**: **K_3G_3-Ada-PA** (Figure 4.32). Copper traces were removed using an alumina flash column in both host-guest PAs before undergoing further chromatographic purification.

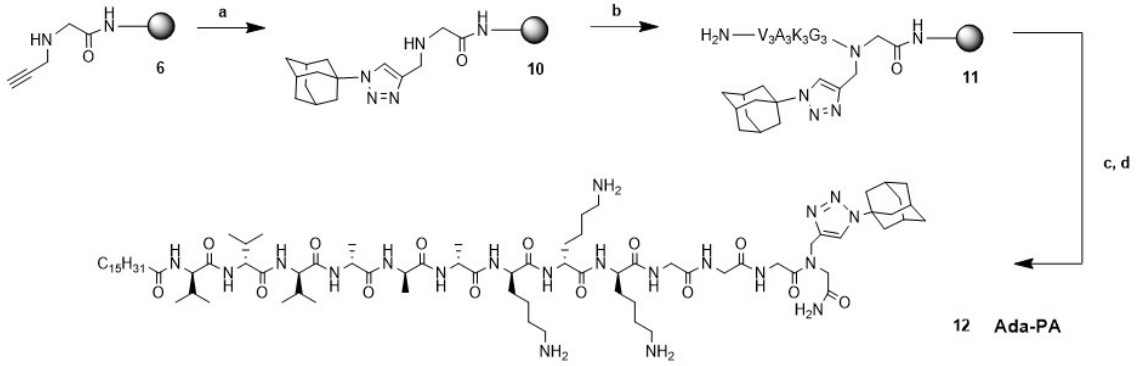

Figure 4.32: *Synthetic route followed for the preparation of **K_3G_3-Ada-PA**. a) CuBr/ascorbic acid/1-azidoadamantane in DMF/acetonitrile/DCM, DIPEA, 2,6-lutidine, r.t., 8 h. b) SPPS c) Palmitic acid/HOBT/DIC 4:4:6 in DMF/DCM 2:3, r.t., 3 h. d) TFA/TIPS/Water, r.t., 3 h.*

4.12.2 Peptide purification and characterisation

Purification of all peptides was carried out through Reverse Phase High-Performance Liquid Chromatography (HPLC) using a 2545 Binary Gradient Preparative HPLC (Waters, USA), a C18 column (Atlantis Prep OBD T3 Column, Waters, USA) and a gradient of 2-100% acetonitrile in water (0.1 v/v% TFA) over 40 min. Detection was carried out concomitantly with 2489 UV/Visible and an electrospray ionisation mass spectrometer detector (ESI-MS) (Waters, USA). Peptide purity was determined by analytical HPLC as well as ESI-MS (Thermo LXQ, Thermo Scientific, USA) and matrix assisted laser/desorption ionisation-time of flight mass spectrometry (MALDI-TOF, Applied Biosystems 4800 Proteomics Analyzer (TOF/TOF)). TFA traces in all the peptides was exchanged for HCl and removed in vacuo, followed by extensive dialysis against deionized water using 100- 500 Da MWCO dialysis tubing (Spectrum Europe B.V., The Netherlands).

4.12.3 β-Cyclodextrin-Gold nanoparticles synthesis

The protocol reported by Shi and co-workers was followed with no further modifications in order to synthesise βCD-AuNPs.[183]

4.12.4 Circular dichroism (CD)

The secondary structure of the PAs was assessed using CD. Peptides were dissolved in water or 4-(2-hydroxyethyl)piperazine-1-ethanesulfonic acid (HEPES) 10 mM saline (155 mM NaCl pH 7.4) at a final concentration of 0.01 wt%, then measured as soon as possible using a 1 mm path-length quartz cuvette in a Pistar-180 spectropolarimeter (Applied Photophysics, Surrey, UK) equipped with a Peltier temperature controller, under a constant nitrogen purging at a constant pressure of 0.7 MPa and temperature of 25 °C. Far UV spectrum were recorded from 190 to 270 nm a wavelength step of 0.5 nm. Each represented spectrum is the average of three consecutive spectra. Temperature variable CD experiments were carried out between 10 ºC and 70 ºC, with a heating rate of 1 ºC/min, and collecting a spectrum every 10 ºC.

4.12.5 Transmission electron microscopy (TEM)

PA 0.05 wt% aqueous solutions were imaged after a negative staining treatment. PA samples were drop casted on holey carbon-coated copper TEM grids (Agar Scientific, Stansted, UK), after 5 minutes incubation, solution excess was removed before incubation with 2 w/v% uranyl acetate for one minute, grids were then washed with ultrapure water for 30s and air dried for 24h at room temperature before imaging. Bright-field TEM imaging was performed on a JEOL 1230 Transmission Electron Microscope operated at an acceleration voltage of 80 kV. All the images were recorded by a Morada CCD camera (Image Systems) and at least six areas were analysed (corresponding to $n \geq 100$ PA fibers).

4.12.6 Scanning electron microscopy (SEM)

PA hydrogels were stepwise dehydrated by immersion in increasingly concentrated ethanol solution (25%, 50%, 70%, 80%, 90%, 95%, 100%), for 5 min twice in each solution. Dehydrated samples were dried using a critical point dryer (K850, Quorum Technologies, UK) and gold coated before imaging on an Inspect F50 (FEI Company, the Netherlands) ($n \geq 5$).

4.12.7 Zeta potential (ζ)

PAs were dissolved in MilliQ water, pH values were adjusted by addition of HCl or NH_4OH, transferred to polycarbonate folded capillary cells where zeta potential measurements were taken in triplicate at 25 °C from pH 3 to 12 using a Zetasizer (Nano-ZS ZEN 3600, Malvern Instruments, UK).

4.12.8 Isothermal titration calorimetry (ITC)

ITC experiments were performed at 25 °C using a MicroCal PEAQ-ITC microcalorimeter (Malvern-Panalytical, UK). PA solutions were prepared in previously filtered 10 mM HEPES buffer, pH 7.4. On a typical experiment 19 injections of 2.0 μL titrant were titrated into the sample cell over 2 s with a stirring speed of 750 rpm and 120 s separation to ensure thermal equilibration. Data were baseline adjusted by subtracting background data obtained from equivalent injections of titrant into the buffer solution. The titration curves were analyzed using the integrated public-domain software packages NITPIC, SEDPHAT and GUSSI.[202,203]

4.12.9 Nuclear magnetic resonance (NMR)

Mixtures of **K_3G_3-Ada-PA** and **K_3G_3-βCD-PA** were prepared in D_2O/CD_3OD reaching a final concentration of 10-12 mg/mL. Two dimensional NOESY NMR spectra were recorded on a Bruker AvanceNEO 600 spectrometer at 298 K.

4.12.10 Thermogravimetric analysis (TGA)

A TA Instruments Q500 Thermogravimetric Analyzer was used to acquire βCD-AuNPs thermograms, temperature programs were followed as described by Shi and co-workers.[183]

4.12.11 Ultraviolet-visible spectroscopy (UV-Vis)

A Perkin Elmer Lambda 35 UV-Vis spectrometer (double-beam, wavelength range 190 - 1100 nm) was used to acquire βCD-AuNPs absorption spectra.

4.12.12 Hydrogel preparation

PAs were dissolved in either water or HEPES buffer, mixed according to the desired **K_3-PA**/**K_3G_3-βCD-PA**/**K_3G_3-Ada-PA** ratio, incubated at 80 °C for 30 min and let slowly cool down to room temperature, then a 30 μL drop was placed onto a polydimethylsiloxane (PDMS) support, injected 15 μL of PBS 0.1 M and incubated overnight at 25 °C to afford 1 wt% hydrogels in all cases.

4.12.13 Epifluorescence microscopy

An inverted epifluorescence widefield Leica DMI4000B microscope (Leica, Germany) equipped with a LEICA DFC300 FX CCD camera was used to visualize FITC (Cyclolab, Hungary) and Nile Red stained peptide aggregates. Peptide solutions were incubated with the fluorescent dye for 30 min at room temperature before imaging and FITC % Texas Red filters were employed.

4.12.14 Stiffness determinations

PA hydrogels rheological characterization was performed with a DHR-3 Rheometer (TA Instruments, USA) equipped with an 8 mm diameter parallel plates geometry. Rheological characteristics were monitored by amplitude sweep, frequency sweep, and the self-healing ability of the gels was assessed through creep-recovery tests. G' (storage modulus) and G"(loss modulus) were measured at 25 °C and a constant frequency of 1 Hz in the 0.01% – 10% strain during the amplitude sweep, while the oscillation frequency experiments were carried out at a 0.1% fixed strain along 0.1 – 100 Hz.

4.12.15 Creep-recovery tests

Creep-recovery tests were performed as follows: an initial 0.1% strain was held for the first 100s, then it was increased to 100% for 100 s, followed by a recovery segment of 0.1% stress for 100 s, the continuous step strains were switched within 200 s for every strain interval.

4.12.16 Hydrogel degradation

PAs gels were placed in suitable glass vials and incubated in HEPES buffer at 25 ºC. Gels degradation/erosion was determined as reported in literature (Figure 4.33).[195]

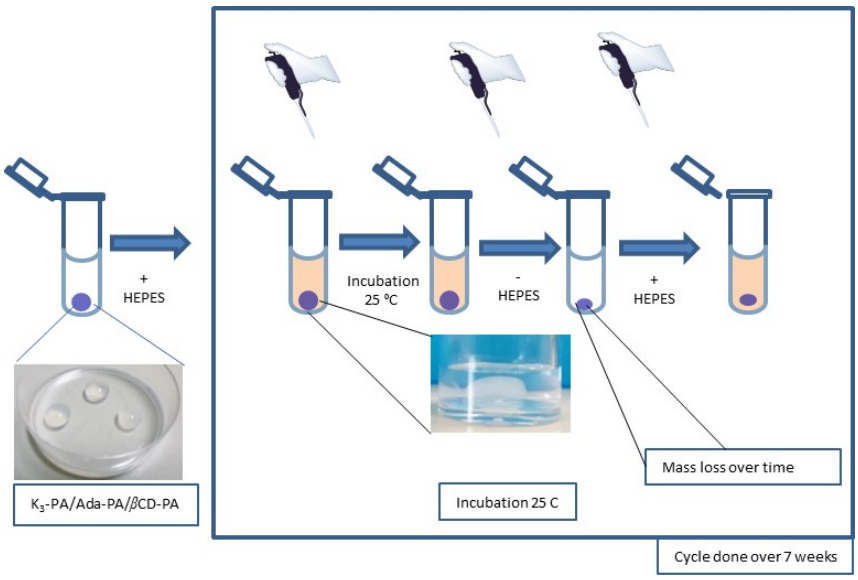

Figure 4.33: *Schematic showing the experimental set-up for degradation assessment of* ***K_3-PA/K_3G_3-βCD-PA/K_3G_3-Ada-PA*** *gels over time (n > 5).*

4.12.17 Cell culture experiments

NIH-3T3 fibroblasts were cultured in DMEM supplemented with 10% FBS and 1% P/S in a humidified incubator (37 °C, 5% CO_2).

4.12.18 Cell viability assays in solution

On a typical experiment 15 000 NIH-3T3 fibroblasts were seeded in a 96-well plate and cultured for 1 day until a monolayer was formed. Cells were incubated with a peptide solution of the desired concentration for 1 h. Peptide was then removed, cells were washed thrice with HBSS and placed with fresh DMEM medium and imaged the next day using the LIVE/DEAD Viability/Cytotoxicity Assay Kit (Thermo Fisher Scientific, UK). Cells were incubated in 10 mM Calcein AM and 1 mM ethidium homodimer-1 (EthD-1) DMEM medium for 30 min before imaging, stained samples were visualised on an inverted epifluorescence widefield Leica DMI4000B microscope (Leica, Germany) equipped with a LEICA DFC300 FX CCD camera.

4.12.19 Cell viability assays in surface cultures

On a typical experiment 5 μL of a 10 mM PA ternary mixture of **K_3-PA**/**K_3G_3-βCD-PA**/**K_3G_3-Ada-PA** (70:15:15) were injected within 50 μL of PBS gelling solution (typically 1 mM PA final concentration). After 30 minutes gelation the excess of PBS was removed and 30-50 000 NIH-3T3 cells were seeded onto the gels.

Gels were kept under orbital agitation for 1 h before static culture for 1, 2 and 7 days. In vitro cell viability was then assessed using the LIVE/DEAD Viability/Cytotoxicity Assay Kit (Molecular Probes), 30 min before imaging hydrogels were incubated in 10 mM Calcein AM and 1 mM ethidium homodimer-1 (EthD-1), stained samples were visualised on an inverted Confocal Laser Scanning Microscope (CLSM) (Leica Laser Scanning Confocal TCS SP2) along with the ImageJ Software (NIH, USA) for reconstructing the 3D images. Cell viability was measured as a ratio of calcein positive cells over total number of cells. All assays were done in at least triplicate.

Chapter 5

Host-guest Mediated Epitope Display on Anionic Peptide Amphiphile-based Hydrogels

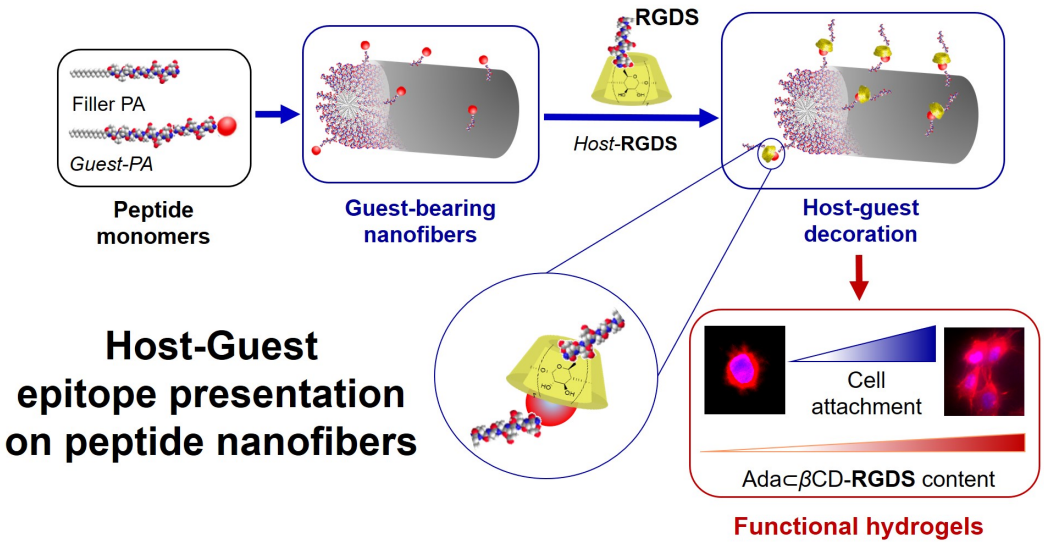

Figure 5.1: *Non-covalent display of RGDS motifs on self-assembled PA hydrogels.*

This chapter describes the ***β*CD/Ada** mediated display of RGDS cell-binding motifs on anionic PA nanofibers. Considerations on the molecular design are presented, followed by a supramolecular aggregation study, finishing with cell attachment studies that evidence the functionality of the gels.

This study will be submitted for publication to *ACS Biomaterials Science and Engineering*:

- **Redondo-Gómez, C.**; Padilla-Lopategui, S.; Azevedo, H. S.; Mata, A. Host-guest-mediated epitope presentation on self-assembled peptide amphiphile hydrogels. *To be submitted to ACS Biomaterials Science and Engineering*.

5.1 Overview

A key feature in biomaterial design is the incorporation of bioactive signals into artificial constructs in order to stimulate tissue regeneration. Most currently used hydrogel cell culture systems depend on the covalent attachment of ECM-derived cell adhesion peptides to either macromolecular units or to smaller self-assembling units, thereby restricting biosignal presentation and response to the static character dictated by their covalent binding to substrate. However, finding new ways to incorporate adhesion epitopes like those present in the on hydrogels would lead to different uses of these scaffolds in cell culture as well as new potential clinical applications.

In this chapter, it is shown that a more dynamic epitope presentation approach based mediated by host-guest interactions is possible. Using PA hydrogels it is demonstrated that the **Ada**/β**CD** pair can be used to tether **RGDS** cell adhesion signals to self-assembled hydrogels.

Hydrogel morphological and rheological behaviour are assessed as well as fibroblast attachment, organisation and spreading responses when cultured atop these scaffolds.

5.2 Introduction

Progress in supramolecular chemistry has led to growing control over molecular self-assembly and has provided a number of robust approaches to design biomaterials with increasing biomimicry, structural complexity and functionality.[204,31,28] As a consequence, remarkable examples of functional polymer,[205] sugar,[206] nucleic acid,[207] and protein-based[208] supramolecular systems have been reported.

Research on synthetic constructs for tissue engineering and regenerative medicine applications has evidenced the importance of mimicking morphological, mechanical aspects and presentation of biochemical cues and viscoelastic behaviour of the ECM.[4,21,66] Hydrogels succeed at featuring these characteristics,[7] thus have drawn attention as cell scaffolds for multiple in vitro and in vivo studies.[209,63,62]

As most hydrogel systems lack the intrinsic cell-binding properties of the ECM[82] functionalisation approaches with cell adhesion promoting peptides are a common strategy to improve biomimicry.[210] Even though dozens of cell adhesion peptides are known,[211] the staggering majority of reports deal with either IKVAV (a sequence found in laminin)[93,212] or RGD (found in fibronectin) as their interaction with integrin receptors and its subsequent signal transduction are well understood.[213] Although many hydrogels are based on polymeric fibrillar components,[214,32] self-assembling peptides like PAs have recently gained increasing attention as they often originate gels with viscoelastic and mass transport properties more similar to the native ECM than polymeric hydrogels do (see Section 2.4).[215,84,216,217]

Fibrillar hydrogels based on PAs have demonstrated promising capacities to emulated ECM characteristics.[96] The formation of nanofiber non-covalent networks rendering a high density of biofunctional epitopes is one of the features that turns PA constructs into highly functional platforms for tissue engineering applications,[98] encompassing cell migration[18,122] and differentiation[108] in vitro as well as in vivo regeneration of blood vessels,[218] cartilage,[127] axons,[123] and enamel.[219]

RGD-based sequences have been successfully incorporated into PA platforms for cell adhesion and cell delivery studies, including variations on linear,[219] branched or cyclic peptide[220] conformations, the presence of a spacer in the PA sequence,[115] epitope density along nanofiber axis[107] and hierarchical structuration of peptide constructs.[116] Research on alternative ways to present biofunctional epitopes like RGD on PA-based biomaterials might help to improve their design, construction and biomimicry capacities.

Host-guest interactions (like the inclusion complex formed between **βCD** and **Ada** motifs)[32,130] have traditionally been employed to modify physicochemical properties of polymer-based hydrogels (see Section 2.5),[82,221] for instance, a recent example by Luong and co-workers reports on pore reduction and variation of viscoelastic properties of RGD and GHK epitopes immobilised covalent poly-methacrylate-based cryogels via **Ada/βCD** binding.[222] Scarce efforts to incorporate host-guest phenomena into supramolecular hydrogels have been reported, like the **βCD**/**Ada** PA gels reported by Redondo-Gómez et al.,[155] (presented in Chapter 4) in which host-guest interactions drove stiffness modulation as well as increases resistance to degradation.

In this chapter the host-guest-mediated tethering of RGDS motifs to self-assembled PA nanofibers is reported as a strategy to improve biological epitope presentation and biomimicry of PA hydrogels. Firstly, the synthesis and characterisation of two anionic adamantane-bearing PAs is presented, then their ability to be incorporated into co-assembled nanofibers is explored from a spectroscopic and rheological point of view. Then, we choose the most suitable Ada-PA derivative to undergo non-covalent functionalisation with a complementary **RGDS-βCD** derivative, lastly, we assess the biological functionality of this binding via in vitro cell adhesion experiments.

5.3 Anionic Guest-Peptide Amphiphiles

5.3.1 Rationale and molecular design

The **Ada/βCD** inclusion complex was chosen to perform the non-covalent binding of epitopes on PA nanofibers because this host-guest pair is perhaps the best characterised and most used in host-guest literature (see Section 2.5).[130] As the presentation of Ada units at the surface of self-assembled PA nanofibers might be used as anchoring points for a variety of **βCD**-bearing binding motifs. The effect of covalent derivatisation of negatively charged PA molecules with **Ada** units was initially investigated, we designed two negatively charged guest PA molecules isostructural to **E_3-PA** (C_{16}-$V_3A_3E_3$: to be further used as epitope diluent or filler PA), whose supramolecular aggregation is known to a good extent.

Table 5.1: Structural information of self-assembling peptides presented in this chapter.

Peptide	Sequence	Use
E_3-PA	$C_{15}H_{31}CONH$-$V_3A_3E_3$-$CONH_2$	Filler-PA
E_3Ada-PA	$C_{15}H_{31}CONH$-$V_3A_3E_3$-(Adamantane)-$CONH_2$	Guest-PA
E_3G_3-PA	$C_{15}H_{31}CONH$-$V_3A_3E_3G_3$-$CONH_2$	Control-PA
E_3G_3Ada-PA	$C_{15}H_{31}CONH$-$V_3A_3E_3G_3$-(Adamantane)-$CONH_2$	Guest-PA
RGDS-βCD	RGDS-(β-Cyclodextrin)	Host-Epitope

Both Ada-bearing guest-PAs comprise an aliphatic palmitoyl tail (C_{16}-) at their N-terminus, followed by a β-sheet forming amino acid sequence (-V_3A_3-) that ensures the formation of high-aspect ratio cylindrical nanofibers. Three ionisable glutamic acid residues (-E_3-) are included immediately after in order to promote nanofiber solubility in water (Figure 5.2).

The use of negatively charged sequences was rationalised in terms if their reduced citotoxicity compared to cationic peptides. It is well accepted that positively charged amphiphiles interact strongly with cell membranes via electrostatic interactions with the negative phospholipid heads, while their hydrophobic domains allow insertion into the membrane through hydrophobic interactions, causing increased permeability and loss of barrier function of target cells.[223]

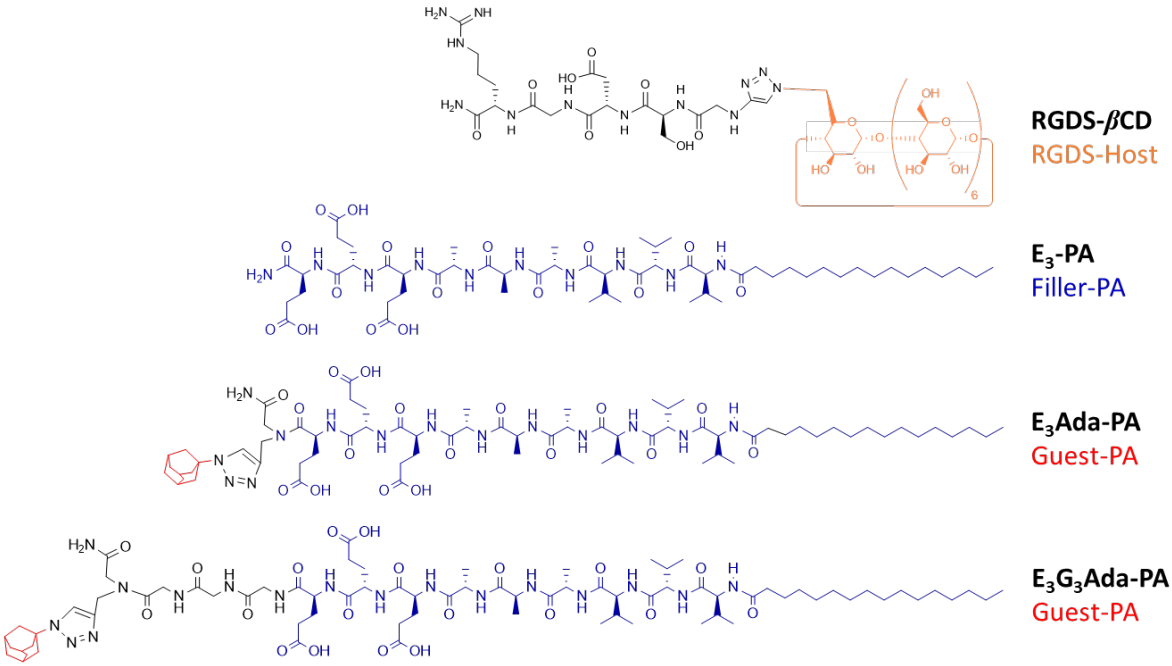

Figure 5.2: *Molecular structures of the self-assembling peptides reported in this study. All PA molecules are isostructural to the negatively charged* ***E*$_3$*-PA**, *in* ***E*$_3$*Ada-PA** *an adamantane moiety was included at the C-terminus. A triglycine spacer was included in* ***E*$_3$*G*$_3$*Ada-PA**, *that bears an adamantane residue after the spacer.* ***βCD-RGDS*** *contains a* ***βCD*** *moiety that is complementary to adamantane residues present in the corresponding guest-PA molecules.*

5.3.2 Purity and characterisation

A combination of peptoid synthesis and copper(I)-catalyzed alkyne-azide cycloaddition (CuAAC) coupling approaches were used to incorporate the Ada units close to the C-terminus of **E$_3$Ada-PA**, while **E$_3$G$_3$Ada-PA** comprised a three-glycine spacer (-G$_3$-) between the Ada units and the PA C-terminus.

This uncharged spacer has a rather flexible nature and spaces out the Ada units some 12.2 Å from the charged glutamic acid residues domain,[115] this spacer was also included to allow further presentation of Ada units when co-assembled with an excess of the filler PA once the PA monomers self-assemble into nanofibers (Figure 5.2).

Synthesis of filler **E$_3$-PA** and control **E$_3$G$_3$-PA** was undertaken following traditional PA SPPS approaches, while guest-PAs: **E$_3$Ada-PA** and **E$_3$G$_3$Ada-PA** were synthesized using standard SSPS followed by purification through RP-HPLC (Table 5.1). Details on their synthesis routes and purification steps can be found in Section 5.10.1 of this thesis.

Filler **E_3-PA** and control **E_3G_3-PA** were obtained with 96% purity, ESI-MS provided mass confirmation of the conjugates: m/z = 1151.8 $[M-H]^-$ and m/z = 1322.8 $[M-H]^-$ respectively (Figure 5.3). Guest-PAs **E_3Ada-PA** and **E_3G_3Ada-PA** were obtained with 98% and 95% purity respectively, ESI-MS provided mass confirmation of the conjugates: m/z = 714.3 $[M+2H]^{2+}$ and m/z = 799.1 $[M+2H]^{2+}$ respectively (Figure 5.4). All of these results are briefed in Table 5.2.

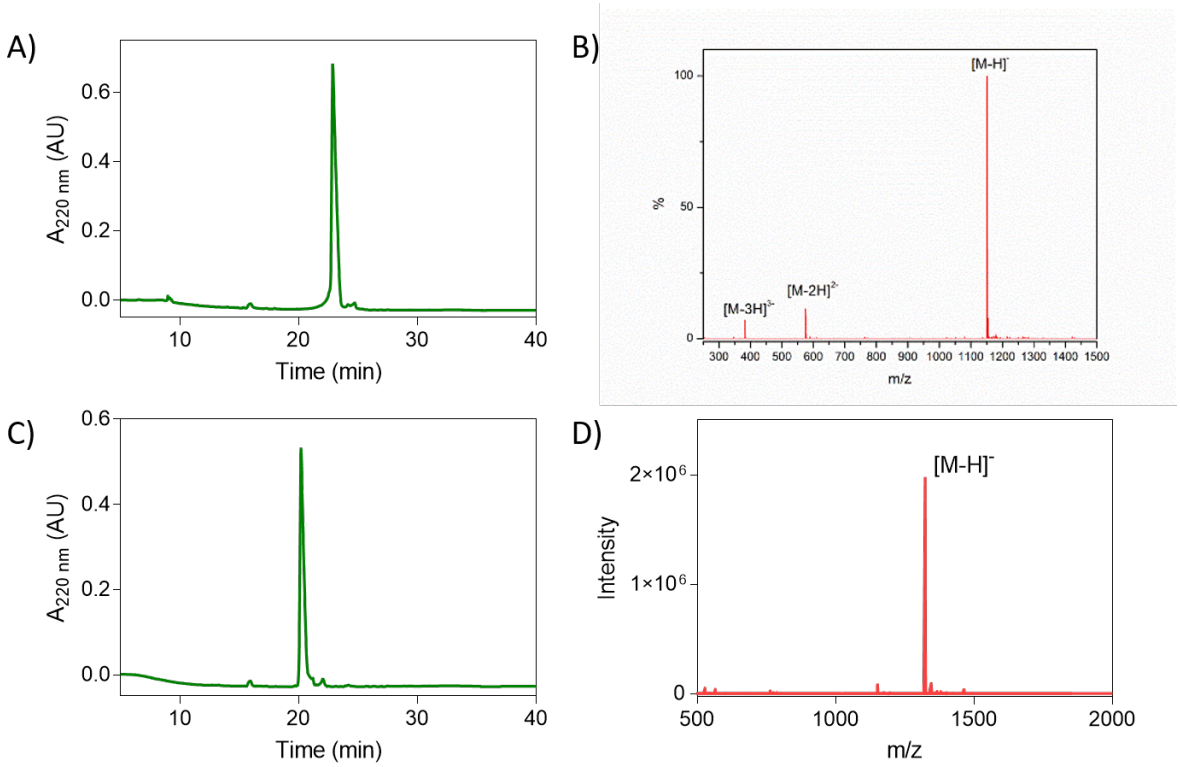

Figure 5.3: *Plots for purity and molecular weight confirmation for **E_3-PA** and **E_3G_3-PA**. A,C) RP-HPLC and B,D) ESI-MS traces respectively.*

Table 5.2: Chemical characterisation of the herein reported anionic peptide amphiphiles.

Peptide	Molecular mass (g/mol)	Found mass (m/z, ∅)	Purity (%, ♯)
E_3-PA	1152.70	1151.8 $[M-H]^-$	96
E_3G_3-PA	1323.76	1322.8 $[M-H]^-$	96
E_3Ada-PA	1425.78	714.3 $[M+2H]^{2+}$	98
E_3G_3Ada-PA	1595.93	799.1 $[M+2H]^{2+}$	95

Notes:
∅ Determined through ESI-MS,
♯ Assessed through RP-HPLC.

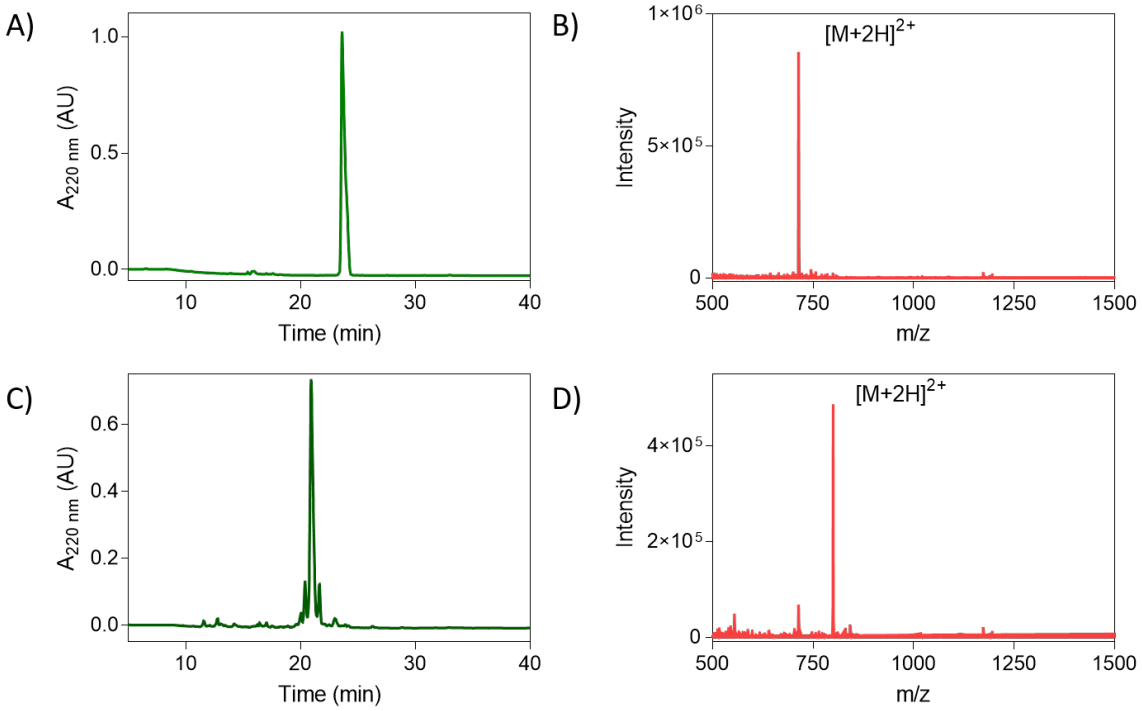

Figure 5.4: *Guest-PAs proof of purity and molecular weight confirmation for* ***E_3Ada-PA*** *and* ***E_3G_3Ada-PA****. A,C) RP-HPLC and B,D) ESI-MS traces respectively.*

5.3.3 Effect of Adamantyl residues on PA self-assembly

Nanofiber self-assembly of unmixed filler PA (**E_3-PA**) and both guest-PAs (**E_3Ada-PA** and **E_3G_3Ada-PA**) was investigated using transmission electron microscopy (TEM). TEM micrographs evidence the presence of nanofibers of around 11-13 nm diameter in both guest-PA solutions at 25 ºC, meanwhile **E_3-PA** originated longer but slightly thinner nanofibers of around 8-10 nm diameter (Figure 5.5B-D). **E_3-PA** originated stand-alone nanofibers (Figure 5.5.B), whereas both guest-PAs nanofibers exhibited a slight tendency to form small bundles.

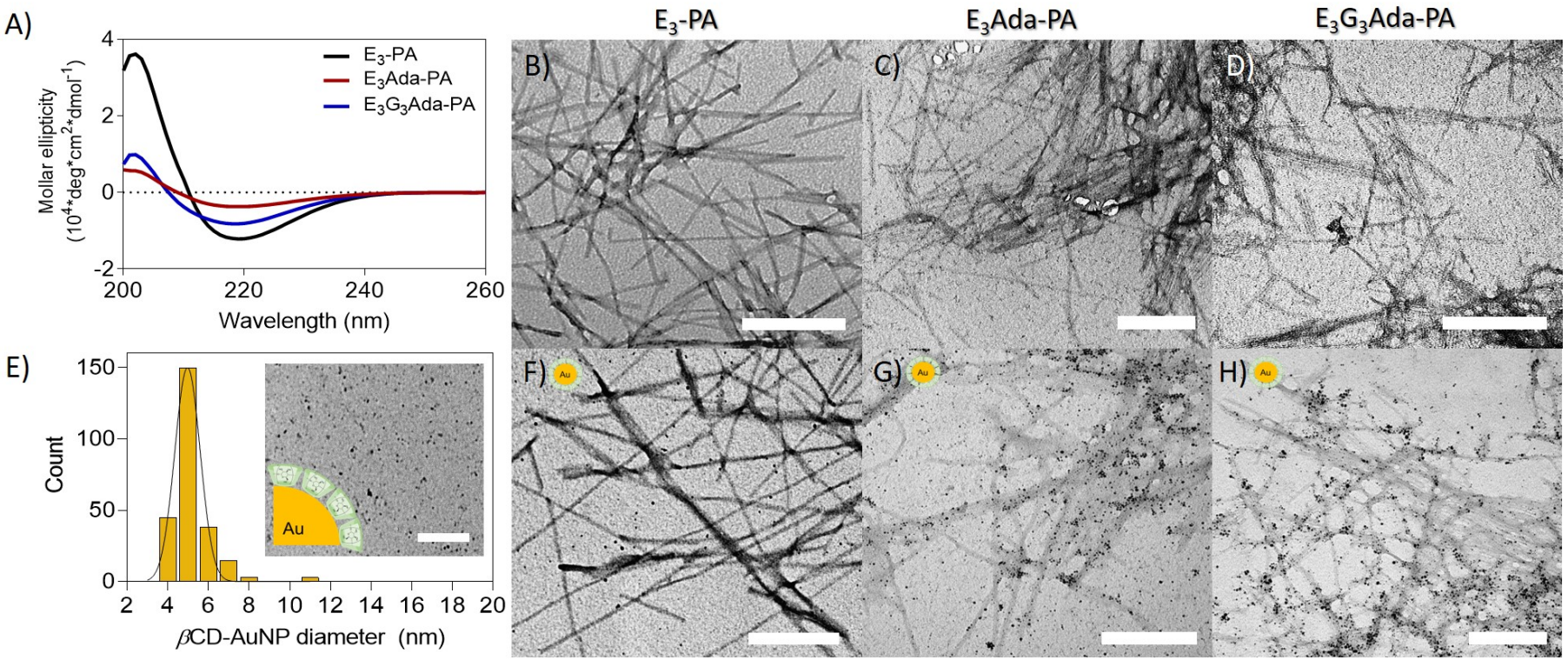

Figure 5.5: *Self-assembly of the herein reported anionic PA derivatives in HEPES buffer. A) Circular dichroism (CD) spectra of* ***E*$_3$*-PA***, ***E*$_3$*Ada-PA***, *and* ***E*$_3$*G*$_3$*Ada-PA*** *indicating the persistence of β-sheets. B–D) Transmission electron microscopy (TEM) images indicate the presence of self-assembled nanofibers in all three* ***E*$_3$*-PA***, ***E*$_3$*Ada-PA***, *and* ***E*$_3$*G*$_3$*Ada-PA*** *cases (scale bars = 250 nm). E) Characterisation of βCD-capped gold nanoparticles (βCD-AuNPs) used to track the presence of adamantyl residues (scale bar = 50 nm). F–H) TEM images of* ***E*$_3$*-PA***, ***E*$_3$*Ada-PA***, *and* ***E*$_3$*G*$_3$*Ada-PA*** *samples incubated with βCD-AuNPs (scale bars = 250 nm).*

Differences in length were observed, as **E_3-PA** nanofibers exhibited longer fiber micron-long sizes in many cases, while guest-PAs originated smaller sub-micron aggregates at this temperature. This is as indication that the presence of **Ada** residues on PA nanofibers may modify the geometric packing parameters of traditional PA backbones, **Ada** residues are rather spherical in shape and of non-polar nature, which allows them to establish van der Waals and hydrophobic interactions amid adjacent units thus promoting their aggregation (Figure 5.5.C-D). A previous report by our group on positively charged PA bearing **Ada** units exhibited a larger tendency to form bundles and originated raft-like objects at millimolar concentration regimes (Figure 4.11 and Section 4.3.5).[155]

5.3.4 Adamantyl moieties effect on nanofiber conformation

As slight interfiber bundling was observed amid guest-PAs, we decided to investigate whatever additional repercussions the presence of **Ada** units may have on the secondary structure of the self-assembled nanofibers. Circular dichroism (CD) spectroscopy showed that all **E_3-PA**, **E_3Ada-PA** and **E_3G_3Ada-PA** presented a β-sheet signature signal,[115] with a positive maximum signal centered at 202 nm and a negative minimum at 219 nm with no evident shifts among the signals (Figure 5.5.A), this absence of wavelength shifts is interpreted as no net increasing in twisting of the β-sheets at the nanofibers core due to the presence of **Ada** units.[224]

Variations in the peak intensities were observed in the three PAs: β-sheet signals were more intense in the case of **E_3-PA**, **E_3G_3Ada-PA** exhibited an almost four-fold reduction in β-sheet signal intensity, while **E_3Ada-PA** showed the least intense signal with a six-fold intensity reduction compared to **E_3-PA**. This intensity reduction can be attributed to the re-arrangement of nanofiber β-sheets into shorter and less regular ones as a result of the presence of Ada units. The presence of the three-glycine spacer appears to be beneficial for β-sheet formation as it spaces out adjacent hydrophobic **Ada** units thus allowing the formation of more ordered β-sheets at the nanofiber core,[224] in other words, **E_3G_3Ada-PA** forms stronger β-sheets than **E_3Ada-PA** but not as stable as **E_3-PA**.

One interesting factor to consider when strength of β-sheets in PAs is discussed has to do with the way water molecules interact with PA assemblies. Overhauser Dynamic Nuclear Polarisation Relaxometry (ODNP) has shown that water molecules are fundamental to structure anionic PA nanofibers, indeed, water molecules exhibit correlation times from 200 ps to 900 ps. These values span the range from fast moving fluid water molecules in the PA nanofiber core to slow-moving water at the nanofiber surface.[16] Introducing hydrophobic **Ada** moities as in **E_3Ada-PA** and **E_3G_3Ada-PA** nanofibers surface might promote water molecules fluidity, thus affecting the associated β-sheets, a similar effect is also expected for water molecules bound to nanofibers with different charges and charge densities.[16]

5.4 Non-covalent binding of Adamantane units

The possibility to confirm the presence of **Ada** binding units atop **E_3Ada-PA** and **E_3G_3Ada-PA** nanofibers surface was explored using TEM. β-Cyclodextrin-capped gold nanoparticles (βCD-AuNPs) presented in Section 4.4 were employed once again for this purpose.[183] βCD-AuNPs were found to exhibit a diameter of (5.6 ± 0.9) nm i.e. about the radius of our PA nanofibers (Figure 5.5.E). In this fashion, **E_3Ada-PA** and **E_3G_3Ada-PA** were incubated with an excess of βCD-AuNPs, finding significant clusters of adsorbed particles in the proximity of both guest-PAs nanofibers (Figure 5.5.G-H).

E_3-PA controls showed little to none βCD-AuNPs adsorption onto nanofibers, which indicates that the host-guest non-covalent binding is the main contributor to βCD-AuNPs attachment to the nanostructures (Figure 5.5.F) rather than an electrostatically driven mechanism. These results confirm that the presence of **Ada** residues in PA monomers does not prevent nanofiber self-assembly and also allows for the establishment of further host-guest interactions with β**CD** binding motifs after nanofiber assembly.

5.5 Structuring PA gels containing E_3-PA/E_3Ada-PA and E_3-PA/E_3G_3Ada-PA

Both **E_3Ada-PA** and **E_3G_3Ada-PA** offer inherent capacities to bind complementary host-units. The possibility to affix pendant **Ada** guest units from these guest-PAs to canonical PA nanofibers was explored by co-assembling them with an excess of filler **E_3-PA**.

Several reasons justify the use of **E_3-PA** as filler/spacer monomer units: As **E_3-PA** contains the same peptide backbone (Figure 5.2) as both guest-PAs a reasonable degree of compatibility amid these units was predicted. Given that the ultimate goal of appending **Ada** units to self-assembled nanofibers is their binding with a suitable epitope-bearing *β***CD**, the longitudinal spacing of **Ada** units along PA nanofibers might contribute to improve further bioactivity when in presence of cells.[113]

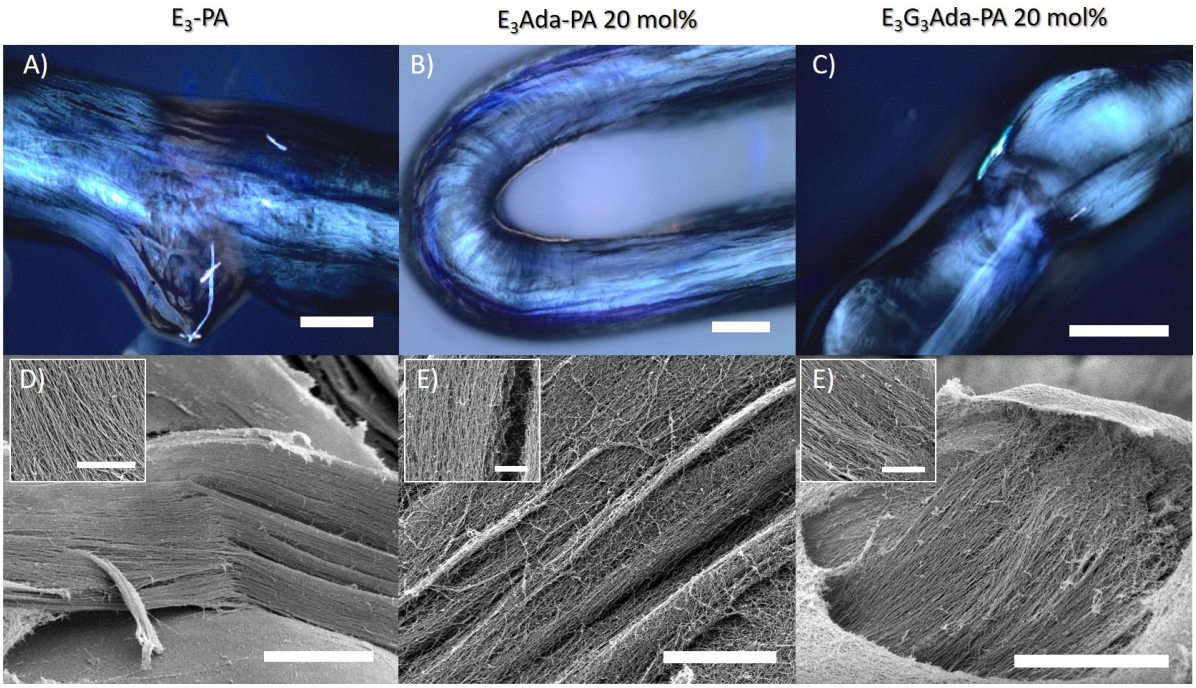

Figure 5.6: *Microstructure characterisation of **E_3-PA**, **E_3-PA/E_3Ada-PA** and **E_3-PA/E_3G_3Ada-PA** aligned hydrogels. A – C) Polarised light microscopy showing the birefringence of single hydrogel strings indicating alignment along the string elongated axis in A) **E_3-PA**, B) **E_3-PA/E_3Ada-PA** 80:20 (mol%) and C) **E_3-PA/E_3G_3Ada-PA** 80:20 (mol%) (scale bars = 1 mm). D) SEM micrographs of **E_3-PA**, E) **E_3-PA/E_3Ada-PA** 80:20 (mol%) and **E_3-PA/E_3G_3Ada-PA** 80:20 (mol%) hydrogels evidencing nanofiber alignment due to elongational flow (scale bars = 10 μm, insets = 2.5 μm).*

Morphological and mechanical properties of these co-assembled nanofibers might be mostly dictated by those of **E_3-PA** as this represents the predominant filler component in the fibers. This prediction gave way to seize the ability of **E_3-PA** filler molecules to confer hierarchical ordering levels via the well-understood entropy driven dehydration-rehydration process reported by Zhang and co-workers (see Figure 2.11).[121]

In order to explore this possibility for our Ada-pendant co-assembled nanofibers guest-PAs solutions containing an excess of **E_3-PA** (80 mol%) and either **E_3Ada-PA** and **E_3G_3Ada-PA** (20 mol%) were prepared. These solutions were heated at 80 ^{o}C, slowly cooled down to room temperature and then manually dragged from a pipette onto a $CaCl_2$ bath, obtaining transparent noodle-shaped viscoelastic strings similar to those originated by **E_3-PA** solutions.[121]

Presence of birefringent domains was found in **E_3-PA** noodle-like strings, as well as in its 80:20 mixtures with either **E_3Ada-PA** or **E_3G_3Ada-PA** (Figure 5.6.A-C). Scanning electron microscopy (SEM) images show that highly parallel oriented filaments are found in either pure **E_3-PA** strings or its guest-PA mixtures (Figure 5.6.D-F). These results show that the presence of **Ada** motifs at the surface of co-assembled PA nanofibers neither disrupts fiber formation nor interferes with their nano- to microscale hierarchical self-assembly.

5.6 Stiffness of E_3-PA/E_3Ada-PA & E_3-PA/E_3G_3Ada-PA co-assemblies

As **Ada** motifs showed no detrimental effects on the structure of co-assembled hydrogel strings, their effect on stiffness of stand-alone hydrogels was assessed using oscillatory rheology. Thermally treated mixtures of **E_3-PA** and different ratios of either **E_3Ada-PA** and **E_3G_3Ada-PA** were turned into gels by injection of an excess of $CaCl_2$. **E_3Ada-PA**-containing gels showed a loss of transparency with an increasing fraction of **E_3Ada-PA**, which reflected on their mechanical properties.

Only a 5 mol% of **E_3Ada-PA** caused a drop in the storage modulus (G') of co-assembled hydrogels, from about 24 kPa in 100 mol% **E_3-PA** hydrogels to around 15 kPa in 95:5 **E_3-PA**/ **E_3Ada-PA** mixtures. Increasing fractions of **E_3Ada-PA** proved adverse as further decrease in G' values was observed. These results indicate little compatibility between **E_3-PA** and **E_3Ada-PA** monomers when forming co-assembled nanofibers, the close proximity of **Ada** residues to negatively charged glutamate units might ultimately generate disruptions in β-sheets in co-assembled nanofibers, thus causing fiber shortening and originating weaker hydrogels (Figure 5.7.A), similar reductions in PA hydrogel stiffness by additions of up to 10% of epitope presenting PA have been reported.[115]

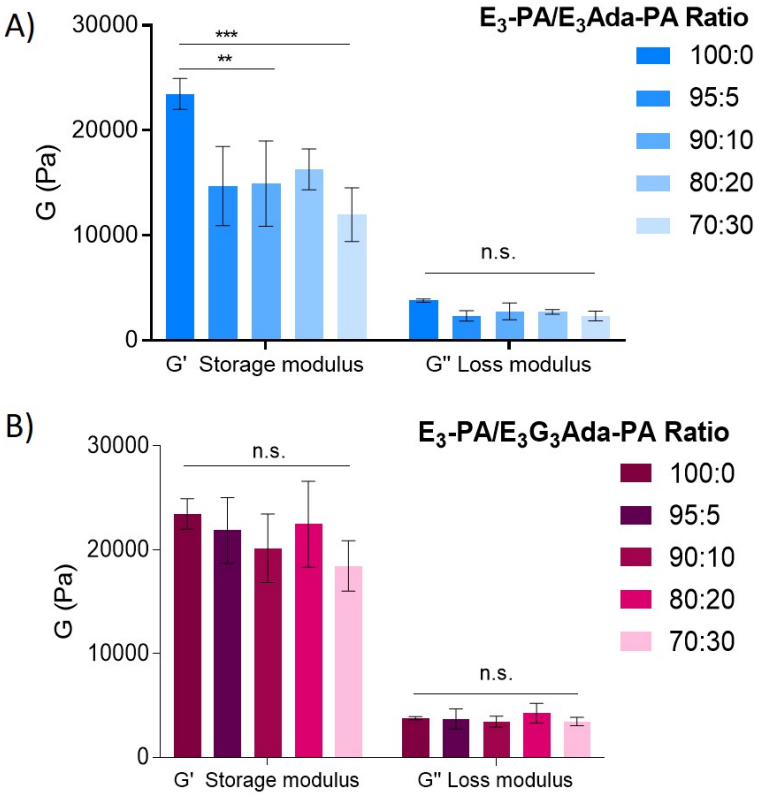

Figure 5.7: *Rheological characterisation of co-assembled **E_3-PA**/**E_3Ada-PA** and **E_3-PA**/**E_3G_3Ada-PA** hydrogels. A) Storage (G') and loss (G") moduli values of hydrogels containing different **E_3-PA**/**E_3Ada-PA** ratios (1 wt%, [$CaCl_2$] = 100 mM) determined by oscillatory rheology. B) Co-assembled **E_3-PA**/**E_3G_3Ada-PA** hydrogels showed no G' nor G" significant dependence on the content of the **Ada**-bearing PA (*** $p < 0.001$; ** $p < 0.01$; n.s. no significant difference; $n > 3$).*

On the other hand, co-assembled hydrogels with increasing **E_3G_3Ada-PA** content remained transparent up to 30 mol% of **Ada**-containing fractions and showed no significant variation in stiffness compared to 100 mol% **E_3-PA** control hydrogels. In this co-assembly scenario, the presence of the three-glycine spacer played a key role in increasing co-assembly compatibility of **E_3-PA** with **E_3G_3Ada-PA**. The independence of G' with **E_3G_3Ada-PA** content is an indicative of self-assembled nanofibers with increased length compared to those originated by co-assembling **E_3Ada-PA** (Figure 5.7.B). As **E_3G_3Ada-PA** showed no interference with the resulting hydrogel mechanical performance when co-assembled with an excess of filler **E_3-PA**, these results indicate that **E_3G_3Ada-PA** is a more suitable PA to further incorporate into co-assembled nanofibers than **E_3Ada-PA**, therefore, only **E_3G_3Ada-PA** was chosen for further studies as guest-PA.

5.7 Non-covalent RGDS-βCD presentation on co-assembled E_3-PA/E_3G_3Ada-PA nanofibers

As rheological studies indicated that **E_3G_3Ada-PA** was a suitable candidate to co-assemble with **E_3-PA** without compromising the resulting mechanical properties of the gel, the formation of host-guest complexes involving the former was studied. As βCD-AuNPs binding studies indicated (Figure 5.5.D and H), **E_3G_3Ada-PA** offers the possibility to bind to **βCD** motifs, in the following studies the **RGDS-βCD** derivative shown in Figure 5.2 was chosen as the epitope-bearer i.e. RGDS-Host (Synthesis details can be found in Section 5.10.1 and Figure 5.15).[225]

RGDS-Host presents two main structural features, on one side it includes a **βCD** unit suitable for binding with **Ada**-containing PA nanofibers, on the other hand it contains an **RGDS** motif, which is known to bind to a variety of integrins including $\alpha v\beta 3$ and $\alpha 5\beta 1$, thereby promoting cell adhesion. In **RGDS-βCD** this peptide cell binding domain is allocated on the primary rim of **βCD** units, thus exposing it on PA nanofiber surface after binding to **Ada** cues via the opposite rim of the **βCD** macrocycle.

In order to demonstrate the formation of this 1:1 host-guest complex we performed NMR studies in solution state. Figure 5.8.A shows ^{1}H-NMR spectra corresponding to **RGDS-βCD** (whose H5 and H3 inner cavity protons are indicated), **E_3G_3Ada-PA** (whose protons from **Ada** units are indicated) and a 1:1 mixture of them, in which some of the **Ada** protons have downfield shifted after binding to **βCD** (Figure 5.8.B) suggesting partial inclusion (Figure 5.8.C).

In order to demonstrate the placing of **Ada** residues inside the **βCD** cavity NOESY experiments were performed. Figure 5.8.D shows cross-peaks between **Ada** protons and H5 and H3 protons from **βCD** cavity (in green) that are completely absent in the NOESY spectrum of **E_3G_3Ada-PA** by itself (Figures 5.9-11). These results confirmed the formation of the non-covalent host-guest complex **E_3G_3Ada-PA•RGDS-βCD** (Figure 5.8.C) and the possibility to use **Ada** cues in PA nanofibers as tethering points for **RGDS-βCD** cell binding motifs.

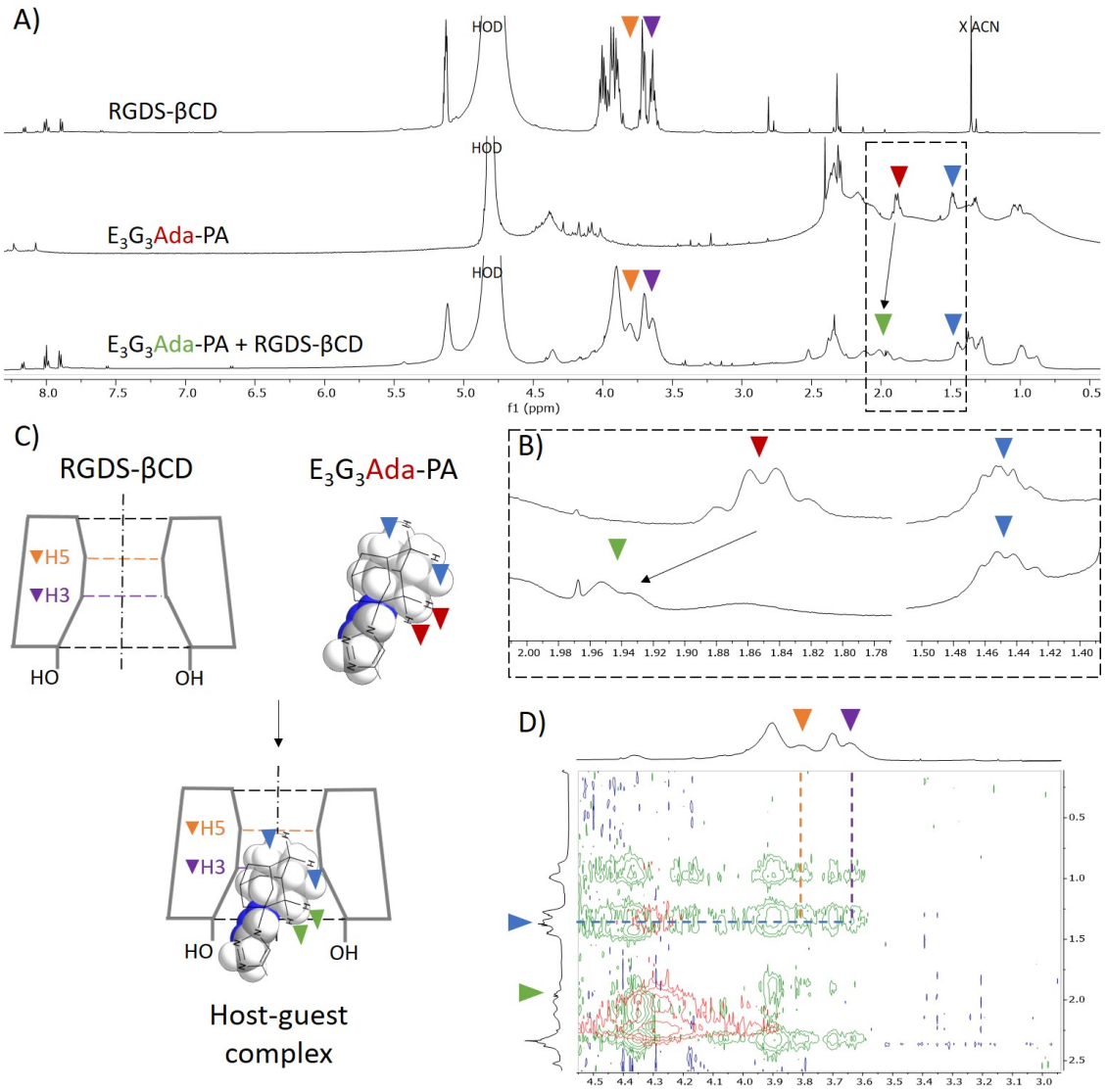

Figure 5.8: *Spectroscopic characterisation of the host-guest inclusion complex formed between* ***RGDS-βCD*** *(Epitope-Host) and* ***E_3G_3Ada-PA*** *(Guest-PA). A) ^{1}H-NMR spectra corresponding to free* ***RGDS-βCD****, free* ***E_3G_3Ada-PA*** *and an equimolar mixture in D_2O, T = 298 K, [Peptide] = 6.5 mM. B) Zoom showing the downfield shift corresponding to adamantyl protons before and after complex formation. C) Schematics illustrating the formation of the 1:1 host-guest complex. D) NOESY experiments demonstrating close proximity of adamantyl* ***E_3G_3Ada-PA*** *protons (green wedges) to H5 and H3 inner cavity****RGDS-βCD*** *protons (orange and purple wedges correspondingly) as cross peaks appear in the green traces, those peaks are absent in the* ***E_3G_3Ada-PA*** *spectrum in absence of* ***RGDS-βCD*** *(red traces).*

5.7.1 E_3G_3Ada-PA•RGDS-βCD effect on nanofiber formation

As spectroscopic evidence of the formation of **E_3G_3Ada-PA•RGDS-βCD** non-covalent units was acquired, we decided to assess the effect of this host-guest binding on self-assembled nanofibers morphology and conformation. CD studies indicated that host-guest complexation of **RGDS-βCD** units does not disrupt β-sheet formation, as a similar β-sheet signature was found in both free and **RGDS-βCD**-bound **E_3G_3Ada-PA** (Figures 5.12.A). Similar host-guest complexations have been reported to drive more dramatic conformational changes in the binding of host-guest-bearing PAs, as Redondo-Gómez and co-workers reported on the host-guest binding of two cationic dodecapeptide amphiphiles (as described in Chapter 4).[155]

The preservation of β-sheets in **E_3G_3Ada-PA•RGDS-βCD** might imply that host-guest binding of shorter peptides can have a less imposing effect on conformational changes of self-assembling peptides. Equimolar mixtures of **E_3G_3Ada-PA/RGDS-βCD** exhibited fibrous morphologies on TEM, implying that host-guest complexations did not alter fiber formation capacities (Figure 5.12.B) in micro and millimolar concentration regimes, thus remaining suitable for further co-assembly with the filler-PA **E_3-PA** in ternary hydrogels.

5.7.2 Ternary E_3-PA/E_3G_3Ada-PA•RGDS-βCD hydrogels

In order to assess the posibility to co-assemble **E_3-PA** and **E_3G_3Ada-PA•RGDS-βCD** units into functional hydrogels, mixtures of the three individual peptides were carefully prepared, incubated at 80 °C, and let to cool down to room temperature before gelifying them by injection of $CaCl_2$. This thermal treatment imprinted the ternary hydrogels with some degree of fiber alignment, as SEM images demonstrated (Figure 5.12.D).

Increasing contents of the **Ada-PA•RGDS-βCD** complex led to different stiffness in the resulting hydrogels, incorporation of 5 mol% and 10 mol% **Ada-PA•RGDS-βCD** units in **E_3-PA** gels originated no significant difference in G' and G" values compared to 100 mol% **E_3-PA** control hydrogels (Figure 5.12.C).

Moreover, fractions higher than 20 mol% **Ada-PA•RGDS-βCD** decreased G' values from 24 kPa to less than 10 kPa, implying a possible detrimental effect in fiber elongation due to electrostatic repulsion or geometric hindrances amid **RGDS-βCD** motifs when present in concentrations higher than 10 mol%. These results show that mechanical properties of ternary hydrogels comprising **E_3-PA** and different amounts of non-covalently presented **RGDS** motifs can be retained as in ummodified **E_3-PA** gels, or modulated as a function of host-guest complex **Ada-PA•RGDS-βCD** concentration.

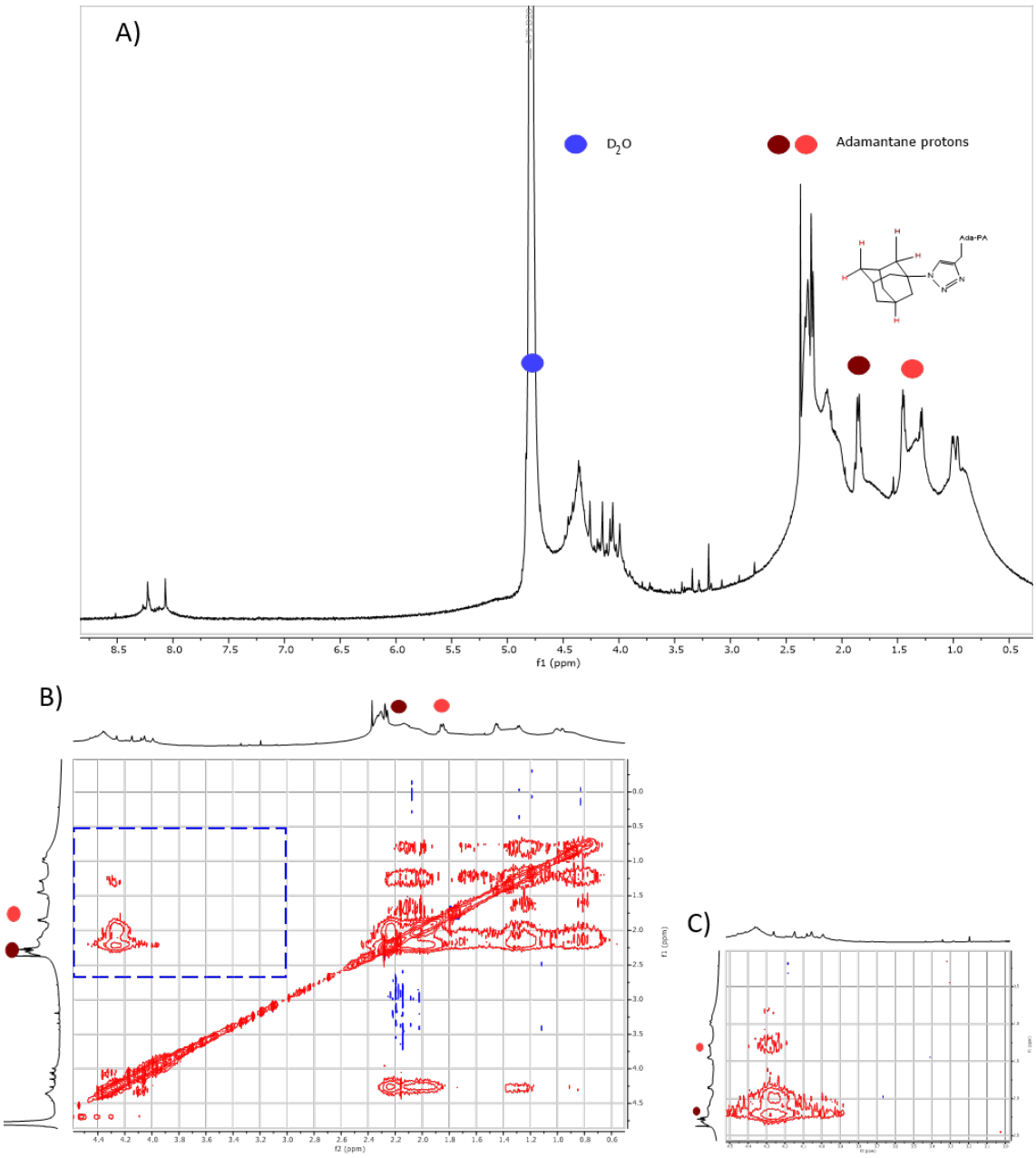

Figure 5.9: *NMR spectra corresponding to* ***E*$_3$*G*$_3$*Ada-PA*** *and its complex with* ***βCD-RGDS****. A)* ^{1}*H-NMR and B) NOESY spectra corresponding to* ***E*$_3$*G*$_3$*Ada-PA*** *(600 MHz, 8.9 mM, D*$_2$*O, 298 K). C) Zoom of the indicated region in blue from panel B.*

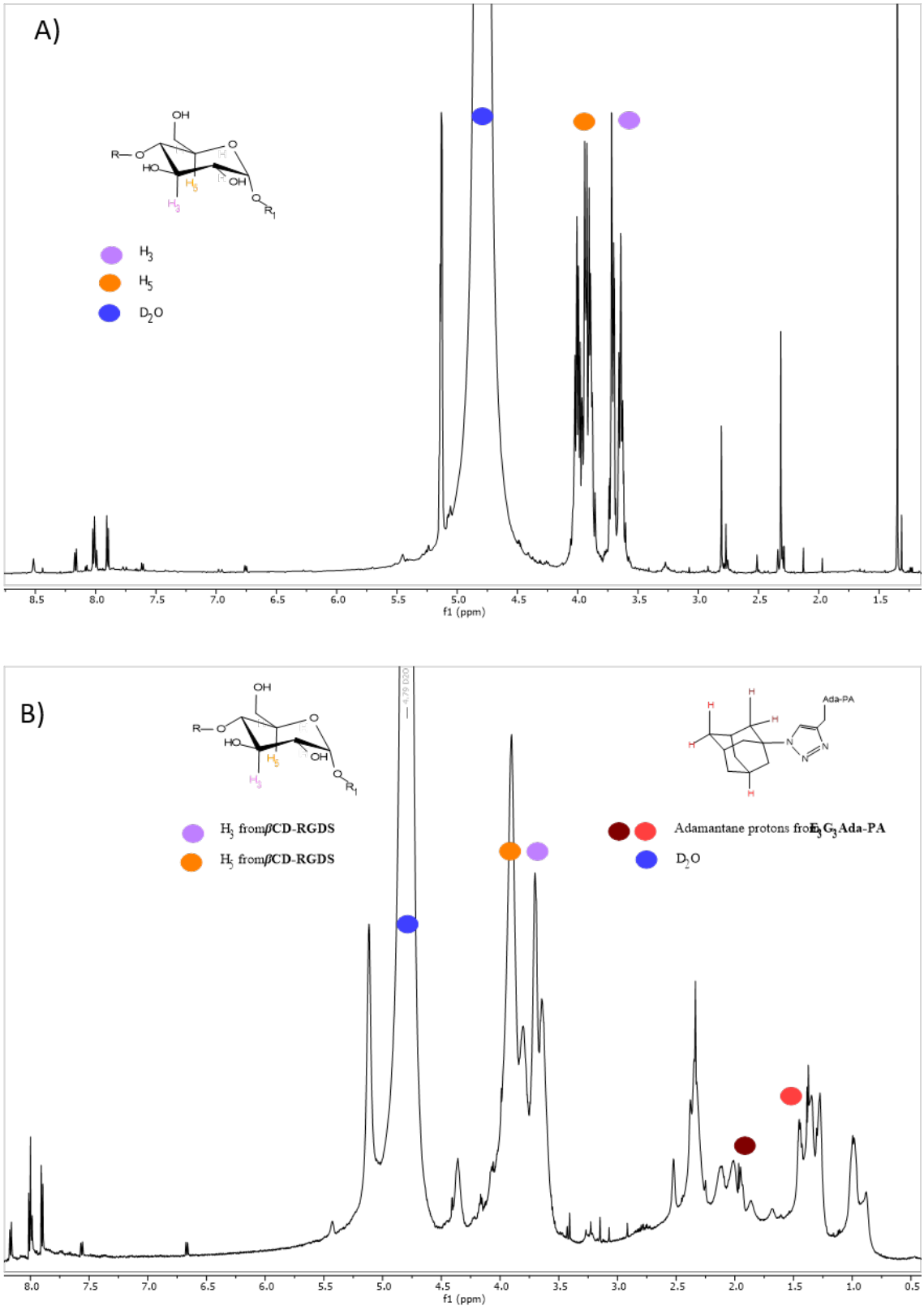

Figure 5.10: *A) ^{1}H-NMR spectrum corresponding to **RGDS-βCD** (600 MHz, 8.5 mM, D_2O, 298 K). B) ^{1}H-NMR spectrum spectra corresponding to **E_3G_3Ada-PA** mixed with **RGDS- βCD** (600 MHz, 8.5 mM each, D_2O, 298 K).*

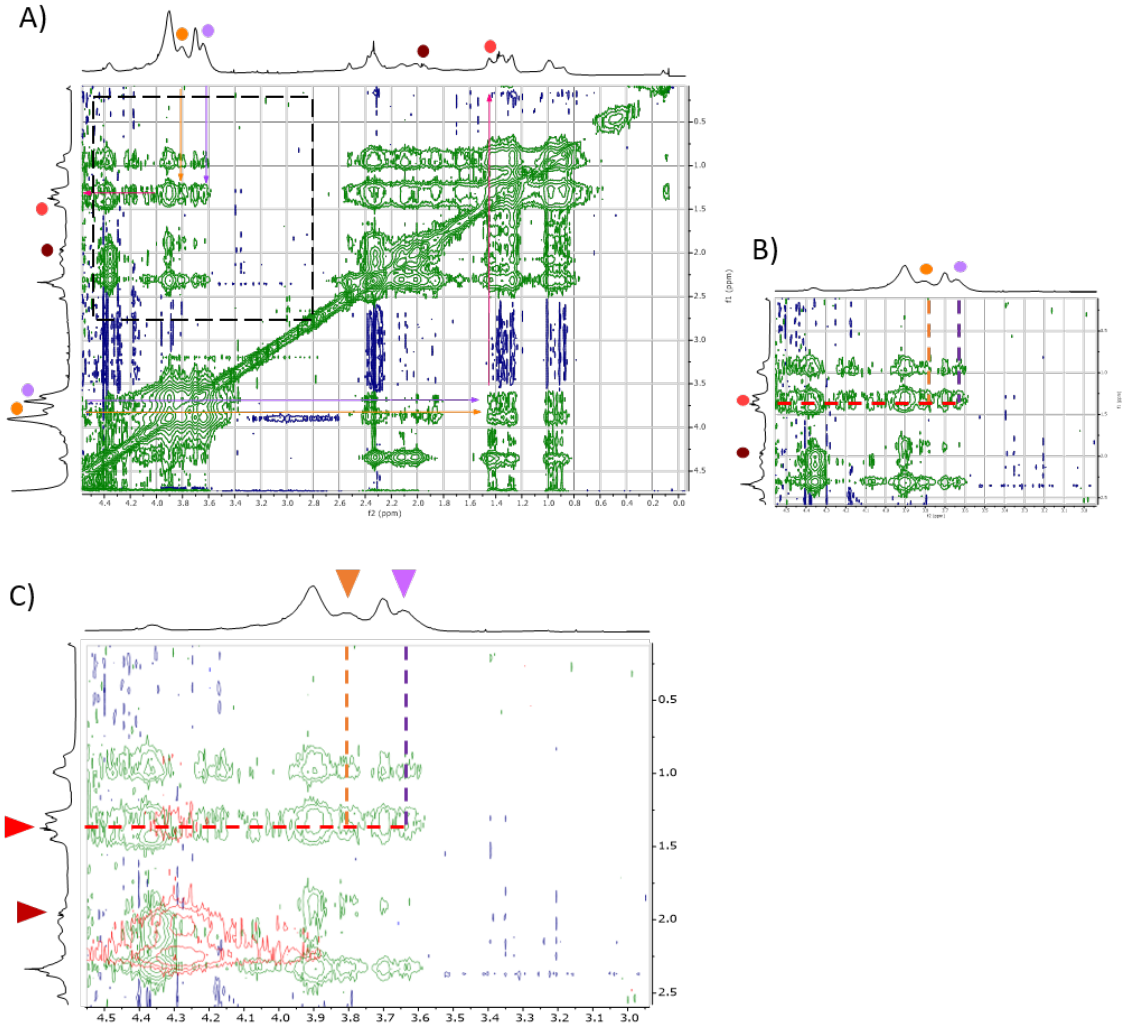

Figure 5.11: *A) NOESY spectra corresponding to* ***E*$_3$*G*$_3$*Ada-PA*** *mixed with* ***RGDS-βCD*** *(600 MHz, 8.5 mM each, D_2O, 298 K). B) Zoom of the indicated region from panel A). C) Superposition of panels C (in red) and G (in green) showing that the cross-peaks in green arise from the interaction between adamantane protons of* ***E*$_3$*G*$_3$*Ada-PA*** *and H3 (violet) and H5 (orange) protons from the cavity of RGDS-βCD.*

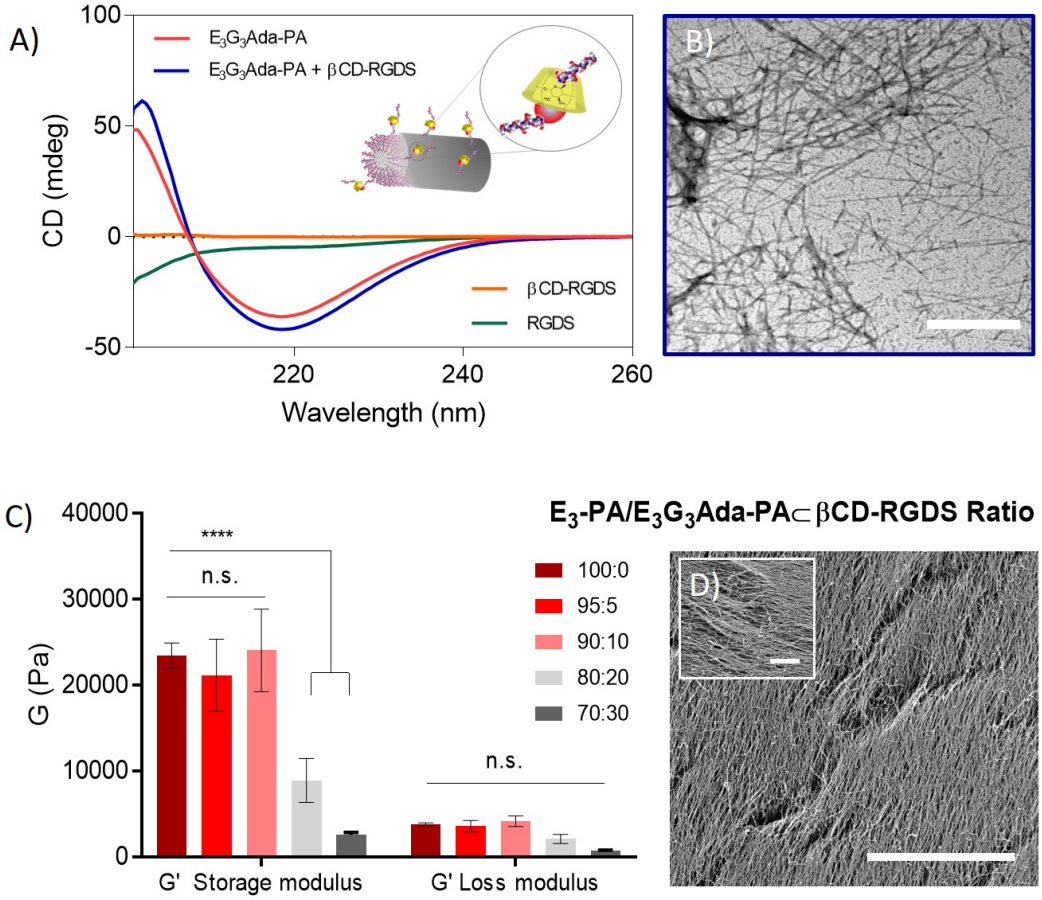

Figure 5.12: *Co-assembly of the **E_3G_3Ada-PA•RGDS-βCD** system. A) CD spectra of free **E_3G_3Ada-PA**, **RGDS-βCD**, RGDS-Peptide, and an equimolar mixture of **E_3G_3Ada-PA/RGDS-βCD** at 25 °C indicating the formation of the complex **E_3G_3Ada-PA•RGDS-βCD**. B) TEM micrograph showing the persistence of nanofibers after **E_3G_3Ada-PA•RGDS-βCD** formation (scale bar = 500 nm). C) Rheological characterisation of co-assembled **E_3-PA /E_3G_3Ada-PA•RGDS-βCD** hydrogels. Storage (G') and loss (G") moduli values of different **E_3-PA / E_3G_3Ada-PA•RGDS-βCD** hydrogels (1 wt%, [$CaCl_2$] = 100 mM, ****p < 0.0001; n.s. no significant difference; n > 3). D) SEM micrograph of a 90:10 thermally treated hydrogel showing the presence of fiber alignment (scale bar = 10 µm, inset = 2.5 µm).*

5.8 Non-covalent RGDS-βCD epitope display on PA hydrogels

Knowing that **RGDS** motifs can be successfully projected out of the PA nanofiber surface via host-guest interactions, we decided to investigate cell response to this non-covalent presentation using in vitro fibroblasts cultures. Cell viability assays on solution showed good citocompatibility of individual components (Figure 5.13), therefore, NIH-3T3 fibroblasts were cultured atop co-asembled **E_3-PA** hydrogels with increasing fractions of **Ada•RGDS-βCD** complex, we hypothesised that increasing contents of host-guest presented **RGDS** epitopes would lead to faster cell attachment and spreading response to the hydrogel scaffolds.

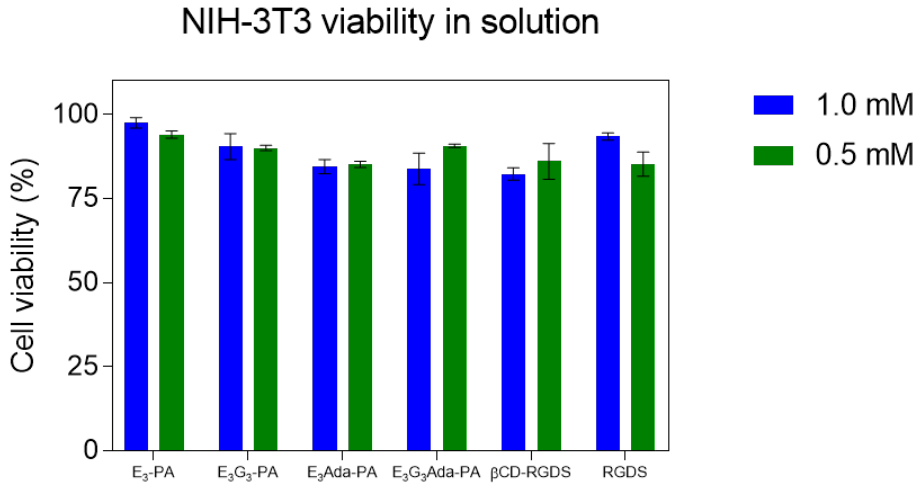

Figure 5.13: *LIVE/DEAD assay on a monolayer of NIH-3T3 fibroblasts after culture in 1.0 mM and 0.5 mM* ***E_3-PA***, ***E_3G_3-PA***, ***E_3Ada-PA***, ***E_3G_3Ada-PA***, ***βCD-RGDS*** *and* ***RGDS*** *solutions.*

Short incubation periods ($\leq$ 3 h) were chosen to evaluate fibroblasts attachment and spreading onto the hydrogels.[226] After incubation cells were fixed and fluorescently stained for actin and nucleus. In this fashion, morphological changes in fibroblasts morphology were tracked and representative cell fluorescence images are shown in Figure 5.14.A.

Qualitatively speaking, fibroblasts cultured for 30 min on **E_3-PA** control hydrogels exhibited little spreading and a rather rounded shape that indicates little to none attachment to the substrate, on the other hand cells cultured atop gels with increasing content of **Ada•RGDS-βCD** appeared more spread and

with rather angular morphologies (for instance the 30 min gel with 20 mol% of **Ada•RGDS-βCD** in Figure 5.14.A). These differences became more notorious after 3 h of culture, when cells on **E_3-PA** control hydrogels started to show more spread polygonal shapes, while cells on **Ada•RGDS-βCD** gels appeared more spread and with a number of cell protruding extensions, indicative of a more advanced stage of attachment and spreading to the hydrogel substrate (compare the same 3h 20 mol% **Ada•RGDS-βCD** gel in Figure 5.14.A).

In addition to cell morphology changes, phalloidin staining also revealed noticeable differences in cell cytoskeleton architecture and actin filaments disposition amongst cultures. After 3 h of culture on **E_3-PA** control hydrogels fibroblasts' cytoskeleton exhibited a rather homogeneous distribution of actin among the cytoplasm and little stress fibers.[227] On the contrary, cells cultured on gels with increasing content of the host-guest pair **Ada•RGDS-βCD** exhibited increasingly organised networks of actin microfilaments, with higher and densely packed contents of actin close to the plasma membrane, a possible indicative of focal adhesion formation as the result of a later spreading stage.[228,229]

We decided to quantify this enhanced fibroblast response to host-guest presented **RGDS** by monitoring changes in cell morphology. For this purpose we opted to use the ratio of projected cell area (A_{cell} indicated by actin content in the cytoskeleton) to cell nucleus area ($A_{nucleus}$ indicated by DAPI staining). This ratio ($A_{cell}/A_{nucleus}$) allows for projected cell area normalisation resulting in a more thorough comparison among cells with similar projected areas but that could undergo different attachment stages, though other measurements like cell aspect-ratio or convex hull can also be used.

Our assays show that hydrogels with increasing fractions of the **Ada•RGDS-βCD** complex anchored to PA nanofibers develop faster cell attachment response than control **E_3-PA** gels. In these **E_3-PA** control gels cell attachment becomes sgnificantly different only after 3 h of culture (red bars, Figure 5.14.B), meanwhile, gels with a 10 mol% fraction of the **Ada•RGDS-βCD** complex showed significant differences after only 1 h of culture (dark blue bars, Figure 5.14.B), and gels with a 20 mol% content developed differences after just 30 min culture (sky blue bars, Figure 5.14.B).

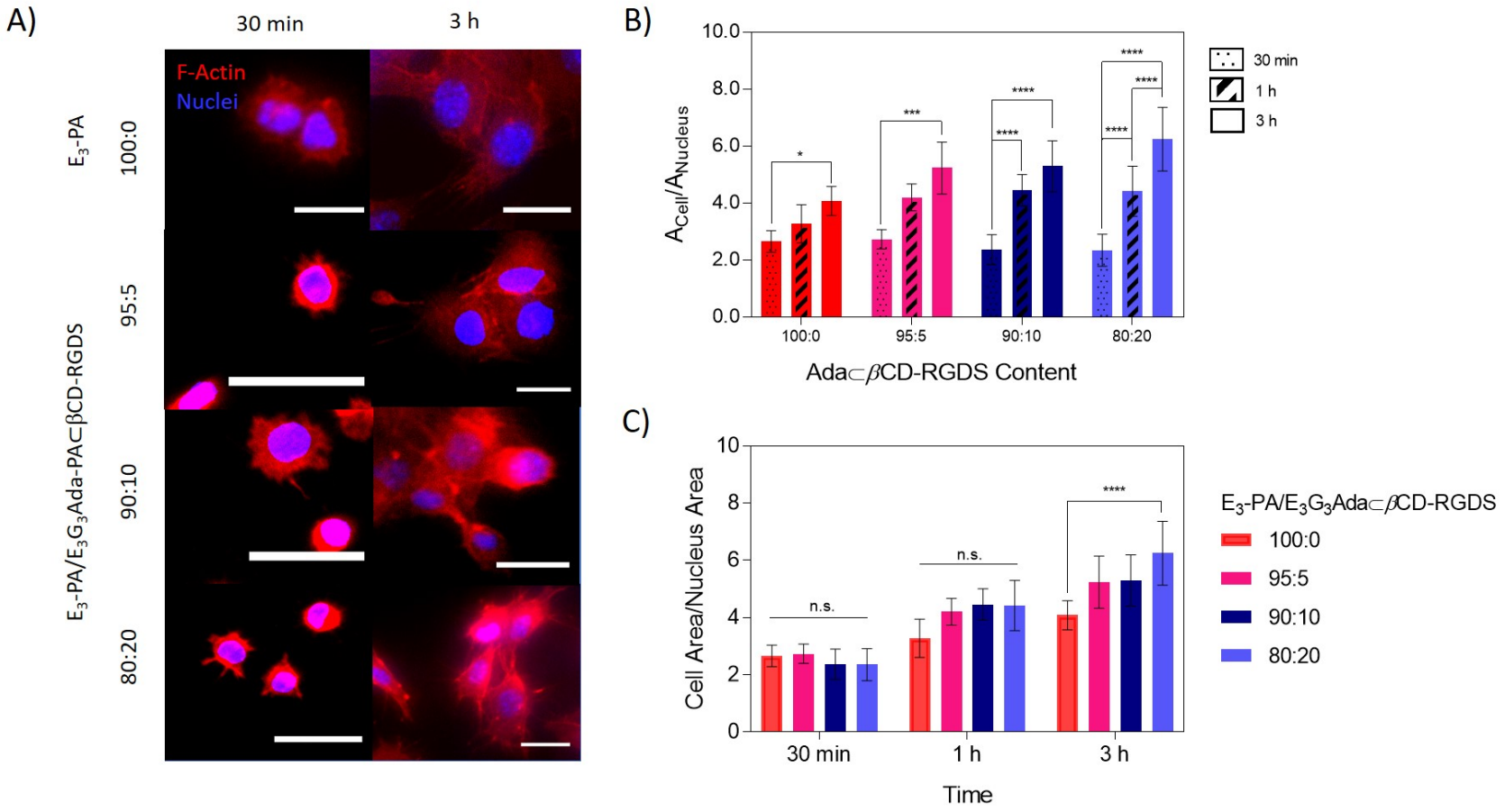

Figure 5.14: *Effect of host-guest-mediated presentation of RGDS motifs on NIH-3T3 fibroblasts attachment to* ***E*$_3$*-PA/E*$_3$*G*$_3$*Ada-PA•βCD-RGDS*** *hydrogels. A) Confocal microscopy images of NIH-3T3 fibroblasts attached to hydrogels with an increasing content of* ***E*$_3$*G*$_3$*Ada-PA•βCD-RGDS*** *units (red staining: Phallodin-rhodamine for F-actin, blue: DAPI for cell nuclei, scale bar = 50 µm). B) NIH-3T3 fibroblast attachment quantified as a function of* ***Ada-PA•βCD-RGDS*** *content, and C) as a function of time (n.s.: no significant difference, * $p < 0.1$, *** $p < 0.001$, **** $p < 0.0001$).*

As no significant differences were found in cell spreading in all samples after 30 min culture (Figure 5.14.C) it can be stated that only initial cell-substrate contact and passive adhesion are taking place, in such way, events in which the presentation of **RGDS** from the substrate do not play a relevant role at this stage.

After 1 h of culture more spread morphologies are found in **Ada·RGDS-βCD** containing hydrogels versus control **E_3-PA** ones (although no significant difference was found), indicating that **RGDS** presentation from the substrates starts playing a role in receptor–ligand binding, in fact, high density presentation of epitopes on PA nanofibers is known to facilitate receptor clustering for signaling and also maximize successful binding between ligands and receptors.[113]

After 3 h of culture all **Ada•RGDS-βCD** containing hydrogels showed significantly different spreading areas compared to **E_3-PA** controls, indicating that fractions of **Ada•RGDS-βCD** as little as 5 mol% are sufficient to trigger late cell spreading events like modulation of cytoskeleton assembly[226] focal adhesion formation, and cell motility, events that have not started to take place in **E_3-PA** control gels at this 3 h stage (Figure 5.14.C).

The observed increase in cell spreading in **RGDS** containing gels but not in **E_3-PA** controls discarts that cells are reacting to hydrogel stiffness[115] rather than RGDS content,[3] and also allows to neglect contributions from serum proteins adsorbed to the nanofiber surface during these early culture stages. Control hydrogels fomulated with an excess of filler **E_3-PA** and 10 mol% of either **E_3G_3-PA/RGDS-βCD** (lacking **Ada** binding units, see Table 5.1) or **E_3G_3-Ada-PA/RGDS** (lacking **βCD** binding units) showed no difference in cell morphology and spreading compared to **E_3-PA** gels, indicating that host-guest-mediated epitope presentation is responsible for the observed cell attachment response in Figure 5.14 experiments rather than electrostatic adsorption of **RGDS-βCD** to nanofibers.[115] Overall, these results indicate that host-guest interactions are fitting to perform presentation of **RGDS** epitopes on PA nanofibers.

5.8.1 Advantages of the host-guest-mediated epitope display approach

Most applications involving co-assembled presentation of epitopes in PA-based hydrogels actually report on the use of concentrations comprised in the range of 5 - 10 mol% reported in Figure 5.14.C, this implies that our non-covalent epitope presentation can achieve similar efficacy as traditional covalent approaches.

Our **Ada/βCD** epitope anchoring approach offers different advantages over conventional covalent epitope attachment. First, nanofiber decoration can be made as a one-pot preparation procedure or can be effectuated post-fiber assembly, thus allowing for versatility.

Second, our host-guest epitope presentation approach relies on the modular assembly of fiber backbone and pendant **Ada** units, these monomer units have the same peptide backbone (i.e. they are isostructural) but can be decorated with a cocktail of different soluble host-epitopes at the same time, the overall non-covalent assembly of our host-guest system allows simple preparation by mixing all the peptide monomer units in the desired ratiometric amounts.

Another possible advantage of non-covalent decoration of PA nanofibers is the posibility choose the order of incorporation of the epitopes, as nanofiber host-guest epitope binding can take place during or after fiber assembly. This modular approach can also allow for the presentation of biomimicry biosignals whose covalent incorporation into a PA sequence would prove synhtetically demanding either by their length, conformational hindrances, overall yield or purification feasability. The dynamic nature of the non-covalent epitope binding does not limit biosignal presentation to static conformational restrictions imposed by traditional covalent bonds, thus allowing for a new spectra of cell responses to the hydrogel scaffold as a function of a particular host-guest system of choice.[31]

Lastly, by choosing a suitable host-guest pair that is stimuli-responsive (including light, pH, ion, redox or thermorresposiveness, see Figure 2.15) PA fibers might be selectively attached or detached to whatever biorrelevant epitope of choice, allowing dynamic on demand regulation of the non-covalent presentation of epitopes on self-assembled peptide nanostructures, whereby making them match the complex time-scales of physiological processes as our cationic host-guest system from Chapter 4 demonstrates (see Figure 4.28.A).

5.9 Closing remarks

In this study we have demonstrated the efficacy of a new high-density epitope presentation strategy on peptide amphiphile-based self-assembled scaffolds mediated by non-covalent interactions. This novel approach relied on the host-guest-mediated presentation of **RGDS** epitopes and led to increased PA nanofiber bioactivity.

Increasing concentrations of non-covalently attached **RGDS** epitopes correlated with incremented cell responses like substrate attachment, spreading and actin organisation as a consequence of the integrin receptor activation driven by the non-covalent presentation of biological cues. We hope that this work may open new molecular design possibilities to enhance biomimicry display on other self-assembled scaffolds relevant to tissue engineering and regenerative medicine applications.

This part of the thesis (including Chapter 5 and Chapter 4) demonstrated the benefits of the convergent incorporation of β**-CD** and **Ada** motifs in PA hydrogels. The next part of the thesis explores the potential to trigger supramolecular gelation by another family of host-guest interactions: those mediated by the cucurbit[n]uril family.

5.10 Materials and methods

All reagents were purchased from Sigma-Aldrich and used without any further purification unless otherwise stated. Phosphate buffered saline (PBS 1x), Dulbecco's Modified Eagle's Medium (DMEM), Hank's Balanced Salt Solution (HBSS), Penicillin/Streptomycin (P/S), and Foetal Bovine Serum (FBS), were obtained from Gibco (Life Technologies).

5.10.1 Peptide synthesis and purification

Peptide amphiphiles and were synthesised using modifications of previously reported SSPS procedures.[230] Guest-PAs were prepared following the same methodology presented in Section 4.12.1.[155]

***β*CD-RGDS** was prepared and purified following the work of Wong and collaborators (Figure 5.15).[225] Peptides were purified using reverse phase HPLC (RP-HPLC) and their identity was confirmed using electrospray ionisation mass spectrometry (ESI-MS).

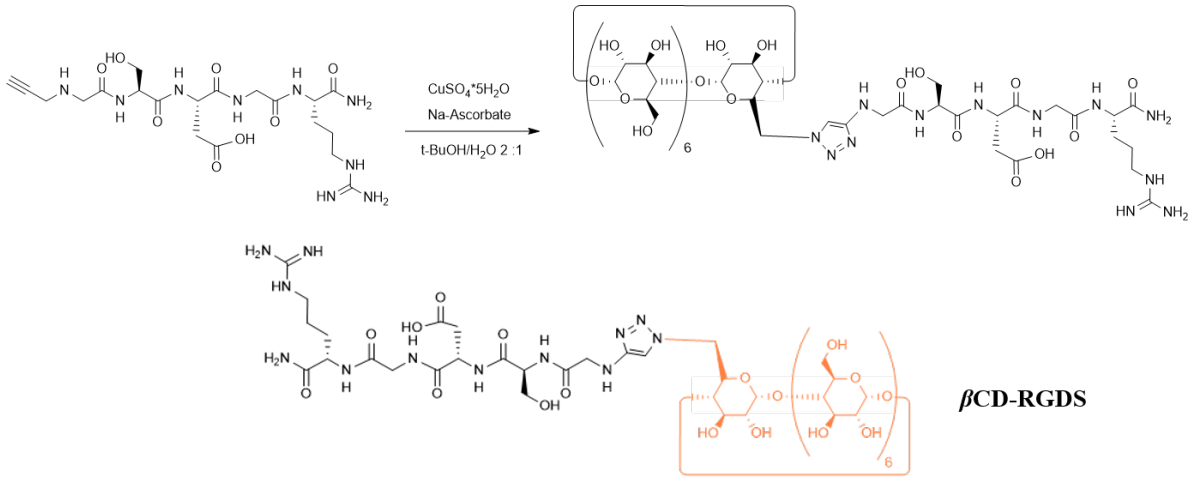

Figure 5.15: *Preparation of β**CD-RGDS** derivative.*[225]

5.10.2 Transmission electron microscopy (TEM)

Peptide 0.05 wt% HEPES solutions were negatively stained as follows: solutions were drop-casted on holey carbon-coated copper TEM grids (Agar Scientific, Stansted, UK), solution excess was blotted after 5 min incubation, then incubated one minute with 2% uranyl acetate, grids were then washed with ultrapure water for 30s and air dried for 24h at room temperature before imaging. Bright-field TEM images were acquired on a JEOL 1230 Transmission Electron Microscope operated at 80 kV. All the images were recorded by a Morada CCD camera (Image Systems) and at least six areas were analysed (corresponding to n $\geq$ 100 PA fibers).

5.10.3 Circular dichroism (CD)

Assessment of secondary structure of self-assembled nanostructures was undertaken with a 1 mm path-length quartz cuvette placed in a Pistar-180 spectropolarimeter (Applied Photophysics, Surrey, UK) equipped with a Peltier temperature controller, under a constant nitrogen purging at a constant pressure of 0.7 MPa and temperature of 25 °C. Peptides were dissolved in HEPES 10 mM saline (155 mM NaCl pH 7.4) reaching a final concentration of 0.01 wt%. Far UV spectra were recorded from 190 to 270 nm a wavelength step of 0.5 nm. Each represented spectrum is the average of three consecutive spectra. Temperature variable CD experiments were carried out between 10 ºC and 70 ºC, with a heating rate of 1 ºC/min, and collecting three spectra every 10 ºC.

5.10.4 Hydrogel preparation

Peptides were dissolved in HEPES buffer at a concentration of 1.5 wt%, mixed thoroughly according to the desired Filler-PA/Host-guest ratio, incubated at 80 °C for 30 min and let to slowly cool down to room temperature, this is called "peptide stock solution". Subsequently, a 30 μL drop of peptide stock solution was placed onto a polydimethylsiloxane (PDMS) support, injected with 15 μL of $CaCl_2$ 100 mM and incubated at 28 ºC and relative humidity of 38% for 24 h to afford 1 wt% self-assembled hydrogels in all cases.

5.10.5 Peptide string formation

An aliquot of 15 μL peptide stock solution was manually dragged from a pipette onto a glass slide covered by a thin layer of $CaCl_2$ 100 mM solution. Noodle-shaped viscoelastic strings were obtained and left to age for at least 15 minutes before using.

5.10.6 Polarised ligh microscopy

An optical microscope with polarising filters (Olympus BX60 Upright compound light microscope) was used to visualise birefringence in the noodle-shaped hydrogel structures. At least three samples were measured per condition ($n \geq 3$).

5.10.7 Scanning electron microscopy (SEM)

PA hydrogels underwent stepwise dehydration, critical point drying and gold coating before SEM imaging. Initially peptide hydrogels were stepwise dehydrated by immersion in increasingly concentrated ethanol solution (20%, 50%, 70%, 80%, 90%, 96%, 100%), for 5 min twice in each solution. Dehydrated samples were dried using a critical point dryer (K850, Quorum Technologies, UK) and gold coated before imaging on an Inspect F50 (FEI Company, the Netherlands) ($n \geq 3$).

5.10.8 Nuclear magnetic resonance (NMR)

E_3G_3Ada-PA was dissolved in D_2O at a final concentration of 10-12 mg/mL (using NaOD to promote peptide solubility) and 1 equivalent of β**CD-RGDS** was added to the mixture. Two dimensional nuclear Overhauser effect spectroscopy (NOESY) NMR spectra were recorded on a Bruker AvanceNEO 600 spectrometer at room temperature.

5.10.9 Rheology

Hydrogels' rheological characterization was performed with a DHR-3 Rheometer (TA Instruments, USA) using an 8 mm diameter parallel plates geometry. G' (storage modulus) and G"(loss modulus) were monitored by amplitude and frequency sweeps. G' and G" moduli were measured at 25 °C and a constant frequency of 1 Hz in the 0.01% – 10% strain during the amplitude sweep, while the oscillation frequency experiments were carried out at a 0.1% fixed strain along 0.1 – 100 Hz.

5.10.10 Cell culture experiments

All cell culture experiments were conducted with a NIH-3T3 fibroblasts cell line. NIH-3T3 fibroblasts were cultured with DMEM medium supplemented with 10% fetal bovine serum (FBS) and 1% penicillin and 1% streptomycin. Cells were maintained in a humidified 5% CO_2 atmosphere at 37 °C.

5.10.11 In vitro cell viability assays

15 000 NIH-3T3 fibroblasts were seeded in a 96-well plate and cultured for 1 day until a monolayer was formed. Cells were incubated with a peptide solution of the desired concentration for 1 h. Peptide was then removed, cells were washed thrice with HBSS and placed with fresh DMEM medium and imaged the next day using the LIVE/DEAD Viability/Cytotoxicity Assay Kit (Thermo Fisher Scientific, UK). Cells were incubated in 10 mM Calcein AM and 1 mM ethidium homodimer-1 (EthD-1) DMEM medium for 30 min before imaging, stained samples were visualised on an inverted epifluorescence widefield Leica DMI4000B microscope (Leica, Germany) equipped with a LEICA DFC300 FX CCD camera.

5.10.12 In vitro cell adhesion assessment

On a typical experiment a 5 μL aliquot of a 10 mM PA ternary mixture of **E_3-PA/E_3G_3Ada-PA•βCD-RGDS** was injected within 50 μL of $CaCl_2$ 100 mM solution (1 mM peptide final concentration). After 30 minutes gelation the excess of $CaCl_2$ was removed and 30 000 NIH-3T3 cells were seeded onto the hydrogels.

Hydrogels ($n \geq 3$) were incubated for 30 min, 1 h and 3 h timepoints in supplemented DMEM before fixation, staining and imaging as follows. Cells were fixed using a 4 wt% paraformaldehyde (PFA) 1x PBS solution overnight at 5 ^{o}C, washed with PBS, blocked with a BSA 2 wt% 1x PBS solution for 2 h, washed with PBS. Samples were firstly stained with DAPI (Sigma-Aldrich) at a 1/5000 dilution for 5min (cell nuclei staining), washed with 1x PBS, then stained with Rhodamine-Phalloidin R415 (Sigma-Aldrich) at a 1/250 dilution in 1x PBS for 40 min (F-Actin staining). Confocal fluorescent images were acquired using a Leica TCS SP2 and Zeiss LSM710 confocal microscopes. Cell adhesion was monitored using Fiji ImageJ software (http://imagej.nih.gov/ij) (NIH, USA) to quantify the ratio of cell area to cell nuclei area ($n \geq 50$ cells per condition).

Part III

Peptide Amphiphiles & Cucurbit[8]uril-Based Interactions

Chapter 6

Peptide Amphiphile Hydrogels Based on a Homoternary Cucurbit[8]uril Host-Guest Complex

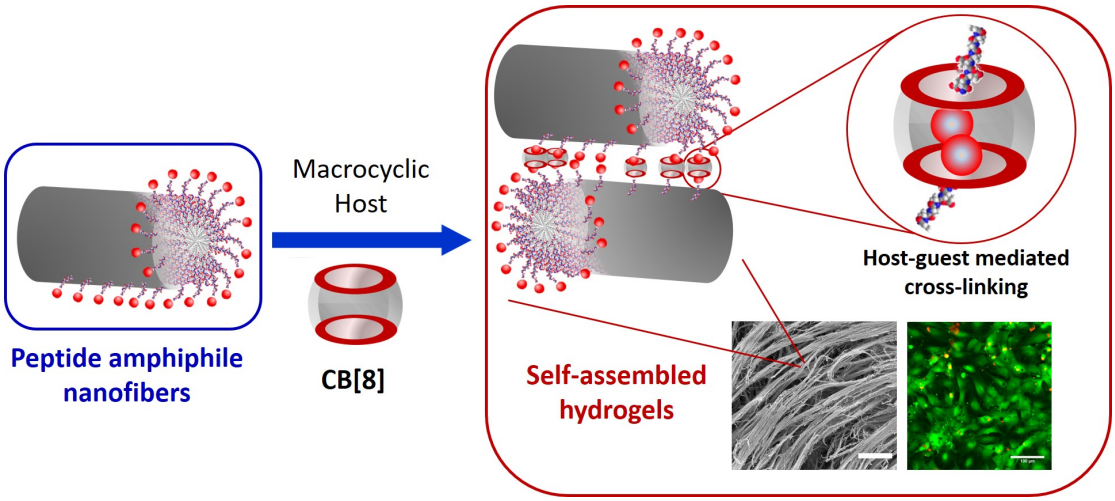

Figure 6.1: ***CB[8]****-guest strategy to dynamically cross-linking PA nanofibers.*

This chapter describes an unreported strategy to generate PA hydrogels based on the formation of a host-guest homoternary complex with **CB[8]** and aromatic amino acid-bearing PA nanofibers. The molecular design is firstly presented, then evidence of the host-guest phenomena is provided, followed by morphological, rheological and cell culture studies.

This study will be submitted for publication to *Biomaterials Science*:

- **Redondo-Gómez, C.**; Padilla-Lopategui, S.; Azevedo, H. S.; Mata, A. Self-assembling peptide amphiphile hydrogels based on a homoternary cucurbit[8]uril host-guest complex. *To be submitted to Biomaterials Science*.

6.1 Overview

Most hydrogels used as scaffolds for tissue engineering and model extracellular matrices for biological studies are based on fibrillar network formation of covalent polymer networks. Supramolecular hydrogels based on PAs are a more promising alternative, as they can recapitulate aspects of native extracellular matrixes in a better way that covalent polymer hydrogels.

Though PA hydrogels are conventionally formed via electrostatic screening, more sophisticated and dynamic hydrogelation mechanisms might help to improve PA design and application. Here we show an unreported host-guest-mediated PA hydrogelation method that relies on the formation of a host-guest homoternary complex with **CB[8]** and aromatic amino acid-bearing PA nanofibers.

As a result of the host-guest non-covalent crosslinking between PA nanofibers, morphological and rheological differences were found when host-guest mediated PA hydrogels were compared to their ion-based equivalents. As both systems exhibited similar biocompatibility, we believe that **CB[8]**-mediated hydrogelation can be used as an additional tool to understand and improve the design of PA, peptide and other supramolecular polymer-based systems of biomedical and clinical relevance.

6.2 Introduction

Supramolecular chemistry provides materials science with powerful approaches to control molecular self-assembly.[31,231] Property control relies on the manipulation of noncovalent forces guiding biomolecular self-organization and recognition processes.[232,233] This often confers reversible, tunable, dynamic and modular control over morphological and functional aspects of the resulting assemblies.[234,21] As a consequence, many functional and precisely organized polymer,[100,235] sugar,[205] nucleic acid,[236] protein,[237,238] peptide,[239,240] and peptide derivative[217]-based supramolecular biomaterials have been reported.

Hydrogels are soft materials suitable for biomedical applications in the light of their molecular-scale control over mechanical and bioresponsive properties.[7,6,241] Unlike polymer-based hydrogels, supramolecular hydrogels are composed of small molecules that self-assemble through non-covalent interactions into often fibrillar 1D objects (see Section 2.3).[38] Supramolecular peptide-based hydrogels rely on this principle by either using nature-inspired motifs (primarily β-sheet formation) or non-native designs to promote self-assembly, which is the case of peptide amphiphiles.[63]

PAs represent a comprehensively studied family of self-assembling peptides programmed to form fibrillar 1D structures in aqueous environments.[96] PA molecules often comprise a lipid hydrophobic tail, a β-sheet forming segment and a hydrophilic polar head of amino acid residues apt to carry biofunctional epitopes. Either pH changes or the presence of metal cations produce charge screening of these segments, thus yielding self-assembled μm-long 1D fibers (see Section 2.4).[194]

As this fibrillar 3D network assembles macroscopic hydrogels that mimic the natural extracellular matrix (ECM) are obtained.[1] These hydrogels have proved their utility in tissue engineering and regenerative medicine applications, as they prompt in vitro cell migration[121] and differentiation[209] as well as in vivo regeneration of axons,[123] blood vessels,[124] myocardium,[107] bone,[125] and cartilage.[127]

Host guest interaction motifs are central in supramolecular materials, and they usually involve the formation of a complex between a suitable macrocycle (most commonly a cyclodextrin or a cucurbit[n]uril) with appended guests on polymer chains (see Section 2.5).[162] Even though the vast majority of efforts to create hydrogels via host–guest interactions have focused on polymer-based hydrogels,[221,82] a recent paper by Redondo-Gómez and collaborators studies the use of host-guest **Ada/βCD** cues as non-covalent crosslinks between PA nanofibers.[155] Nevertheless no reports on cucurbit[n]uril-PA based systems are found in literature.

Cucurbit[8]uril (**CB[8]**) is a macrocyclic octamer of glycoluril units bound together by 16 methylene bridges (Figure 6.2).[146,242] **CB[8]** features two identical polar portals to a hydrophobic cavity, large enough to simultaneously accommodate two organic guests,[73] thus forming highly stable ternary complexes with a variety of small chemical species,[243,244] including aromatic amino acids: tyrosine (Y),[149] phenylalanine (F) and tryptophan (W, see Section 2.5).

These last two amino acids have been reported to selectively bind to **CB[8]** forming a 2:1 homoternary complex in several systems, including tri-[245] and oligopeptides,[246] and macromolecular systems including proteins,[247] enzymes,[248] polysaccharide derivatives,[140,249] intracellular drug delivery systems,[250] as well as polymer nanoparticles,[251] and styrenic polymer-based hydrogels.[252]

In this chapter, we describe the synthesis and self-assembly study of new PA class (Figure 6.2), able to undergo conventional ion-mediated gelation but also forms supramolecular gels via an unreported gelation mechanism via homoternary host-guest complex with **CB[8]**. Thorough spectroscopic characterisation of the host-guest complexation mechanism is provided, as well as a comparison of the hydrogels' mechanical properties and their suitability to be used in cell culture scaffolds for tissue engineering applications.

6.3 Guest-PA molecules suitable for CB[8] binding

6.3.1 Rationale and molecular design

As aromatic amino acids (most reports are on phenylalanine and tryptophan) are known to form a complex with **CB[8]**[252,245] we investigated the effect of presenting these aromatic amino acids at the surface of self-assembled PA nanofibers. In this study we designed two anionic guest PA molecules isostructural to **E_3-PA** (C_{16}-$V_3A_3E_3$), whose supramolecular aggregation is known to a good extent.

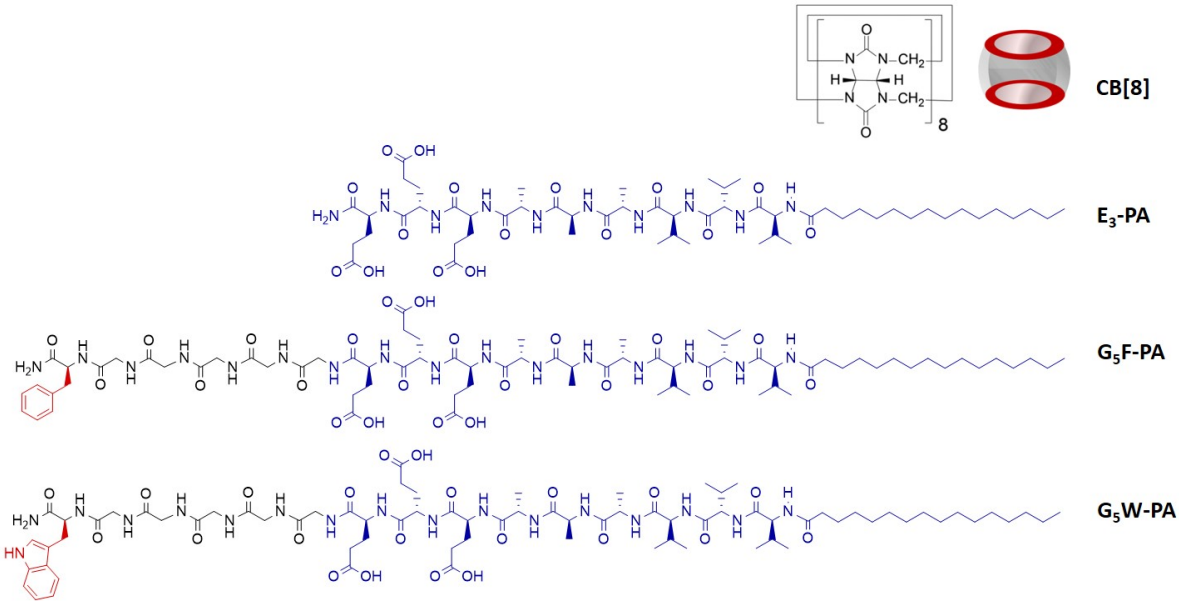

Figure 6.2: *Molecular structures of the peptide amphiphile (PA) molecules reported in this study. All PA molecules are isostructural to the negatively charged **E_3-PA**. Five glycine residues were included as spacer, followed by either a phenylalanine or a tryptophan residue in **G_5F-PA** and **G_5W-PA** respectively.*

Both guest-PAs (sequence: C_{16}-$V_3A_3E_3G_5X$) comprise an aliphatic palmitoyl tail C_{16}- at their N-terminus, followed by a β-sheet forming amino acid sequence -V_3A_3- that ensures the formation of high-aspect ratio nanofibers. Three ionisable glutamic acid residues -E_3- are included immediately after in order to promote nanofiber solubility in water. In order to promote display of aromatic amino acid residues (X) a pentaglycine -G_5- spacer was included after the negatively charged region, the insertion of this glycine pentad allows for a flexible, uncharged spacer that separates further amino acid residues approximately 19.3 Å from the negatively charged fiber region.[115]

Table 6.1: Structural information of peptide amphiphiles presented in this chapter.

Peptide	Sequence	Use
E_3-PA	$C_{15}H_{31}CONH\text{-}V_3A_3E_3\text{-}CONH_2$	Control-PA
G_5F-PA	$C_{15}H_{31}CONH\text{-}V_3A_3E_3G_5F\text{-}CONH_2$	Guest-PA
G_5W-PA	$C_{15}H_{31}CONH\text{-}V_3A_3E_3G_5W\text{-}CONH_2$	Guest-PA

This structural feature combination allows for surface display of either a phenylalanine (X = F in **G_5F-PA**) or a tryptophan (X = W in **G_5W-PA**) residue once the PA monomers self-assemble into nanostructures (Figure 6.2).

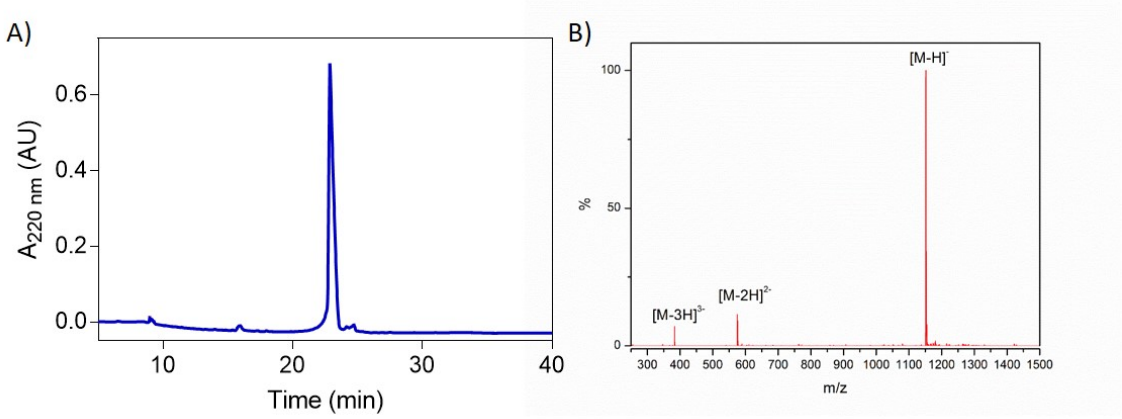

Figure 6.3: *Purity and sequence confirmation corresponding to **E_3-PA**. A) RP-HPLC and B) ESI-MS traces corresponding to **E_3-PA**.*

Control **E_3-PA**, and guest-PAs: **G_5F-PA** and **G_5W-PA** were synthesized using standard solid-state peptide synthesis (SSPS) followed by purification through RP-HPLC. Further synthesis and characterization details can be found in Section 6.9.2 (Figures 6.3, 6.4, 6.5). All of these results are briefed in Table 6.2.

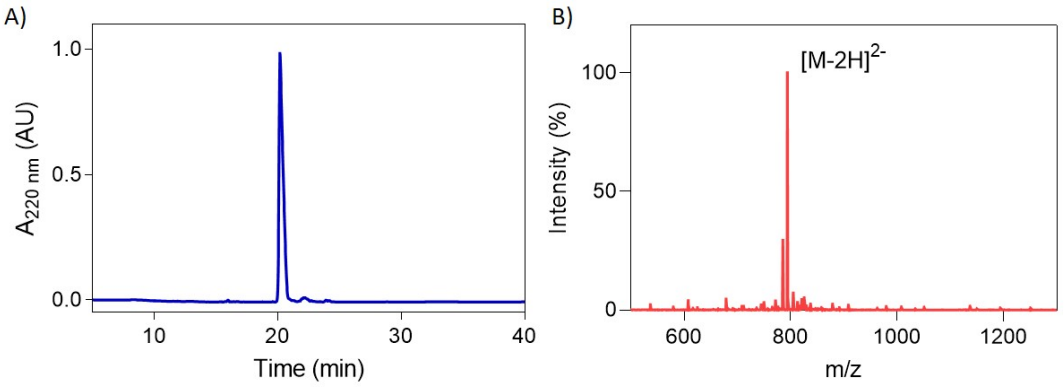

Figure 6.4: *Purity and sequence confirmation corresponding to **G_5F-PA**. A) RP-HPLC and B) ESI-MS traces corresponding to **G_5F-PA**.*

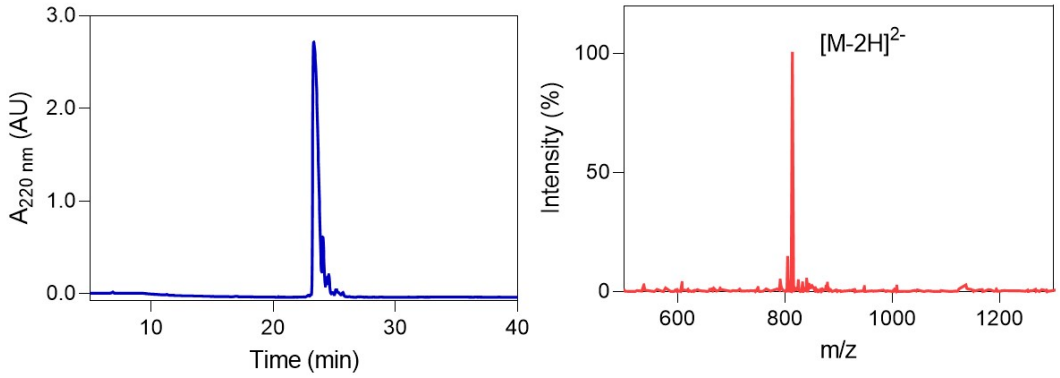

Figure 6.5: *Purity and sequence confirmation corresponding to* ***G_5W-PA****. A) RP-HPLC and B) ESI-MS traces corresponding to* ***G_5W-PA****.*

Table 6.2: Chemical characterisation of the herein reported anionic peptide amphiphiles.

Peptide	Calculated (m/z)	Found (m/z, Ø)	Purity (%, ♯)
E_3-PA	1152.70	1151.7 $[M-H]^-$	96
G_5F-PA	1584.88	791.44 $[M-2H]^{2-}$	97
G_5W-PA	1623.89	813.58 $[M-2H]^{2-}$	95

Notes:
Ø Determined through ESI-MS,
♯ Assessed through RP-HPLC.

6.3.2 Guest-PAs supramolecular self-assembly in solution

Self-assembled **G_5F-PA** and **G_5W-PA** nanofiber formation was investigated using transmission electron microscopy (TEM). TEM micrographs evidence the presence of micron-long nanofibers of around 11-14 nm diameter in both guest-PA solutions at 25 ºC. **G_5F-PA** originated stand-alone nanofibers (Figure 6.6.A), whereas **G_5W-PA** nanofibers appear to coalesce into submicron-size bundles (Figure 6.6.C). A more robust stacking between adjacent indole rings in **G_5W-PA** can account for this tendency to form bundles, which was not observed in **G_5F-PA** under the same micromolar concentration regime .

Negatively charged PA molecules analogue to **E_3-PA** (therefore, analogue to **G_5F-PA** and **G_5W-PA** as well) offer the possibility to access hierarchical nanofiber ordering levels via a entropy driven dehydration-rehydration process (see Section 2.4.3 and Figure 2.11).[121]

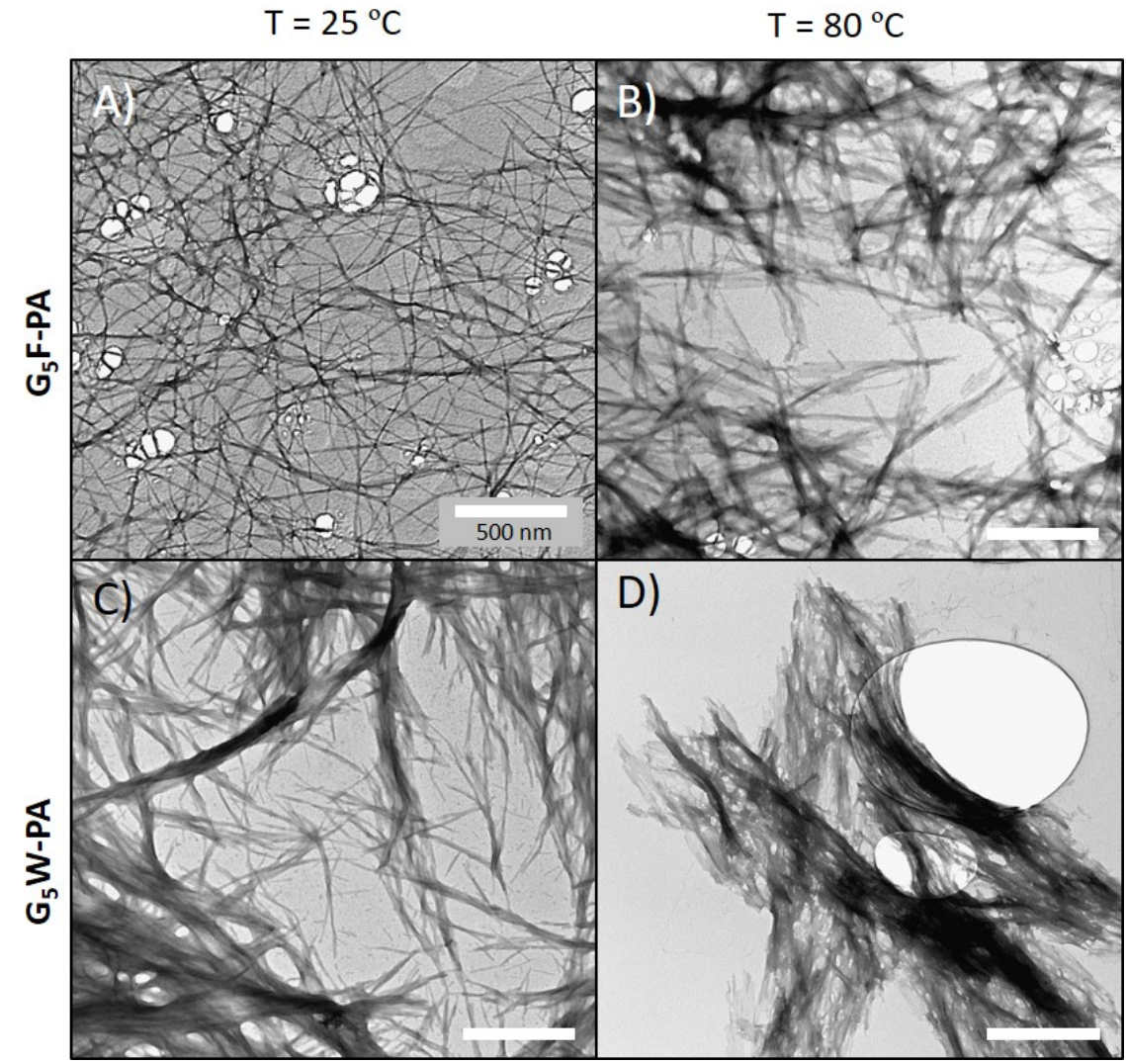

Figure 6.6: *Self-assembly of* ***G*$_5$*F-PA*** *and* ***G*$_5$*W-PA*** *into nanofibers. A) TEM micrographs of* ***G*$_5$*F-PA*** *and C)* ***G*$_5$*W-PA*** *at 25 ºC. B, D) TEM micrographs of the same PA samples thermally treated at 80 ºC ([****G*$_5$*F-PA****] = [****G*$_5$*W-PA****] = 63 μM, in HEPES buffer).*

In order to explore this possibility for our guest-PAs **G$_5$F-PA** and **G$_5$W-PA** solutions were heated at 80 ºC and then slowly cooled down to room temperature. In the case of **G$_5$F-PA** TEM micrographs evidence formation of intertwined filaments with larger diameters than the pristine nanofibers (Figure 6.6.B), meanwhile **G$_5$W-PA** bundles turned into micron-size aggregates with highly parallel oriented filaments (Figure 6.6.D). These results show that the presence of **G$_5$F** or **G$_5$W** motifs at the surface of PA nanofibers neither disrupts fiber formation nor interferes with their nano- to microscale hierarchical self-assembly.

6.4 Guest-PAs-CB[8] host-guest interactions

As PA nanofibers with pendant phenylalanine and tryptophan amino acids were found to assemble in solution, it was hypothesised that these aromatic residues might form their corresponding inclusion complex with **CB[8]**.

6.4.1 Homoternary complex formation

^{1}H-NMR spectroscopy revealed changes in the chemical shifts of the signals between 7.1 and 7.8 ppm , corresponding to the protons of the phenyl and indole ring in **G_5F-PA** and **G_5W-PA**, suggesting their placement in a new magnetic environment when in presence of **CB[8]** (Figures 6.7 and 6.8).

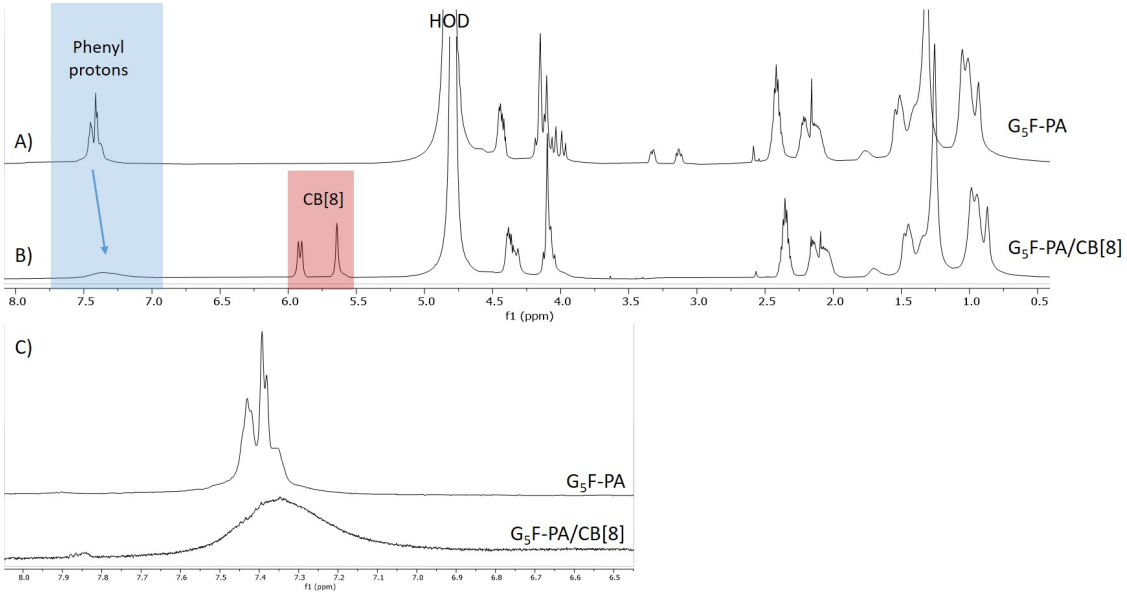

Figure 6.7: *^{1}H-NMR spectra corresponding to A) **G_5F-PA**, B) its **CB[8]** homoternary complex (**G_5F-PA**)$_2$•**CB[8]**, and C) a zoom of the aromatic region from both spectra (600 MHz, 4.1 mM, D_2O/ND_4OD, 298 K).*

Monitoring of aromatic motifs fluorescence through the method of continuous variations[253] (Figure 6.9) allowed to construct the Job Plots shown in (Figure 6.10.A), whose maxima around 0.66 PA mole fraction confirm the expected 2:1 binding mode and the formation of the homoternary complexes (**G_5F-PA**)$_2$•**CB[8]** and (**G_5W-PA**)$_2$•**CB[8]**. The slightly steeper triangular-like shape originated by **G_5F-PA** might be an indicator of a greater affinity towards **CB[8]** than **G_5W-PA**, in any case both complexes should exhibit high binding equilibrium constants (K_{eq} up to 10^{12} M^{-2}).[252]

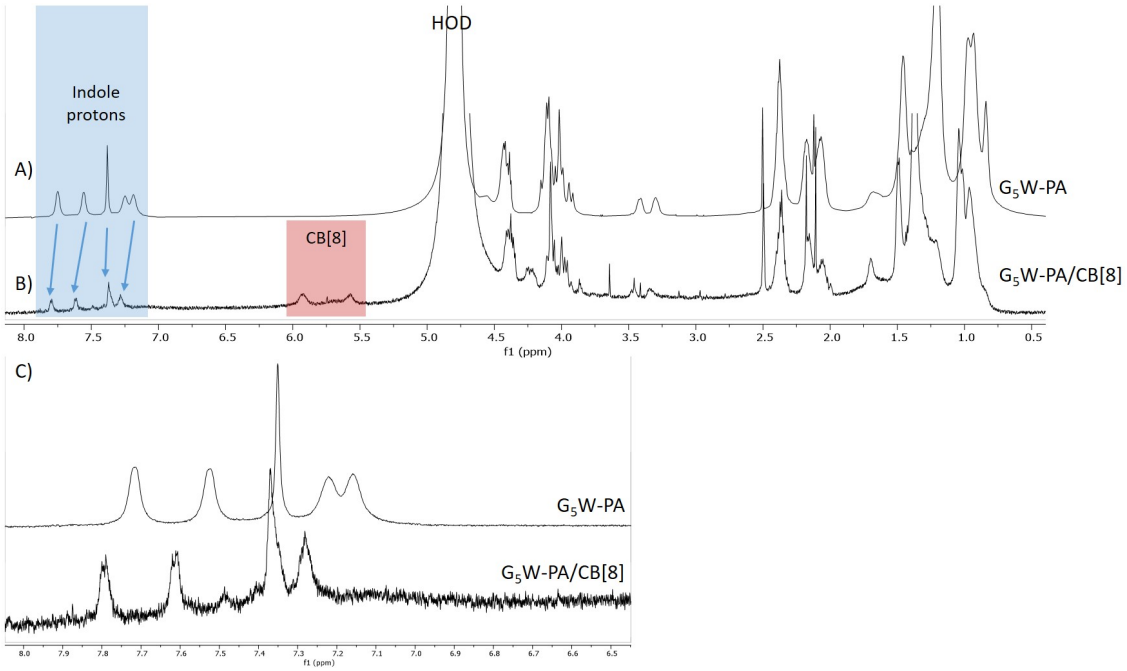

Figure 6.8: *^{1}H-NMR spectra corresponding to A) **G_5W-PA**, B) its **CB[8]** homoternary complex (**G_5W-PA**)$_2$•**CB[8]**, and C) a zoom of the aromatic region from both spectra (600 MHz, 3.8 mM, D_2O/ND_4OD, 298 K).*

There are a collection of intermolecular events taking place while these complexes form. Inclusion of PA molecules can be accounted by the release of 'high-energy' water upon complexation, as well as the formation of hydrogen bond between N-H protons from peptide bonds and both of **CB[8]** carbonyl portals,[147] and aromatic interactions between the aromatic amino acids. In fact, aromatic interactions seem to play a key role, as **CB[8]** appears not to interact with PA molecules lacking the **G_5F** or **G_5W** motifs as circular dichroism (CD) studies of **E_3-PA/CB[8]** revealed (Figure 6.10.B). These results demonstrate that PA molecules can take part in homoternary host-guest complexations with a suitable macrocyclic host.

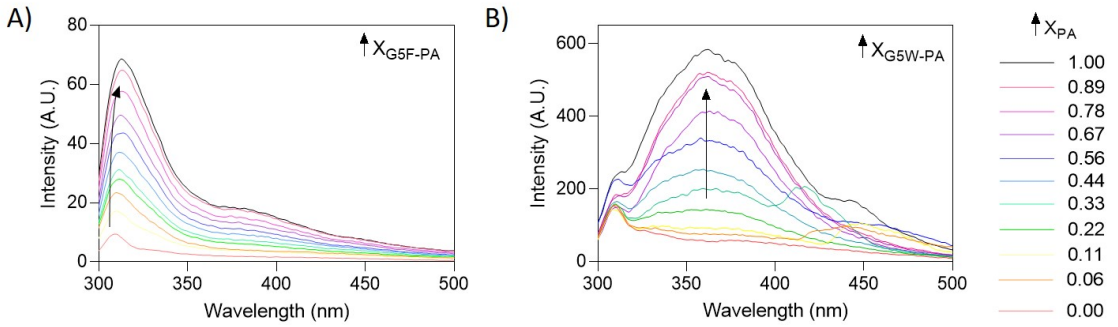

Figure 6.9: *Fluorescence spectra of increasing molar ratio of PA:**CB[8]** employed for Job Plot analysis.*

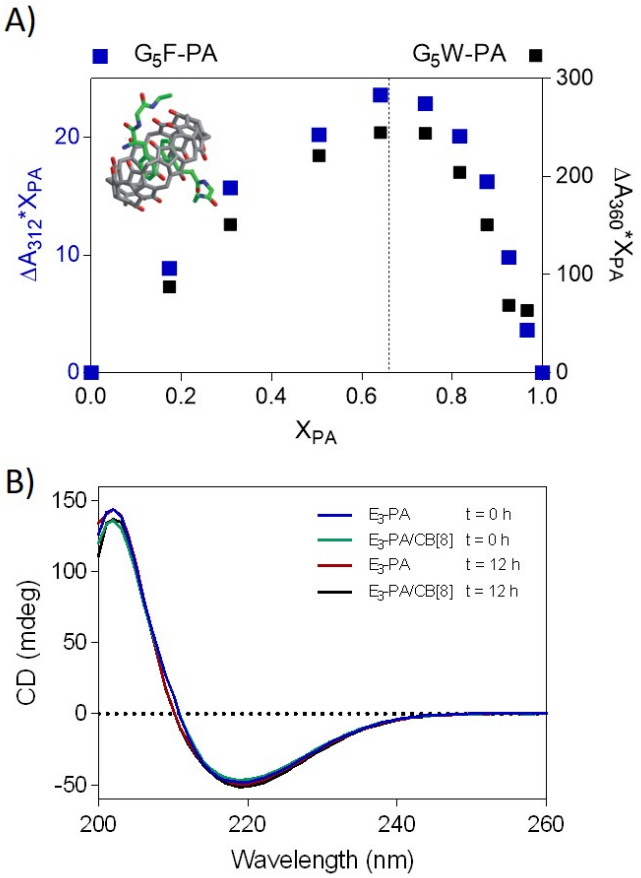

Figure 6.10: *Host-guest interaction between PAs and their complementary macrocyclic host **CB[8]** in aqueous media. A) Fluorescence spectroscopy revealed the formation of (**G$_5$F-PA**)$_2$•**CB[8]** and (**G$_5$W-PA**)$_2$•**CB[8]** 2:1 complexes. B) Circular dichroism (CD) evidences no molecular binding between control **E$_3$-PA** and **CB[8]**.*

6.4.2 CB[8]/Guest-PA interactions affect fiber conformation

As complexation between (**G$_5$F-PA**)$_2$•**CB[8]** and (**G$_5$W-PA**)$_2$•**CB[8]** was evidenced, we decided to investigate whatever repercussions these complexations might have on the secondary structure of the self-assembled nanofibers. CD investigations showed that both **G$_5$F-PA** and **G$_5$W-PA** nanofibers exhibit a β-sheet signature signal characterised by a positive maximum centred at 205 and 203 nm respectively (Figure 6.11.A,D), whereas in presence of **CB[8]** both signals experience a 1 nm red-shift and a significant intensity increment, a similar shift was observed in the negative minima centered around 220 and 218 nm. These red-shifts can be attributed to increasing levels of twisting of the β-sheets at the nanofibers core, while the intensity increase can be the result of re-arrangement of these β-sheets into longer and more regular ones as a result of the binding with **CB[8]** host units.[224]

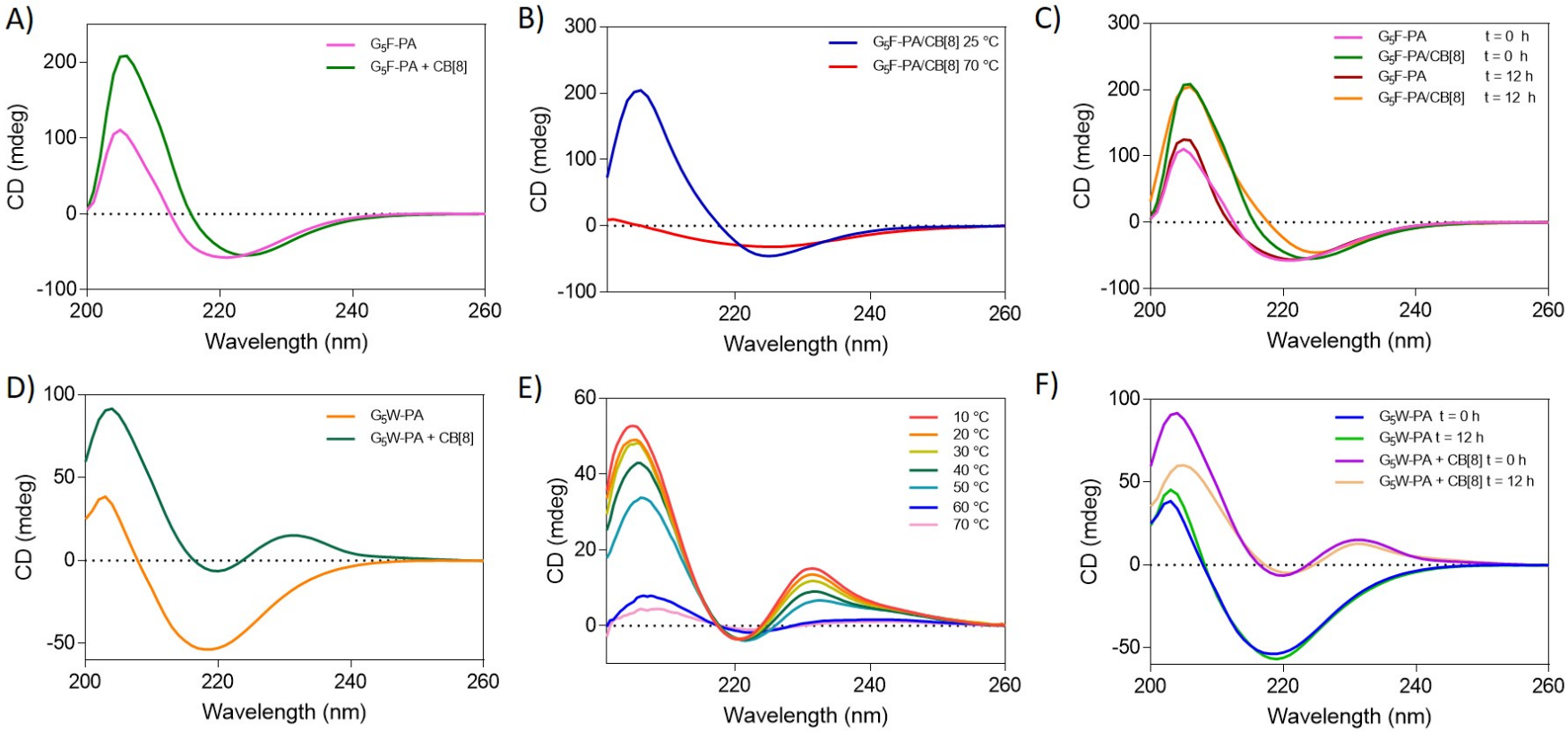

Figure 6.11: *Guest-PAs secondary structure assessment in presence of* ***CB[8]*** *in aqueous media. A) CD spectra of* $\boldsymbol{G_5}$***F-PA*** *and its* ***CB[8]*** *mixture exhibit β-sheet conformations. B) Temperature variable CD shows how these β-sheets are temperature sensitive. C) Time evolution of* $\boldsymbol{G_5}$***F-PA*** *self-assembled nanofibers and the ternary complex* $(\boldsymbol{G_5}$***F-PA***$)_2\bullet$***CB[8]***. *D)* $\boldsymbol{G_5}$***W-PA*** *nanofibers exhibit β-sheet conformation, while interaction with* ***CB[8]*** *produces radical changes in its CD spectra. E) CD studies indicate that* $(\boldsymbol{G_5}$***W-PA***$)_2\bullet$***CB[8]***. *formation is temperature sensitive. F)* $\boldsymbol{G_5}$***W-PA*** *shows little time-evolution in its secondary structure, while the ternary complex* ***CB[8]***$\bullet(\boldsymbol{G_5}$***W-PA***$)_2$ *exhibits loss of β-sheet content after 12 h of incubation at 25 ºC (*$[\boldsymbol{G_5}$***F-PA***$] = [\boldsymbol{G_5}$***W-PA***$] = 63$ *μM, in HEPES saline buffer).*

In the case of **G_5W-PA**/**CB[8]** mixtures, an important intensity increase took place, accompanied by the notorious appearance of a positive maximum at 231 nm (Figure 6.11.D). Even though a positive band at this wavelength can be associated to disulphide bonds, we can discard this possibility,[254] and attribute it to close intermolecular contacts between indole rings from adjacent tryptophan residues,[255,256] as in the case of PEG-ylated tryptophan-containing amphiphiles.[257]

CD investigations showed how the formation of homoternary $(PA)_2$•**CB[8]** complexes is temperature sensitive, maintaining significant degrees of interaction at physiologically relevant temperatures, and being disassembled above 60 ºC (Figure 6.11.B,E). $(PA)_2$•**CB[8]** complexes exhibited conformational changes after 12 h of ageing. The negative minimum originally centered at 223 nm in (**G_5F-PA**)$_2$•**CB[8]** nanofibers exhibited a 3 nm red-shift indicating further β-sheet twisting after initial fiber preparation (Figure 6.11.C), while the (**G_5W-PA**)$_2$•**CB[8]** positive maximum lost about 25% of its initial intensity, indicating a possible loss of β-sheet length and regularity due to ageing (Figure 6.11.F). These findings are in good agreement with other host-guest PA systems based on **Ada**/**βCD** interactions.[155] These results show that supramolecular complexations at the periphery of guest-PA nanofibers can lead to conformational changes in peptide monomer units.

6.5 Self-assembled hydrogels based on PA-CB[8] host-guest interactions

6.5.1 CB[8] triggers PA hydrogelation

Having assessed how the formation of homoternary $(PA)_2$•**CB[8]** complexes occurring at diluted concentration regimes, we decided to investigate if this non-covalent union can be used to dynamically cross-link PA nanofibers at higher concentrations relevant to hydrogel formulation. When a 350 μM solution of **CB[8]** was injected into **G_5F-PA** about 6 mM solution, a transparent 1 wt% gel was obtained. **G_5W-PA** rendered a more turbid gel.

Gelation of both PA solutions represented a macroscopic reflection of changes in self-assembly at the molecular level, therefore we proceeded to assess those changes in the microstructure of the gels.

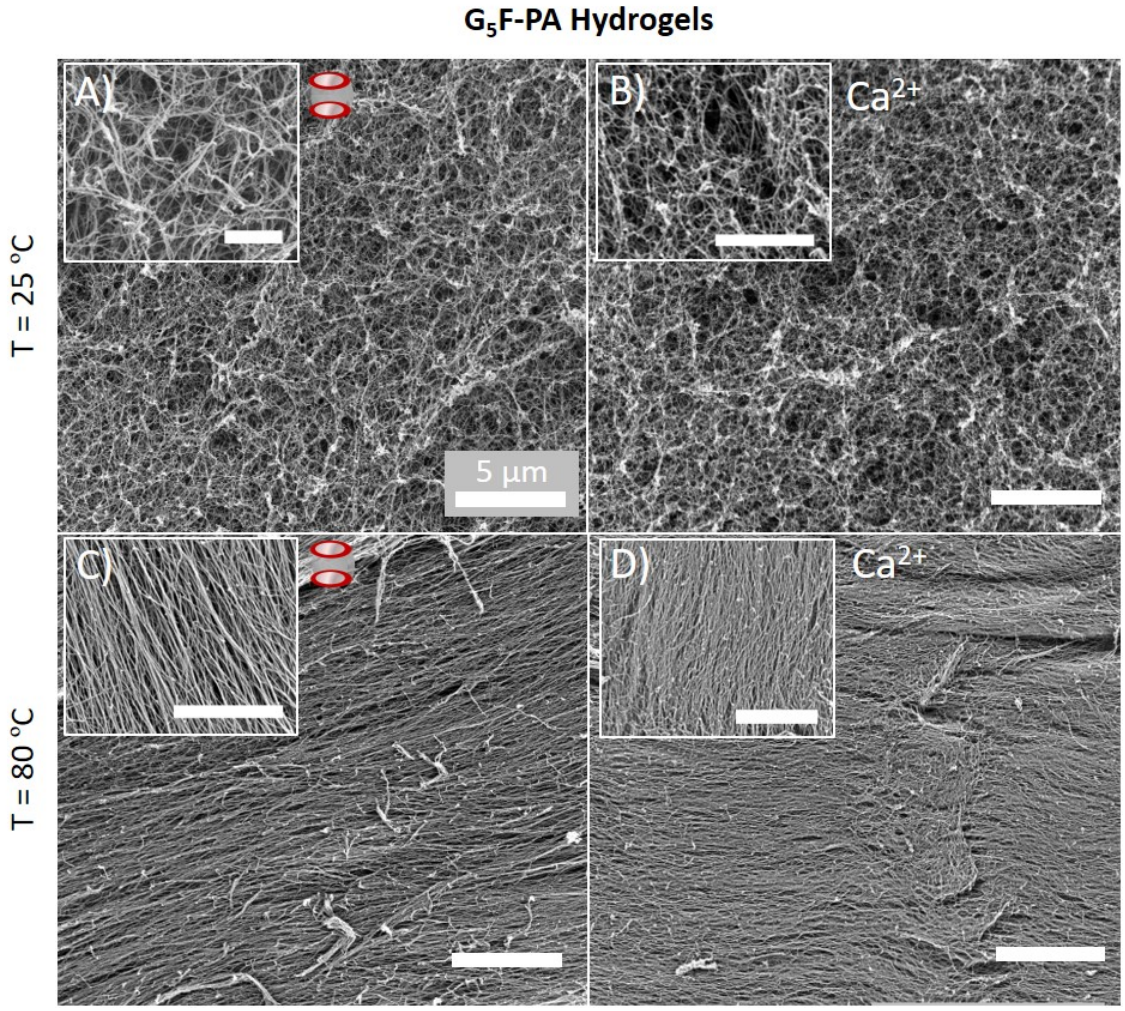

Figure 6.12: *Microstructure analysis of **G_5F-PA**-based hydrogels showing nanofiber persistence and alignment due to thermal treatment in **CB[8]** and Ca^{2+}-based gels. A-D) SEM micrographs of **G_5F-PA** hydrogels: A) non-heated **CB[8]**-based B) non-heated Ca^{2+}-based C) heated **CB[8]**-based, and D) heated Ca^{2+}-based. (1 wt% gels in all cases, [**CB[8]**] = 350 µM, [Ca^{2+}] = 50 mM, scale bars = 5 µm, inset scale bars = 2 µm).*

Scanning electron microscopy (SEM) images exhibit the persistence of a fibrillar 3D network of over micron-length nanofibers in the case of **G_5F-PA/CB[8]** hydrogels (Figure 6.12.A). Meanwhile **G_5W-PA/CB[8]** hydrogels exhibited shorter fiber arrays, randomly stacked forming a three-dimensional network (Figure 6.13).

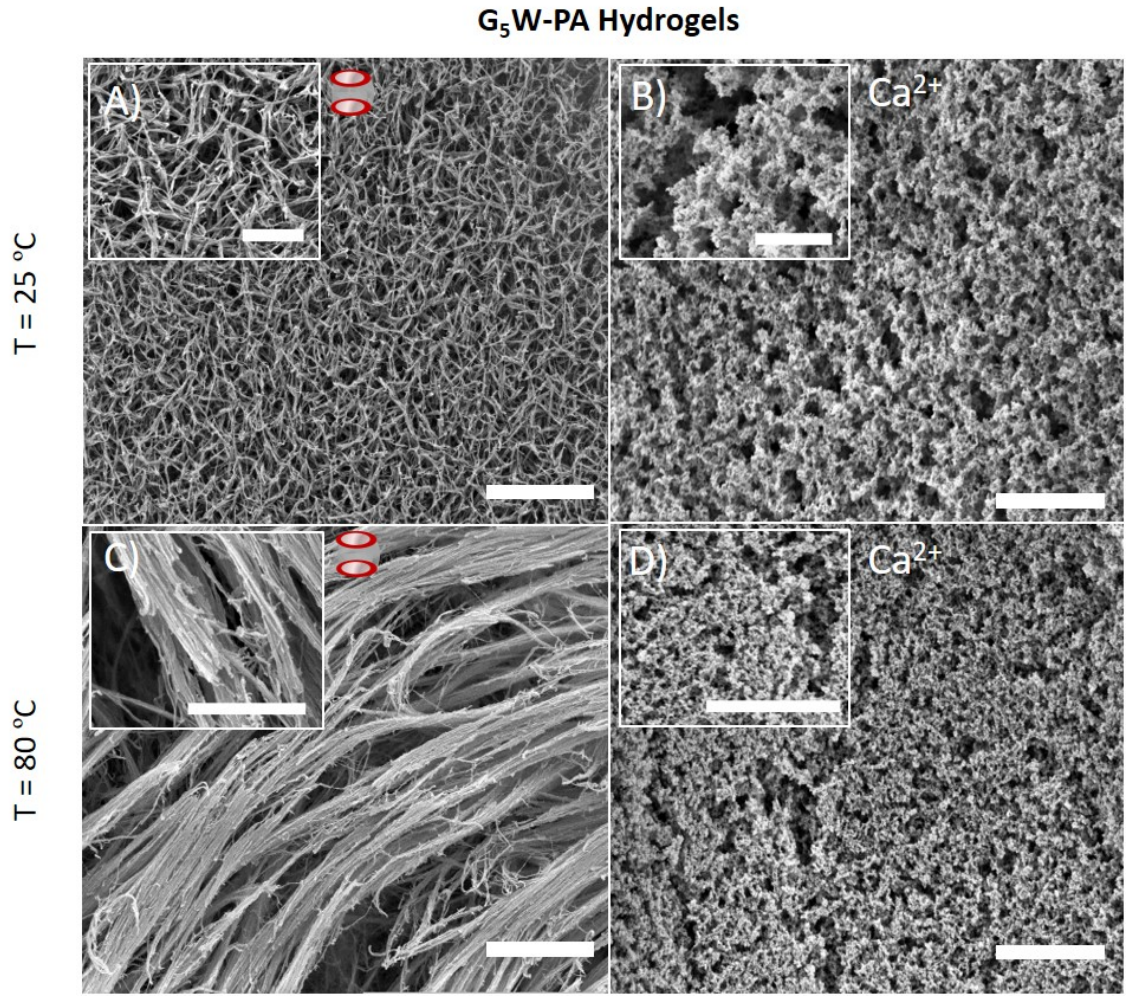

Figure 6.13: *Microstructure analysis of* ***G*$_5$*W-PA****-based hydrogels showing nanofiber persistence and alignment due to thermal treatment in* ***CB[8]*** *and* Ca^{2+}*-based gels. A-D) SEM micrographs of* ***G*$_5$*W-PA*** *hydrogels: A) non-heated* ***CB[8]****-based B) non-heated* Ca^{2+}*-based C) heated* ***CB[8]****-based, and D) heated* Ca^{2+}*-based (1 wt% gels in all cases, [****CB[8]****] = 350 µM, [*Ca^{2+}*] = 50 mM, scale bars = 5 µm, inset scale bars = 2 µm).*

Thermally treated guest-PA solutions were also subjected to gelation via **CB[8]** complex formation, thermally treated **G$_5$F-PA**/**CB[8]** hydrogels exhibited nanofiber alignment across micron scales (Figure 6.12.C), meanwhile thermally treated **G$_5$W-PA**/**CB[8]** hydrogels presented twisted filaments made of bundled peptide fibrils. Thermal treatment appears to promote parallel alignment of nanofibers (Figure 6.13.C) into peptide fibrils of greater size than those found in TEM images of non-gelated **G$_5$W-PA** solutions (Figure 6.12.D) as a result of fiber interaction with **CB[8]** (Figure 6.14).

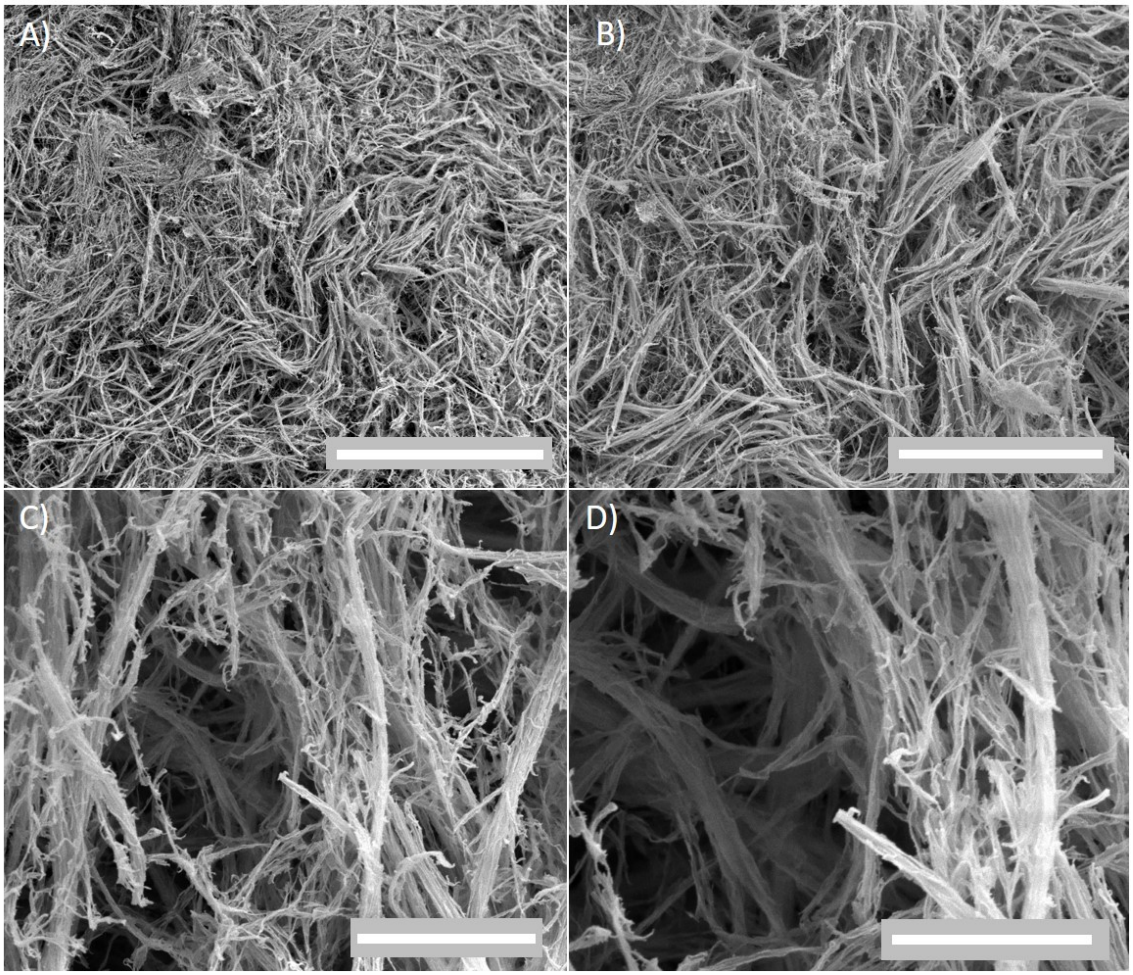

Figure 6.14: *SEM micrographs corresponding to* ***G_5W-PA/CB[8]*** *hydrogels (scale bars = 75 µm, 38 µm, 3.8 µm, and 2.3 µm respectively).*

Similar apparition of bundled and twisted fiber morphologies of varying diameters has been reported by Freeman and co-workers,[17] the emergence of such morphologies is attributed to large-scale spatial redistribution of molecules, directed by strong noncovalent electrostatics and Watson-Crick DNA base-pairing. Our study might contribute to add host-guest complexations to this list of interactions. The above discussed results show how the combination of simple thermal alignment of nanofibrillar materials and the dynamic cross-linking ability of **CB[8]** can lead access to further hierarchical ordering levels in self-assembled peptide-based hydrogels.

6.5.2 CB[8]-based versus Ca^{2+}-based PA hydrogelation

PAs traditionally form self-supporting gels from solutions upon pH changes or addition of metal ions.[194] **G_5F-PA** and **G_5W-PA** were found to be no exception, as addition of $CaCl_2$ (as source of Ca^{2+} ions) rendered transparent gels in every case. Room temperature **G_5F-PA** solutions originated anisotropic fibrillar 3D networks (Figure 6.12.B), meanwhile thermally treated **G_5F-PA** solutions rendered regularly aligned nanofibers (Figure 6.12.D) similar to their analogue **CB[8]**-based gels in both cases.

G_5W-PA Ca^{2+}-based hydrogels exhibited significant differences both in the room temperature (Figure 6.13.B) and thermally treated cases when compared to their **CB[8]**-based analogue gels. No fibrillar network formation was observed, but the presence of a continuous assembly of amorphous particles was found instead Figure 6.13.D).

The herein reported host-guest-based mechanism and the traditional ion-based gelation approach showed similar capacities to render fiber formation and alignment in **G_5F-PA** gels, meanwhile the host-guest gelation mechanism allowed to access further structuring capacities in **G_5F-PA** that the ion-bridging mechanism could not afford. These results show that **CB[8]**-induced non-covalent crosslinking of nanofibers can be employed as a tool to promote further organization in non-covalent polymer-based biomaterials.

6.6 Mechanical properties of Guest PAs-CB[8] hydrogels

Given these results, we reasoned that morphological differences in peptide architectures observed in **CB[8]**-based and Ca^{2+}-based hydrogels should have impactful repercussions on the mechanical properties of the resulting materials. In order to test this hypothesis, stiffness and response to deformation of the hydrogels were assessed through oscillating rheology.

6.6.1 Rheological characterisation of CB[8]-based PA hydrogels

Amplitude and frequency sweep experiments were used to quantify the storage (G') and loss (G") moduli of **CB[8]**-based gels (Figures 6.15 & 6.16). Viscoelastic behaviour was found in both thermally treated hydrogel systems, G' values were greater than G" in every case, confirming the materials exhibit a predominantly elastic rather than viscous character (Figure 6.17). **G_5F-PA/CB[8]** gels exhibited significantly larger G' values (4.7 ± 1.3 kPa, $p < 0.0001$) than those of **G_5W-PA/CB[8]** hydrogels (1.2 ± 0.2 kPa, Figure 6.17.C, Table 6.3).

Table 6.3: Storage (G') and loss (G") moduli of selected self-assembled PA hydrogels presented in this chapter $^{\forall}$

Hydrogel	G' (Storage modulus, Pa)	G" (Loss modulus, Pa)
G_5F-PA / CB[8] 350 μM	4749 ± 1355	1914 ± 649
G_5F-PA / $CaCl_2$ 30 mM	4423 ± 223	735 ± 57
G_5W-PA / CB[8] 350 μM	1281 ± 261	445 ± 223
G_5W-PA / $CaCl_2$ 50 mM	2117 ± 772	468 ± 153

Note: $^{\forall}$ ± S.D. n > 3.

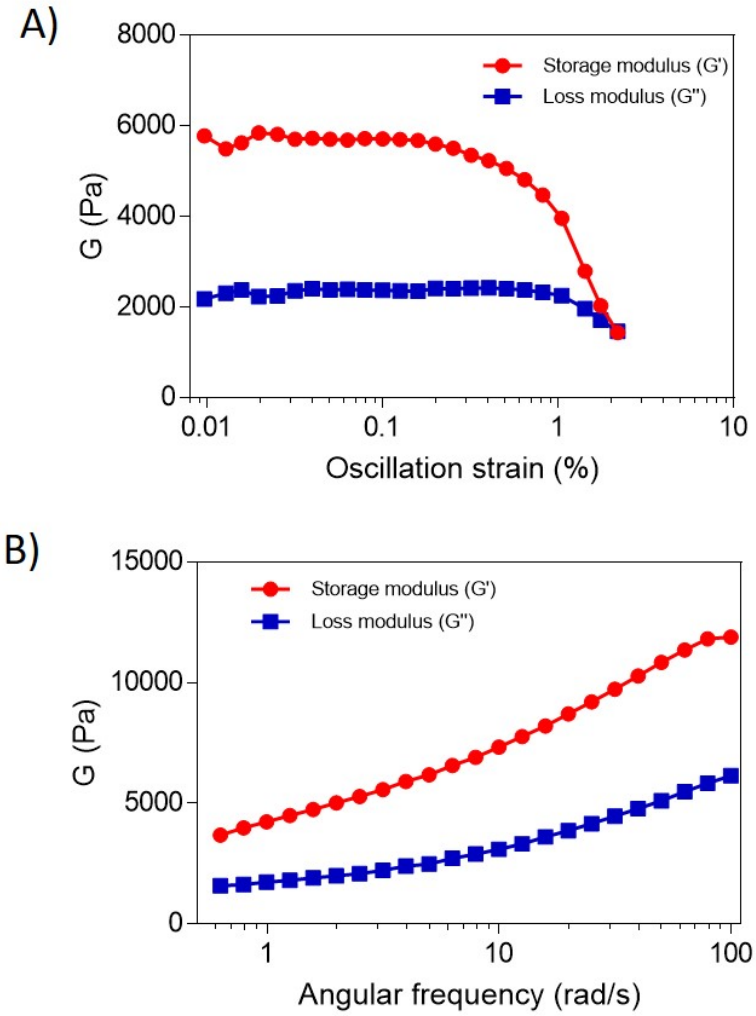

Figure 6.15: *Dynamic rheology experiments on* ***G*$_5$*F-PA/CB[8]*** *hydrogels. A) Oscillatory strain and B) oscillatory frequency sweeps of a representative* ***G*$_5$*F-PA/CB[8]*** *gel (1 wt%).*

These differences can be explained in terms of the length of highly aligned fiber aggregates found in **G$_5$F-PA/CB[8]** (Figure 6.12C) compared to the shorter and more heterogeneous filamentous aggregates found in **G$_5$W-PA/CB[8]** gels (Figure 6.13.C, Figure 6.14). These findings are in accordance with other reports on hydrogels based on rigid polymer chains with pendant phenylalanine or tryptophan amino acids, where phenylalanine unit affords much stronger hydrogel materials than its tryptophan counterpart,[252] contradicting the initial intuitive guess that tryptophan-based gels might be stiffer due to increased aromatic interactions between adjacent interfiber indole rings.

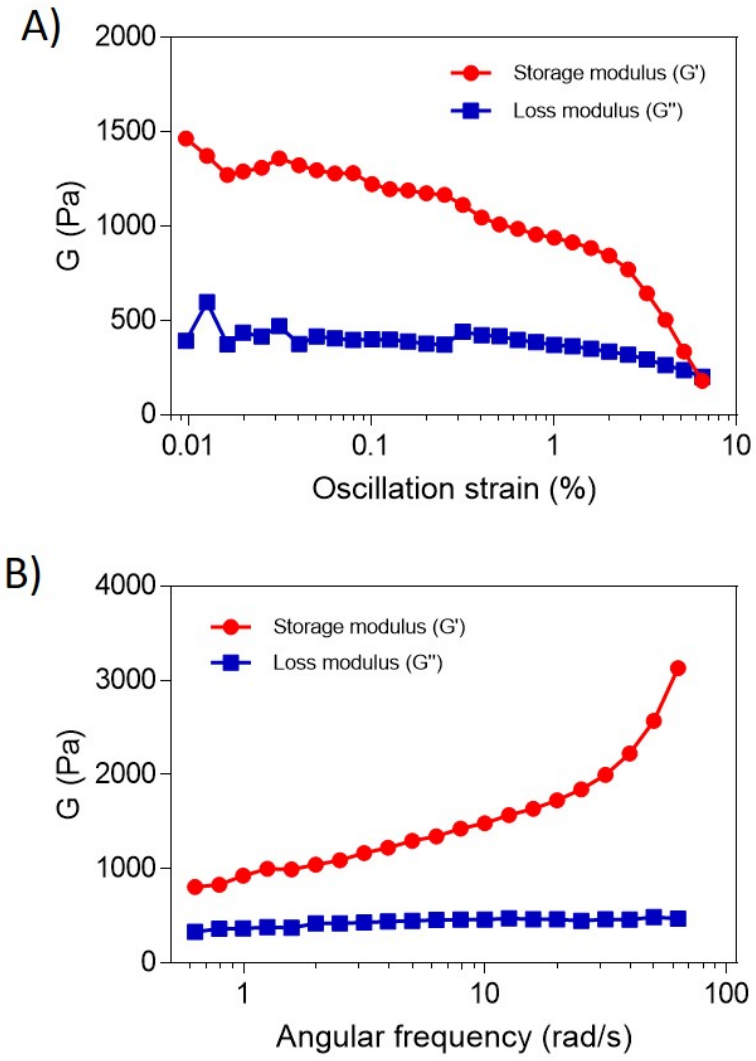

Figure 6.16: *Dynamic rheology experiments on* ***G_5W-PA/CB[8]*** *hydrogels.A) Oscillatory strain and B) oscillatory frequency sweeps of a representative* ***G_5W-PA/CB[8]*** *gel (1 wt%).*

Stiffness of ion-based PA gels can be tuned as a function of Ca^{2+} ions, we took advantage of this property to prepare **G_5F-PA** and **G_5W-PA** hydrogels with similar stiffness values to our dynamically crosslinked PA/**CB[8]** gels. **G_5F-PA**/Ca^{2+} gels required the use of [$CaCl_2$] = 30 mM to emulate stiffness values of **G_5F-PA/CB[8]** (crosslinked with [**CB[8]**] = 350 μM), whereas a higher $CaCl_2$ concentration of 50 mM was necessary in the case of **G_5W-PA**/Ca^{2+} gels prepared under equivalent conditions (Figure 6.17).

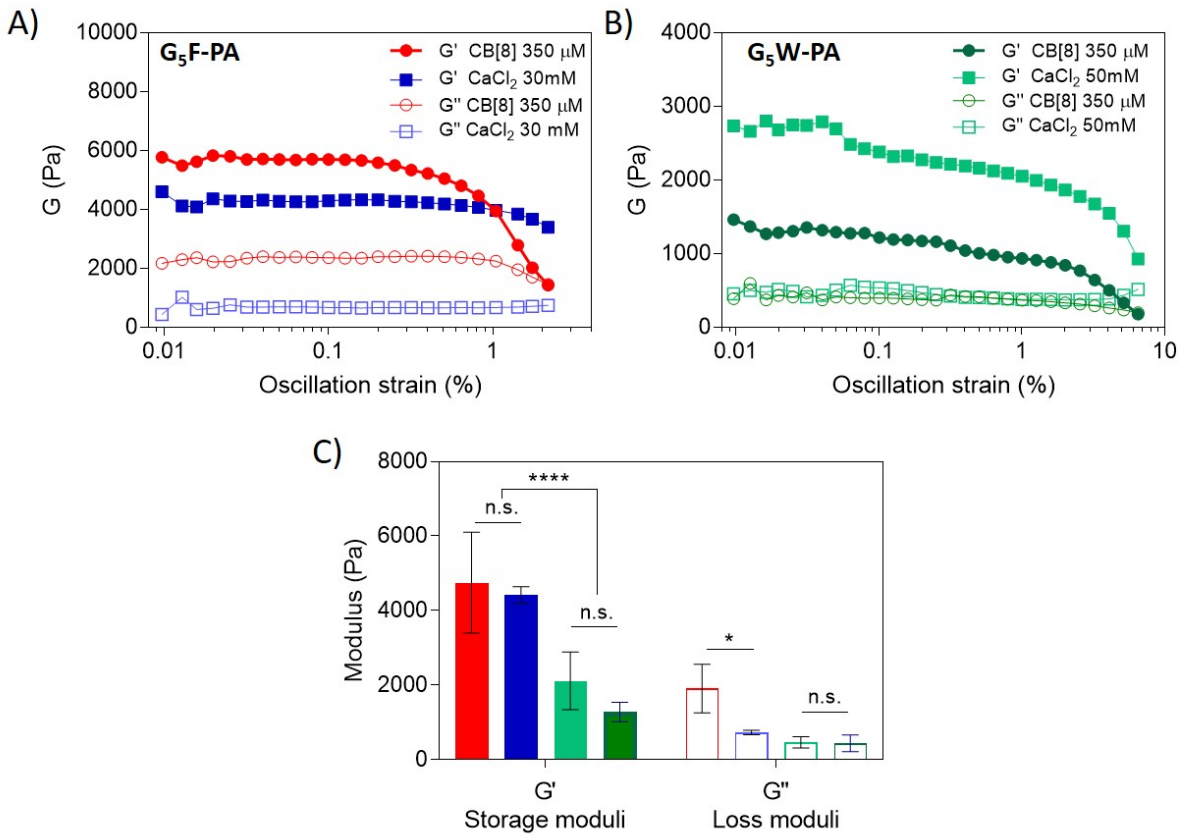

Figure 6.17: *Dynamic rheology characterisation of **CB[8]** and Ca^{2+}-based self-assembled hydrogels. A) Oscillation strain sweep experiments on 1 wt% **G_5F-PA** hydrogels based on **CB[8]** and Ca^{2+} ([**CB[8]**] = 350 µM, [$CaCl_2$] = 30 mM, from thermally treated PA solutions). B) Oscillation strain sweep experiments on 1 wt% **G_5W-PA** hydrogels based on **CB[8]** and $CaCl_2$ ([**CB[8]**] = 350 µM, [$CaCl_2$] = 50 mM, from thermally treated PA solutions). C) Storage (G') and loss (G") moduli corresponding to **G_5F-PA** and **G_5W-PA** hydrogels (* $p < 0.05$, **** $p < 0.0001$, $n > 3$; n.s. no significant difference).*

6.6.2 Interfiber dynamics in CB[8]-based and Ca^{2+}-based hydrogels

In Ca^{2+}-based gels self-assembly of PAs is triggered by electrostatic counterion screening, meanwhile in **CB[8]**-based gels self-assembly occurs due to hampering of aromatic amino acids mostly due to $\pi - \pi$ interactions. Simple stoichiometry calculations show that formation of **CB[8]**-based gels required the presence of one **CB[8]** molecule per every 30 aromatic binding sites in the guest-PA nanofibers periphery, meanwhile it took a 3:1 excess ratio of calcium ions to carboxylate binding sites in Ca^{2+}-based gels to afford similar mechanical properties as maximum metal ion-PA interactions are achieved.

Additional interfiber interactions take place on both cases, i.e. stabilisation via van der Waals and hydrophobic forces and hydrogen bonding.[194] These results indicate that host-guest interactions can drive more efficient PA gelation than electrostatic forces as the ones involved in Ca^{2+}-based gels.

One last significant finding from the rheological comparison of Ca^{2+}-based and **CB[8]**-based hydrogels was the values of the loss tangents. Loss tangent is a measure of the ratio of energy lost to energy stored during gel cyclic deformation,[86] and it can be easily calculated as tan δ = G”/G’. Values of tan δ for **G_5F-PA** & **G_5W-PA** Ca^{2+}-based gels happened to be smaller than those corresponding to equivalent **CB[8]**-based gels. This indicates that the electrostatic mechanism originates gels with greater elastic character than the host-guest driven ones.

Even though both hydrogel classes rely on non-covalent interfiber contacts, transient and non-specific electrostatic ion bridging lacks the intricacies of molecular binding and recognition events that lead to **CB[8]**-guest complex formation. The recruitment of a second interfiber PA monomer unit in our (**Guest-PA**)$_2$•**CB[8]** crosslinks ultimately determines the mechanical properties of the hydrogels. As supramolecular gels translate molecular-scale information into materials performance,[85] it is possible that interfiber fixation of PA anchoring points can limit sliding of the nanofibers during stress deformations.

Similar **CB[8]**-phenylalanine and tryptophan covalent systems indicate that the binding of the second aromatic guest dictates gel stiffness, i.e. greater mechanical strength is produced as a result of a higher energetic barrier of dissociation of the complex.[196] Reduction in PA dynamic exchange due to recruiting into binding sites has been observed in coarse-grain molecular dynamics simulations.[17] These results show that **CB[8]**-PA complexations can be employed to modulate nanofiber morphology and mechanical performance of peptide fibers and their resulting hydrogels.

6.7 Biocompatibility of Guest PA-CB[8] hydrogels

6.7.1 Biological relevance of CB[8]-PA hydrogels

In general, PA-based gels are highly suitable substrates to use as cell culture scaffolds, as they recapitulate mechanical and morphological aspects of native ECM. **CB[8]**-based PA hydrogels might be relevant in different in vivo therapeutic scenarios, especially in those where an excess of gelator counterions could become detrimental. For instance, ion-rich environments could influence enzyme activity and protein conformation, cause osmotic unbalances, hinder cargo delivery by formation of electrostatic complexes with drugs, or affect cell function and phenotype, as in the case of stem cell fate. Also, PA-based hydrogels exhibit shear-thinning and fast recovery properties,[92] enabling minimally invasive administration routes in biomedical applications.

6.7.2 Cell culture studies

To assess the potential of our host-guest crosslinked PA hydrogels to be used in biological applications, in vitro culture of NIH-3T3 fibroblasts over **G_5F-PA** and **G_5W-PA** (both **CB[8]** and $CaCl_2$-based) hydrogels was performed (Figure 6.19.A). Host-guest crosslinked, and electrostatics-based gels exhibited similar cell viability values of over 95% after 24 h of culture compared to tissue culture plastic controls (Figure 6.19.B). These high cell viabilities correlate with results obtained in cell viability assays in solution, as the presence of **CB[8]** proved not to be detrimental in fibroblasts cell response neither in the gel state nor when presented to a monolayer of cells in solution state (Figure 6.18), same positive cell response was observed when the self-assembled **G_5F-PA** and **G_5W-PA** nanofibers.

Recent studies on CB[7]/PEG-based hydrogels report on the pivotal role of host-guest affinity in dictating supramolecular hydrogel properties after in vivo implantation,[258] suggesting that our **G_5F-PA/CB[8]** and **G_5W-PA/CB[8]** hydrogels are likely to drive different cell infiltration behaviours and material clearance after implantation.

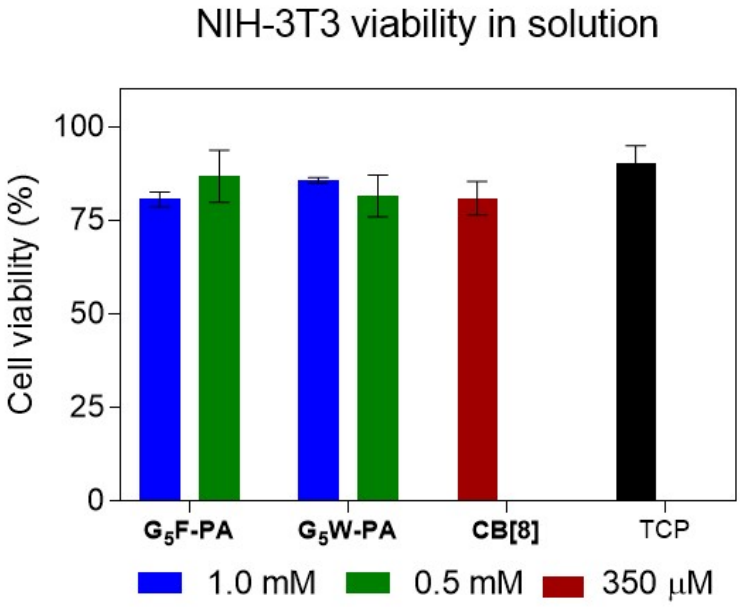

Figure 6.18: *NIH-3T3 fibroblasts LIVE-DEAD results assay after culture with the indicated solutions, TCP as control.*

The possibility to prepare guest-PA gels incorporating both Ca^{2+} and **CB[8]**-driven gelation was also preliminary explored, finding that the resulting gels do not differ in transparency or stiffness compared to Ca^{2+}-based only and **CB[8]**-based only hydrogels. This suggests that synergistic use of both mechanisms can exploited in circumstances were a precise gel architecture or stiffness is desired without the presence of ion-rich environments. Such systems could be used as disease models in calcification involved pathologies like heterotopic ossification (the formation of bone in soft tissues), where muscle or spinal cord injury animal models are currently used.[259]

If “smarter” PA and self-assembling peptide-based materials are desired then their role must go beyond the simple presentation of cell-adhesive epitopes or the modulation of mechanical properties, towards truly mimicking ECM spatiotemporal dynamic properties.[260,1] This will require involving the same dynamic non-covalent interactions that are present in natural matrix materials.[31] We believe host-guest mediated PA hydrogels point in that direction and we hope that further research on them can lead to improvements in stem cell-based and other regenerative therapies.

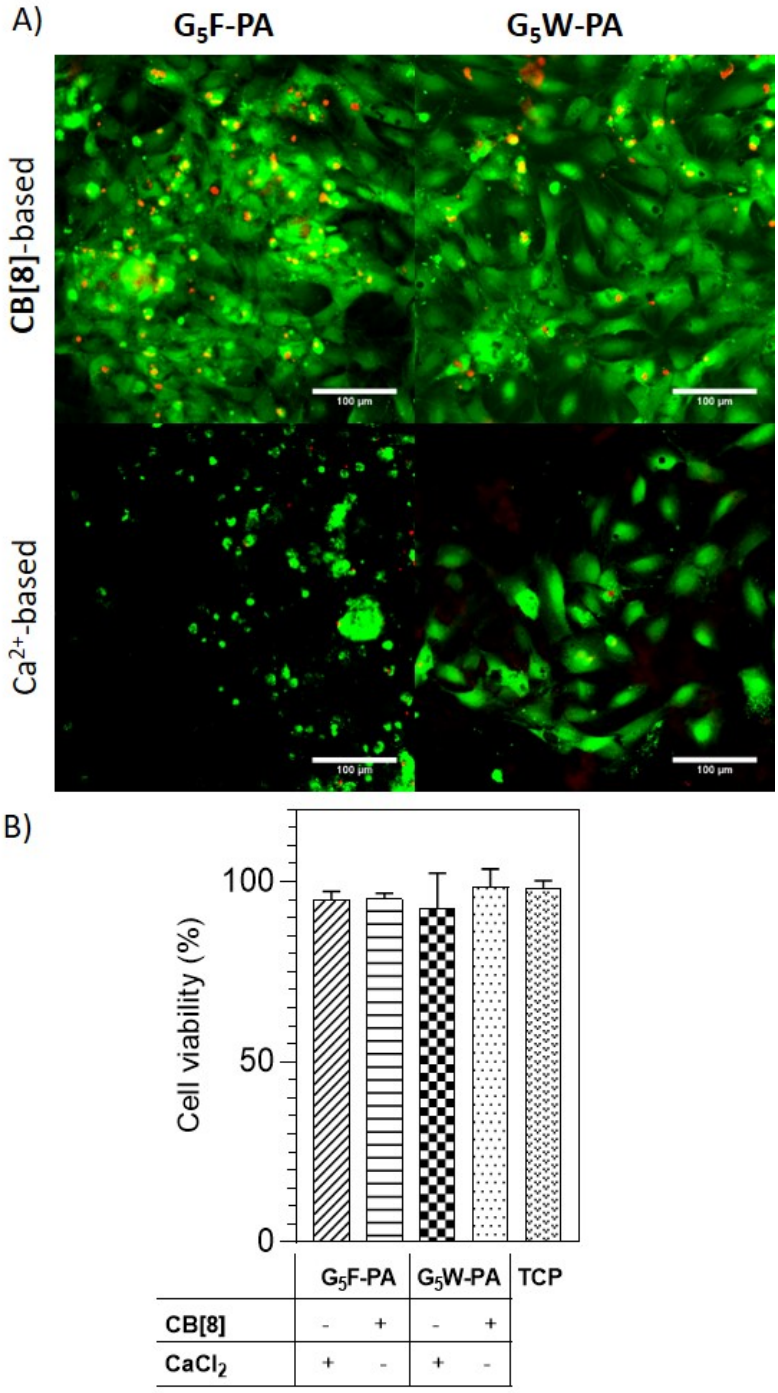

Figure 6.19: *Cell viability studies of NIH-3T3 fibroblasts cultured atop **CB[8]** and Ca^{2+}-based PA-hydrogels. A) LIVE/DEAD images from the cell-seeded hydrogels (green: calcein AM, alive cells; red: ethidium homodimer-1 (EthD-1), dead cells). B) Cell viability values after 24 h of culture onto **G_5F-PA** and **G_5W-PA** hydrogels ([**CB[8]**] = 350 µM, [$CaCl_2$]**G_5F** = 30 mM, [$CaCl_2$]**G_5W** = 50 mM, from thermally treated PA solutions).*

6.8 Closing remarks

In this study, we report on the synthesis, supramolecular aggregation, and structural characterisation of the unreported **CB[8]**-guest mediated dimerisation of peptide amphiphiles containing phenylalanine and tryptophan motifs. **CB[8]**-driven PA gelation showed great potential to maintain and guide PA nanofiber hierarchical organisation, thus representing a promising mechanism to understand and guide precision organisation and functionality in other supramolecular polymer-based biomaterials.

Our work evidences the benefits of merging the self-assembling dynamic properties of PA nanofibers and the high stability of (**Guest-PA**)$_2$•**CB[8]** cross-links, as **CB[8]**-based gels achieved similar mechanical properties and suitability for cell culture to gels involving ion-rich conditions, nonetheless involving only a minimal fraction of interfiber contacts. **CB[8]**-based PA gels may find applications in the development of therapies for disease and regenerative medicine.

This chapter demonstrated the benefits of the incorporation of **CB[8]** in PA hydrogels, thus closing the experimental chapters. The next chapter of the thesis provides the final remarks and conclusions.

6.9 Materials and methods

6.9.1 Materials

Cucurbit[8]uril (**CB[8]** hydrate, 99+%) was purchased from abcr GmbH (Karlsruhe, Germany). Phosphate buffered saline (PBS 1x), 4-(2-hydroxyethyl) piperazine-1-ethanesulfonic acid (HEPES), Dulbecco's Modified Eagle's Medium (DMEM), Hank's Balanced Salt Solution (HBSS), Penicillin/Streptomycin (P/S), and Fetal Bovine Serum (FBS), were obtained from Gibco (Life Technologies). All other reagents were purchased from Sigma-Aldrich and used without any further purification unless otherwise stated.

6.9.2 Peptide synthesis and purification

Peptide amphiphiles (PAs) **E_3-PA**, **G_5F-PA** and **G_5W-PA** were synthesised using modifications of previously reported solid phase peptide synthesis (SPPS) procedures.[230] PAs were purified using reverse phase HPLC (RP-HPLC) using a 2545 Binary Gradient Preparative HPLC (Waters, USA) and a C18 column (Atlantis Prep OBD T3 Column, Waters, USA). Peptide identity was confirmed using electrospray ionisation mass spectrometry (ESI-MS, Thermo LXQ, Thermo Scientific, USA).

6.9.3 Nuclear magnetic resonance (NMR)

PAs were dissolved in D_2O at a final concentration of 4-6 mg/mL (ammonium-d_4 deuteroxide ND_4OD was added to promote peptide solubility) and 1 equivalent of **CB[8]** in D_2O was added to the mixture. Spectra were acquired using a Bruker AvanceNEO 600 spectrometer at 298 K.

6.9.4 Fluorescence spectroscopy

Fluorescence spectra were recorded on a LS55 spectrofluorimeter with Xenon pulsed flash lamp (Perkin Elmer, MA, USA). Measurements were made using a 10 mm path-length cuvette at 25 °C and a λ_{exc} = 280 nm. Emission spectra were recorded from 300 nm to 600 nm in each case.

6.9.5 Circular dichroism (CD)

CD measurements were made using a 1 mm path-length quartz cuvette placed in a Pistar-180 spectropolarimeter (Applied Photophysics, Surrey, UK) equipped with a Peltier temperature controller, under a constant nitrogen purging at a constant pressure of 0.7 MPa and temperature of 25 °C. Peptides were dissolved in HEPES 10 mM saline (155 mM, NaCl pH 7.4) reaching a final concentration of 0.01 wt%. Far UV spectra were recorded from 190 to 260 nm a wavelength step of 0.5 nm. Each represented spectrum is the average of three consecutive spectra. Temperature variable CD experiments were carried out between 10 ºC and 70 ºC, with a heating rate of 1 ºC/min.

6.9.6 Transmission electron microscopy (TEM)

PA 0.05 wt% HEPES solutions were negatively stained as follows: solutions were drop-casted on holey carbon-coated copper TEM grids (Agar Scientific, Stansted, UK), solution excess was blotted after 5 min incubation, then incubated one minute with 2% uranyl acetate, grids were then washed with ultrapure water for 30s and air dried for 24h at room temperature before imaging. Bright-field TEM images were acquired on a JEOL 1230 Transmission Electron Microscope operated at 80 kV. All the images were recorded by a Morada CCD camera (Image Systems) and at least six areas were analysed (corresponding to n $\geq$ 100 PA fibers).

6.9.7 Gel preparation

In a typical example of hydrogelation procedure, PAs were dissolved in HEPES saline at a concentration of 1.5 wt% incubated at 80 ºC for 30 min and let slowly cool down to 25 ºC ("peptide stock solution"). Subsequently, a 30 μL drop of peptide stock solution was placed onto a poly-dimethylsiloxane (PDMS) support, injected with 15 μL of either $CaCl_2$ 100 mM or saturated **CB[8]** 350 μM solution and incubated at 28 ºC for 24 h to afford 1 wt% hydrogels in all cases.

6.9.8 Scanning electron microscopy (SEM)

PA hydrogel samples underwent stepwise dehydration, critical point drying and gold coating before SEM imaging. Initially PA hydrogels were stepwise dehydrated by immersion in increasingly concentrated ethanol solution (20%, 50%, 70%, 80%, 90%, 96%, 100%), for 5 min twice in each solution. Dehydrated samples were dried using a critical point dryer (K850, Quorum Technologies, UK) and gold coated before imaging on an Inspect F50 (FEI Company, the Netherlands) ($n \geq 3$).

6.9.9 Oscillating rheology

Rheological characterisation was performed with a DHR-3 Rheometer (TA Instruments, USA) using an 8 mm diameter parallel plates geometry. G' (storage modulus) and G" (loss modulus) of hydrogels were monitored by amplitude and frequency sweeps. G' and G" moduli were measured at 25 °C and a constant frequency of 1 Hz in the 0.01%– 10% strain during the amplitude sweep, while the oscillation frequency experiments were carried out at a 0.1% fixed strain along a 0.1 – 100 Hz range.

6.9.10 Cell culture experiments

All cell culture experiments were conducted using NIH-3T3 fibroblasts. NIH-3T3 fibroblasts were cultured with DMEM medium supplemented with 10$% fetal bovine serum (FBS) and 1% penicillin and 1% streptomycin. Cells were maintained in a humidified 5% CO_2 atmosphere at 37 °C during culture.

6.9.11 In vitro cell viability assays on hydrogel surface

Hydrogels were sterilised using UV light for 30 min prior to culture. Typically, 30 000 NIH-3T3 fibroblasts were seeded on top of a hydrogel, placed under orbital agitation for 1 h and then incubated for 24 h until LIVE/DEAD imaging. A LIVE/DEAD Viability/Cytotoxicity Assay Kit (Thermo Fisher Scientific, UK) was used. Cells were incubated in 10 mM Calcein AM and 1 mM ethidium homodimer-1 (EthD-1) DMEM medium for 30 min before imaging, stained samples were visualised on an inverted epifluorescence widefield Leica DMI4000B microscope (Leica, Germany) equipped with a LEICA DFC300 FX CCD camera.

Part IV

Concluding remarks

Chapter 7

Conclusions and Future Perspectives

This chapter summarises the overall findings of the research work in relation to the thesis aim and objectives. The chapter is divided into three parts addressing each objective in turn. Each part contains a summary of findings, a perspective on the significance of the work, and a suggestions for future work based on the limitations of the studies.

7.1 Summary

The thesis intended to conceive novel peptide amphiphile-based materials based on the convergence of peptide self-assembly and host-guest interactions to successfully integrate the benefits of these self-assembling systems and the dynamic capacities and versatility of host-guest interactions.

The herein presented collection of projects demonstrated that molecular designs incorporating PA host-guest-mediated nanofiber anchoring, epitope presentation and non-covalent dimerisation can be turned into functional biomaterials with enhanced capacities to emulate dynamic complexity aspects of native extracellular matrixes. Thereby, validating the relevance of the overall thesis aim.

This concluding chapter provides a review of each of the three experimental studies (Chapters 4-6), corresponding to three thesis objectives (Section 3.2). Each section is divided into a summary of findings as well as perspectives and suggestions for future work.

7.2 β-Cyclodextrin/Adamantane nanofiber anchoring on cationic PA hydrogels

The first thesis objective was to prepare tunable hydrogel scaffolds based on the host-guest binding of complementary PA molecules bearing **Ada** and **βCD** motifs. The study presented in Chapter 4 aimed to address this objective.

7.2.1 Summary of findings

The synthesis, supramolecular aggregation, and mechanical improvement of a new family of PA hydrogels based on the dynamic noncovalent binding of **β-cyclodextrin** and **adamantane** motifs were presented.

This study demonstrated that systematic variations of **K_3-PA** (Figure 4.7) by covalent attachment of **Ada** (in **K_3G_3-Ada-PA**) or **βCD** residues (in **K_3G_3-βCD-PA**) can actually lead to formation of unreported peptide assemblies (Figure 4.11), originate unforeseen effects on peptide packing into nanofibers (Figure 4.2) and allow for the formation of host-guest complexes at the surface of PA nanofibers (Figure 4.15).

This non-covalent complexation allowed for dynamic intermolecular binding of PA units both in solution (Figure 4.22) and the gel state (Figure 4.23) rendering an approach that can keep peptide concentration constant and originate stiffer self-assembled hydrogels as a function of host-guest units concentration along **K_3-PA** diluted nanofibers (Figure 4.26) while increasing gel lifespan and retaining bioactivity (Figure 4.28). The findings of this study suggest that host-guest interactions represent an attractive and viable tool to not only improve mechanical and structural features in PA-based hydrogels, but also to further incorporate dynamic guests and structural complexity levels of PA hydrogels useful for developing novel therapies for disease and regenerative medicine.

7.2.2 Perspectives & future work

As the staggering majority of hydrogels comprising host-guest units are polymer-based ones (Figure 2.6),[32,73,77] this study aims to stimulate more supramolecular hydrogels (specially self-assembling peptide-based ones) integrating concepts of supramolecular polimerisation and host-guest interactions (Figure 2.2).

Efforts in this direction are likely to increase our understanding of the dynamic complexity ECM-like materials eliciting beneficial cell-responses as better biochemical and biophysical recapitulation of the native ECM is achieved,[31] including the potential to instruct cell fate via stiffness control of the hydrogel substrate.[197,82]

As the incorporation of host-guest motifs does not interfere with self-healing and shear thinning capacities of PA hydrogels (as shown in Figure 4.27) their incorporation as part of functional bio-inks for use in additive manufacture techniques will gain momentum, as current reports on 3D self-assembling peptides[79] and PA-bioprinting demonstrate.[192]

As progress on PA-based platforms advance, they will likely become available to more diverse audiences, therefore control of stiffness on demand might be fundamental for biofabrication processes or the development of novel therapies involving the assembly and disassembly of PA-based constructs. The correct choice of a suitable host-guest pair might allow responsiveness to a variety of stimuli, including thermal, redox, light and ion-responsiveness (Figure 2.15), thus adding a dynamic dimension to PA-based biomaterials and helping collaborative dialog between cell biologists, materials scientists and engineers to tackle the demands imposed by increasing biological complexity,[82] demands such as biosignal display, which is addressed in the following section.

7.3 β-Cyclodextrin/Adamantane-mediated epitope display on anionic PA hydrogels

The second thesis objective was to display cell adhesion epitopes on PA hydrogels through **βCD/Ada** host-guest-mediated tethering to self-assembled nanofibers. The study presented in Chapter 5 aimed to address this objective.

7.3.1 Summary of findings

This study presented the design of two Ada-bearing PA molecules and their suitability to undergo further host-guest complexation with a complementary **RGDS-βCD** derivative. The results from this study throw light on the influence of spacer length when it comes to present Ada residues on self-assembled nanofibers, as a Ada-PA without a three-glycine spacer was found to be detrimental for β-sheet formation (Figure 5.5) and subsequent hydrogel mechanical properties (Figure 5.7).

Formation of **E_3G_3Ada-PA•RGDS-βCD** units (Figure 5.8) led to preservation of β-sheets when the host-guest complex was presented along **E_3-PA** diluted nanofibers (Figure 5.12), implying that further use of this kind of hydrogel as a cell culture scaffold might not impose additional mechanical impediments for cells to struggle with when cell-substrate interactions take place.

The present study, however, makes several noteworthy contributions to new biosignal presentation strategies. The herein described **RGDS** epitope presentation strategy mediated by non-covalent interactions proved effective to prompt morphological changes in 3T3 fibroblasts due to attachment, spreading and cytoskeleton organisation in response to the host-guest-mediated display of **RGDS** in PA gels (Figure 5.14). Overall, this study demonstrates that carefully chosen molecular design can lead to effective host-guest-mediated tethering of **RGDS** epitopes by **βCD/Ada** as a strategy to increase PA nanofiber bioactivity.

7.3.2 Perspectives & future work

This research has thrown up several questions in need of further investigation. Further work needs to be done in the following areas: more studies are required regarding the length on the glycine spacer used in Guest-PAs, as longer spacer lengths might improve **βCD**/**Ada**-mediated biosignal presentation, as studied by Sur et al.[115] in the case of covalent epitope attachment to PA nanofibers. Also, the possibility to attach other biologically relevant epitopes apart from **RGDS** by attachment to **βCD** can be explored.[211] As **βCD** offers the possibility to attach up to 7 **RGDS** sequences at once (using the free primary hydroxyl groups from the primary rim), the use of similar macrocyclic units might offer the possibility to present even higher epitope densities on PA nanofibers using per-functionalised cyclodextrins.

The herein presented host-guest-mediated epitope presentation employed the well known **β-CD**/**Ada** pair, but further studies can actually used other host-guest pairs (Figure 2.15).[130] In fact, part of this study involved the preparation of UV light-responsive azobenzene-PA and redox-responsive ferrocene-PA derivatives, unfortunately these conjugates could not undergo purification (neither by RP-HPLC nor dialysis) due to their low water solubility and strong tendency to aggregate in acetonitrile solutions.

More hydrophilic designs of this type of derivative might imprint stimuli responsiveness to PA-hydrogels, thereby resulting in **on-demand spatiotemporal bioactivity presentation** useful in clinical therapies or preparation of nanomaterials. For instance, a PA gel with pendant azobenzene units could be reversibly bound to an **αCD** functionalized with the **RGD** peptide (thus forming azo-RGD complexes) in the trans-configuration, thus promoting cell attachment; while irradiation of the gel with UV light might induce isomerisation of the azobenzene cues to the cis-configuration, resulting in the release of **azo-RGD** and cells from the PA scaffold.[261] Removal of UV radiation allows formation of new **azo-RGD** units as the trans-configuration is regained, allowing for reversible epitope presentation, in fact, similar cycles of trans–cis–trans isomerization in cyclo(RGDFK) monolayers leads to reinforcement of cell adhesion, perhaps as the result of cell adhesion stimulation via mechanical forces.[261,262]

So far supramolecular hydrogels have successfully provided ECM-like 3D cell microenvironments, however, no use of synchro-nous regulations of matrix stiffness, shape and size, and degradation[263] are yet spread in PA hydrogels as in other organogels[264] or polymeric hydrogels like those HA-based.[265] To date there is only one report on PA gels where structural and biochemical reversibility can be achieved, in this case via peptide-DNA conjugates that happen to also alter the phenotype of neural cells in contact with these materials.[17] Other PA platforms capable of responding to specific stimuli (e.g., light, magnetic and electrochemical stimulations) are sill required, and it is anticipated that the study presented in Chapter 5 has gone some way towards enhancing our understanding and design of such materials in future.

7.4 Cucurbit[8]uril-driven PA hydrogelation

The third thesis objective was to develop hydrogels relying on the dynamic non-covalent PA dimerisation mediated by **CB[8]**. The study presented in Chapter 6 aimed to address this objective by showing **CB[8]-PA** hydrogels as alternatives to conventionally ion-generated PA scaffolds.

7.4.1 Summary of findings

The evidence from this study suggests that pH changes and electrostatic counterion screening are not the only viable way to prompt PA hydrogelation, as **CB[8]**-mediated homoternary complexation of aromatic-bearing proved to originate self-sustaining gels without the presence of ions, and occurring at physiological pH values (Figure 6.17).

The results of this study indicate that variations of only one amino acid in Guest-PAs (by going from phenylalanine in **G_5F-PA** to tryptophan in **G_5W-PA** originated tremendous spectroscopic (Figure 6.11) and morphological differences in presence of **CB[8]** (Figures 6.12 & 6.13) even though both amino acids bear aromatic side chains and their gelation is likely to share a similar host-guest-mediated mechanism. Both Guest-PAs exhibited β-sheet conformations in presence of **CB[8]**, though their time and temperature-driven evolution exhibited differences.

In particular, **G_5W-PA** exhibited promising abilities to generate temperature-driven supra-molecular structures (Figure 6.14), and even though these fibrillar aggregates had consequences on the resulting hydrogel stiffness (Figure 6.17) this effect can be attenuated by diluting the peptide along self assembled nanofibers with a filler-PA like **E_3-PA**.

Finally, both ion-based and **CB[8]**-based Guest-PA hydrogels achieved similar mechanical properties and suitability for in vitro cell studies (Figure 6.19). As this study merges features of host-guest interactions and supramolecular gelation (Figure 2.2) it is anticipated that it might help to integrate both families of supramolecular biomaterials thus enhancing their future molecular design.

7.4.2 Perspectives & future work

As this study accounts for an unreported mechanism to drive PA-hydrogelation many questions are in need of further investigation. Further work needs to be done to establish the ability of **CB[8]** (and other members of the cucurbit[n]uril family) to dynamically dimerise PA nanofibers. More work needs to be done regarding the binding kinetics and thermodynamics of the system, as the high density presentation of the aromatic motifs in PA nanofibers might have an effect (perhaps a cooperative one) on the traditionally accepted parameters (measured as free molecules or macromolecular conjugates).[266]

Self-assembled nanofibers bearing Guest-PA monomers might be useful to tether proteins and small molecule drugs able to undergo complexation with **CB[8]**, thereby forming drug delivery system with dynamics controlled not only by supramolecular polimerisation parameters but also by **CB[8]** affinity.[162,32]

An interesting possibility allowed by the **CB[8]**-driven non-covalent binding is the preparation of double network hydrogels simultaneously incorporating macromolecular units bearing aromatic amino acids (like phenylalanine or tryptophan) and supramolecular PA-nanofibers bearing the same amino acids. Such systems might help move forward the design of more adaptive and biologically relevant hydrogel biomaterials[83] useful in clinical models, tissue engineering relevant constructs or regenerative therapies.

Appendix A

Related Publications & Collaborations

This appendix summarises all published material (publications, collaborations and book chapter) and provides a list of all conference presentations concerning this thesis.

A.I Publications derived from this thesis

A.I.1 Book chapter

- Okesola, B.; **Redondo-Gómez, C.**; Mata, A. *"Multicomponent self-assembly: Supramolecular design of complex hydrogels for biomedical applications"* in "Self-Assembling Biomaterials: Molecular Design, Characterization and Application in Biology and Medicine" Elsevier, ISBN: 978-0-08-102015-9 (2018).

A.I.2 Papers

- **Redondo-Gómez, C.**; Abdouni, Y.; Becer, R.; Mata, A. *Self-assembling hydrogels based on a complementary host-guest peptide amphiphile pair.* Biomacromolecules (2019) 20, 6, 2276-2285.
- **Redondo-Gómez, C.**; Padilla-Lopategui, S.; Azevedo, H. S.; Mata, A. *Host-guest-mediated epitope presentation on self-assembled peptide amphiphile hydrogels. To be submitted to ACS Biomaterials Science and Engineering*.
- **Redondo-Gómez, C.**; Padilla-Lopategui, S.; Azevedo, H. S.; Mata, A. Self-assembling peptide amphiphile hydrogels based on a homoternary cucurbit[8]uril host-guest complex. *To be submitted to Biomaterials Science*.

A.II Collaborations

- Hedegaard, C. L.; Collin, E.; **Redondo-Gómez, C.**; Nguyen, L. T. H.; Woei Ng, K.; Castrejón-Pita, A. A.; Castrejón-Pita, J. R.; Mata, A. *Hydrodynamically guided hierarchical self-assembly of peptide-protein bioinks* Adv. Funct. Mater. (2018) 1703716.
- Hedegaard, C. L.; **Redondo-Gómez, C.**; Tan, B. Y.; Woei Ng, K.; Loessner, D.; Mata, A. *Peptide-protein co-assembling hydrogel as an effective 3D model of ovarian cancer. Submitted to Science Advances*.
- Ajovalasit, A.; **Redondo-Gómez, C.**; Sabatino, M. A.; Dispenza, C.; Mata, A. *Carboxylated-xyloglucan and peptide amphiphile co-assembly for wound healing application.* Manuscript in preparation.
- Anna M. Majkowska, A. M.; Inostroza-Brito, K.; **Redondo-Gómez, C.**; Collin, E.; Rice, A.; Rodríguez Cabello, C.; Mata, A. *Interfacial self-assembly in hybrid bioactive scaffolds.* Manuscript in preparation.
- Collin, E.; **Redondo-Gómez, C.**; Martin, C.; Okesola, B.; Inostroza-Brito, K.; Mata, A. *Effect of peptide amphiphiles charges on cell viability.* Manuscript in preparation.
- Abdouni, Y.; M. ter Huurne, G. M.; Monaco, A.; **Redondo-Gómez, C.**; Yilmaz, G.; Meijer, E. W.; Palmans, A. R. A.; Becer, C. R. Supramolecular Single-Chain Folding Polymeric Glyconanoparticles. Manuscript in preparation.

A.III Conferences and Poster Presentations

- **Redondo-Gómez, C.**; Mata, A. “Stabilising Peptide Amphiphile-based biomaterials through Host-Guest complexations”, Sao Paulo School of Advanced Science on Biophysical Methods to Study Biomolecular Interactions, Brazil, 10/2017. Best poster presentation winner.
- **Redondo-Gómez, C.**; Mata, A. “Stabilising Peptide Amphiphile-based biomaterials through Host-Guest complexations”, Industry Liaison Forum, Queen Mary University of London, London, United Kingdom, 11/2017.
- **Redondo-Gómez, C.**; Mata, A. “Self-assembling hydrogels based on a complementary host-guest peptide amphiphile pair”, Industry Liaison Forum, Queen Mary University of London, London, United Kingdom, 11/2018.
- **Redondo-Gómez, C.**; Abdouni, Y.; Becer, C. R.: Mata, A. “Self-assembling hydrogels based on a complementary host-guest peptide amphiphile pair”, XIV International Symposium on Macrocyclic and Supramolecular Chemistry, Lecce, Italy, 2019.

Bibliography

[1] George S. Hussey, Jenna L. Dziki, and Stephen F. Badylak. Extracellular matrix-based materials for regenerative medicine. *Nature Reviews Materials*, 3(7):159–173, 2018.

[2] Florian Rehfeldt, Adam J. Engler, Adam Eckhardt, Fariyal Ahmed, and Dennis E. Discher. Cell responses to the mechanochemical microenvironment-Implications for regenerative medicine and drug delivery. *Advanced Drug Delivery Reviews*, 59(13):1329–1339, 2007.

[3] Adam J Engler, Shamik Sen, H Lee Sweeney, and Dennis E Discher. Matrix Elasticity Directs Stem Cell Lineage Specification. *Cell*, 126(4):677–689, aug 2006.

[4] Steven R. Caliari and Jason A. Burdick. A practical guide to hydrogels for cell culture. *Nature Methods*, 13(5):405–414, 2016.

[5] Chun Yang, Mark W. Tibbitt, Lena Basta, and Kristi S. Anseth. Mechanical memory and dosing influence stem cell fate. *Nature Materials*, 13(6):645–652, jun 2014.

[6] Jason A. Burdick and William L. Murphy. Moving from static to dynamic complexity in hydrogel design. *Nature Communications*, 3:1–8, 2012.

[7] Nicholas A. Peppas, J. Zach Hilt, Ali Khademhosseini, and Robert Langer. Hydrogels in biology and medicine: From molecular principles to bionanotechnology. *Advanced Materials*, 18(11):1345–1360, 2006.

[8] Chris S. Hughes, Lynne M. Postovit, and Gilles A. Lajoie. Matrigel: a complex protein mixture required for optimal growth of cell culture. *Proteomics*, 10(9):1886–1890, 2010.

[9] Eric H. Nguyen, William T. Daly, Ngoc Nhi T. Le, Mitra Farnoodian, David G. Belair, Michael P. Schwartz, Connie S. Lebakken, Gene E. Ananiev, Mohammad Ali Saghiri, Thomas B. Knudsen, Nader Sheibani, and William L. Murphy. Versatile synthetic alternatives to Matrigel for vascular toxicity screening and stem cell expansion. *Nature Biomedical Engineering*, 1(7):1–14, 2017.

[10] Jieling Li, Ruirui Xing, Shuo Bai, and Xuehai Yan. Recent advances of self-assembling peptide-based hydrogels for biomedical applications. *Soft Matter*, 15(8):1704–1715, 2019.

[11] Jie Zhan, Yanbin Cai, Shenglu Ji, Shuangshuang He, Yi Cao, Dan Ding, Ling Wang, and Zhimou Yang. Spatiotemporal Control of Supramolecular Self-Assembly and Function. *ACS Applied Materials and Interfaces*, 9(11):10012–10018, 2017.

[12] Ehud Gazit. Self-assembled peptide nanostructures: The design of molecular building blocks and their technological utilization. *Chemical Society Reviews*, 36(8):1263–1269, 2007.

[13] Chengqian Yuan, Wei Ji, Ruirui Xing, Junbai Li, Ehud Gazit, and Xuehai Yan. Hierarchically oriented organization in supramolecular peptide crystals. *Nature Reviews Chemistry*, 3(10):567–588, 2019.

[14] J. C. Stendahl, M. S. Rao, M. O. Guler, and S. I. Stupp. Intermolecular Forces in the Self-Assembly of Peptide Amphiphile Nanofibers. *Advanced Functional Materials*, 16(4):499–508, mar 2006.

[15] Sanket A. Deshmukh, Lee A. Solomon, Ganesh Kamath, H. Christopher Fry, and Subramanian K.R.S. Sankaranarayanan. Water ordering controls the dynamic equilibrium of micelle-fibre formation in self-assembly of peptide amphiphiles. *Nature Communications*, 7:1–11, 2016.

[16] Songi Han, Monica Olvera de la Cruz, Christina J. Newcomb, Julia H. Ortony, Samuel I. Stupp, Timothy J. Keller, Elad Deiss-Yehiely, Baofu Qiao, and Liam C. Palmer. Water Dynamics from the Surface to the Interior of a Supramolecular Nanostructure. *Journal of the American Chemical Society*, 139(26):8915–8921, 2017.

[17] Ronit Freeman, Ming Han, Zaida Álvarez, Jacob A. Lewis, James R. Wester, Nicholas Stephanopoulos, Mark T. McClendon, Cheyenne Lynsky, Jacqueline M. Godbe, Hussain Sangji, Erik Luijten, and Samuel I. Stupp. Reversible self-assembly of superstructured networks. *Science*, 362(6416):808–813, nov 2018.

[18] Shuming Zhang, Megan A. Greenfield, Alvaro Mata, Liam C. Palmer, Ronit Bitton, Jason R. Mantei, Conrado Aparicio, Monica Olvera de la Cruz, and Samuel I. Stupp. A self-assembly pathway to aligned monodomain gels. *Nature Materials*, 9(7):594–601, jul 2010.

[19] Ramille M. Capito, Helena S. Azevedo, Yuri S. Velichko, Alvaro Mata, and Samuel I. Stupp. Self-assembly of large and small molecules into hierarchically ordered sacs and membranes. *Science*, 319(5871):1812–1816, 2008.

[20] Karla E Inostroza-brito, Estelle C Collin, Anna Majkowska, Sherif Elsharkawy, Alistair Rice, E Armando, Río Hernández, Xin Xiao, José Rodríguez-cabello, and Alvaro Mata. Acta Biomaterialia Cross-linking of a biopolymer-peptide co-assembling system. *Acta Biomaterialia*, 58:80–89, 2017.

[21] Babatunde O. Okesola, Carlos Redondo-Gómez, and Alvaro Mata. Multicomponent self-assembly: Supramolecular design of complex hydrogels for biomedical applications. In *Self-assembling Biomaterials*, pages 371–397. Elsevier, 2018.

[22] Jean-Marie Lehn. Perspectives in Supramolecular Chemistry—From Molecular Recognition towards Molecular Information Processing and Self-Organization. *Angewandte Chemie International Edition in English*, 29(11):1304–1319, nov 1990.

[23] Jean Marie Lehn. Towards complex matter: Supramolecular chemistry and self-organization. *European Review*, 17(2):263–280, 2009.

[24] Christopher E. Wilmer, Jiwon Kim, Bartosz A. Grzybowski, Kyle J. M. Bishop, and Kevin P. Browne. Self-assembly: from crystals to cells. *Soft Matter*, 5(6):1110, 2009.

[25] George M. Whitesides and Bartosz Grzybowski. Self-assembly at all scales. *Science*, 295(5564):2418–2421, 2002.

[26] George M. Whitesides and Mila Boncheva. Beyond molecules: Self-assembly of mesoscopic and macroscopic components. *Proceedings of the National Academy of Sciences of the United States of America*, 99(8):4769–4774, 2002.

[27] Shuguang Zhang. Fabrication of novel biomaterials through molecular self-assembly. *Nature Biotechnology*, 21(10):1171–1178, 2003.

[28] Ana C. Mendes, Erkan T. Baran, Rui L. Reis, and Helena S. Azevedo. Self-assembly in nature: Using the principles of nature to create complex nanobiomaterials. *Wiley Interdisciplinary Reviews: Nanomedicine and Nanobiotechnology*, 5(6):582–612, 2013.

[29] Elisha Krieg, Maartje M.C. Bastings, Pol Besenius, and Boris Rybtchinski. Supramolecular polymers in aqueous media. *Chemical Reviews*, 116(4):2414–2477, 2016.

[30] Yingfeng Tu, Fei Peng, Alaa Adawy, Yongjun Men, Loai K.E.A. Abdelmohsen, and Daniela A. Wilson. Mimicking the Cell: Bio-inspired functions of supramolecular assemblies. *Chemical Reviews*, 116(4):2023–2078, 2016.

[31] Matthew J. Webber, Eric A. Appel, E. W. Meijer, and Robert Langer. Supramolecular biomaterials. *Nature Materials*, 15(1):13–26, 2015.

[32] Joseph L. Mann, Anthony C. Yu, Gillie Agmon, and Eric A. Appel. Supramolecular polymeric biomaterials. *Biomaterials Science*, 6(1):10–37, 2018.

[33] Lauren E. Buerkle, Horst A. Von Recum, and Stuart J. Rowan. Toward potential supramolecular tissue engineering scaffolds based on guanosine derivatives. *Chemical Science*, 3(2):564–572, 2012.

[34] Kazuki Fukushima, Shaoqiong Liu, Hong Wu, Amanda C. Engler, Daniel J. Coady, Hareem Maune, Jed Pitera, Alshakim Nelson, Nikken Wiradharma, Shrinivas Venkataraman, Yuan Huang, Weimin Fan, Jackie Y. Ying, Yi Yan Yang, and James L. Hedrick. Supramolecular high-aspect ratio assemblies with strong antifungal activity. *Nature Communications*, 4, 2013.

[35] Christianus M.A. Leenders, Tristan Mes, Matthew B. Baker, Marcel M.E. Koenigs, Pol Besenius, Anja R.A. Palmans, and E. W. Meijer. From supramolecular polymers to hydrogel materials. *Materials Horizons*, 1(1):116–120, 2014.

[36] Mark Burnworth, Liming Tang, Justin R. Kumpfer, Andrew J. Duncan, Frederick L. Beyer, Gina L. Fiore, Stuart J. Rowan, and Christoph Weder. Optically healable supramolecular polymers. *Nature*, 472(7343):334–337, 2011.

[37] Claudine Fouquey, Jean-Marie -M Lehn, and Anne-Marie -M Levelut. Molecular recognition directed self-assembly of supramolecular liquid crystalline polymers from complementary chiral components. *Advanced Materials*, 2(5):254–257, 1990.

[38] Richard G. Weiss. The past, present, and future of molecular gels. What is the status of the field, and where is it going? *Journal of the American Chemical Society*, 136(21):7519–7530, 2014.

[39] Roman V. Kazantsev, Faifan Tantakitti, Roya Zandi, Tao Yu, Job Boekhoven, Samuel I. Stupp, Julia H. Ortony, George C. Schatz, Jiahe Li, Monica Olvera de la Cruz, Christina J. Newcomb, Gajendra S. Shekhawat, Xin Wang, Ellen Zhuang, and Liam C. Palmer. Energy landscapes and functions of supramolecular systems. *Nature Materials*, 15(4):469–476, 2016.

[40] Marius Wehner and Frank Würthner. Supramolecular polymerization through kinetic pathway control and living chain growth. *Nature Reviews Chemistry*, dec 2019.

[41] Shuguang Zhang, Todd Holmes, Curtis Lockshin, and Alexander Rich. Spontaneous assembly of a self-complementary oligopeptide to form a stable macroscopic membrane. *Proceedings of the National Academy of Sciences of the United States of America*, 90(8):3334–3338, 1993.

[42] Shuguang Zhang. Self-assembling peptide materials. *Amino Acids, Peptides and Proteins*, 37:40–65, 2012.

[43] Jun Chen and Xuenong Zou. Self-assemble peptide biomaterials and their biomedical applications. *Bioactive Materials*, 4(October 2018):120–131, 2019.

[44] Helena S. Azevedo. *Biomaterials Inspired by Biology: From Molecules to Self-Assembly*. Elsevier Inc., 2019.

[45] S. Maude, L. R. Tai, R. P. W. Davies, B. Liu, S. A. Harris, P. J. Kocienski, and A. Aggeli. Peptide Synthesis and Self-Assembly. In Deming T., editor, *Peptide-Based Materials. Topics in Current Chemistry*, pages 27–69. 2011.

[46] A. Aggeli, M Boden N Bell, J N Keen, P F Knowles, T C B McLeish, M. Pitkeathly, and S E Radford. Responsive gels formed by the spontaneous self-assembly of peptides into polymeric ß-sheet tapes.symbol. .symbol. *Nature*, 386(062/10):259–262, 1997.

[47] Sylvain Vauthey, Steve Santoso, Haiyan Gong, Nicki Watson, and Shuguang Zhang. Molecular self-assembly of surfactant-like peptides to form nanotubes and nanovesicles. *Proceedings of the National Academy of Sciences of the United States of America*, 99(8):5355–5360, 2002.

[48] He Dong, Sergey E. Paramonov, Lorenzo Aulisa, Erica L. Bakota, and Jeffrey D. Hartgerink. Self-assembly of multidomain peptides: Balancing molecular frustration controls conformation and nanostructure. *Journal of the American Chemical Society*, 129(41):12468–12472, 2007.

[49] Lisa Pakstis, Joel P. Schneider, Karthikan Rajagopal, Juliana Kretsinger, Bulent Ozbas, and Darrin J. Pochan. Responsive Hydrogels from the Intramolecular Folding and Self-Assembly of a Designed Peptide. *Journal of the American Chemical Society*, 124(50):15030–15037, 2002.

[50] Yang Li and S Michael Yu. Targeting and mimicking collagens via triple helical peptide assembly. *Current Opinion in Chemical Biology*, 17(6):968–975, dec 2013.

[51] Jordan M. Fletcher, Robert L. Harniman, Frederick R.H. Barnes, Aimee L. Boyle, Andrew Collins, Judith Mantell, Thomas H. Sharp, Massimo Antognozzi, Paula J. Booth, Noah Linden, Mervyn J. Miles, Richard B. Sessions, Paul Verkade, and Derek N. Woolfson. Self-assembling cages from coiled-coil peptide modules. *Science*, 340(6132):595–599, 2013.

[52] Andrew M. Smith, Richard J. Williams, Claire Tang, Paolo Coppo, Richard F. Collins, Michael L. Turner, Alberto Saiani, and Rein V. Ulijn. Fmoc-diphenylalanine self assembles to a hydrogel via a novel architecture based on π-π interlocked β-sheets. *Advanced Materials*, 20(1):37–41, 2008.

[53] Scott Fleming and Rein V. Ulijn. Design of nanostructures based on aromatic peptide amphiphiles. *Chemical Society Reviews*, 43(23):8150–8177, 2014.

[54] Santu Bera, Sudipta Mondal, Bin Xue, Linda J. W. Shimon, Yi Cao, and Ehud Gazit. Rigid helical-like assemblies from a self-aggregating tripeptide. *Nature Materials*, 18:503–509, 2019.

[55] Matthew J. Webber, Eric J. Berns, and Samuel I. Stupp. Supramolecular nanofibers of peptide amphiphiles for medicine. *Israel Journal of Chemistry*, 53(8):530–554, 2013.

[56] J. D. Hartgerink, E. Beniash, and S. I. Stupp. Peptide-amphiphile nanofibers: A versatile scaffold for the preparation of self-assembling materials. *Proceedings of the National Academy of Sciences*, 99(8):5133–5138, 2002.

[57] Luciano Galantini, M. Chiara di Gregorio, Marta Gubitosi, Leana Travaglini, José Vázquez Tato, Aida Jover, Francisco Meijide, Victor H. Soto Tellini, and Nicolae V. Pavel. Bile salts and derivatives: Rigid unconventional amphiphiles as dispersants, carriers and superstructure building blocks. *Current Opinion in Colloid and Interface Science*, 20(3):170–182, 2015.

[58] Supratim Banerjee, Rajat K. Das, and Uday Maitra. Supramolecular gels 'in action'. *Journal of Materials Chemistry*, 19(37):6649–6687, 2009.

[59] Niek Zweep and Jan H. van Esch. CHAPTER 1. The Design of Molecular Gelators. In Beatriu Beatriu Escuder and J. F. Miravet, editors, *Functional Molecular Gels*, pages 1–29. 2014.

[60] R. Nagarajan. Molecular packing parameter and surfactant self-assembly: The neglected role of the surfactant tail. *Langmuir*, 18(1):31–38, 2002.

[61] Muruganathan Ramanathan, Lok Kumar Shrestha, Taizo Mori, Qingmin Ji, Jonathan P. Hill, and Katsuhiko Ariga. Amphiphile nanoarchitectonics: From basic physical chemistry to advanced applications. *Physical Chemistry Chemical Physics*, 15(26):10580–10611, 2013.

[62] Yu Shrike Zhang and Ali Khademhosseini. Advances in engineering hydrogels. *Science*, 356(6337), 2017.

[63] Elisabeth Prince and Eugenia Kumacheva. Design and applications of man-made biomimetic fibrillar hydrogels. *Nature Reviews Materials*, 2019.

[64] Seliktar Dror. Designing Cell-Compatible Hydrogels for Biomedical Applications. *Science*, 336(6085):1124–1128, jun 2012.

[65] Achilleas D. Theocharis, Spyros S. Skandalis, Chrysostomi Gialeli, and Nikos K. Karamanos. Extracellular matrix structure. *Advanced Drug Delivery Reviews*, 97:4–27, 2016.

[66] M. P. Lutolf and J. A. Hubbell. Synthetic biomaterials as instructive extracellular microenvironments for morphogenesis in tissue engineering. *Nature Biotechnology*, 23(1):47–55, 2005.

[67] Renato V. Iozzo and Maria A. Gubbiotti. Extracellular matrix: The driving force of mammalian diseases. *Matrix Biology*, 71-72:1–9, 2018.

[68] Tapio Ihanamäki, Lauri J Pelliniemi, and Eero Vuorio. Collagens and collagen-related matrix components in the human and mouse eye. *Progress in Retinal and Eye Research*, 23(4):403–434, jul 2004.

[69] Hikmet Geckil, Feng Xu, Xiaohui Zhang, SangJun Moon, and Utkan Demirci. Engineering hydrogels as extracellular matrix mimics. *Nanomedicine*, 5(3):469–484, apr 2010.

[70] Yulin Li, João Rodrigues, and Helena Tomás. Injectable and biodegradable hydrogels: Gelation, biodegradation and biomedical applications. *Chemical Society Reviews*, 41(6):2193–2221, 2012.

[71] Raquel Silva, Ben Fabry, and Aldo R. Boccaccini. Fibrous protein-based hydrogels for cell encapsulation. *Biomaterials*, 35(25):6727–6738, aug 2014.

[72] Mark W. Tibbitt, Christopher B. Rodell, Jason A. Burdick, and Kristi S. Anseth. Progress in material design for biomedical applications. *Proceedings of the National Academy of Sciences*, 112(47):14444–14451, 2015.

[73] Eric A. Appel, Jesús Del Barrio, Xian Jun Loh, and Oren A. Scherman. Supramolecular polymeric hydrogels. *Chemical Society Reviews*, 41(18):6195–6214, 2012.

[74] Tao Lin Sun, Takayuki Kurokawa, Shinya Kuroda, Abu Bin Ihsan, Taigo Akasaki, Koshiro Sato, Md Anamul Haque, Tasuku Nakajima, and Jian Ping Gong. Physical hydrogels composed of polyampholytes demonstrate high toughness and viscoelasticity. *Nature Materials*, 12(10):932–937, 2013.

[75] C.-C. Hsu, C. Zhang, M. J. Tauber, B. Arman, R. A. Mashelkar, A. Phadke, S. Varghese, A. K. Lele, and G. Arya. Rapid self-healing hydrogels. *Proceedings of the National Academy of Sciences*, 109(12):4383–4388, 2012.

[76] Masaki Nakahata, Yoshinori Takashima, Hiroyasu Yamaguchi, and Akira Harada. Redox-responsive self-healing materials formed from host-guest polymers. *Nature Communications*, 2(1):511–516, 2011.

[77] Jie Zhou, Jie Li, Xuewen Du, and Bing Xu. Supramolecular biofunctional materials. *Biomaterials*, 129:1–27, 2017.

[78] Mohsen Doostmohammadi, Atefeh Ameri, Reza Mohammadinejad, Negar Dehghannoudeh, Ibrahim M Banat, Mandana Ohadi, and Gholamreza Dehghannoudeh. Hydrogels For Peptide Hormones Delivery: Therapeutic And Tissue Engineering Applications. *Drug Design, Development and Therapy*, Volume 13:3405–3418, sep 2019.

[79] Bella Raphael, Tony Khalil, Victoria L. Workman, Andrew Smith, Cameron P. Brown, Charles Streuli, Alberto Saiani, and Marco Domingos. 3D cell bioprinting of self-assembling peptide-based hydrogels. *Materials Letters*, 190:103–106, 2017.

[80] Deepak Kumar, Victoria L. Workman, Marie O'Brien, Jane McLaren, Lisa White, Krish Ragunath, Felicity Rose, Alberto Saiani, and Julie E. Gough. Peptide Hydrogels—A Tissue Engineering Strategy for the Prevention of Oesophageal Strictures. *Advanced Functional Materials*, 27(38), 2017.

[81] Simon Wan, Samantha Borland, Stephen M. Richardson, Catherine L.R. Merry, Alberto Saiani, and Julie E. Gough. Self-assembling peptide hydrogel for intervertebral disc tissue engineering. *Acta Biomaterialia*, 46:29–40, 2016.

[82] Adrianne M. Rosales and Kristi S. Anseth. The design of reversible hydrogels to capture extracellular matrix dynamics. *Nature Reviews Materials*, 1(2):1–15, 2016.

[83] Rienk Eelkema and Andrij Pich. Pros and Cons: Supramolecular or Macromolecular: What Is Best for Functional Hydrogels with Advanced Properties? *Advanced Materials*, 1906012:1906012, jan 2020.

[84] Joel H. Collier, Jai S. Rudra, Joshua Z. Gasiorowski, and Jangwook P. Jung. Multi-component extracellular matrices based on peptide self-assembly. *Chemical Society Reviews*, 39(9):3413–3424, 2010.

[85] Phillip R.A. Chivers and David K. Smith. Shaping and structuring supramolecular gels. *Nature Reviews Materials*, 4(7):463–478, 2019.

[86] Hiroshi Murata. Rheology - Theory and Application to Biomaterials. In *Polymerization*, pages 403–423. InTech, sep 2012.

[87] M. L. Oyen. Mechanical characterisation of hydrogel materials. *International Materials Reviews*, 59(1):44–59, 2014.

[88] Romano Lapasin. Rheological Characterization of Hydrogels. In *Polysaccharide Hydrogels*, volume 14, pages 83–137. Pan Stanford, nov 2015.

[89] F C Mackintosh, J. Kas, and P. A. Janmey. Elasticity of Semi-flexible polymer networks. *Physical Review Letters*, 75(24):4425, 1995.

[90] P G de Gennes. *Scaling Concepts in Polymer Physics*. Cornell University Press, 1979.

[91] Bulent Ozbas, Karthikan Rajagopal, Joel P. Schneider, and Damn J. Pochan. Semiflexible chain networks formed via self-assembly of β-hairpin molecules. *Physical Review Letters*, 93(26 I):1–4, 2004.

[92] Megan A. Greenfield, Jessica R. Hoffman, Monica Olvera De La Cruz, and Samuel I. Stupp. Tunable mechanics of peptide nanofiber gels. *Langmuir*, 26(5):3641–3647, 2010.

[93] Shantanu Sur, Christina J. Newcomb, Matthew J. Webber, and Samuel I. Stupp. Tuning supramolecular mechanics to guide neuron development. *Biomaterials*, 34(20):4749–4757, 2013.

[94] E. Thomas Pashuck, Honggang Cui, and Samuel I. Stupp. Tuning Supramolecular Rigidity of Peptide Fibers through Molecular Structure. *Journal of the American Chemical Society*, 132(17):6041–6046, 2010.

[95] Brian Amsden. An Obstruction-Scaling Model for Diffusion in Homogeneous Hydrogels. *Macromolecules*, 32(3):874–879, 1999.

[96] J. D. Hartgerink, E. Beniash, and S. I. Stupp. Self-assembly and mineralization of peptide-amphiphile nanofibers. *Science*, 294(5547):1684–1688, nov 2001.

[97] Kohei Sato, Mark P. Hendricks, Liam C. Palmer, and Samuel I. Stupp. Peptide supramolecular materials for therapeutics. *Chemical Society Reviews*, 47(20):7539–7551, 2018.

[98] Mark P. Hendricks, Kohei Sato, Liam C. Palmer, and Samuel I. Stupp. Supramolecular Assembly of Peptide Amphiphiles. *Accounts of Chemical Research*, 50(10):2440–2448, 2017.

[99] L. Brunsveld, B. J.B. Folmer, E. W. Meijer, and R. P. Sijbesma. Supramolecular polymers. *Chemical Reviews*, 101(12):4071–4097, 2001.

[100] Jean François Lutz, Jean Marie Lehn, E. W. Meijer, and Krzysztof Matyjaszewski. From precision polymers to complex materials and systems. *Nature Reviews Materials*, 1(16024), 2016.

[101] Roman V. Kazantsev, Faifan Tantakitti, Roya Zandi, Tao Yu, Job Boekhoven, Samuel I. Stupp, Julia H. Ortony, George C. Schatz, Jiahe Li, Monica Olvera de la Cruz, Christina J. Newcomb, Gajendra S. Shekhawat, Xin Wang, Ellen Zhuang, and Liam C. Palmer. Energy landscapes and functions of supramolecular systems. *Nature Materials*, 15(4):469–476, 2016.

[102] Peter A. Korevaar, Christina J. Newcomb, E. W. Meijer, and Samuel I. Stupp. Pathway selection in peptide amphiphile assembly. *Journal of the American Chemical Society*, 136(24):8540–8543, 2014.

[103] Keith W. MacRenaris, Claudio Luchinat, Emily A. Waters, Thomas J. Meade, Mark T. McClendon, Adam T. Preslar, Chad R. Haney, Samantha S. Sefick, Tyson J. Moyer, Samuel I. Stupp, and Giacomo Parigi. Gd(III)-Labeled Peptide Nanofibers for Reporting on Biomaterial Localization in Vivo . *ACS Nano*, 8(7):7325–7332, 2014.

[104] Mustafa O. Guler, Stephen Soukasene, James F. Hulvat, and Samuel I. Stupp. Presentation and recognition of biotin on nanofibers formed by branched peptide amphiphiles. *Nano Letters*, 5(2):249–252, 2005.

[105] Mustafa O. Guler, Lorraine Hsu, Stephen Soukasene, Daniel A. Harrington, James F. Hulvat, and Samuel I. Stupp. Presentation of RGDS Epitopes on Self-Assembled Nanofibers of Branched Peptide Amphiphiles. *Biomacromolecules*, 7(6):1855–1863, jun 2006.

[106] Eduard Sleep, Feng Chen, Andrew D. Schneider, Joseph A. Weiner, Sohaib Z. Hashmi, Erin L. Hsu, Michael S. Schallmo, Karina M. Katchko, Zhilin Yu, Sungsoo S. Lee, Zaida Álvarez, Samuel I. Stupp, Ralph W. Cook, Wellington K. Hsu, Danielle S. Chun, Gurmit Singh, Chawon Yun, Mark T. McClendon, Timmy Fyrner, Stuart R. Stock, Justin T. Smith, and Ryan D. Freshman. Sulfated glycopeptide nanostructures for multipotent protein activation. *Nature Nanotechnology*, 12(8):821–829, 2017.

[107] Matthew J. Webber, Xiaoqiang Han, S. N. Prasanna Murthy, Kanya Rajangam, Samuel I. Stupp, and Jon W. Lomasney. Capturing the stem cell paracrine effect using heparin-presenting nanofibres to treat cardiovascular diseases. *Journal of Tissue Engineering and Regenerative Medicine*, 4(8):600–610, dec 2010.

[108] Gabriel A. Silva, Catherine Czeisler, Krista L. Niece, Elia Beniash, Daniel A. Harrington, John A. Kessler, and Samuel I. Stupp. Selective Differentiation of Neural Progenitor Cells by High-Epitope Density Nanofibers. *Science*, 303(5662):1352–1355, 2004.

[109] Steve R. Bull, Liam C. Palmer, Nathaniel J. Fry, Megan A. Greenfield, Benjamin W. Messmore, Thomas J. Meade, and Samuel I. Stupp. A templating approach for monodisperse self-assembled organic nanostructures. *Journal of the American Chemical Society*, 130(9):2742–2743, 2008.

[110] Zhilin Yu, Faifan Tantakitti, Tao Yu, Liam C. Palmer, George C. Schatz, and Samuel I. Stupp. Simultaneous covalent and noncovalent hybrid polymerizations. *Science*, 351(6272):497–502, 2016.

[111] Krista L. Niece, Jeffrey D. Hartgerink, Jack J. J. M. Donners, and Samuel I. Stupp. Self-Assembly Combining Two Bioactive Peptide-Amphiphile Molecules into Nanofibers by Electrostatic Attraction. *J. Am. Chem. Soc.*, 125:7146–7147, 2003.

[112] Christina J. Newcomb, Shantanu Sur, Julia H. Ortony, One-Sun Lee, John B. Matson, Job Boekhoven, Jeong Min Yu, George C. Schatz, and Samuel I. Stupp. Cell death versus cell survival instructed by supramolecular cohesion of nanostructures. *Nature Communications*, 5(1):3321, may 2014.

[113] Hannah Storrie, Mustafa O. Guler, Suha N. Abu-Amara, Tova Volberg, Mukti Rao, Benjamin Geiger, and Samuel I. Stupp. Supramolecular crafting of cell adhesion. *Biomaterials*, 28(31):4608–4618, 2007.

[114] Matthew J. Webber, Jörn Tongers, Marie Ange Renault, Jerome G. Roncalli, Douglas W. Losordo, and Samuel I. Stupp. Development of bioactive peptide amphiphiles for therapeutic cell delivery. *Acta Biomaterialia*, 6(1):3–11, 2010.

[115] Shantanu Sur, Faifan Tantakitti, John B. Matson, and Samuel I. Stupp. Epitope topography controls bioactivity in supramolecular nanofibers. *Biomaterials Science*, 3(3):520–532, 2015.

[116] Eric J. Berns, Shantanu Sur, Liuliu Pan, Joshua E. Goldberger, Sunitha Suresh, Shuming Zhang, John A. Kessler, and Samuel I. Stupp. Aligned neurite outgrowth and directed cell migration in self-assembled monodomain gels. *Biomaterials*, 35(1):185–195, 2014.

[117] Ramille M Capito, Helena S Azevedo, Yuri S Velichko, Alvaro Mata, and Samuel I Stupp. Self-Assembly of Large and Small Molecules into Hierarchically Ordered Sacs and Membranes. *Science*, 319(5871):1812–1816, mar 2008.

[118] R. Helen Zha, Yuri S. Velichko, Ronit Bitton, and Samuel I. Stupp. Molecular design for growth of supramolecular membranes with hierarchical structure. *Soft Matter*, 12(5):1401–1410, 2016.

[119] Karla E. Inostroza-Brito, Estelle Collin, Orit Siton-Mendelson, Katherine H. Smith, Amàlia Monge-Marcet, Daniela S. Ferreira, Raúl Pérez Rodríguez, Matilde Alonso, José Carlos Rodríguez-Cabello, Rui L. Reis, Francesc Sagués, Lorenzo Botto, Ronit Bitton, Helena S. Azevedo, and Alvaro Mata. Co-Assembly, spatiotemporal control and morphogenesis of a hybrid protein-peptide system. *Nature Chemistry*, 7(11):897–904, 2015.

[120] Honggang Cui, Matthew J. Webber, and Samuel I. Stupp. Self-assembly of peptide amphiphiles: From molecules to nanostructures to biomaterials. *Biopolymers*, 94(1):1–18, jan 2010.

[121] Yi Zhang, Yuhong Bai, and Bing Yan. Functionalized carbon nanotubes for potential medicinal applications. *Drug Discovery Today*, 15(11-12):428–435, jun 2010.

[122] Alvaro Mata, Lorraine Hsu, Ramille Capito, Conrado Aparicio, Karl Henrikson, and Samuel I. Stupp. Micropatterning of bioactive self-assembling gels. *Soft Matter*, 5(6):1228, 2009.

[123] Mark T. McClendon, Anisa Yalom, Eric J. Berns, Akishige Hokugo, Samuel I. Stupp, Reza Jarrahy, Igor Spigelman, Andrew Li, Nicholas Stephanopoulos, and Luis A. Segovia. A bioengineered peripheral nerve construct using aligned peptide amphiphile nanofibers. *Biomaterials*, 35(31):8780–8790, 2014.

[124] M. J. Webber, J. Tongers, C. J. Newcomb, K.-T. Marquardt, J. Bauersachs, D. W. Losordo, and S. I. Stupp. Supramolecular nanostructures that mimic VEGF as a strategy for ischemic tissue repair. *Proceedings of the National Academy of Sciences*, 108(33):13438–13443, aug 2011.

[125] Alvaro Mata, Yanbiao Geng, Karl J. Henrikson, Conrado Aparicio, Stuart R. Stock, Robert L. Satcher, and Samuel I. Stupp. Bone regeneration mediated by biomimetic mineralization of a nanofiber matrix. *Biomaterials*, 31(23):6004–6012, aug 2010.

[126] Timothy D Sargeant, Samuel I Stupp, Alvaro Mata, Zhan Huang, Chung-Yan Koh, Pablo Bringas, Malcolm L Snead, and James F Hulvat. Bioactive Nanofibers Instruct Cells to Proliferate and Differentiate During Enamel Regeneration. *Journal of Bone and Mineral Research*, 23(12):1995–2006, 2008.

[127] Ramille N. Shah, Nirav A. Shah, Marc M. Del Rosario Lim, Caleb Hsieh, Gordon Nuber, and Samuel I. Stupp. Supramolecular design of self-assembling nanofibers for cartilage regeneration. *Proceedings of the National Academy of Sciences*, 107(8):3293–3298, feb 2010.

[128] Daniel J. Toft, Tyson J. Moyer, Stephany M. Standley, Yves Ruff, Andrey Ugolkov, Samuel I. Stupp, and Vincent L. Cryns. Coassembled cytotoxic and pegylated peptide amphiphiles form filamentous nanostructures with potent antitumor activity in models of breast cancer. *ACS Nano*, 6(9):7956–7965, 2012.

[129] Anthony C. Yu, Lyndsay M. Stapleton, Joseph L. Mann, and Eric A. Appel. Self-assembled biomaterials using host-guest interactions. In *Self-assembling Biomaterials*, pages 205–231. Elsevier, 2018.

[130] Bernhard V.K.J. Schmidt and Christopher Barner-Kowollik. Dynamic Macromolecular Material Design—The Versatility of Cyclodextrin-Based Host–Guest Chemistry. *Angewandte Chemie - International Edition*, 56(29):8350–8369, 2017.

[131] Don Wook Lee Kimoon Kim, Young Ho Ko, Su Hyun Lee, Selvapalam Narayanan. Composition for odor removal comprising cucurbituril, 2013.

[132] Nial J. Wheate and Christina Limantoro. Cucurbit[n]urils as excipients in pharmaceutical dosage forms. *Supramolecular Chemistry*, 28(9-10):849–856, 2016.

[133] Frank Davis and Séamus Higson. *Macrocycles*. 2011.

[134] Xiaoke Li, Changjun Zou, and Chanchan Cui. Synthesis and characterization of a novel *β*-cyclodextrin modified cationic polyacrylamide and its application for enhancing oil recovery. *Starch - Stärke*, 67(7-8):673–682, jul 2015.

[135] Christopher B. Highley, Christopher B. Rodell, and Jason A. Burdick. Direct 3D Printing of Shear-Thinning Hydrogels into Self-Healing Hydrogels. *Advanced Materials*, 27(34):5075–5079, 2015.

[136] Simge G. Yüz, Julia Ricken, and Seraphine V. Wegner. Independent Control over Multiple Cell Types in Space and Time Using Orthogonal Blue and Red Light Switchable Cell Interactions. *Advanced Science*, 5(8):1–6, 2018.

[137] Dawid Kedracki, Jancy Nixon Abraham, Enora Prado, and Corinne Nardin. Assembly of Biohybrid Polymers. In *Macromolecular Self-assembly*, pages 193–229. John Wiley & Sons, Inc., Hoboken, New Jersey, aug 2016.

[138] Anika M Jonker, Dennis W P M Lowik, and Jan C M van Hest. Peptide-and protein-based hydrogels. *Chemistry of Materials*, 24(5):759–773, 2012.

[139] Quan Luo, Chunxi Hou, Yushi Bai, Ruibing Wang, and Junqiu Liu. Protein Assembly: Versatile Approaches to Construct Highly Ordered Nanostructures. *Chemical Reviews*, 116(22):13571–13632, 2016.

[140] Matthew J. Rowland, Marina Atgie, Dominique Hoogland, and Oren A. Scherman. Preparation and Supramolecular Recognition of Multivalent Peptide-Polysaccharide Conjugates by Cucurbit[8]uril in Hydrogel Formation. *Biomacromolecules*, 16(8):2436–2443, 2015.

[141] Mikhail V. Rekharsky and Yoshihisa Inoue. Complexation Thermodynamics of Cyclodextrins. *Chemical Reviews*, 98(5):1875–1918, jul 1998.

[142] Akihito Hashidzume, Fumitaka Ito, Itsuro Tomatsu, and Akira Harada. Macromolecular Recognition by Polymer-Carrying Cyclodextrins: Interaction of a Polymer Bearing Cyclodextrin Moieties with Poly(acrylamide)s Bearing Aromatic Side Chains. *Macromolecular Rapid Communications*, 26(14):1151–1154, jul 2005.

[143] Frank van de Manakker, Kevin Braeckmans, Najim el Morabit, Stefaan C. De Smedt, Cornelus F. van Nostrum, and Wim E. Hennink. Protein-Release Behavior of Self-Assembled PEG- *β* -Cyclodextrin/PEG-Cholesterol Hydrogels. *Advanced Functional Materials*, 19(18):2992–3001, sep 2009.

[144] Yan-Li Zhao and J. Fraser Stoddart. Azobenzene-Based Light-Responsive Hydrogel System †. *Langmuir*, 25(15):8442–8446, aug 2009.

[145] Kang Moo Huh, Hajime Tomita, Won Kyu Lee, Tooru Ooya, and Nobuhiko Yui. Synthesis of $$-Cyclodextrin-Conjugated Poly($$-lysine)s and Their Inclusion Complexation Behavior. *Macromolecular Rapid Communications*, 23(3):179–182, feb 2002.

[146] Jason Lagona, Pritam Mukhopadhyay, Sriparna Chakrabarti, and Lyle Isaacs. The cucurbit[n]uril family. *Angewandte Chemie - International Edition*, 44(31):4844–4870, 2005.

[147] Steven J. Barrow, Setu Kasera, Matthew J. Rowland, Jesús Del Barrio, and Oren A. Scherman. Cucurbituril-Based Molecular Recognition. *Chemical Reviews*, 115(22):12320–12406, 2015.

[148] Jae Wook Lee, S. Samal, N. Selvapalam, Hee Joon Kim, and Kimoon Kim. Cucurbituril homologues and derivatives: New opportunities in supramolecular chemistry. *Accounts of Chemical Research*, 36(8):621–630, 2003.

[149] Guanglu Wu, David E. Clarke, Ce Wu, and Oren A. Scherman. Oligopeptide-CB[8] complexation with switchable binding pathways. *Organic and Biomolecular Chemistry*, 17(14):3514–3520, 2019.

[150] Urs Rauwald and Oren A. Scherman. Supramolecular Block Copolymers with Cucurbit[8]uril in Water. *Angewandte Chemie International Edition*, 47(21):3950–3953, may 2008.

[151] Dorothee Wasserberg, Vinod Subramaniam, Luc Brunsveld, Li Zhang, Dana A. Uhlenheuer, Christian Blum, and Hoang Nguyen. Modulation of Protein Dimerization by a Supramolecular Host-Guest System. *Chemistry - A European Journal*, 15(35):8779–8790, 2009.

[152] Olga J.G.M. Goor, Ralph P.G. Bosmans, Luc Brunsveld, and Patricia Y.W. Dankers. Cucurbituril-mediated immobilization of fluorescent proteins on supramolecular biomaterials. *Journal of Polymer Science, Part A: Polymer Chemistry*, 55(21):3607–3616, 2017.

[153] Jin Geng, Frank Biedermann, Jameel M. Zayed, Feng Tian, and Oren A. Scherman. Supramolecular Glycopolymers in Water: A Reversible Route Toward Multivalent Carbohydrate–Lectin Conjugates Using Cucurbit[8]uril. *Macromolecules*, 44(11):4276–4281, jun 2011.

[154] Eric A. Appel, Frank Biedermann, Urs Rauwald, Samuel T. Jones, Jameel M. Zayed, and Oren A. Scherman. Supramolecular cross-linked networks via host-guest complexation with cucurbit[8]uril. *Journal of the American Chemical Society*, 132(40):14251–14260, 2010.

[155] Carlos Redondo-Gómez, Yamin Abdouni, C. Remzi Becer, and Alvaro Mata. Self-Assembling Hydrogels Based on a Complementary Host–Guest Peptide Amphiphile Pair. *Biomacromolecules*, 20(6):2276–2285, jun 2019.

[156] Elizabeth C. Wu, Shuguang Zhang, and Charlotte A E Hauser. Self-assembling peptides as cell-interactive scaffolds. *Advanced Functional Materials*, 22(3):456–468, 2012.

[157] Zhen Gang Wang and Baoquan Ding. DNA-based self-assembly for functional nanomaterials. *Advanced Materials*, 25(28):3905–3914, 2013.

[158] Richard J. Williams, Andrew M. Smith, Richard Collins, Nigel Hodson, Apurba K. Das, and Rein V. Ulijn. Enzyme-assisted self-assembly under thermodynamic control. *Nature Nanotechnology*, 4(1):19–24, jan 2009.

[159] Daniela S. Ferreira, Alexandra P. Marques, Rui L. Reis, and Helena S. Azevedo. Hyaluronan and self-assembling peptides as building blocks to reconstruct the extracellular environment in skin tissue. *Biomaterials Science*, 1(9):952, 2013.

[160] Nathaniel Huebsch, David J. Mooney, Darinka Klumpers, Georg N. Duda, Max Darnell, Ovijit Chaudhuri, James C. Weaver, Hong-pyo Lee, Luo Gu, Sidi A. Bencherif, Evi Lippens, Darinka Klumpers, Max Darnell, Sidi A. Bencherif, James C. Weaver, Nathaniel Huebsch, Hong-pyo Lee, Evi Lippens, Georg N. Duda, and David J. Mooney. Hydrogels with tunable stress relaxation regulate stem cell fate and activity. *Nature Materials*, 15(3):326–334, mar 2016.

[161] William J. Hadden, Jennifer L. Young, Andrew W. Holle, Meg L. McFetridge, Du Yong Kim, Philip Wijesinghe, Hermes Taylor-Weiner, Jessica H. Wen, Andrew R. Lee, Karen Bieback, Ba-Ngu Vo, David D. Sampson, Brendan F. Kennedy, Joachim P. Spatz, Adam J. Engler, and Yu Suk Choi. Stem cell migration and mechanotransduction on linear stiffness gradient hydrogels. *Proceedings of the National Academy of Sciences*, 114(22):5647–5652, may 2017.

[162] Siena M. Mantooth, Brizzia G. Munoz-Robles, and Matthew J. Webber. Dynamic Hydrogels from Host–Guest Supramolecular Interactions. *Macromolecular Bioscience*, 19(1):1–12, 2019.

[163] Hui Yang, Bin Yuan, Xi Zhang, and Oren A. Scherman. Supramolecular chemistry at interfaces: Host-guest interactions for fabricating multifunctional biointerfaces. *Accounts of Chemical Research*, 47(7):2106–2115, 2014.

[164] Akira Harada, Yoshinori Takashima, and Masaki Nakahata. Supramolecular polymeric materials via cyclodextrin-guest interactions. *Accounts of Chemical Research*, 47(7):2128–2140, 2014.

[165] Yamin Abdouni, Gökhan Yilmaz, and C. Remzi Becer. Sequence Controlled Polymers from a Novel *β*-Cyclodextrin Core. *Macromolecular Rapid Communications*, 38(24):1700501, dec 2017.

[166] Qiang Zhang, Lu Su, Jennifer Collins, Guosong Chen, Russell Wallis, Daniel A. Mitchell, David M. Haddleton, and C. Remzi Becer. Dendritic cell lectin-targeting sentinel-like unimolecular glycoconjugates to release an anti-HIV drug. *Journal of the American Chemical Society*, 136(11):4325–4332, mar 2014.

[167] Gokhan Yilmaz, Veselina Uzunova, Richard Napier, and C. Remzi Becer. Single-Chain Glycopolymer Folding via Host-Guest Interactions and Its Unprecedented Effect on DC-SIGN Binding. *Biomacromolecules*, 19(7):3040–3047, jul 2018.

[168] Yung Chih Lin, Po I. Wang, and Shiao Wei Kuo. Water-soluble, stable helical polypeptide-grafted cyclodextrin bioconjugates: Synthesis, secondary and self-assembly structures, and inclusion complex with guest compounds. *Soft Matter*, 8(37):9676–9684, 2012.

[169] Frank Versluis, Jens Voskuhl, Marc C.A. Stuart, Jelle B. Bultema, Seda Kehr, Bart Jan Ravoo, and Alexander Kros. Power struggles between oligopeptides and cyclodextrin vesicles. *Soft Matter*, 8(33):8770–8777, 2012.

[170] Shan-Shan Xue, Cai-Ping Tan, Mu-He Chen, Jian-Jun Cao, Dong-Yang Zhang, Rui-Rong Ye, Liang-Nian Ji, and Zong-Wan Mao. Tumor-targeted supramolecular nanoparticles self-assembled from a ruthenium-*β*-cyclodextrin complex and an adamantane-functionalized peptide. *Chemical Communications*, 53(5):842–845, 2017.

[171] M. A. Hossain, K. Hamasaki, K. Takahashi, H. Mihara, and A. Ueno. Guest-induced diminishment in fluorescence quenching and molecule sensing ability of a novel cyclodextrin-peptide conjugate [7]. *Journal of the American Chemical Society*, 123(30):7435–7436, 2001.

[172] Yara Ruiz García, Jan Zelenka, Y. Vladimir Pabon, Abhishek Iyer, Miloš Buděšínský, Tomáš Kraus, C. I. Edvard Smith, and Annemieke Madder. Cyclodextrin-peptide conjugates for sequence specific DNA binding. *Organic and Biomolecular Chemistry*, 13(18):5273–5278, 2015.

[173] Zhilin Yu, Aykut Erbas, Faifan Tantakitti, Liam C. Palmer, Joshua A. Jackman, Monica Olvera De La Cruz, Nam Joon Cho, and Samuel I. Stupp. Coassembly of Peptide Amphiphiles and Lipids into Supramolecular Nanostructures Driven by Anionâ'Ï€ Interactions. *Journal of the American Chemical Society*, 139(23):7823–7830, 2017.

[174] Vida Castro, Hortensia Rodríguez, and Fernando Albericio. CuAAC: An Efficient Click Chemistry Reaction on Solid Phase. *ACS Combinatorial Science*, 18(1):1–14, 2016.

[175] C. Allen Bush, Susanta K. Sarkar, and Kenneth D. Kopple. Circular Dichroism of (*β* Turns in Peptides and Proteins. *Biochemistry*, 17(23):4951–4954, 1978.

[176] Suhaas Aluri, Martha K. Pastuszka, Ara S. Moses, and J. Andrew MacKay. Elastin-like peptide amphiphiles form nanofibers with tunable length. *Biomacromolecules*, 13(9):2645–2654, 2012.

[177] Mingjie Zhang and Hans J Vogels. THE JOURNAL OF BIOLOGICAL CHEMISTRY Determination of the Side Chain p K a Values of the Lysine Residues in Calmodulin*. 268(30):22420–22428, 1993.

[178] Mitsuru Nagasawa. *Physical Chemistry of Polyelectrolyte Solutions*, volume 158. 2015.

[179] Daniel G. Isom, Carlos A. Castañed, Brian R. Cannon, and Bertrand E. García-Moreno. Large shifts in pKa values of lysine residues buried inside a protein. *Proceedings of the National Academy of Sciences of the United States of America*, 108(13):5260–5265, 2011.

[180] Ritchie Chen, Sarah A. Shelby, Ronald N. Zuckermann, Ryan A. Mesch, Christian Kisielowski, Ki Tae Nam, Tammy K. Chu, Li Tan, Philip H. Choi, Michael D. Connolly, Amanda B. Marciel, Byoung-Chul Lee, Sarah A. Shelby, Philip H. Choi, Amanda B. Marciel, Ritchie Chen, Li Tan, Tammy K. Chu, Ryan A. Mesch, Byoung-Chul Lee, Michael D. Connolly, Christian Kisielowski, and Ronald N. Zuckermann. Free-floating ultrathin two-dimensional crystals from sequence-specific peptoid polymers. *Nature Materials*, 9(5):454–460, may 2010.

[181] Peter A. Korevaar, Christina J. Newcomb, E. W. Meijer, and Samuel I. Stupp. Pathway selection in peptide amphiphile assembly. *Journal of the American Chemical Society*, 136(24):8540–8543, 2014.

[182] Alper D. Ozkan, Ayse B. Tekinay, Mustafa O. Guler, and E. Deniz Tekin. Effects of temperature, pH and counterions on the stability of peptide amphiphile nanofiber structures. *RSC Advances*, 6(106):104201–104214, 2016.

[183] Yi Shi, Jerry Goodisman, and James C. Dabrowiak. Cyclodextrin capped gold nanoparticles as a delivery vehicle for a prodrug of cisplatin. *Inorganic Chemistry*, 52(16):9418–9426, 2013.

[184] Stefanie C. Lange, Jan Unsleber, Patrick Drücker, Hans Joachim Galla, Mark P. Waller, and Bart Jan Ravoo. PH response and molecular recognition in a low molecular weight peptide hydrogel. *Organic and Biomolecular Chemistry*, 13(2):561–569, 2015.

[185] Guang Yang, Xiang Zhang, Zdravko Kochovski, Yufei Zhang, Bin Dai, Fuji Sakai, Lin Jiang, Yan Lu, Matthias Ballauff, Xueming Li, Cong Liu, Guosong Chen, and Ming Jiang. Precise and Reversible Protein-Microtubule-Like Structure with Helicity Driven by Dual Supramolecular Interactions. *Journal of the American Chemical Society*, 138(6):1932–1937, 2016.

[186] Jorge Carrazana, Aida Jover, Francisco Meijide, Victor H. Soto, and José Vázquez Tato. Complexation of adamantyl compounds by *β*-cyclodextrin and monoaminoderivatives. *Journal of Physical Chemistry B*, 109(19):9719–9726, 2005.

[187] Joseph B. Lambert, Eugene P. Mazzola, and Clark D. Ridge. *Nuclear Magnetic Resonance Spectroscopy: An Introduction to Principles, Applications, and Experimental Methods*. Wiley, 2nd edition, 2018.

[188] Mark P Foster, Craig A Mcelroy, and Carlos D Amero. Current Topics Solution NMR of Large Molecules and Assemblies †. *Current*, 46(2), 2007.

[189] Liam C. Palmer, Benjamin Weber, Wei Ji, Matthias Barz, Kohei Sato, Samuel I. Stupp, Wei Ji, Liam C. Palmer, Benjamin Weber, Matthias Barz, and Samuel I. Stupp. Programmable Assembly of Peptide Amphiphile via Noncovalent-to-Covalent Bond Conversion. *Journal of the American Chemical Society*, 139(26):8995–9000, 2017.

[190] Mohammad Aref Khalily, Melis Goktas, and Mustafa O. Guler. Tuning viscoelastic properties of supramolecular peptide gels via dynamic covalent crosslinking. *Organic and Biomolecular Chemistry*, 13(7):1983–1987, 2015.

[191] Joel M. Anderson, Adinarayana Andukuri, Dong Jin Lim, and Ho Wook Jun. Modulating the gelation properties of self-assembling peptide amphiphiles. *ACS Nano*, 3(11):3447–3454, nov 2009.

[192] Clara L. Hedegaard, Estelle C. Collin, Carlos Redondo-Gómez, Luong T.H. Nguyen, Kee Woei Ng, Alfonso A. Castrejón-Pita, J. Rafael Castrejón-Pita, and Alvaro Mata. Hydrodynamically Guided Hierarchical Self-Assembly of Peptide–Protein Bioinks. *Advanced Functional Materials*, 28(16):1–13, 2018.

[193] Sergey E. Paramonov, Ho Wook Jun, and Jeffrey D. Hartgerink. Self-assembly of peptide-amphiphile nanofibers: The roles of hydrogen bonding and amphiphilic packing. *Journal of the American Chemical Society*, 128(22):7291–7298, 2006.

[194] John C. Stendahl, Mukti S. Rao, Mustafa O. Guler, Samuel I. Stupp, By John C Stendahl, Mukti S. Rao, Mustafa O. Guler, and Samuel I. Stupp. Intermolecular forces in the self-assembly of peptide amphiphile nanofibers. *Advanced Functional Materials*, 16(4):499–508, 2006.

[195] Shangyang Li, Lin Zhang, Bo Wang, Mingfang Ma, Pengyao Xing, Xiaoxiao Chu, Yimeng Zhang, and Aiyou Hao. An easy approach for constructing vesicles by using aromatic molecules with *β*-cyclodextrin. *Soft Matter*, 11(9):1767–1777, 2015.

[196] Eric A. Appel, Rebecca A. Forster, Matthew J. Rowland, and Oren A. Scherman. The control of cargo release from physically crosslinked hydrogels by crosslink dynamics. *Biomaterials*, 35(37):9897–9903, 2014.

[197] Jae-Won Shin and David J. Mooney. Extracellular matrix stiffness causes systematic variations in proliferation and chemosensitivity in myeloid leukemias. *Proceedings of the National Academy of Sciences*, 113(43):12126–12131, 2016.

[198] Ronald N. Zuckermann, Janice M. Kerr, Walter H. Moosf, and Stephen B.H. Kent. Efficient Method for the Preparation of Peptoids [Oligo(N-substituted glycines)] by Submonomer Solid-Phase Synthesis. *Journal of the American Chemical Society*, 114(26):10646–10647, 1992.

[199] Weihua Tang and Siu Choon Ng. Facile synthesis of mono-6-amino-6-deoxy-α-, β-, γ-cyclodextrin hydrochlorides for molecular recognition, chiral separation and drug delivery. *Nature Protocols*, 3(4):691–697, 2008.

[200] Shihua Wang, Lin Yu, Pinhua Li, Lingguo Meng, and Lei Wang. Copper(I) iodide catalyzed cross-coupling reaction of terminal alkynes with 1-bromoalkynes: A simple synthesis of unsymmetrical buta-1,3-diynes. *Synthesis*, (10):1541–1546, 2011.

[201] Belhu B. Metaferia, Matthew Rittler, Jinesh S. Gheeya, Albert Lee, Heidi Hempel, Alberto Plaza, William G. Stetler-Stevenson, Carole A. Bewley, and Javed Khan. Synthesis of novel cyclic NGR/RGD peptide analogs via on resin click chemistry. *Bioorganic and Medicinal Chemistry Letters*, 20(24):7337–7340, 2010.

[202] Sandro Keller, Carolyn Vargas, Huaying Zhao, Grzegorz Piszczek, Chad A Brautigam, and Peter Schuck. High-Precision Isothermal Titration Calorimetry with Automated Peak-Shape Analysis. *Analytical Chemistry*, 84(11):5066–5073, jun 2012.

[203] Chad A. Brautigam, Huaying Zhao, Carolyn Vargas, Sandro Keller, and Peter Schuck. Integration and global analysis of isothermal titration calorimetry data for studying macromolecular interactions. *Nature Protocols*, 11(5):882–894, may 2016.

[204] Jenny Brinkmann, Emanuela Cavatorta, Shrikrishnan Sankaran, Bettina Schmidt, Jasper Van Weerd, and Pascal Jonkheijm. About supramolecular systems for dynamically probing cells. *Chemical Society Reviews*, 43(13):4449–4469, 2014.

[205] Marco Paolino, Franka Ennen, Stefania Lamponi, Mihaela Cernescu, Brigitte Voit, Andrea Cappelli, Dietmar Appelhans, and Hartmut Komber. Cyclodextrin-Adamantane Host–Guest Interactions on the Surface of Biocompatible Adamantyl-Modified Glycodendrimers. *Macromolecules*, 46(9):3215–3227, may 2013.

[206] Martina Delbianco, Priya Bharate, Silvia Varela-Aramburu, and Peter H. Seeberger. Carbohydrates in supramolecular chemistry. *Chemical Reviews*, 116(4):1693–1752, 2016.

[207] Alex Buchberger, Chad R Simmons, Nour Eddine Fahmi, Ronit Freeman, and Nicholas Stephanopoulos. Hierarchical Assembly of Nucleic Acid/Coiled-Coil Peptide Nanostructures. *Journal of the American Chemical Society*, page jacs.9b11158, jan 2020.

[208] Hector Garcia-Seisdedos, Charly Empereur-Mot, Nadav Elad, and Emmanuel D. Levy. Proteins evolve on the edge of supramolecular self-assembly. *Nature*, 548(7666):244–247, 2017.

[209] Gabriel A Silva, Gabriel A Silva, Catherine Czeisler, Krista L Niece, Elia Beniash, Daniel A Harrington, John A Kessler, and Samuel I Stupp. Selective Differentiation of Neural Progenitor Cells by High – Epitope Density Nanofibers. *Science*, 303(February):1352–1355, 2014.

[210] Amy Y. Clark, Karen E. Martin, José R. García, Christopher T. Johnson, Hannah S. Theriault, Woojin M. Han, Dennis W. Zhou, Edward A. Botchwey, and Andrés J. García. Integrin-specific hydrogels modulate transplanted human bone marrow-derived mesenchymal stem cell survival, engraftment, and reparative activities. *Nature Communications*, 11(1):114, dec 2020.

[211] Nick Huettner, Tim R. Dargaville, and Aurelien Forget. Discovering Cell-Adhesion Peptides in Tissue Engineering: Beyond RGD. *Trends in Biotechnology*, 36(4):372–383, 2018.

[212] I. Ceren Yasa, Nuray Gunduz, Murat Kilinc, Mustafa O. Guler, and Ayse B. Tekinay. Basal Lamina Mimetic Nanofibrous Peptide Networks for Skeletal Myogenesis. *Scientific Reports*, 5:1–13, 2015.

[213] Jian Ping Xiong, Thilo Stehle, Rongguang Zhang, Andrzej Joachimiak, Matthias Frech, Simon L. Goodman, and M. Amin Arnaout. Crystal structure of the extracellular segment of integrin $\alpha V\beta 3$ in complex with an Arg-Gly-Asp ligand. *Science*, 296(5565):151–155, 2002.

[214] Mingjun Zhou, Yulia Shmidov, John B. Matson, and Ronit Bitton. Multi-scale characterization of thermoresponsive dendritic elastin-like peptides. *Colloids and Surfaces B: Biointerfaces*, 153:141–151, 2017.

[215] Jiayang Li, Yi Kuang, Yuan Gao, Xuewen Du, Junfeng Shi, and Bing Xu. D -amino acids boost the selectivity and confer supramolecular hydrogels of a nonsteroidal anti-inflammatory drug (NSAID). *Journal of the American Chemical Society*, 135(2):542–545, 2013.

[216] Nicholas Stephanopoulos, Julia H. Ortony, and Samuel I. Stupp. Self-assembly for the synthesis of functional biomaterials. *Acta Materialia*, 61(3):912–930, 2013.

[217] Beom Jin Kim, Dongsik Yang, and Bing Xu. Emerging Applications of Supramolecular Peptide Assemblies. *Trends in Chemistry*, pages 1–13, 2019.

[218] Matthew J. Webber, Christina J. Newcomb, Ronit Bitton, and Samuel I. Stupp. Switching of self-assembly in a peptide nanostructure with a specific enzyme. *Soft Matter*, 7(20):9665–9672, 2011.

[219] Zhan Huang, Christina J. Newcomb, Pablo Bringas, Samuel I. Stupp, and Malcolm L. Snead. Biological synthesis of tooth enamel instructed by an artificial matrix. *Biomaterials*, 31(35):9202–9211, 2010.

[220] Hannah Storrie, Mustafa O. Guler, Suha N. Abu-Amara, Tova Volberg, Mukti Rao, Benjamin Geiger, and Samuel I. Stupp. Supramolecular crafting of cell adhesion. *Biomaterials*, 28(31):4608–4618, 2007.

[221] Margarita Vázquez-González and Itamar Willner. Stimuli-responsive Biomolecule-based Hydrogels and their Applications. *Angewandte Chemie International Edition*, page 10.1002/anie.201907670, nov 2019.

[222] Thai Duong Luong, Mohamed Zoughaib, Ruslan Garifullin, Svetlana Kuznetsova, Mustafa O. Guler, and Timur I. Abdullin. In situ functionalization of poly(hydroxyethyl methacrylate) cryogels with oligopeptides via *β*-cyclodextrin-adamantane complexation for studying cell-instructive peptide environment. *ACS Applied Bio Materials*, page acsabm.9b01059, dec 2019.

[223] Ziqing Jiang, Adriana I. Vasil, John D. Hale, Robert E.W. Hancock, Michael L. Vasil, and Robert S. Hodges. Effects of net charge and the number of positively charged residues on the biological activity of amphipathic *α*-helical cationic antimicrobial peptides. *Biopolymers - Peptide Science Section*, 90(3):369–383, 2008.

[224] E. Thomas Pashuck, Honggang Cui, and Samuel I. Stupp. Tuning Supramolecular Rigidity of Peptide Fibers through Molecular Structure. *Journal of the American Chemical Society*, 132(17):6041–6046, 2010.

[225] Li Yen Wong, Bingzhao Xia, Ernst Wolvetang, and Justin Cooper-White. Targeted, Stimuli-Responsive Delivery of Plasmid DNA and miRNAs Using a Facile Self-Assembled Supramolecular Nanoparticle System. *Biomacromolecules*, 19(2):353–363, 2018.

[226] Martin J. Humphries. Cell Adhesion Assays. In *Methods in Molecular Biology, Extracellular Matrix Protocols, vol. 522*, pages 203–210. 2009.

[227] Stéphanie Pellegrin and Harry Mellor. Actin stress fibers. *Journal of Cell Science*, 120(20):3491–3499, 2007.

[228] James L. McGrath. Cell Spreading: The Power to Simplify. *Current Biology*, 17(10):357–358, 2007.

[229] J. Thomas Parsons, Alan Rick Horwitz, and Martin A. Schwartz. Cell adhesion: Integrating cytoskeletal dynamics and cellular tension. *Nature Reviews Molecular Cell Biology*, 11(9):633–643, 2010.

[230] Alvaro Mata, Liam Palmer, Esther Tejeda-Montes, and Samuel I. Stupp. Design of Biomolecules for Nanoengineered Biomaterials for Regenerative Medicine. volume 811, pages 39–49. Humana Press, Totowa, NJ, 2012.

[231] Douglas Philp and J. Fraser Stoddart. Self-Assembly in natural and unnatural systems. *Angewandte Chemie (International Edition in English)*, 35(11):1154–1196, 1996.

[232] Jean Marie Lehn. Toward self-organization and complex matter. *Science*, 295(5564):2400–2403, 2002.

[233] Ana C. Mendes, Erkan T. Baran, Rui L. Reis, and Helena S. Azevedo. Self-assembly in nature: Using the principles of nature to create complex nanobiomaterials. *Wiley Interdisciplinary Reviews: Nanomedicine and Nanobiotechnology*, 5(6):582–612, 2013.

[234] O. J.G.M. Goor and P. Y.W. Dankers. *Advances in the Development of Supramolecular Polymeric Biomaterials*, volume 5. Elsevier Inc., 2 edition, 2017.

[235] Elham Radvar and Helena S. Azevedo. Supramolecular Peptide/Polymer Hybrid Hydrogels for Biomedical Applications. *Macromolecular Bioscience*, 19(1):1–16, 2019.

[236] Jasmina Gačanin, Christopher V. Synatschke, and Tanja Weil. Biomedical Applications of DNA-Based Hydrogels. *Advanced Functional Materials*, 1906253, 2019.

[237] Quan Luo, Chunxi Hou, Yushi Bai, Ruibing Wang, and Junqiu Liu. Protein Assembly: Versatile Approaches to Construct Highly Ordered Nanostructures. *Chemical Reviews*, 116(22):13571–13632, 2016.

[238] Rein V. Ulijn and Ayala Lampel. Order/Disorder in Protein and Peptide-Based Biomaterials. *Israel Journal of Chemistry*, pages 1–13, 2019.

[239] Antara Dasgupta, Julfikar Hassan Mondal, and Debapratim Das. Peptide hydrogels. *RSC Advances*, 3(24):9117–9149, 2013.

[240] Rein V. Ulijn and Andrew M. Smith. Designing peptide based nanomaterials. *Chemical Society Reviews*, 37(4):664–675, 2008.

[241] Jeanie L. Drury and David J. Mooney. Hydrogels for tissue engineering: scaffold design variables and applications. *Biomaterials*, 24(24):4337–4351, nov 2003.

[242] Debapratim Das and Oren A. Scherman. Cucurbituril: At the interface of small molecule host-guest chemistry and dynamic aggregates. *Israel Journal of Chemistry*, 51(5-6):537–550, 2011.

[243] Steven J. Barrow, Setu Kasera, Matthew J. Rowland, Jesús Del Barrio, and Oren A. Scherman. Cucurbituril-Based Molecular Recognition. *Chemical Reviews*, 115(22):12320–12406, 2015.

[244] Elena Pazos, Paula Novo, Carlos Peinador, Angel E. Kaifer, and Marcos D. García. Cucurbit[8]uril (CB[8])-Based Supramolecular Switches. *Angewandte Chemie - International Edition*, 58(2):403–416, 2019.

[245] Lisa M. Heitmann, Alexander B. Taylor, P. John Hart, and Adam R. Urbach. Sequence-Specific Recognition and Cooperative Dimerization of N-Terminal Aromatic Peptides in Aqueous Solution by a Synthetic Host sequences in aqueous solution with high affinity and selectivity. *J. Am. Chem. Soc*, 128:12574–12581, 2006.

[246] Silvia Sonzini, Seán T.J. Ryan, and Oren A. Scherman. Supramolecular dimerisation of middle-chain Phe pentapeptides via CB[8] host-guest homoternary complex formation. *Chemical Communications*, 49(78):8779–8781, 2013.

[247] Chunyan Zhao, Aaron Tan, Giorgia Pastorin, and Han Kiat Ho. Nanomaterial scaffolds for stem cell proliferation and differentiation in tissue engineering. *Biotechnology Advances*, 31(5):654–668, sep 2013.

[248] Dung T. Dang, Hoang D. Nguyen, Maarten Merkx, and Luc Brunsveld. Supramolecular control of enzyme activity through cucurbit[8]uril-mediated dimerization. *Angewandte Chemie - International Edition*, 52(10):2915–2919, 2013.

[249] Yuan-Fu Ding, Tianlei Sun, Shengke Li, Qiaoxian Huang, Ludan Yue, Liangkui Zhu, and Ruibing Wang. Oral Colon-Targeted Konjac Glucomannan Hydrogel Constructed through Noncovalent Cross-Linking by Cucurbit[8]uril for Ulcerative Colitis Therapy. *ACS Applied Bio Materials*, page acsabm.9b00676, aug 2019.

[250] Haishi Qiao, Jing Jia, Haowen Shen, Sibo Zhao, Enping Chen, Wei Chen, Bin Di, and Chi Hu. Capping Silica Nanoparticles with Tryptophan-Mediated Cucurbit[8]uril Complex for Targeted Intracellular Drug Delivery Triggered by Tumor-Overexpressed IDO1 Enzyme. *Advanced Healthcare Materials*, 8(13):1–10, 2019.

[251] Owen S. Fenton, Mark W. Tibbitt, Eric A. Appel, Siddharth Jhunjhunwala, Matthew J. Webber, and Robert Langer. Injectable Polymer-Nanoparticle Hydrogels for Local Immune Cell Recruitment. *Biomacromolecules*, 20:4430–4436, 2019.

[252] Matthew J. Rowland, Eric A. Appel, Roger J. Coulston, and Oren A. Scherman. Dynamically crosslinked materials via recognition of amino acids by cucurbit[8]uril. *Journal of Materials Chemistry B*, 1(23):2904, 2013.

[253] Joseph S. Renny, Laura L. Tomasevich, Evan H. Tallmadge, and David B. Collum. Method of continuous variations: Applications of job plots to the study of molecular associations in organometallic chemistry. *Angewandte Chemie - International Edition*, 52(46):11998–12013, 2013.

[254] R. C. Hider, G. Kupryszewski, P. Rekowski, and B. Lammek. Origin of the positive 225-230 nm circular dichroism band in proteins. Its application to conformational analysis. *Biophysical Chemistry*, 31(1-2):45–51, 1988.

[255] Dick Andersson, Uno Carlsson, and Per Ola Freskgard. Contribution of tryptophan residues to the CD spectrum of the extracellular domain of human tissue factor: Application in folding studies and prediction of secondary structure. *European Journal of Biochemistry*, 268(4):1118–1128, 2001.

[256] Robert W. Woody. Contributions of tryptophan side chains to the far-ultraviolet circular dichroism of proteins. *European Biophysics Journal*, 23(4):253–262, 1994.

[257] Carlo Diaferia, Nicole Balasco, Teresa Sibillano, Cinzia Giannini, Luigi Vitagliano, Giancarlo Morelli, and Antonella Accardo. Structural Characterization of Self-Assembled Tetra-Tryptophan Based Nanostructures: Variations on a Common Theme. *ChemPhysChem*, 19(13):1635–1642, 2018.

[258] Lei Zou, Adam S. Braegelman, and Matthew J. Webber. Dynamic Supramolecular Hydrogels Spanning an Unprecedented Range of Host–Guest Affinity. *ACS Applied Materials & Interfaces*, pages 8–13, 2019.

[259] Carolyn Meyers, Jeffrey Lisiecki, Sarah Miller, Adam Levin, Laura Fayad, Catherine Ding, Takashi Sono, Edward McCarthy, Benjamin Levi, and Aaron W James. Heterotopic Ossification: A Comprehensive Review. *JBMR Plus*, 3(4):e10172, 2019.

[260] Adrianne M. Rosales, Sebastián L. Vega, Frank W. DelRio, Jason A. Burdick, and Kristi S. Anseth. Hydrogels with Reversible Mechanics to Probe Dynamic Cell Microenvironments. *Angewandte Chemie - International Edition*, 56(40):12132–12136, 2017.

[261] Bárbara Santos Gomes, Bárbara Simões, and Paula M. Mendes. The increasing dynamic, functional complexity of bio-interface materials. *Nature Reviews Chemistry*, 2(3):0120, 2018.

[262] Laith F. Kadem, K. Grace Suana, Michelle Holz, Wei Wang, Hannes Westerhaus, Rainer Herges, and Christine Selhuber-Unkel. High-Frequency Mechanostimulation of Cell Adhesion. *Angewandte Chemie - International Edition*, 56(1):225–229, 2017.

[263] Yuqing Dong, Guorui Jin, Yuan Hong, Hongyuan Zhu, Tian Jian Lu, Feng Xu, Dan Bai, and Min Lin. Engineering the Cell Microenvironment Using Novel Photoresponsive Hydrogels. *ACS Applied Materials and Interfaces*, 10(15):12374–12389, 2018.

[264] Xingyuan Yang, Guanxin Zhang, and Deqing Zhang. Stimuli responsive gels based on low molecular weight gelators. *Journal of Materials Chemistry*, 22(1):38–50, 2012.

[265] Adrianne M. Rosales, Christopher B. Rodell, Minna H. Chen, Matthew G. Morrow, Kristi S. Anseth, and Jason A. Burdick. Reversible Control of Network Properties in Azobenzene-Containing Hyaluronic Acid-Based Hydrogels. *Bioconjugate Chemistry*, 29(4):905–913, apr 2018.

[266] Eric A. Appel, Rebecca A. Forster, Alexandros Koutsioubas, Chris Toprakcioglu, and Oren A. Scherman. Activation energies control the macroscopic properties of physically cross-linked materials. *Angewandte Chemie - International Edition*, 53(38):10038–10043, 2014.